The University Of Sheffield.

Process Simulation of Power Generation Systems with CO_2 Capture

By:

Usman Ali

A thesis submitted in partial fulfilment of the requirements for the degree of Doctor of Philosophy

The University of Sheffield
Energy Engineering Research Group
Faculty of Engineering

September 2016

The candidate confirms that the work submitted is his own and that appropriate credit has been given where reference has been made to the work of others. The contribution of the candidate and the other authors to this work due to jointly-authored publications has been explicitly mentioned below.

The work presented in Chapter 3 of the thesis has appeared as part of the publications as follows:

Ali, U., T. Best, K.N. Finney, C.F. Palma, K.J. Hughes, D.B. Ingham, and M. Pourkashanian, *Process Simulation and Thermodynamic Analysis of a Micro Turbine with Post-combustion CO_2 Capture and Exhaust Gas Recirculation*, Energy Procedia, 2014. 63(0): p. 986-996.

and in,

Ali, U., K.J. Hughes, D.B. Ingham, L. Ma, and M. Pourkashanian, *Effect of the CO_2 enhancement on the performance of a micro gas turbine with a pilot-scale CO_2 capture plant.* Chemical Engineering Research and Design, 2017. 117: p. 11-23.

The work presented in Chapter 4 of the thesis has appeared as part of the publications as follows:

Ali, U., K.J. Hughes, D.B. Ingham, L. Ma, and M. Pourkashanian, *Effect of the CO_2 enhancement on the performance of a micro gas turbine with a pilot-scale CO_2 capture plant.* Chemical Engineering Research and Design, 2017. 117: p. 11-23.

and in,

Ali, U., C.F. Palma, K.J. Hughes, D.B. Ingham, L. Ma, and M. Pourkashanian, *Impact of the operating conditions and position of exhaust gas recirculation on the performance of a micro gas turbine*, in Computer Aided Chemical Engineering, J.K.H. Krist V. Gernaey and G. Rafiqul, Editors. 2015, Elsevier. p. 2417-2422.

The work presented in Chapter 5 of the thesis has appeared as part of the publication as follows:

Ali, U., C.F. Palma, K.J. Hughes, D.B. Ingham, L. Ma, and M. Pourkashanian. *Thermodynamic analysis and process system comparison of the exhaust gas recirculated, steam injected and humidified micro gas turbine,* in *Turbine Technical Conference and Exposition*. 2015. Montreal, Canada: GT2015-42454, Proceedings of ASME Turbo Expo 2015.

The work presented in Chapter 6 of the thesis has appeared as part or full of the publications as follows:

Ali, U., E.O. Agbonghae, K.J. Hughes, D.B. Ingham, L. Ma, and M. Pourkashanian, *Techno-economic process design of a commercial-scale amine-based CO_2 capture system for natural gas combined cycle power plant with exhaust gas recirculation.* Applied Thermal Engineering, 2016. 103: p. 747-758.

in,

Akram, M., U. Ali, T. Best, S. Blakey, K. Finney, and M. Pourkashanian, *Performance evaluation of PACT Pilot-plant for CO_2 capture from gas turbines with Exhaust Gas Recycle.* International Journal of Greenhouse Gas Control, 2016, 47: p. 137-150.

and in,

Ali, U., J. Szuhánszki, M. Akram, C.F. Palma, K.J. Hughes, D.B. Ingham, L. Ma, and M. Pourkashanian, *Sensitivity of Post-Combustion CO_2 Capture at Pilot Scale Level*, In *3rd Post Combustion Capture Conference (PCCC3)*: Boundary Dam Site, Canada, 8th – 11th September, 2015.

The work presented in Chapter 7 of the thesis has appeared as part of the publication as follows:

Ali, U., E.O. Agbonghae, K.J. Hughes, D.B. Ingham, L. Ma, and M. Pourkashanian, *Techno-economic process design of a commercial-scale amine-based CO_2 capture system for natural gas combined cycle power plant with exhaust gas recirculation.* Applied Thermal Engineering, 2016. 103: p. 747-758.

The contributions from the co-authors T. Best, K. N. Finney, M. Akram, J. Szuhánszki and S. Blakey have not appeared in the thesis. The contribution of C. Font Palma was to give suggestions to shape the research work and publications. The other authors were supervisors who have acted in an advisory role giving suggestions about the research direction.

Acknowledgement

I wish to acknowledge and pay special thanks to the supervisory team; Prof M. Pourkashanian, Prof D. B. Ingham, Prof L. Ma and Dr K. J. Hughes for the proper guidance, timely contributions and moral support. It's all due to their remarkable suggestions, keen interest, constructive criticism and responsive discussions throughout the period which have played a key role in the completion of this research work. I am also indebted to the post doctorate research fellows, particularly, Dr C. F. Palma for their valuable input and suggestions. It is all because of the above support that I am able to realize this work. I also wish to express my gratitude to the ETII staff at the University of Leeds and the Energy2050 Staff at the University of Sheffield for their help and assistance.

I take this opportunity to express my profound gratitude to my Father and Late Mother; for their sincere love, continuous motivation and unending prayers. I wish to pay thanks to my loving brothers and sister for their support and faith in me.

I would like to thank the Grant provided by the University of Engineering and Technology, Lahore, Pakistan and the partial support by the University of Leeds and University of Sheffield, UK for carrying out my research work.

Finally, I express gratitude and praise to Almighty God, the creator of the universe, who is beneficial and merciful, guided me in difficult and congeal circumstances, and who endowed me with the will to undertake this work.

Publications and Conferences

Journal

[1] **Ali, U.**, C. Font-Palma, H. Nikpey, M. Mansouri, M. Akram, K.N. Finney, T. Best, N.B. Mohd Said, M. Assadi, and M. Pourkashanian, *Benchmarking of a micro gas turbine model integrated with post-combustion CO_2 capture*, Energy, 2016 [Under review].

[2] **Ali, U.**, K.J. Hughes, D.B. Ingham, L. Ma, and M. Pourkashanian, *Effect of the CO_2 enhancement on the performance of a micro gas turbine with a pilot-scale CO_2 capture plant.* Chemical Engineering Research and Design, 2017. 117: p. 11-23.

[3] **Ali, U.**, E.O. Agbonghae, K.J. Hughes, D.B. Ingham, L. Ma, and M. Pourkashanian, *Techno-economic process design of a commercial-scale amine-based CO_2 capture system for natural gas combined cycle power plant with exhaust gas recirculation.* Applied Thermal Engineering, 2016. 103: p. 747-758.

[4] Akram, M., **U. Ali**, T. Best, S. Blakey, K. Finney, and M. Pourkashanian, *Performance evaluation of PACT Pilot-plant for CO_2 capture from gas turbines with Exhaust Gas Recycle.* International Journal of Greenhouse Gas Control, 2016. 47: p. 137-150.

[5a] **Ali, U.**, C.F. Palma, K.J. Hughes, D.B. Ingham, L. Ma, and M. Pourkashanian, *Impact of the operating conditions and position of exhaust gas recirculation on the performance of a micro gas turbine*, in Computer Aided Chemical Engineering, J.K.H. Krist V. Gernaey and G. Rafiqul, Editors. 2015, Elsevier. p. 2417-2422.

[6a] **Ali, U.**, T. Best, K.N. Finney, C.F. Palma, K.J. Hughes, D.B. Ingham, and M. Pourkashanian, *Process Simulation and Thermodynamic Analysis of a Micro Turbine with Post-combustion CO_2 Capture and Exhaust Gas Recirculation*, Energy Procedia, 2014. 63(0): p. 986-996.

Conference

[5b] **Ali, U.**, C.F. Palma, K.J. Hughes, D.B. Ingham, L. Ma, and M. Pourkashanian, *Impact of the operating conditions and position of exhaust gas recirculation on the performance of a micro gas turbine*, In *Process System Engineering and European Syposium for Computer Aided Process Engineering (PSE2015/ESCAPE25)*: Copenhagen, Denmark, 31st May – 4th June, 2015.

[6b] **Ali, U.**, T. Best, K.N. Finney, C.F. Palma, K.J. Hughes, D.B. Ingham, and M. Pourkashanian, *Process Simulation and Thermodynamic Analysis of a Micro Turbine with Post-combustion CO_2 Capture and Exhaust Gas Recirculation*, In *12th International Conference on Greenhouse Gas Control Technolgies (GHGT-12)*: Austin, Texas, 5th -9th October, 2014.

[7] **Ali, U.**, J. Szuhánszki, M. Akram, C.F. Palma, K.J. Hughes, D.B. Ingham, L. Ma, and M. Pourkashanian, *Sensitivity of Post-Combustion CO_2 Capture at Pilot Scale Level*, In *3rd Post Combustion Capture Conference (PCCC3)*: Boundary Dam Site, Canada, 8th – 11th September, 2015.

[8] **Ali, U.**, C.F. Palma, K.J. Hughes, D.B. Ingham, L. Ma, and M. Pourkashanian. *Thermodynamic analysis and process system comparison of the exhaust gas recirculated, steam injected and humidified micro gas turbine*, in *Turbine Technical Conference and Exposition*. 2015. Montreal, Canada: GT2015-42454,Proceedings of ASME Turbo Expo 2015.

Abstract

The increase in the anthropogenic greenhouse gases has severely damaged the environment in terms of pollution and global climate change. It is capturing the carbon dioxide from the present and future power plants that could save the climate. The post-combustion CO_2 capture system using amine wet scrubbing is investigated in detail for natural-gas fired power plant from pilot-scale to commercial-scale level.

The research work is focussed on the investigation of the different innovative modifications to the micro gas turbine (MGT) including exhaust gas recirculation (EGR), steam injection and humid air turbine. The process models are developed for both MGT and pilot-scale amine-based CO_2 capture plant. The MGT model is tuned and validated with extensive experimental data at different part load conditions for base case, CO_2, steam and simultaneous CO_2 and steam injection to the default MGT. The thermodynamic behaviour, emissions, system efficiency and the sensitivity of the base case MGT for ambient conditions are explored. The robust model is extended for EGR, steam injection and humid air turbine system models; and process system performance comparison for the different modifications is assessed for possible recommendation. In addition, the impact of the operating conditions and locations of the EGR on the performance of the MGT is also analysed. Further, the effect of the enhanced CO_2 on the extensively validated pilot-scale amine-based CO_2 capture plant integrated with MGT is examined. In addition, the sensitivity analysis of the pilot-scale amine-based CO_2 capture model is studied to quantify the effect of the operating parameters on the system performance and to estimate the optimum operating envelope. The EGR at 55 % resulted in a 20.5 % decrease in specific reboiler duty from the pilot-scale amine-based CO_2 capture plant at the CO_2 capture rate of 90 % for monoethanolamine at 30 wt. % aqueous solution.

Furthermore, a techno-economic process design and/or scale-up of the commercial-scale amine-based CO_2 capture system to service about 650 MW_e of the natural gas-fired power plant system with and without EGR is investigated for varying EGR percentage. Finally, thorough comparative potential for the natural gas, coal, biomass fired and co-firing of coal and biomass power plants integrated with CO_2

capture and CO_2 compressions system are explored for different cases of each power plant. The biomass firing resulted in about 40 % increase in fuel flow rate for the constant heat input case while it resulted in 30 % derating of the power output for the constant fuel flow rate case. The comparative potential of gas-CCS, coal-CCS and BECCS has shown that the NGCC with EGR resulted in the least efficiency penalty on integration with CO_2 capture and compression system due to the higher net efficiency. However, coal and biomass fired power plant resulted in the least specific losses per unit of the CO_2 capture on integration with CO_2 capture and compression system due to the higher specific CO_2 capture.

Table of Contents

List of Tables

List of Figures

Nomenclature

Acronyms/Abbreviations

Acronym	Description
Abs	Absorber column
ACP	Amine capture plant
AmH	Amine
APGTF	Advanced Power Generation Technology Forum
APH	Air pre-heater
AR5	Assessment Report 5
ASME	American Society of Mechanical Engineers
ASU	Air Separation Unit
B	Biomass
BECCS	Bio Energy Carbon Capture and Storage
C	Coal
CAPEX	Capital expenditure of the plant
CC	Carbon Capture
CCGT	Closed Cycle Gas Turbine
CCP	CO_2 capture unit
CCS	Carbon Capture and Storage
CCU	CO_2 compression unit
CDT	Compressor discharge temperature
CDP	Compressor discharge pressure
CFD	Computational Fluid Dynamics
CFF	Constant fuel flow rate
CHI	Constant heat input

CHP	Combined Heat and Power
COP	Conference of Parties
CW	Cooling water
DCS	Distributed power generation
DEA	Diethanolamine
DECC	Department of Energy and Climate Change.
DGA	Diglycolamine
DIPA	Diisopropanolamine
DLN	Dry low NO_x
DoE	Department of Energy
DRIASI	Dual-Recuperated-Inter-cooled-After-cooled Steam Injected cycle
EGR	Exhaust Gas Recirculation
EM	Economiser
ENRTL	Electrolyte Non Random Two Liquid
ESP	Electrostatic precipitator
ETII	Energy Technology Innovation Initiative
EU	European Union
FGD	Flue gas desulphurization
FWH	Feed water heater
GE	General Electric
GHG	Greenhouse gases
G/L	Gas/Liquid
GMF	Gas mixing facility
GT	Gas turbine
gPROMS	general PROcess Modelling System
HAT	Humid air turbine
HHV	Higher heating value

HP	High pressure
HRSG	Heat recovery steam generator
ID	Induced draft
IEA	International Energy Agency
IGCC	Integrated Gasification Combined Cycle
IGV	Inlet guide vane
IMTP	INTALOX Metal Tower Packing
Inc	Incorporation
IP	Intermediate pressure
IPCC	Intergovernmental Panel on Climate Change
ISO	International Standards Organization
L/G	Liquid to gas ratio
LHV	Lower heating value
Liq.	Liquid
LNG	Liquefied natural gas
LOTHECO	Low Temperature Heat Combined Cycle
LP	Low pressure
MDEA	Monodiethanolamine
MEA	Monoethanolamine
MGT	Micro gas turbine
NGCC	Natural gas combined cycle
OCGT	Open cycle gas turbine
OCP	Oxy-fuel combustion plant
OECD	Organization for Economic Co-operation and Development
OPEX	Operating expenditure of plant
ReMoVe	Research, Monitoring and Verification
RIGES	Renewable Intensive Global Energy Scenario

PACT	Pilot scale Advanced Capture Technology
PCC	Post combustion capture
PFD	Process flow diagram
PH	Power and heat
PR	Peng-Robinson
PV	Pressure volume
RD&D	Research Development and Demonstration
RH	Re-heater
SCCP	Solvent based Carbon Capture Plant
SCR	Selective catalytic reduction reactor
SH	Super-heater
ST	Steam turbine
STIG	Steam injected
tcm	trillion cubic meter
TEA	Triethylamine
Tech	Technology
TEG	Tetraethylene glycol
TEMA	Tubular Exchanger Manufacturers Association
TIT	Turbine inlet temperature
TOT	Turbine outlet temperature
TOTEX	Total expenditure of plant
TS	Temperature entropy
UHC	Unburned hydro carbons
UK	United Kingdom
UKCCSRC	United Kingdom Carbon Capture and Storage Research Center
UNFCC	United Nations Framework on Climate Change
UKSDAP	UK CO_2 Storage Appraisal Project

US	United State
Vap.	Vapour
WEO	World Energy Outlook
WWC	Water wash column
X	Base

List of Symbols

Symbol	Description	Units
A1, A2, A3…	Reacting species	
A_i	Pre exponential factor for forward reaction	[mol/m^{3}s]
A_i^j	Pre exponential factor for backward reaction	[mol/m^{3}s]
c_p	Molar specific heat at constant pressure	[J/mol-K]
c_{p_a}	Molar specific heat at constant pressure for air	[J/mol-K]
c_{p_f}	Molar specific heat at constant pressure for fuel	[J/mol-K]
c_{p_g}	Molar specific heat at constant pressure for flue gas	[J/mol-K]
c_v	Molar specific heat at constant volume	[J/mol-K]
E_i	Activation energy for forward reaction	[J/mol]
E_i^j	Activation energy for backward reaction	[J/mol]
f	Fugacity coefficient	[bar]
f_i	Fugacity coefficient for ith specie	[bar]
f_i^o	Fugacity coefficient for ith specie at the standard state	[bar]
G	Gibbs energy	[J]
G_i^o	Gibbs energy for ith specie at standard state	[J]
G^t	Total Gibbs energy	[J]
ΔG^o	Gibbs energy change at standard state	[J]
H	Enthalpy	[J/mol]
H_1	Enthalpy at compressor inlet	[J/mol]
H_2	Enthalpy at compressor outlet	[J/mol]
H'	Head	[m]
i	Interest rate	[%]
K	Equilibrium constant	
K_j	Equilibrium constant for jth chemical reaction	

k_{AmH}	Rate constant for reaction between CO_2 and alkanolamine	[m^3/mols]
k_X	Rate constant for reaction between zwitterion and base	
k_{CO_2}	Observed rate constant for reaction based on zwitterion mechanism	[m^3/mols]
k_{H_2O}	Rate constant for reaction between CO_2 and water molecule	
k_i	Rate constant for forward reaction	[m^3/mols]
k_i^j	Rate constant for backward reaction	[m^3/mols]
k_{OH}	Rate constant for reaction between CO_2 molecule and hydroxyl ion	
k_1	Rate constant for forward reaction	
k_2	Rate constant for backward reaction	
M	Molecular weight	[g/gmol]
$\dot{m}$	Mass flow rate	[g/s]
$\dot{m}_{in}$	Mass flow rate at compressor inlet	[g/s]
$\dot{m}_{in,cr}$	Corrected mass flow rate at compressor inlet	[g/s]
N	Rotational speed	[rpm]
N_{cr}	Corrected rotational speed	[rpm]
n	number of moles of the reacting specie	[mol]
n_i	number of moles of the i^{th} reacting specie	[mol]
P	Pressure	[bar]
P_{amb}	Pressure at ambient conditions	[bar]
P_{in}	Pressure at compressor inlet	[bar]
P^o	Pressure at standard state	[bar]
P_{ref}	Pressure at reference condition	[bar]
P_s	Stripper pressure	[bar]
P_1	Pressure at compressor inlet	[bar]
P_2	Pressure at compressor outlet	[bar]

P_3	Pressure at combustor outlet/turbine inlet	[bar]
P_4	Pressure at turbine outlet	[bar]
Q	Amount of energy transfer in terms of heat	[J]
Q_{23}	Heat released during combustion	[J]
R	Universal molar gas constant	[J/K mol]
RH	Relative humidity	[%]
r	Pressure ratio	
R	Apparent rate of reaction of CO_2 molecule with alkanolamine	[mol/m^3s]
R_{CO_2}	Observed rate of reaction of CO_2 molecule with alkanolamine	[mol/m^3s]
R_i	Rate of reaction for i^{th} reaction	[mol/m^3s]
R'	Apparent rate of reaction of CO_2 with water molecule	[mol/m^3s]
R''	Apparent rate of reaction of CO_2 molecule with hydroxide ion	[mol/m^3s]
S	Entropy	[J/mol-K]
s	Service life of the plant	[yrs]
T	Temperature	[K]
T_{amb}	Temperature at ambient conditions	[K]
T_G	Temperature of flue gas	[K]
T_f	Temperature of fuel stream	[K]
T_{in}	Temperature at compressor inlet	[K]
T_L	Temperature of liquid	[K]
T_{ref}	Temperature at reference condition	[K]
T_1	Temperature at compressor inlet	[K]
T_{2_i}	Isentropic temperature at compressor outlet	[K]
T_2	Temperature at compressor outlet	[K]

T_3	Temperature at combustor outlet/turbine inlet	[K]
T_{4_i}	Isentropic temperature at turbine outlet	[K]
T_4	Temperature at turbine outlet	[K]
ΔT	Temperature difference	[K]
u	Velocity	[m/s]
u_1	Velocity at compressor inlet	[m/s]
u_2	Velocity at compressor outlet	[m/s]
V	Volume	[m^3]
v	Reacting coefficient specie	
v_i	i^{th} reacting coefficient specie	
$v_{i,j}$	i^{th} reacting coefficient specie for j^{th} reaction	
W	Amount of energy transfer in terms of work	[J]
W_c	Amount of energy transfer in terms of actual work	[J]
W_{c_a}	Actual work required by compressor	[J]
W_{c_i}	Isentropic work required by compressor	[J]
W_{in}	Work required by compressor	[J]
W_{out}	Work produced by turbine	[J]
W_{t_a}	Actual work produced by turbine	[J]
W_{t_i}	Isentropic work produced by turbine	[J]
W_{12}	Work required by compressor	[J]
W_{34}	Work produced by turbine	[J]
wt.	Weight percentage	[%]
X_1	Scaling factor	
X_2	Scaling factor	
x_i	Extended reaction rate constant for forward reaction	[m^3/mols]
x_i^j	Extended reaction rate constant for forward reaction	[m^3/mols]
y	Specie molar concentration	[mol%]

z	Compressibility factor

Superscripts

Symbol	Description
o	Standard state
t	Total
j	Backward reaction

Subscripts

Symbol	Description
1,2,3,...	Number of species, or streams of the PFD
a	Actual
a	Air
amb	Ambient
AmH	Amine
b	Combustor
c	Compressor
cr	Corrected
e	Electrical
f	Fuel
G	Gas
g	Flue gas
i	Isentropic
i	Forward reaction
i	Number of species
in	Inlet
j	Number of chemical reaction
j	Number of chemical reaction in the chemical reaction set
L	Liquid
max	Maximum

o	Standard state
out	Outlet
P	Pressure
ref	Reference state
s	Stripper
T	Temperature
th	Thermal
t	Turbine
X	Base
v	Volume

Greek Letters

Symbol	Description	Units
α	Base component	
α	Maximum to minimum temperature of the cycle	
α	solvent loading	mol mol^{-1}
β	Fuel to air ratio	
Γ	Integration constant	
Γ_i	Integration constant for i^{th} specie	
γ	Isentropic coefficient (c_p/c_v)	
δ	Pressure ratio	
ε	Heat exchanger effectiveness	[%]
η	Efficiency	[%]
η_b	Efficiency of combustor	[%]
η_c	Efficiency of compressor	[%]
η_t	Efficiency of turbine	[%]
θ	Temperature ratio	
μ	Activity coefficient	
μ_i	Activity coefficient of the i^{th} specie	
π	Product overall spices	
Φ	Ratio of fugacity coefficient	
Φ_i	Ratio of fugacity coefficient for i^{th} specie	
φ	Extent of chemical reaction	[mol]

φ_i	Extent of chemical reaction for the i^{th} specie	[mol]
Ψ	CO_2 capture rate	[%]
ω	Amine solvent mass strength	[%]

Chapter 1
Introduction

This chapter deals with the general introduction to the topic on which the research work is presented in this thesis. The main emphasis is on the set goals and objectives of the research work depending on the need basis at the present time.

1.1 Background

The world population is going to increase to 8.6 billion in 2035 and the urbanization factor is enhancing with higher demand for electricity; with 1.7 billion more energy consumers [1]. Currently 1.2 billion people lack the access to electricity and 2.7 billion people do cooking using biomass as the fuel [1, 2]. Further, more than 2 million people die each year due to the effect of indoor and outdoor air pollution [3].

The world energy trend is changing and this will influence the energy market and trade [1]. Our energy supply system is under the long phase of transition from the conventional power generation systems to more sustainable systems with low carbon emissions in order to deal with the increasing trend of greenhouse gas emissions that severely affect the environment, resulting in global warming and climate change [1, 4]. The United Nations Framework Convention on Climate Change (UNFCC) established that the human activities are substantially increasing the emissions of greenhouse gases into the atmosphere, thus resulting in the warming of the global environment and this effects both nature and mankind [5]. The aim of the UNFCC is to maintain the atmospheric greenhouse gases at a certain minimum level in order to minimize the adverse effects on the global climate [5]. The IPCC, in its fourth assessment report, concludes that the observed temperature rise in the atmosphere over the last few years is likely to continue to increase due to the emissions of anthropogenic greenhouse gases [6, 7]. The synthesis report by the IPCC [8] confirms that human activities influence and cause the global warming and mitigation technologies need to be adopted to limit this effect. Due to human

activities there is a marked increase in the long-lived greenhouse gases carbon dioxide, methane, nitrous oxide and fluorinated gases into the atmosphere [6, 9]. Of these greenhouse gases (GHG), the major share is in the carbon dioxide which is being released abundantly by the power generation sector [1, 6, 7]. The effect of the GHG emissions on the global climate is overwhelming [10] and COP21 put renewed interest towards carbon abatement technologies needed to achieve the balance between emissions by different sources and removals by sinks for the anthropogenic GHG's [11].

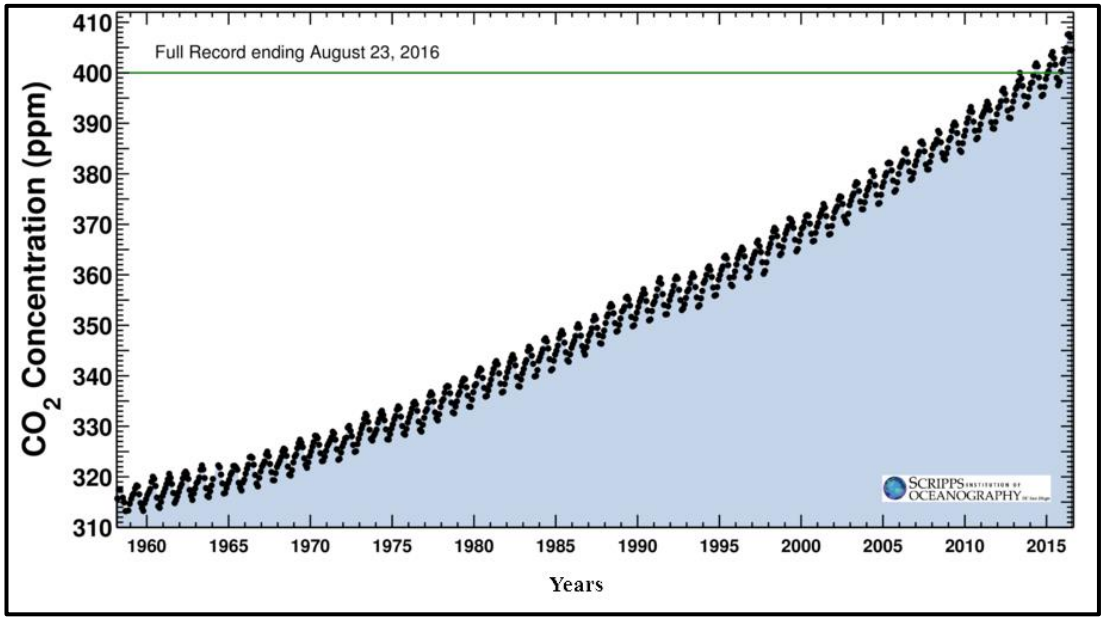

Figure 1.1 Greenhouse gas emissions into the atmosphere at Mauna Loa Observatory (latest CO_2 reading of August 23, 2016 is 402.03 ppm) [12].

The options that can rapidly reduce and/or remove large tons of CO_2 from atmosphere will be part of the energy mix in near future [13]. There is a major share of power production, heat generation and transport in the release of carbon dioxide emissions which contribute in a great context in the global climate change [7]. The carbon dioxide emissions have increased significantly over the past few years and have crossed a level of 400 ppm according to the daily record measurements of the historical Keeling curves as illustrated by Figure 1.1 compared to the pre-industrial era emission level of 280 ppm [7, 12, 14].

Restricting the warming temperature to 2 ^{o}C, and the CO_2 emissions to 450 ppm, for the climate goal is becoming stringent as four-fifths of the CO_2 emissions by 2035 are already locked-in by the present power production sector [1, 15]. Fossil fuel combustion is the dominant source for the generation of power in order to achieve

the ever increasing thirst for energy and being the major reason for the emission of the carbon dioxide [2, 6, 16]. The working group (III) contribution to AR5 of IPCC [13], recommended that the decarbonizing of the energy supply sector is the major mitigation strategy. To have a deep cut in the global CO_2 emissions, there is a wide consensus that there is a need to have changes to the existing and developing power generation systems [17].

1.1.1 Coal as Fuel

Coal is the most widely distributed, abundantly available and single largest primary energy supply [1, 6, 7, 18, 19]. Combustion of fossil fuels, such as coal, oil and natural gas, emits carbon dioxide into the atmosphere. Reliable electricity supply is one of the basic needs for the increase in the living standards and the developing countries mostly rely on coal for the power generation [18]. The proportion of electricity generation from the coal is increasing day by day and thus has many environmental concerns relating to the use of coal for power generation, and in particular the greenhouse gas carbon dioxide [1, 6, 7, 18, 20].

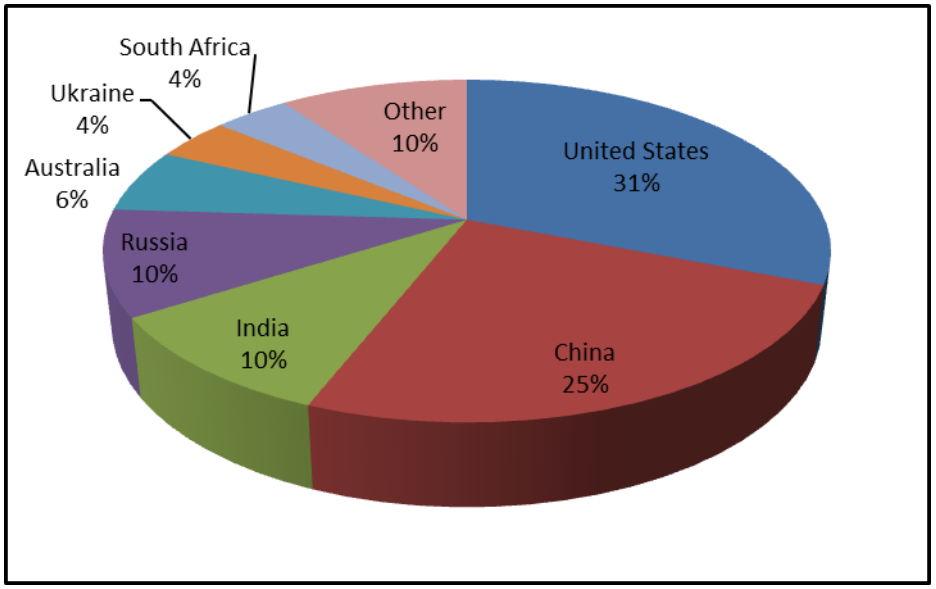

Figure 1.2 World hard coal reserves by country – end 2010 (Total reserves 728 billion tonnes) [21].

Coal met 45% of the energy demand of the globe between 2001-2011 and it will have to decrease to a 25% share in the energy demand by 2035 [1]. Coal is mainly used for power production and fuel production, out of which 65% of the world coal consumption is in the power sector and 27% is in industry [1]. World Energy Outlook (WEO) [1] predicts that the coal reserves are sufficient for about 132 years

of power production based on the 2011 level and Figure 1.2 represents the different country's share in the total of 728 billion tonnes of world hard coal reserves [1].

Over the world, the coal share in CO_2 emission was 71%, oil 17% and gas 12% as reported in the literature [1]. For the same energy equivalent amount of fuel, coal emits 68% more CO_2 than natural gas and 42% more than oil [1]. According to the International Energy Agency (IEA) analyses, the globally installed coal-fired power plants accounts for more than 8.5 Giga tonnes of carbon dioxide emissions per year and it represents approximately one-quarter of the global carbon dioxide emissions [20]. Further, an additional 1000 GW of coal-fired power generation capacity is coming by 2035, with more than 1600 GW of installed capacity of coal-fired power generation system present in 2010 [20]. As there is rapid and gradual expansion of the coal-fired power generation system in the countries such as China and India, due to the growing demand of the energy and the coal remains the cheapest power generation option in these Asian countries [1, 19]. Therefore coal will remain as the major source for the electricity production globally in the coming years [1, 19].

1.1.2 Natural Gas as Fuel

Natural gas is a relatively clean fossil fuel, and in the future energy mix, the share of the natural gas power plant is expected to grow. Natural gas power plants are relatively cheap, flexible in operation since it controls and emits less CO_2 and NO_x and nearly zero SO_2 compared to other fossil fuels. The natural gas is easy to burn fuel as the requirements of the transport to the burner are simple and the burning or ignition characteristics are good as compared to the coal. Gas demand for the particular power generation depends on the comparative price of the coal and gas which vary and most power generators switch from gas to coal during winter as the gas price and residential consumption for space heating increases [9, 19]. The global total conventional recoverable resources of the natural gas amounts to approximately 790 tcm and they are sufficient for 230 years consumption at the present rate of usage as reported by the WEO [1]. There is a boost in the gas demand with the increase of the gas power stations response and also due to the increasing attention for reducing the carbon dioxide emissions from the power generation system [1, 22]. The natural gas power plant mainly comes in the form of the open cycle gas turbine (OCGT), or combined cycle gas turbine (CCGT), and appears to be most stimulating, in terms of the efficiency, ease of operation, economy, and

environmental aspects [1]. The natural gas turbine power generation systems became more important after 1990, as the machine cost decreases and the efficiency in comparison to the coal fired power generation systems increases [19]. The share of the natural gas is rising among all other fossil fuels due to its low carbon intensity [2]. Further, the share of the gas in the global energy demand is more pronounced as predicted by the IEA [23], as shown in Figure 1.3.

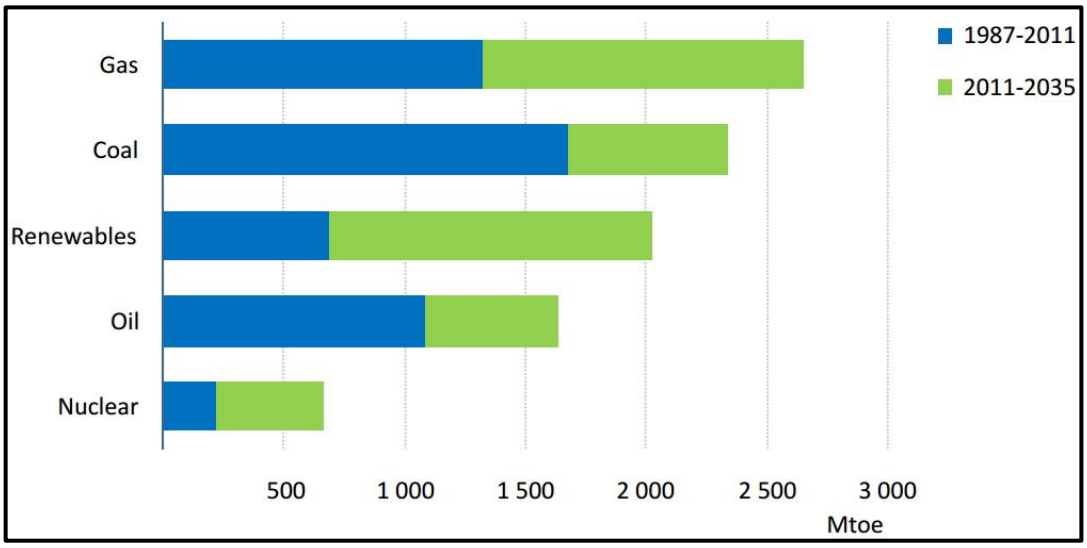

Figure 1.3 Growth in the total primary energy demand [23].

Due to stringent environmental emission regulations and continuing efforts for the reduction of carbon dioxide from the power generation systems, improved efficiency is demanded from the power generation systems with reduced toxic and noxious emissions. The gas turbine technology provides the future clean and cost effective way of controlling the carbon dioxide emissions for the cogeneration systems of heat and power generation in the distributed power generation regime [24]. Therefore natural gas is going to dominate in the energy market and the main contribution will be towards the simple or the combined cycle systems and the major development will be in the distributed power generation, and especially the micro gas turbines will be at the front line for meeting the needs of the electrical and thermal energy demand of the costumers [25]. Although much work needs to be done on this in order to increase the power and efficiency of the gas turbines, and to shift the power scale to the micro level gas turbines in the distributed power generation regime and to compete with the conventional and the emerging technologies. There is a need to move towards the efficient power generation systems and eliminating the less

efficient ones, adopting distribution systems and smart grid systems, with greater use of the combined heat and power generation systems with minimum loses [1].

1.1.3 Biomass as Fuel

Biomass is un-fossilized organic material that is renewable in nature. Biomass as a fuel mainly consists of woody plants/wastes, herbaceous plants/grasses, aquatic plants and manures [26, 27]. Biomass provides almost 10 % of the global energy supply as predicted by the IEA and plays an important role for cooking and space heating in developing countries [28]. The technological developments, surplus food/crop wastes and climate change threat have renewed interest towards the use of biomass for power production [27]. The biomass is considered to be (nearly) carbon-neutral fuel, as the CO_2 released during the combustion of the biomass is consumed by the biomass when it is replanted. Therefore, in closed-loop life cycle analysis the bioenergy is considered to be a zero-emission fuel provided that the gap between instantaneous release of the CO_2 during combustion of the biomass and its uptake by newly planted biomass is small. Task 38 of the IEA for bioenergy [29], have mentioned different technologies which can use biomass to effectively reduce the atmospheric CO_2. The major challenges towards the development and deployment of the biomass for power generation through standalone biomass-fired power plants or co-firing of coal and biomass are the economical and sustainable availability of biomass rather than technical in nature [30]. The United Nations Conference on Environment and Development, the renewable intensive global energy scenario (RIGES), suggested that half of the world primary energy demand will be met by biomass by 2050 [27].

1.2 Climate Change Mitigation

In order to reduce the worsening effect of the carbon emissions in the atmosphere in terms of pollution, global climate change and global warming has led to a shift in the dependence from the carbon sources towards low- or non-carbon sources for the generation of the power in a sustainable way [1, 6]. The policies, research, and capital all should be directed towards the development and deployment of carbon abatement technologies in order to save the environment [1]. There are differences in the geographical distribution of the fossil fuels for the power generation, as depicted in Figure 1.2, and the technological and structural changes in the

production systems, consumption and the trade patterns due to the rural and urban distribution of the population varies through the globe [6]. To reduce the carbon dioxide emissions, the carbon-intensive fuels should be replaced by cleaner and sustainable technologies, such as switching from coal towards natural gas or biomass, and depending more on nuclear and renewable energies [6]. However, new carbon abatement technologies, such as underground coal gasification, carbon capture and storage, renewables and nuclear should be adopted on a commercial-scale to reduce emissions in order to achieve the desired goals [1]. The stabilization of greenhouse gases into the atmosphere can be achieved by using non-carbon resources: renewable energy, such as biomass, solar and wind energy [31]. Of all the new power plants, approximately one third will replace those plants which will be retired by 2035, while half of the newly installed capacity will be of renewables as reported by WEO [1]. The following strategy is often proposed for CO_2 emissions abatement, and includes [1, 6, 19, 31-34]:

- Improving generation efficiency.
- Reducing carbon intensity.
- Replacing hydrocarbons by renewable and nuclear.
- Altering the present power production techniques/developing new innovative power generation techniques.
- Innovative and cost effective capture technologies.

Raising the overall plant efficiency by 1 percentage point will result in a 3 % reduction in carbon dioxide emissions [18]. In the coming years, power generation will continue to be dependent on fossil fuels, which will lead to the increase in emissions of carbon dioxide into the atmosphere [31]. No more than one third of the present reserves can be consumed before 2050 if the target of the 450 ppm scenario of the 2 ^{o}C goal mater allies and the carbon abatement technologies to be properly adopted [1]. However, countries with low levels of modern energy services rarely rely on the efficiency or carbon abatement technologies [1]. These countries rather concentrate on the supply or the meeting of the public demand by building new capacities [1]. Carbon capture and storage is an important technological option to allow societies to maintain their existing carbon based infrastructure, while minimizing the carbon dioxide concentration into the atmosphere [31].

1.2.1 Carbon Dioxide Capture and Storage

The only technology that can reduce or mitigate the carbon dioxide emissions from large power generation systems is the carbon dioxide capture and storage [35]. Carbon dioxide capture and storage consists of separating carbon dioxide from the large point sources, transporting carbon dioxide to the location where it can be stored intact from the atmosphere in the underground storage for longer periods of time [35, 36]. In order to achieve deep cuts in worldwide carbon dioxide emissions, all newly built coal fired power plants must be equipped with carbon dioxide capture and storage, and all present plants having a significant lifetime must be carbon dioxide capture and storage retrofitted [20]. Carbon dioxide capture and storage technology should also be considered and adopted for already locked-in carbon dioxide emissions for limiting the global temperature rise below 2°C [1].

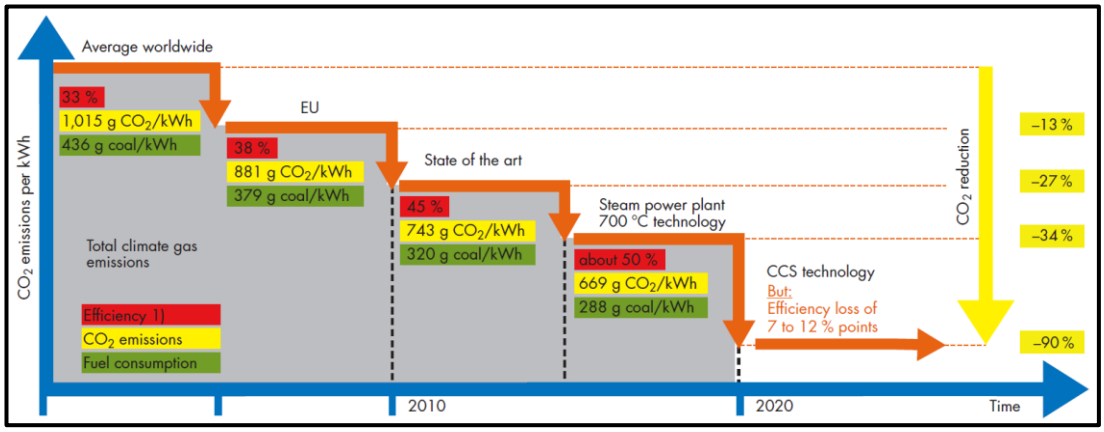

Figure 1.4 Power plant efficiency as a function of carbon dioxide emission reduction [37].

As long as fossil fuels continue to play a major share in the global energy mix, there will be no climate friendly solution other than carbon capture and storage for power generation sector [38]. Carbon capture and storage is likely to play a part of the 13 % cumulative emissions reductions by 2050, not only from power generation but also from industrial sector [16]. The major barriers to the development of the carbon capture and storage is the higher costs, insufficient support schemes and subsidies to the fossil fuels [39]. Carbon dioxide capture, pressurization and injection requires energy, which reduces the overall energy efficiency of the power plant and this increases the cost of the process and typical values for the efficiency loss lies between 6-12% [35]. Carbon dioxide capture and storage would save 2.5 giga tons of the carbon dioxide in 2035, so carbon dioxide capture and storage will be a major

abatement technology after 2020 [1]. There are approximately 15 large-scale facilities in operation with CCS worldwide [16]. The first and oldest carbon capture and storage project is the Sleipner oil and gas carbon dioxide capture and storage project, which has completed 20 years of successful operation by storing 1 Mt/yr of CO_2 to the deep saline reservoir. The first carbon capture and storage project from the power plant is the Boundary Dam Power Station, Estevan, Saskatchewan, Canada. This project is based on 139 MW of the coal-fired power plant using post-combustion CO_2 capture technology. The captured CO_2 is used for the enhanced oil recovery and/or stored in Auistore through 66 km pipeline. Further, in the Canada Shell Quest carbon dioxide capture and storage project is based on capturing 1.2 Mt/yr of the CO_2 from oil sands which will be later stored in the saline acquifers. In United States, the CO_2 is being used for enhanced oil recovery using 6600 km of the CO_2 pipeline. Further, Kemper County, Mississippi is integrated gasification combined cycle based on 582 MW with 3 Mt/yr of the CO_2 capture which will be used for enhanced oil recovery. The Petra Nova carbon dioxide capture and storage project will be based on 240 MW of slip stream from 610 MW coal-fired facility resulting in 1.4 Mt/yr of CO_2 capture which will be transported through 132 km pipeline for enhanced oil recovery. In addition, the Gorgon CO_2 injection project in Australia is already injecting 3.4 Mt/yr of the CO_2. The industrial carbon capture and storage project of pre-combustion steel production in Abu Dhabi is planned to capture 0.8 Mt/yr of the CO_2 to be used for the enhanced oil recovery. In United Kingdom, the Peterhead CO_2 capture and storage project from 385 MW of gas fired using post- combustion carbon capture and the Whiterose oxy-fuel carbon dioxide capture and storage projects were scraped due to government decision of abolishing the £1 bn funding.

However, the existing power capacity is likely to be unsuitable for carbon dioxide capture and storage retrofit, either the plant efficiency is too low and/or its capacity is too small [18]. Further, a number of the various technical factors which must be considered for the retrofitting, includes access to CO_2 storage, site space for CO_2 capture plant, further the gas cleaning performances if required, cooling, heating and power requirements [40, 41]. The retrofit triangle indicates that the three key interlinked requirements are; ability of add capture, access to secure storage and economic and social viability [40, 41]. In conclusion, the retrofit to the specific facility depends on a site specific basis [40, 42], however, the number of power

plants are relatively small. This carbon dioxide emissions reduction, by the increase of the power plant efficiency, is visible through the Figure 1.4 [18]. Further, to reach the targets set for 2100, the development and deployment of bioenergy carbon capture and storage is also essential [13]. Carbon capture and storage, bioenergy and combination of both in terms of bioenergy carbon capture and storage will be an integral part of limiting global warming to below 2 ^{o}C [13].

1.2.2 Carbon Dioxide Capture and Storage Steps

Carbon dioxide capture and storage involves three components or stages for the mitigation of the carbon dioxide from the large point sources. The three stages of the carbon dioxide capture and storage are as follows:

i. Carbon dioxide capture.
ii. Carbon dioxide transport.
iii. Carbon dioxide storage/sequestration.

Carbon dioxide capture involves the separation of the carbon dioxide from the gases before or after combustion. Next is the transport step which involves the carrying of the captured carbon dioxide to the storage location where it can be kept in isolation from the atmosphere. The captured carbon dioxide is compressed before transportation and the storage involves either injection of carbon dioxide in a deep ocean, underground geological formations or industrial fixation into inorganic metal carbonates.

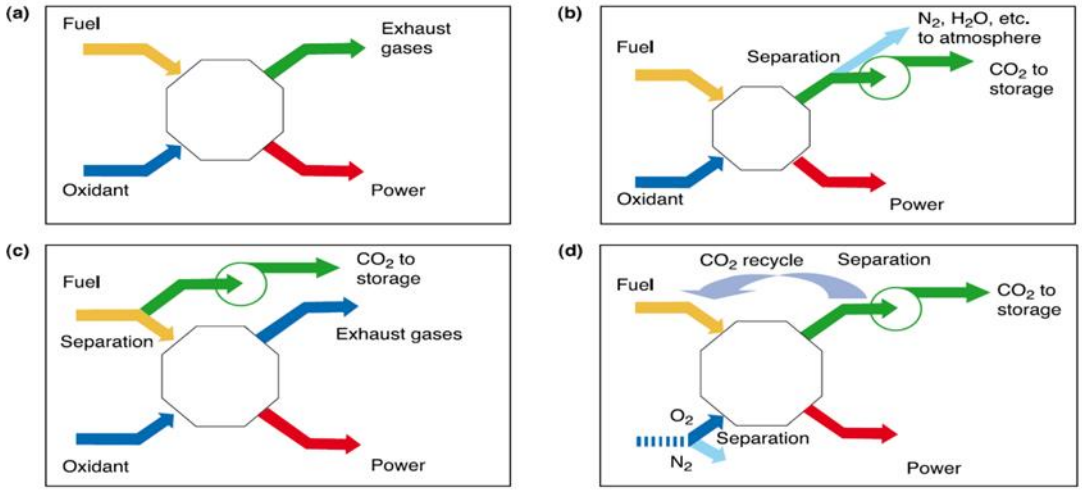

Figure 1.5 Schematic of the Carbon Capture technologies (a) Conventional power plant; (b) Post-combustion carbon dioxide capture; (c) Pre-combustion carbon dioxide capture; and (d) Oxy-fuel combustion carbon dioxide capture [43].

1.2.2.1 Carbon Dioxide Capture

The carbon dioxide is captured from large emission sources, such as the power plants and industries and it is concentrated before transportation [36]. Capture technologies pave the path for the development of low carbon or zero-emission electricity for the end use [36]. Several technologies are in the research, development and demonstration phase, while the most considered and developed are as classified in Figure 1.5 [1, 4, 6, 31-33, 36, 44, 45];

i. Post-combustion carbon dioxide capture.
ii. Pre-combustion carbon dioxide capture.
iii. Oxy-fuel combustion carbon dioxide capture.

The capture process requires energy and it reduces the overall efficiency of the power generation leading to more fuel consumption making system less mass and energy intensive; so research and development is needed to develop novelty in these processes to make them acceptable with a smaller efficiency loss [6, 36].

1.2.2.1.1 Post-Combustion Carbon Dioxide Capture

Post-combustion carbon dioxide capture involves the removal of carbon dioxide from the flue gas of the conventional power plants [46]. The conventional power plants generate the flue gas, which contains diluted carbon dioxide with nitrogen and other impurities [31, 34, 36, 45]. The fuel is combusted in the air which is about four-fifths nitrogen and after the removal of the NO_x and SO_2 the carbon dioxide is captured to be transported and injected into the storage, as shown in Figure 1.5 (b). The low concentration of the carbon dioxide in the flue gas creates a technical challenge for the development of energy intensive and cost effective process for the capture of the carbon dioxide [31, 36, 44, 45]. The various technologies referred for post-combustion capture includes absorption, adsorption, gas separation membranes, and cryogenic distillation [6, 31, 34, 36, 45]. The most important technique adopted for post-combustion capture involve; absorption and striping columns using chemical or physical solvents having an affinity to readily absorb or desorb carbon dioxide [45, 46]. However, separation is mostly performed using chemical solvents, such as mono ethanolamine (MEA), chilled ammonia or sterically hindered amines [45, 46]. Amine absorption is a proven technology in the process industry [6, 46].

Further, amines are available in three forms, each with its own advantages and disadvantages for use as a carbon dioxide solvent [34, 45].

1.2.2.1.2 Pre-Combustion Carbon Dioxide Capture

This process is mostly used in relation with Integrated Gasification Combined Cycle (IGCC) power plants, where syngas containing carbon monoxide, carbon dioxide and hydrogen are obtained using gasification while carbon monoxide is converted into carbon dioxide by a shift reactor and the carbon dioxide is separated from the rest of the hydrogen before it is combusted into the gas turbine [18, 36, 46]. There are two main routes for this process, namely steam reforming or limited oxygen to the primary fuel [36]. As the partial pressure of the carbon dioxide produced is higher; physical solvents can be applied for the separation of the carbon dioxide [34, 46]. The separated carbon dioxide is then sent to the storage location as shown in Figure 1.5 (c). The process is also known as fuel decarbonisation and the aim of this process is to convert carbon fuel into carbon-less fuel and converting carbon energy into hydrogen [31, 46]. IGCC uses a combination of gas and steam turbines to produce electricity [18]. Due to the higher capital cost of the plant construction, complexity, little experience of large scale power generation through IGCC, and less demonstration, make it less viable [46].

1.2.2.1.3 Oxy-Combustion Carbon Dioxide Capture

The oxy-fuel carbon dioxide combustion involves the elimination of the nitrogen from the flue gas by combusting the fuel in either pure oxygen or a mixture of pure oxygen and carbon dioxide rich recycled flue gas [36]. By eliminating nitrogen, the flue gas mainly consists of carbon dioxide and water vapour and a concentrated stream of carbon dioxide can be easily produced for transport and storage by simply condensing the water vapour [18, 31, 32]. The pure oxygen for oxy-fuel combustion is produced by cryogenic air separation or membranes [31, 32]. In the cryogenic air separation unit, the air is first compressed then trace impurities, such as water, carbon dioxide and hydrocarbons, which could accumulate into the system with time is removed. The air is cooled to the desired temperature in the heat exchangers against the returning liquids and sent to the double distillation column for the separation into the desired components with a specified purity level [36]. A schematic of the oxy-combustion capture is shown in Figure 1.5 (d). The

combustion of fuel in pure oxygen results in high temperatures as compared to the combustion in air [32]. The recycled carbon dioxide controls the flame temperature as well as compensates for the missing nitrogen [18, 31, 32, 46]. The flue gas contains primarily carbon dioxide, with impurities such as SO_2, NO_x, HCl and Hg depending on the type of the fuel used with some inerts, such as nitrogen, oxygen and argon depending upon the oxidant stream or the air-ingress into the system [36]. The carbon dioxide concentrated flue gas is divided into three streams; the first one is recycled back into the furnace, the second one to transport and dry the coal feed while the third as the product gas [36]. The flue gas, which contains mainly carbon dioxide, is cooled and water vapours are removed through condensation, after which the dried carbon dioxide is compressed to be transported for storage.

1.2.2.2 Carbon Dioxide Transport

Transport is the intermediate stage between carbon dioxide capture and storage and it links between the sources and storage sites [35, 36]. Natural gas, oil, condensate, water and many hydrocarbons are transported through pipelines over thousands of kilometres; both on-shore and off-shore, in deserts, over mountains, through populated and open areas [36]. Carbon dioxide is transported in three states; solid, liquid and gas in pipelines, ship-, rail- and road-tankers [31, 35, 36]. Transporting carbon dioxide in solid state is not a cost effective means for the transport [31, 35]. Carbon dioxide transport through pipelines is the most favourable, cost-effective and reliable method for transporting a large bulk of carbon dioxide [31, 36]. Pipelines can be connected to various emission points and large collections can be obtained at lower cost [31, 36]. However, carbon dioxide is transported through ships when the carbon dioxide is to be moved over long distances or overseas [31]. The carbon dioxide is transported at high pressure which reduces its volume and makes it denser and in the super-critical state through pipelines and shipment [31, 35, 36]. From an operational point of view, safety risk, maintenance and technically the optimum operating and design conditions are of prime importance for pipeline transport [31, 35, 36].

1.2.2.3 Carbon Dioxide Storage

Carbon dioxide storage or sequestration is the last stage of the carbon dioxide mitigation technique and stores carbon dioxide for a longer period of time without contact with the atmosphere [31]. There are three ways through which carbon

dioxide can be stored including; geological storage, ocean storage and mineralisation [31, 35, 36]. In geological storage, the carbon dioxide is immobilised in a gaseous or supercritical state by the physical trapping into geological formations [31, 35]. The geological storage options include: depleted oil and gas reservoirs in combination with enhanced recovery, deep saline aquifers, and un-minable coal mines with enhanced coal bed methane recovery [31, 35, 36]. The injection of the carbon dioxide into well-defined and managed location will retain it underground for the longer period of time and the likelihood of the carbon dioxide to be retained for 1000 years is 99 % [36]. Carbon dioxide can also be injected into the depths of the ocean where it forms hydrates which are heavier than water plumes and therefore sink towards the bottom of the ocean and remains isolated for millions of years [31, 35, 36]. The ocean is considered to be the largest storage of the carbon dioxide, however, with the increase in concentration of the carbon dioxide in the ocean the acidification and serious concerns to the aquatic life arose [31]. The mineralization involves the chemical reaction of carbon dioxide and the formation of the inorganic carbonates such as natural rock [31, 35, 36]. It is the safest and the permanent solution for the carbon dioxide storage [31, 36]. The higher cost of the mineralization and the eco-concerns to the ocean storage the underground storage seems to be the most feasible option [31].

1.3 United Kingdom Perspective

According to the statistical releases; the provisional figures of the greenhouse gas emissions for the year 2015 released by the Department of Energy and Climate Change (DECC) [47], were 3 % lower as compared to the 2014 and 38 % lower as compared the 1990 emissions level as shown in Figure 1.6. Carbon dioxide emission accounted for 82 % of the total greenhouse gas emissions in 2014 [47]. The major contribution to the carbon dioxide emissions by source sector in 2015 (provisional) was 34 % by energy supply, 29 % by transport, 17 % by business, etc. [47]. Coal is the second largest fuel after natural gas and it contributes to 29 % in the electricity generation and 25 % in the carbon dioxide emission as compared to the other fuels such as oil and natural gas as shown in Figure 1.7 (a) and (b), respectively [9].

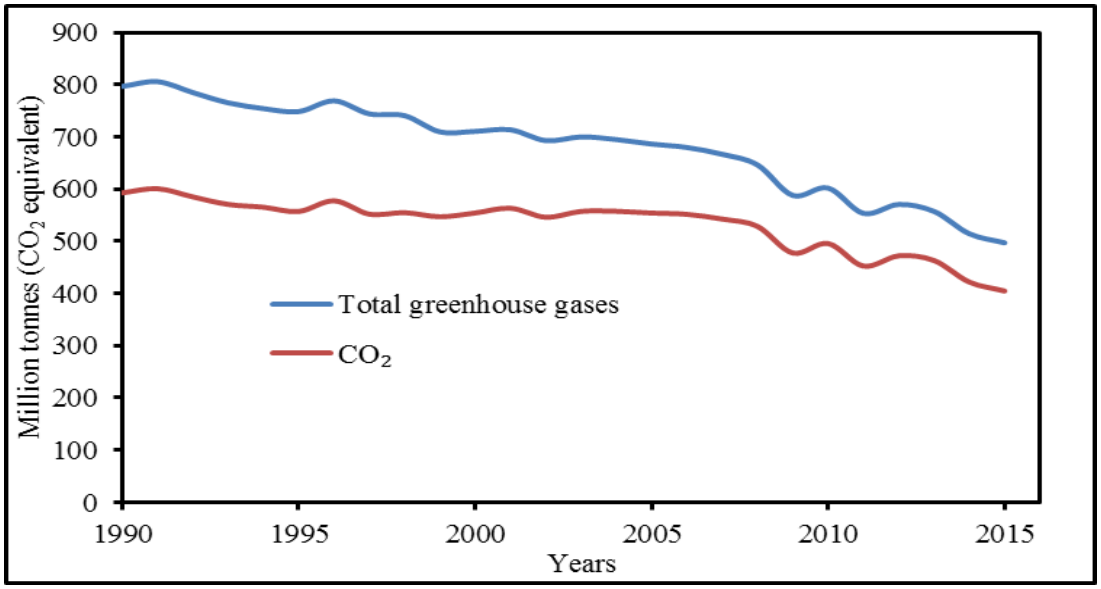

Figure 1.6 Emissions of greenhouse gasses in United kingdom, 1990 – 2015 (with values for 2015 as provisional) [47].

There are a total of 18 coal-fired power plants in the UK with an installed capacity of 24 GW and with an average age of 40 years as reported by the IEA [9]. The United Kingdom has been set with different objectives by the DECC and UK Advanced Power Generation Technology Forum (APGTF) which includes: 80 % reduction in the greenhouse gas emissions by 2050 (based on the 1990 timeline).

(a) (b)

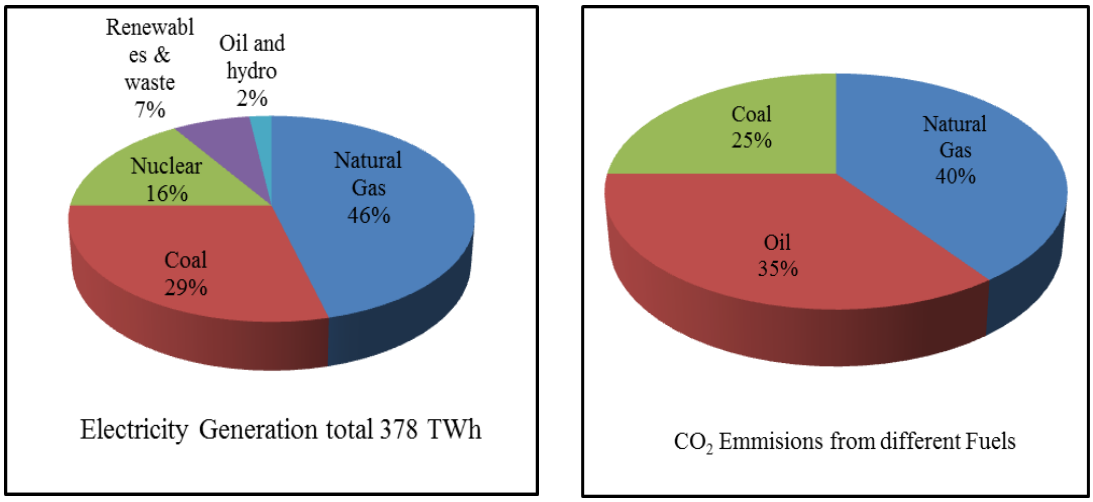

Figure 1.7 Contribution of different energy resources in (a) electricity generation, and (b) fuels [9].

Natural gas is the most abundantly used fuel in the United Kingdom as shown in Figure 1.7. The power generation through the natural gas in Europe has tripled in the last 10 years [48]. According to Pilavachi [49], the United Kingdom has a 12 million

natural gas boiler market and if 25 % of this were shifted to a micro cogeneration system then this will result in 25 % of the United Kingdom's electricity demand. However, a higher natural gas price will reduce the development of the natural gas turbine system. The United Kingdom government has developed a secure policy by promoting energy efficiency measures by reducing the energy demand, or by maximising the reliance on the indigenous energy resources [9].

1.4 The Challenges for Research

The energy demand is going to increase more than one third by the year 2035 [1]. Further, there is a growing trend in the emissions from different sources, and this will result in a worsening effect on the environment in terms of ozone depletion, climate change worldwide and global warming [1, 6, 15]. Due of the uncertainties in the constant supply of power from the renewable sources and a retreat from the nuclear resources; fossil fuels will continue to play a dominant role in the energy supply worldwide [1]. There is a wide consensus and awareness around the world on the mitigation of carbon dioxide emissions and to adopt carbon dioxide capture and storage techniques in terms of retrofit to the existing power plants, or be fitted with the new power plants [1, 6, 19]. Carbon dioxide emissions form the conventional power plants result in a diluted flue gas stream and its capture is of high cost. Although, the capture of the carbon dioxide from the concentrated flue gas stream through exhaust gas recirculation is more easy and cost effective. Further, at present, much research, development and demonstration work is being carried out across the world. The process investigation of the gas turbine with either exhaust gas recirculation and/or the humidification of the air are the core areas which have not been extensively studied. It is necessary to make the natural gas power plants, including exhaust gas recirculation coupled to the carbon capture system, to be the next solution for the power generation sector; making it technically and economically feasible. Therefore, the understanding of the system, initially at pilot-scale level is important for being a replica of the commercial-scale system and then its application to the commercial-scale level to suggest some viable options and solutions. Micro gas turbines are one of the secure, economical and environmentally viable options for the power and heat generation at the distributed power generation level and an accessible option for research in academia to further its integration with pilot-scale with carbon dioxide capture plant can also be assessed to recommend

findings for commercial-scale system. The process system analysis of the system for different modifications, along with the sensitivity analysis of the operational parameters, will help us to better understand the system. Further, comparison of the different power generation systems, such as using coal and biomass as fuel with natural gas fired systems, will give an insight for the better options for the future energy mix whilst keeping the targets of reducing the carbon dioxide emissions in to the context.

1.5 Aims and Objectives

Today, process system analysis is a vital tool for the investigation and to better apprehend the process thermodynamic, transport and kinetic properties and for generating the data for the process understanding. The aim of the research work to be presented in this thesis is to develop an optimized micro gas turbine integrated to the pilot-based amine-based CO_2 capture system including exhaust gas recirculation. The objectives are to extend the gained understanding to the commercial-scale application of natural gas fired power plants including exhaust gas recirculation further, coupled to the CO_2 capture plant. Here the aims and objectives that are set for the research work are presented which includes the following:

i. Development of an effective systematic approach for the process system analysis of natural gas fired systems coupled to CO_2 capture technology.

ii. Development of validated process models for micro gas turbine and pilot-scale amine-based CO_2 capture plants and investigating the sensitivity of the system against key operational scenarios.

iii. Investigation of an optimal way of exhaust gas recirculation to the micro gas turbine and assessment of the impact on the integrated pilot-scale amine-based CO_2 capture system. Further, assessing the effect of steam injection and humidification of the air on the performance of the micro gas turbine.

iv. Techno-economic process design and/or scale-up of amine-based CO_2 capture system for commercial scale application of natural gas combined cycle power plant with and without exhaust gas recirculation.

v. Assessing the comparative potential of natural gas combined cycle power plants integrated with CO_2 capture and compression system with and without exhaust gas recirculation against the coal and biomass fired power plants integrated with CO_2 capture and compression system.

1.6 Novelty and Contribution

The research work presented in this thesis is continuously being disseminated in peer-reviewed journal and conference publications. The list of peer-reviewed journal and conference publications are given in page iv. Further, the work presented in the thesis is based on the novel process system analysis being adopted. The major novel approaches adopted in this research work can be listed as follows:

- Integration of MGT with a pilot-scale CO_2 capture plant (both validated experimentally) is novel in a way, namely the pure CO_2 is injected at the MGT inlet. The injected CO_2 results in enhancement of the CO_2 in the flue gas which is beneficial for analysis with the CO_2 capture plant at higher CO_2 concentrations in the flue gas.
- The micro gas turbine analysed in this research work has a very low concertation of the CO_2 in the flue gas. The treatment of the low CO_2 concentration range from 1.4 to 4.9 mol% through a pilot-scale amine-based CO_2 capture plant is never being reported in the literature. However, the overall range studied in the research work presented in this thesis varies from 1.4 to 14.4 mol%.
- The optimization of the EGR cycle in terms of the position and conditions of the EGR is reported.
- The comparative potential of the MGT-EGR, MGT-STIG and MGT-HAT and more especially in terms of the thermodynamic parameters is a contribution towards the literature.
- The scale-up approach is novel in which design methodology is adopted by using the process modelling tool along with economic parameters as an optimization parameter – for commercial-scale CO_2 capture plant design and/or scale up.
- The full-scale modelling of the integrated power plant with CO_2 capture and compression system for biomass fuel switch for two cases and co-firing of coal and biomass is reported for the first time and its comparison with NGCC

with and without EGR and coal-fired power plant integrated with the CO_2 capture and compression system.

1.7 Organization of the Thesis

The thesis is organized into 9 chapters where the present Chapter 1 presents the general background of the area in which the research work is carried out. In Chapter 2, a brief overview of the gas turbine system and amine-based CO_2 system is presented. In addition, the process chemistry and thermodynamics of the systems under investigations is explained along with generalized modelling algorithm. Further, techniques and tools to be used in this thesis are elaborated in Chapter 2. Chapter 3 presents the validated micro gas turbine model along with sensitivity of the key operational parameters to assess the performance of the micro gas turbine. The optimum exhaust gas recirculation system for a micro gas turbine is investigated in Chapter 4. Further, the effect synthetic exhaust gas recirculation in terms of CO_2 injection to the micro gas turbine is assessed and the developed models are validated against the extensive set of experimental data for CO_2 injection at different part load conditions. In continuation to Chapters 3 and 4, the Chapter 5 presents the micro gas turbine model validation against steam injection and performance assessment and comparison of the different alterations of micro gas turbine, including, exhaust gas recirculation, steam injection and humid air turbine system. In Chapter 6, the pilot-scale amine-based CO_2 capture plant is presented. The validation of the pilot-scale system against an extensive set of experimental data and the sensitivity of the plant for key operating parameters are investigated. The developed validated model of the amine-based CO_2 capture system is used to perform a techno-economic process design and/or scale-up of the amine-based CO_2 capture system for commercial-scale application to a natural gas fired combined cycle power plant with and without exhaust gas recirculation, in Chapter 7. Chapter 8 compares the performance of the systems studied in Chapter 7 with coal and biomass fired power plants, and the comparative potential of each system is assessed for integration with a CO_2 capture and compression system. Finally, in Chapter 9 the conclusion are drawn based on the research work presented in the thesis and recommendations are presented for the possible future research work.

Chapter 2
Review of Literature and Techniques

This chapter is focussed on a literature review regarding the gas turbine system and the CO_2 capture system. Further thermodynamics of the different systems which will be investigated and the modelling algorithm of the techniques adopted in this thesis are presented. In the first section, the gas turbines, with its different modifications are presented with a literature review of the respective modification. In addition, the thermodynamics are explained to have a better understanding of the process and to build the process model based on this background knowledge. In the second section of the chapter, the post combustion CO_2 capture (PCC) technology is evaluated with emphasis on reactive absorption and desorption using aqueous monoethanolamine as the solvent. Further, the thermodynamic background of the CO_2 capture system for the MEA-based system is elaborated. In the third section of the chapter, the general modelling strategy and its algorithm adopted in the present research work is presented.

2.1 Gas Turbine System

2.1.1 Historical Review

In 1867, the German Werner von Siemens, after discovering the operating principle of the electrodynamics, developed the first “dynamo” [50]. It is believed that the first gas turbine was developed by Barber in Great Britain and by Stolze in Berlin [50]. While the first successful attempt was by the French scientists Armengoud and Lemale in 1904 [50]. Giampaolo [51] gave the complete chronological development of the gas turbine through the ages from 130 BC, the reaction steam turbine principle by Hero of Alexandria to the first commercial axial compressor and turbine in 1938. The main theme of the research at that time was to shift from the accelerating pistons, cranks and rods of the diesel piston engines and from the boiler, condenser, water pumps, treatment sections of the bulky steam turbine plants,

towards the more stable and cleaner power production techniques [50]. In the present day, the gas turbine components efficiency have peaked at 85 to 90 %, with the pressure ratio 35:1 and turbine inlet temperature 1650 K [52, 53].

The gas turbine system burns fuel to run the turbines in order to generate electricity and this result in historical improvements in terms of the efficiency, operation, reliability and environmental performance of the overall system [54]. Global warming issues have led to the shift towards the low carbon or the clean carbon technologies which result in the smaller emissions of the greenhouse gases in to the atmosphere [55]. The natural gas fired turbine systems in comparison to the coal combustion processes has led to the control of the anthropogenic greenhouse gases. The prime objective is to develop an efficient and cost effective compressor and turbine units, low emission combustion systems and optimize the overall system in terms of the operability and control which results in more energy output from the gas turbine with an increased plant efficiency and decreased energy cost [48, 56, 57]. There are number of parameters and factors which effect the characteristic performance of the gas turbine for the prediction of the accurate behaviour of the gas turbine; the design and the operating conditions of the system can be properly diagnosed [55].

Massardo and Scialo [58] have studied a thermo-economic analysis of the gas turbine system and presented a cost analysis along with important thermodynamic parameters, such as efficiency, specific work, and pressure ratio. Jeong et al. [59] have performed an inverse performance analysis for the estimation of the characteristic performance of the gas turbine in comparison to the measured data available and concluded that the full operating performance of the gas turbine should be in hand for the user to run it precisely. Zhang et al. [60] have carried out a thermodynamic analysis of the gas turbine fired with different variations of the syn-gas and concluded that the heating value has a strong influence on the power generated from the gas turbine. The LNG fuelled combined cycle, with carbon dioxide as the working fluid in the Brayton cycle, have been investigated for a virtually zero emission system by Zhang et al. [61]. Chiaramonti et al. [62] have studied the emissions of CO and NO_x from liquid fuels, especially biodiesel and vegetable oil, in comparison to diesel when injected into the micro turbine and

measured the physical properties and estimated the combustion behaviour and emissions at the outlet

2.1.2 Distributed Power Generation

Distributed generation is the local generation of the electrical, thermal and mechanical energy at the consumer site [48]. Distributed power generation is the small scale modular power generation technology, either integrated or in stand-alone mode, near the end user [63]. The power market in different countries is now decentralised and various independent, distributed power generation producers have developed [64]. Distributed power generation systems have led to the advancement of small or micro power sources, including combined heat and power engines, fuel cells, reciprocating engines, and micro gas turbines, renewable systems including solar systems, wind turbines, biomass or bagasse gasifiers, waste cogeneration units and small hydro units [48, 63, 65, 66].

The distributed generation technologies are becoming more efficient and reliable as the transmission and distribution losses are reduced due to the generation of the power on-site near the load [67]. The distributed technologies are becoming more popular and utilize the waste heat recovery units and thermally active systems [67]. From the available distributed power generation resources, the micro gas turbine appears to be the most advanced and most easily adoptable for decentralised heat and power generation modes [65]. The trend of combined heat and power generation is increasing with the increase in efficiency and performance of different power generation techniques [48]. In spite of the potential benefits for the use of the mini-, and micro- gas turbines for distributed power generation, there are some technical and non-technical barriers which have reduced its growth through the market [48]. The factors, such as cost, efficiency, reliability operability, environmental emissions and safety concerns, need some improvements before the micro gas turbines may be fully adopted in the industrial and commercial sectors [48]. Micro gas turbines can be adopted for the any types of load operation, including peak load, part load, stand-alone, grid-connected, emergency and/or remote operation in either only the power generation mode or the combined heat and power generation mode [63, 68]. Micro gas turbines can also be connected with other technologies, such as fuel cells, wind turbines and PVs, for hybrid power generation [63].

2.1.3 Micro Gas Turbine

The micro gas turbine (MGT) is single stage; single shaft low pressure gas turbines either as a simple gas cycle, a recuperated one or a combined heat and power system. The micro gas turbines are the most efficient, highly reliable with low emissions power and heat generation system [48, 69]. The schematic of combined heat and power MGT is shown in Figure 2.1. MGT's can be operated in different operational modes, such as grid connected, stand-alone or dual mode with either base load, peak shaving or load following capabilities [63, 68]. The fuel capabilities for the MGT includes both gas and liquid fuels or bio gas with automatic switches between the different mode of operations [68].

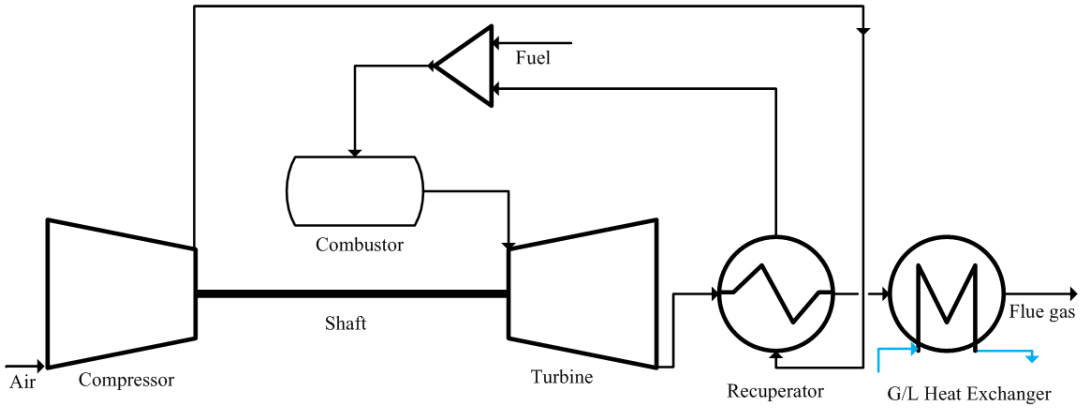

Figure 2.1 Schematic of the combined heat and power micro gas turbine.

MGT's came into the energy market between 1950 and 1970, replacing the trivial reciprocating piston engines. The first generation MGT's were used for generating electricity for buses, airplanes and other commercial transport means [25, 68]. With the advancement in the distributed energy technologies in the era of 1980 and 1990; the MGT's have become more popular in the stationary energy power generation system and in the mid 1990's with its reuse in the automobile sector in hybrid vehicles and also major car manufacturing companies started projects on the development of MGT's [25, 68]. Poullikkas [70] and Nascimento et al. [68] gave a comprehensive list of the turbine manufacturers with their rated power and efficiency. This thesis is focused on the MGT as it is a low emission, reliable and efficient combined heat and power generation system that competes with the combined heat and power reciprocating engines. Further, MGT is a good and accessible option for research purposes and the performance outcomes can provide recommendations for the commercial-scale gas turbines.

The gas turbines can be classified as either non-injected gas turbines or injected gas turbines. In the injected gas turbines, the injection might be of the exhaust gas, water, steam or any other fluid. The further classification of the non-injected and injected gas turbine is as follows:

i. Non-Injected gas turbines [70, 71].
    a. Gas to gas recuperated cycle.
    b. Brayton-Diesel cycle.
    c. Brayton-Stirling cycle.
    d. Chemical recuperated cycle.
    e. Combined cycle.
    f. Kalina cycle.
    g. Brayton-Fuel cell cycle.

ii. Injected gas turbines [70, 71].
    a. EGR cycle.
    b. STIG cycle.
    c. Wet compression cycle.
    d. Evaporation cycle.
    e. Cheng cycle.
    f. HAT cycle.
    g. LOTHECO/DRIASI cycle.

There is no standard range or scale to which the MGT can be defined and each researcher defines it in some arbitrary scale. The current set of available MGT's range is under 500 kW_e with an efficiency in the range of 25 to 30 %, maximum cycle temperature 800 to 1000 ^oC, and pressure ratio 3 to 5 [25, 48, 65, 68, 72]. Pilavachi et al. [48] have mentioned the benefits of the MGT system, especially in comparison to the reciprocation engines. The various features that MGT's offered include the variable speed, multi fuel capabilities, light weight, compact size per unit of the power generation, small number of moving parts, high grade waste heat, low friction and little balancing requirements, low maintenance requirements, low noise and environmental pollution [48, 68, 73]. The reduced emission level of carbon dioxide, oxides of sulphur and nitrogen for MGT combined heat and power generation, have developed greater potential for the MGT's in the market in the present scenario of reducing GHG emissions. The feasibility of the micro gas

turbines for the grid connected mode needs to be more frequent and part load condition operation needs further flexibility. The fuel flexibility options for the multi fuel burning in the MGT's need to be developed with time to have lower emissions from the system [49]. Pilavachi et al. [48] have shown different market potentials of the MGT, including paper and pulp, chemicals, food and brewages, textiles, mining, oil and gas; in different mode of operation, such as continuous combined heat and power generation, peak and emergency power production, and onsite and remote power production. The MGT's are now able to peep and spread into the energy market due to their flexible and cost effective operation [74]. The exhaust gas from the turbine takes much of the heat energy with itself and is wasted. In order to utilise this waste of the heat, the heat exchanger, known as the recuperator is installed to pre-heat the air going to the combustion section [66]. The waste heat after the recuperator can be used for heating, absorption refrigeration, air conditioning, or desalination and the selection of the perspective technique depends on the grade of the heat, efficiency, and the power factor [49]. Recuperated gas turbines offer unique characteristics for dealing with the part load performance and this is in contrast to the simple cycle analysis [65] and this will be discussed in Sections 2.1.3.2 and 2.1.3.3.

2.1.3.1 Micro Gas Turbine Performance

Miniaturisation has an influence on the performance of the gas turbine system and the scale down effect on the gas turbine to the MGT system level will affect its construction to seamless surfaces and will influence the characteristics of the MGT's [75, 76]. Kurt et al. [24] concluded that the modelling of the gas turbine systems results in important information which can be used for the analysis, design, control and optimization of the system. The MGT performance parameters include engine inlet temperature, compressor discharge temperature and pressure, fuel and air flow rates, turbine exit temperature, and exhaust gas temperature; while the component characteristic parameters which will assist the analysis of the performance include the parameters such as the turbine inlet temperature, compressor and turbine efficiency, recuperator effectiveness, and electrical and thermal efficiency [65]. The performance criteria will assist to keep the behaviour of the system at or close to the peak level [24]. The turbine inlet temperature and the pressure ratio are the two key important factors which effect the net power output and the efficiency of the gas turbine and the other considerations which needs attention include better component

design, more efficient combustion techniques and high temperatures with-standing materials [64]. The highest temperature in the cycle is dictated by the material to be used in the gas turbine [24]. An increase in the component efficiencies of the turbine and compressor results in an increase in the net power output with a decrease in the specific fuel consumption and an increase in the overall efficiency [57]. The increase in the compressor efficiency decreases the work of the compression and increases the work of the expansion and improves the performance of the cycle.

Geographical regions with high ambient temperature results in an increase in the specific air consumption and this causes more compressor work with a reduced net power output from the cycle and thus the efficiency decreases [57, 77]. The ambient temperature effect increases the net power output in the winter and decreases it in the summer [24]. De Sa et al. [78] have developed a direct connection between the ambient temperature and the decrease of the gas turbine output and concluded with a relationship that "with every K rise in the ambient condition the gas turbine loses 0.1 % efficiency and 1.47 MW of the gross power generated". The inlet air can be cooled by different systems, including evaporative media coolers, saturated systems, sprayers/fogging systems, over spray systems, and mechanical vapour compression/absorption chillers [64, 78, 79]. However, care must be taken for the inlet temperature adjustment by adopting the evaporative coolers or chillers in order to avoid the condensation or the carry away of the water as this affects the performance of the compressor [70]. The saturated air or the media cooler can increase the humidity levels of the air and this result in an increase in the power and efficiency of the system. Further, this assists in the reduction of the NO_x emissions from the gas turbine [64]. The turbine inlet temperature is limited and not increased as the hot section cooling is not feasible in the case of the MGT's.

The thermal efficiency and a net power output increases as the turbine inlet temperature and pressure ratio increases, but with a decrease in the ambient temperature [24, 78]. The specific fuel consumption decreases with increasing the compressor inlet temperature and the pressure ratio, while it increases with an increase in the turbine inlet temperature [24]. However, the recuperator effectiveness is quite insensitive with respect to the variation of the turbine inlet temperature and the turbine efficiency, while the recuperator effectiveness increases with the power reduction due to the decrease in the mass flow rate through the heat exchanger [56,

65]. The increase in the pressure ratio of the compressor results in a temperature rise in the compressed air and this decreases the exhaust gas temperature [71].

2.1.3.2 Part Load Operation

Various options which exist for the part load operation including variable speed, variable inlet guide vane/variable area nozzle and fuel control operations. Maintaining the high turbine outlet temperature results in the enhancement of the part load efficiency as the temperature of the recuperator gas inlet increases [56]. The fuel control option reduces the recuperator effect, which in turn results in a decrease in the efficiency of the system, while a variable speed causes a greater difference between the turbine exhaust temperature and the exhaust gas temperature and this results in an excessive heat extraction at the recuperator and thus an efficiency enhancement [56].

The exhaust gas recirculation not only increases the efficiency and performance at the part load operation but also it enhances the dynamic response of the system, and consequently reduces the NO_x formation in the combustor [80]. By lowering the power level for the open or combined cycle gas turbine systems; efficiency decreases and in order to maintain it at the same level for reduced power level than, the peak cycle temperature or the pressure ratio, or both, needs to be reduced [80]. It has been established that the presence of the combustion products in the air will limit the peak temperature by varying oxygen concentration in the oxidant stream and will also retard the formation of the nitrous oxides in the combustor exhaust [80].

2.1.3.3 Recuperator Impact

The recuperator is not just a matrix type heat exchanger, it may be a surface type heat exchanger for a stationary type gas turbine application for both a low pressure ratio and a low turbine inlet temperature MGT system [56]. The conventional stainless steel recuperator can be replaced with inconel or ceramics for high temperature turbine exhaust gas stream operations [48]. The barriers for the advancement of the recuperator, other than lower efficiency, are higher cost, maintenance issues, material temperature restrictions, fouling and corrosion caused by the exhaust gases of the combustion chamber [49]. The recuperator requires a smooth variation of the turbine exhaust temperature during transient conditions in

order to avoid the thermal metal stress in the recuperator [74]. The important characteristics for the recuperator to be fitted in the micro gas turbine with higher field acceptance should be the compact size, light weight, low cost, higher effectiveness, high reliability, low maintenance, structural integrity and be adoptable for massive auto production with the minimum number of parts and be easily fabricated [73]. Ferrari et al. [81, 82] have performed steady state and dynamic performance studies on the recuperated Turbec T100 MGT in electrical grid connected and standalone configurations and studied the effects on the effectiveness of the recuperator. Kesseli et al. [83] have provided a comprehensive design guide for gas turbine engineers for the conversion of the simple gas turbine cycle to the recuperated one based on the effectiveness, pressure drop and cost.

2.1.4 Water/Steam Injected Gas Turbines

At the beginning of the 20^{th} century, materials were not able to withstand the high temperature of the combustion gases and the cooling of the combustor through different means had to be adapted by including the water or steam injection in the gas turbines [64]. In the first gas turbine, the compressor was cooled by the injected water and the combustor was cooled by a jacket around the combustor with the water flowing in it and the evaporated water from the jacket was injected into the combustor [64]. According to Jonson and Yan [64], different humidified gas turbines cycle systems include the direct water injected cycles, the evaporative cycles and the steam injected cycles. The schematic of the micro gas turbine with an auto generated steam injection is shown in Figure 2.2.

The humidified gas turbine offers several advantages, such as high efficiency, more net power output, reduced specific fuel consumption, increased control on the NO_x emissions from the combustor, reduced cost per unit of power produced, and increased part load performance characteristics [64]. The exhaust heat of the gas turbine cycle can be utilised to generate the steam which can then be used in the bottoming Rankine cycle, or it can be injected into the combustion chamber or to humidify the compressed air [70]. Water/steam injection results in an increased mass flow with an increased specific heat content through the turbine [70, 71]. Thus, the water/steam injection results in an increased net power output as the work for the compressor remains the same and the amount of the fluid expanding through the turbine increases [71, 84]. Humidifying the combustion chamber with water replaces

the compressed air used for the combustor cooling and uses the energy of the combustion gases for the water evaporation [64, 85]. In the 1990s, the water injection appears to be the most efficient technique for the control of the NO_x emissions with the additional advantage in the increase of the net power output [64]. In the late 1990s, the dry low NO_x burners were introduced with lean combustion systems in order to reduce the NO_x formation [64]. The water injection decreases the equilibrium temperature of the combustion and thus decreases the NO_x emissions while the steam reduces the presence of the oxygen molecules and increases the concentration of the OH atoms which reduces the NO_x emissions. However, the use of the water results in an increase in the operational cost of the gas turbine with the additional drawbacks of corrosion, erosion and instability of the combustion with CO and unburned hydrocarbon (UHC) emissions [64].

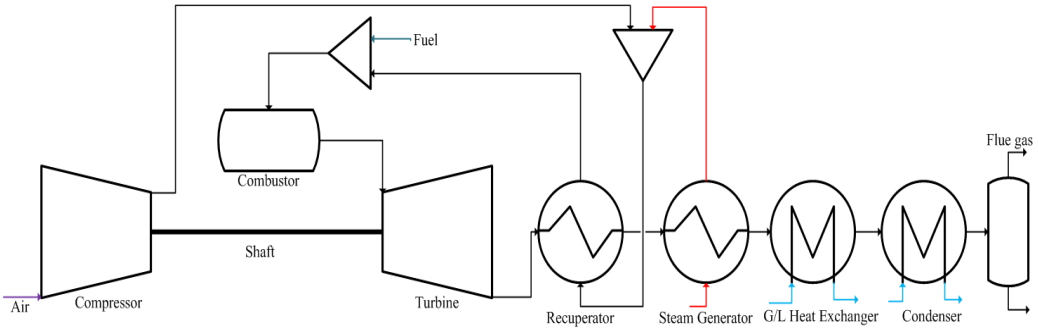

Figure 2.2 Schematic of the micro gas turbine with an auto generated steam injection.

The direct water injection into the fast moving high pressure stream of air results in the flashing of the hot water and it almost saturates the air [64]. The injection of the water at the air inlet of the compressor results in the humid/saturated air depending on the conditions or the wet compression which is initially adapted for the compressor blade cleaning during the technology development and these injections are limited by the saturation limit of the inlet air and the irreversibilities related to the air-water mixture [64, 84]. The water/steam can be injected into the compressed air after the compressor in the recuperator and there demonstration plants can be found in the literature [64, 84, 85].

Steam injection systems work if the steam pressure is higher than the compressor exit pressure and it should be in the superheated state [71]. The major concern for the water or steam injection system includes the loss of the water from the system and this can be in the form of vapour plumes, the cost incurred on the water

purification, and the cost for the steam raising [70, 71]. Humidified working fluids result in a less density system and this result in an increase in the gas turbine cycle efficiency [70]. Steam injection results in lower thermal efficiency when steam is auto generated from the exhaust of the gas turbine, with more CO and UHC emissions [49]. However, the auto generation of the steam from the exhaust gas of the gas turbine is limited by the pinch point limitation of the steam generator and quality of the waste heat available at the downstream of the gas turbine. Since the steam generator works at constant temperature and this is due to low quality of the heat available in the flue gas and it cannot be properly extracted due to isothermal boiling.

2.1.5 Humid Air Turbines

As stated in Section 2.1.4, the steam generation and injection is limited due to the pinch point for auto steam generation, however, the problems concerning the steam generation can be solved by modifying the cycle to the evaporation one which results in the injection of the water at different saturation temperatures [70, 71]. The pinch point limitation of the boiler, plus the problem of not utilizing the low grade heat to evaporate the water, limits the steam injection process in comparison to the humidification tower in which the air is saturated with water and the process of the humidification is the non-isothermal in comparison to the isothermal boiling [64]. In the humidification tower, there is direct contact between the hot air and the water over the packing or trays and as a result of the simultaneous heat and mass transfer, the hot saturated humid air leaves the top section of the column [64]. The heat of compression and the exhaust gas through the turbine is sufficient to evaporate the water and subsequently it can be injected into the cycle [70, 71]. The schematic of the humid air turbine cycle for the micro gas turbine is shown in Figure 2.3. Poullikkas [70] has given a comprehensive classification of the advanced cycle gas turbines, including steam injected gas turbines and/or humid air turbines, and the basis of the classification was either the steam is mixed with the working fluid or it is not. The humid air turbine (HAT) cycle is the advanced evaporative gas turbine cycle developed from the evaporative regenerative cycle and it increases the cycle power output and efficiency [70].

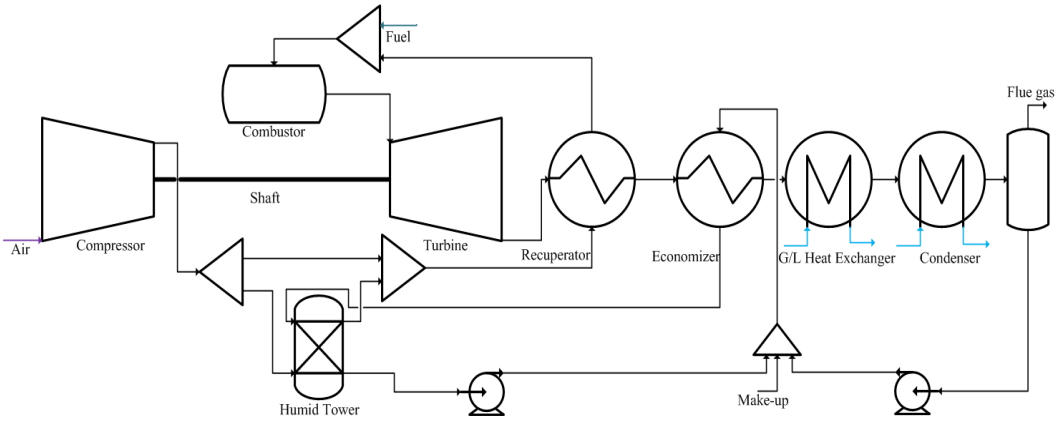

Figure 2.3 Schematic of the micro gas turbine with a humidification system.

The saturator of the HAT cycle, either the plate or the packing type column, can be used to saturate the air with water in a step wise manner as air moves up the column and the mode of contact may be either counter current or co current between air and water [70]. A varying amount of water may set the cycle into the part load operation without effecting the efficiency of the cycle and it shows a good part load performance characteristic as compared to simple gas turbine systems [70]. The humidification of the gas turbine results in a flow mismatch in the cycle as a result of the increased flow rate through the turbine as compared to the compressor unit [71]. The HAT cycle has a significant advantages, in terms of higher thermal efficiency and low NO_x emissions, with the benefit of the water recycle by the condensation of the water through the exhaust and forwarding the CO_2 rich stream to the CO_2 capture system for the purification [86]. The humidified air turbines are versatile, flexible and capable of meeting high ambient temperature performance characteristics by changing the water addition and getting the adjusted outputs in the distribution power generation systems with the additional benefit of a CO_2 capture ready system [64]. The HAT's are advanced further through cascaded systems, compressed air storage systems for off-peak power load management, HAT's with topping or bottoming cycles for cogeneration of power and heat, and the fuel modifications to the gas turbines [64]. For higher pressure ratios, the evaporative gas turbines show a superior performance as compared to the steam injected gas turbines, while at lower pressure ratios it is vice versa [64].

The evaporative MGT can be traced in the literature [87, 88]. The evaporative MGT result in the augmentation of the power and the specific work [87] and show better thermo-economic analysis as compared to the conventional dry MGT's [88]. The

humidification results in the enhancement of the CO_2 concentration in the exhaust gas and it will reduce the cost of the PCC technology [64]. In order to minimize the effect of the high ambient temperature, the water or steam can be injected in to the gas turbine system [77]. Water or steam injection can be incorporated to provide seasonal demand loads of the distributed generation and at part load conditions, water or steam injection leads to a higher power generation efficiency [77]. In MGT systems, the water or steam injection theoretical studies can be traced in the literature while the technological aspects of the water or steam injection needs to be studied or further investigated [77]. The exhaust gas temperature after the recuperator is mostly low, and the steam generation is not viable as compared to the hot water generation which can be injected at the inlet of either the recuperator or the combustor [77]. The injection of the water at the inlet of either the recuperator or the combustor have different thermodynamic effects on the system as the water injection at the recuperator inlet vaporizes as a result of the interaction with the hot side and utilizes the thermal energy while the injection of the water at the combustor inlet penalizes the efficiency of the MGT system [77, 84].

2.1.6 Exhaust Gas Recirculation

Exhaust gas recirculation (EGR) is an innovative mode of gas turbine operation in which the exhaust gas is split: one part being emitted while the other part is dried before being recirculated to the gas turbine inlet. The benefits of EGR are a decreased flow rate with higher concentration of CO_2 in the exhaust gas, which results in a decreased energy penalty when integrated with a CO_2 capture system. The schematic of the exhaust gas recirculation for the micro gas turbine can be found in Figure 2.4. In EGR, the part of the exhaust gas is recirculated back to the system and it is first investigated and proposed by Earnest [80] for a combined cycle system. EGR results in the enhancement of the CO_2 concentration in the exhaust gas of the turbine with reduced flow rate and if it is integrated with PCC technology that it will result in benefit due to the lower energy requirements of the PCC technology. However, the application of the EGR results in combustion issues in terms of flame instability, CO and UHC emissions due to the changing fluid nature of the oxidant stream. However, the literature recommends minimum oxygen concentration to be present in the oxidant stream after EGR to avoid these issues [89-92]. Further, Cameretti et al. [93-96] have reported a CFD analysis of the combustor when EGR

is applied to the MGT and the impact of different fuels on the performance of the MGT through CFD analysis.

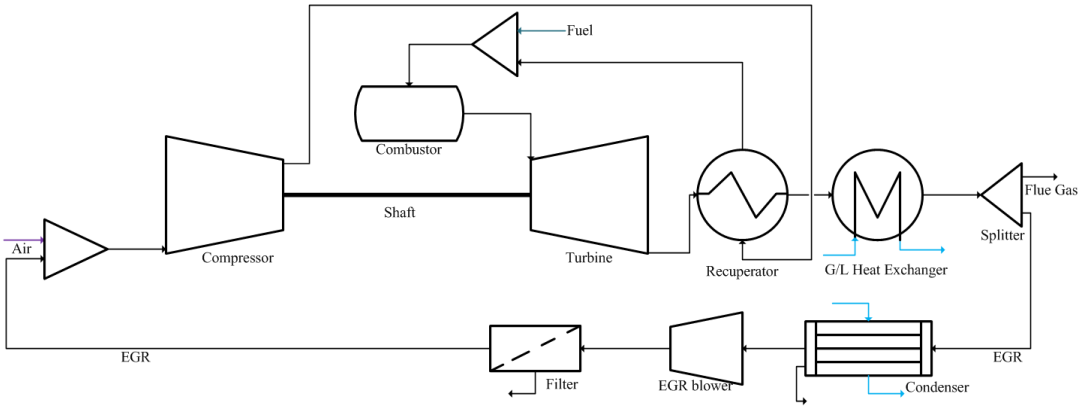

Figure 2.4 Schematic of micro gas turbine with exhaust gas recirculation

The mild or flameless combustion can be one of the opportunities through which the NO_x release through the micro gas turbine can be reduced by employing the EGR for diluting the oxygen in the inlet air [93, 94]. An abridged definition of the mild combustion culled from Cavaliere and Joannon [97] where more details can be referred, is given as follows:

> *"A combustion process is named Mild when the inlet temperature of the reactant mixture is higher than mixture self-ignition temperature whereas the maximum allowable temperature increase with respect to inlet temperature during combustion is lower than mixture self-ignition temperature (in Kelvin)".*

The EGR on one side decreases the temperature of the combustion section and on the other side dilutes the oxidant stream. This results in the minimization of the thermal NO_x formation mechanism [93, 94]. The part load operation may lead to an increase in the NO_x formation due to the increase in supply of the fuel, to maintain the stable flame [94]. The exhaust gas recuperation, along with its recirculation to the compressor inlet, results in a near zero emission cycle [94, 98]. The flameless combustion offers significant losses in the NO_x emissions from the MGT system with added benefit of EGR. The main component in the NO_x emissions is the thermal NO and this can be controlled by either reducing the combustion temperature, or by reducing the residence time in the combustor [98]. The EGR, and the use of the recuperator, results in the reduction of the NO_x emission from the

MGT system and this leads the combustion into the mild or flameless region due to the increase in the equivalence ratio [95]. The EGR results in a reduced flow towards the heat extraction unit and this is counter balanced by the pollution control capacity of the EGR [95].

However, most of the literature reports EGR percentages below 50 %, however, there is potential to increase the EGR percentage beyond 50 % since the oxygen concentration at the combustor inlet is higher than the minimum oxygen concentration. In the literature, the injection of the EGR location into the gas turbine is assumed to be the compressor inlet. However, there are some other potential locations, such as compressor discharge location and combustor inlet location, which needs to be investigated and optimized. Further, the operating conditions of the EGR stream also needs optimization as the temperature and water content in the EGR stream affects the performance of the compressor and gas turbine as a whole.

2.1.6.1 Literature Review of Exhaust Gas Recirculation

Sipocz and Assadi [99] integrated a post-combustion CO_2 capture plant with a 400 MW combined cycle at 40 % EGR with a focus on the methods to reduce the reboiler duty by the steam extraction, and by using an external biomass fired boiler. Jonshagen et al. [100] developed an IPSE Pro model for the 300 MW GE 109 FB, combined cycle at 40 % EGR and studied the effect of the EGR on the isentropic exponent and gas constant, resulting in 8 % CO_2 in the outlet with a focus on the effect on the heat flux diagrams for the HRSG with different alterations for integration with the CO_2 capture system. Studies have also included the effect of the EGR on the performance of the post-combustion CO_2 capture plant. A common conclusion may be drawn from the reported literature [101-105] that the EGR may enhance the performance of the gas turbine when integrated with a carbon capture system. Based on techno-economic analyses, EGR may offer an opportunity to reduce cost and offer economic benefits for the CO_2 capture system [101, 106-108]. For commercial scale gas turbines, the effect of the EGR on the NGCC power plant is quantified by Canepa et al. [103] and Li et al. [105] while economic evaluation has been performed by Biliyok et al. [101] and Canepa & Wang [107].

Most of the literature pertains to commercial-scale combined cycle systems with an exhaust gas that already has higher CO_2 content than in the MGT. However, the CO_2

concentration in the exhaust gas of the MGT is much lower, it ranges from 1.5 to 1.8 mol% while the commercial-scale natural gas-fired turbines have CO_2 concentrations in the range 3.8 to 4.4 mol% [103-105, 108]. For MGT with EGR, the literature reports only 40 % and 50 % EGR ratios [109, 110]. They have compared the EGR and HAT cycle and studied the effect of the ambient temperature on the system performance. Cameretti et al. [93, 96] studied the effect of the EGR on the performance of the MGT for different types of fuels and the reduction of NO_x through CFD modelling of the MGT. It is important to note that some work on the effect of the EGR on the performance and a sensitivity analysis of the ambient temperature for the MGT with EGR have been reported in the literature [109-111].

2.2 Thermodynamics of the Gas Turbine

From the number of widely adopted means of producing power, such as hydro systems and coal power plants, the most efficient means of producing power is the gas turbine. The steam power plants are bulkiest; however, if the moving fluid steam is replaced by hot gas to expand through the turbine, then the steam cycle resembles that of the gas turbine cycle. Scientists and researchers started thinking about shaft generated power in comparison to piston engines and the gas turbine industry has progressed swiftly with varying numbers of applications [53]. For the expansion of the gas through the turbine, the fluid gas must have sufficient pressure to move the turbine and drive the shaft that is coupled to it. If the compressed air directly goes into the turbine then the power generated by the turbine is consumed by the compressor and the net power result is zero. The power produced by the turbine can be enhanced if the expanding gas has more energy and the system results in a net power output which is able to be extracted for use.

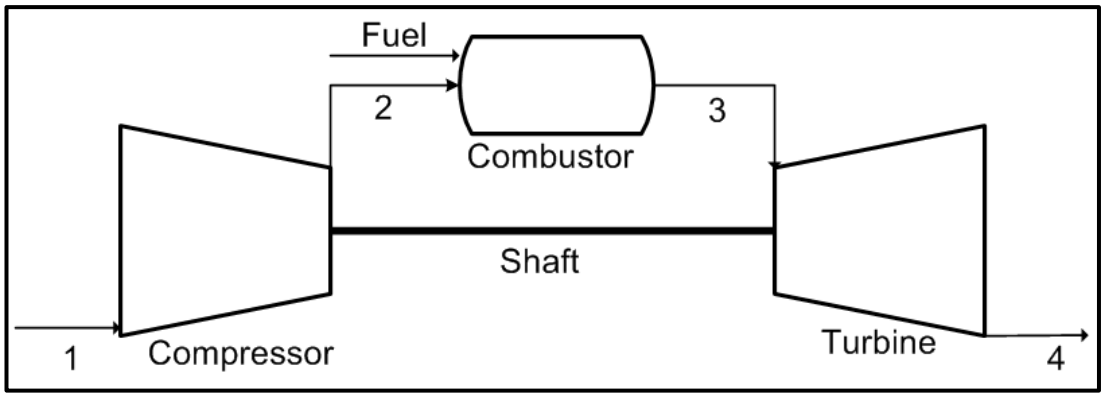

Figure 2.5 Schematic of the simple gas turbine.

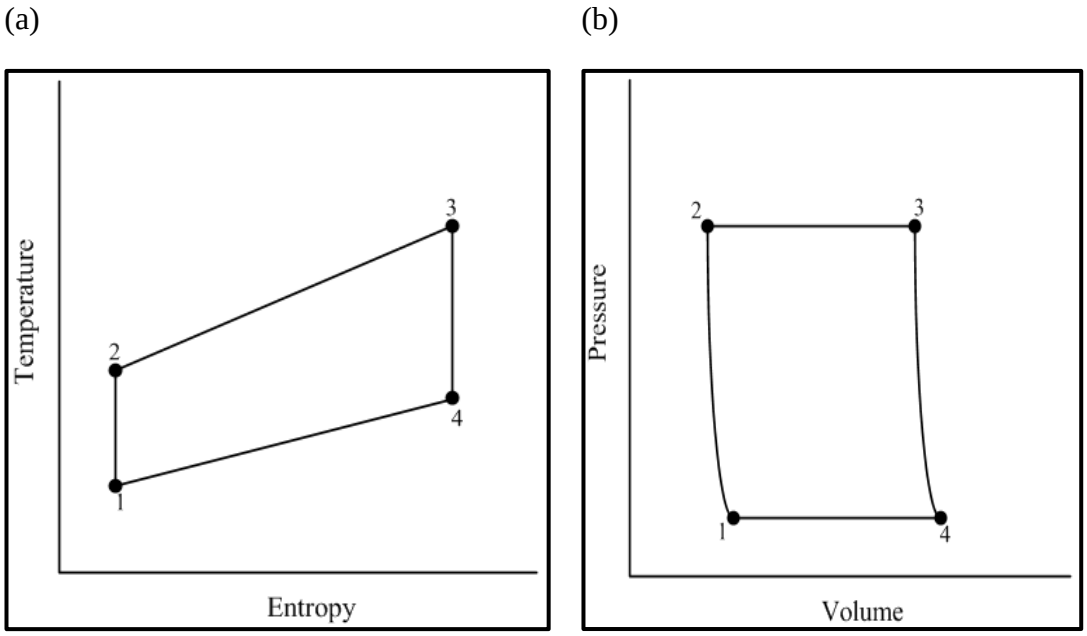

Figure 2.6 Thermodynamic diagrams of the simple gas turbine (a) TS diagram; and (b) PV diagram.

The preferable means of providing the energy is to perform the combustion of the fuel in the combustion chamber with the compressed air and then the expansion of the hot working fluid results in the net power output. This forms the simplest arrangement of the gas turbine, as shown in Figure 2.5. There are loses which occur, both in the compressor and in the turbine which increases the power absorbed by the compressor and reduces the power output of the turbine. Also there is a limit to which the fuel can be added to the combustion section of the turbine and this defines the net power output of that particular system [53]. The historical development of the gas turbine, in general, and the micro gas turbine, in particular, are explored in Sections 2.1.1 and 2.1.3, respectively. The important factors which dictate the performance of the gas turbine cycle are the component efficiencies and the maximum temperatures to which the materials of the turbine can withstand. The higher the temperature of the combustion gases for the expansion in the turbine, the higher is the efficiency of the cycle and thus the higher will be the net power output of the cycle. The limiting temperature is determined by the metallurgical limits of the materials of construction of the turbine blades. The thermodynamics of the gas turbine is based on the Ideal Brayton (or Joule) cycle which assumes a closed cycle with air acting as the working fluid. The working fluid is compressed in the compressor, then heat is added in the combustor, in the next step expansion occurs

in the turbine and finally the heat is rejected to the atmosphere and the working fluid traces back in the compressor for compression.

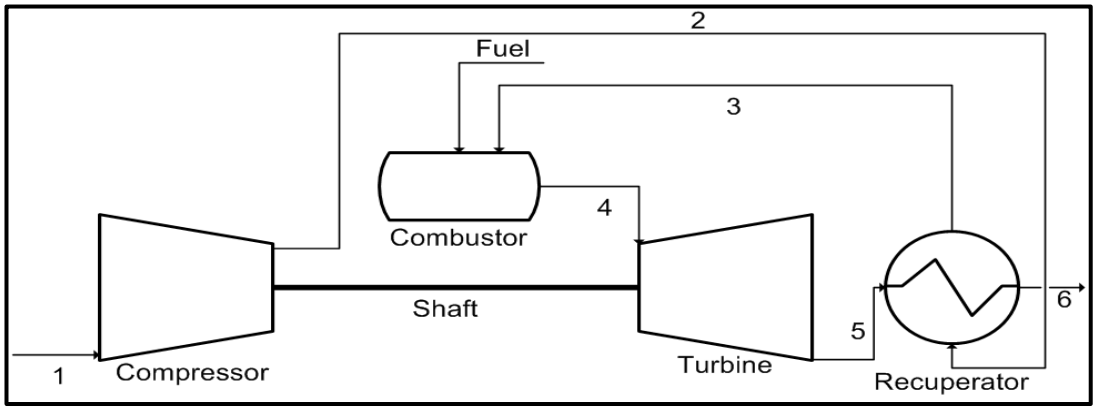

Figure 2.7 Schematic of a recuperated gas turbine.

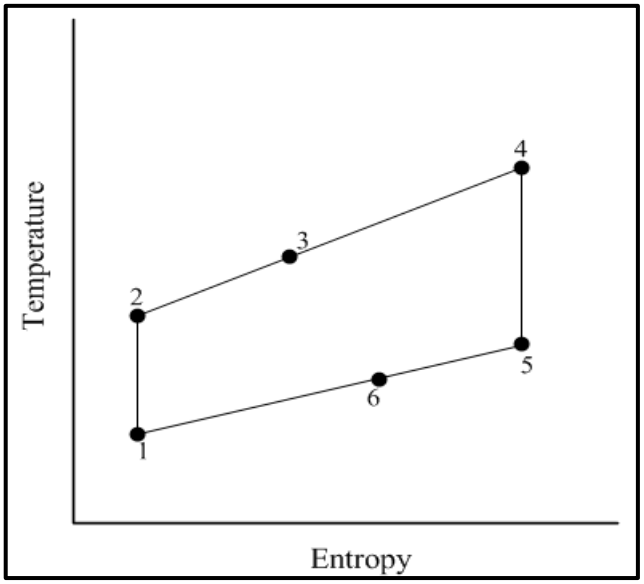

Figure 2.8 TS diagram schematic of a recuperated gas turbine.

The ideal Brayton cycle consists of four steady state steps, including two isentropic steps and two constant pressure steps. The thermodynamically Brayton cycle consists of the isentropic compression of the air from step 1 to step 2, the heat addition to the air at constant pressure in the combustor from step 2 to 3, the isentropic expansion in the turbine from step 3 to 4, and the heat rejection at constant pressure from step 4 to back step 1 and this completes the cycle. These steps are schematically shown in Figure 2.5, and Figure 2.6 (a) and (b). Various options exist through which the efficiency of the cycle can be enhanced, such as through the intercooling between the compressor stages, reheating between the turbine stages, heat extraction through the exhaust gas to preheat the combustion air,

cogeneration, etc. This resulted in increased complexity, weight and cost of the gas turbine system.

2.2.1 Gas Turbine with Recuperator

In a simple gas turbine, the exhaust gas from the turbine is at a sufficiently higher temperature and is wasted to the atmosphere, while this temperature is sufficient to raise the temperature of the compressed air before entering the combustor in order to reduce the specific fuel consumption.

This is usually done by employing a heat exchanger, termed the recuperator/regenerator in order to preheat the compressor air from the hot exhaust of the turbine. The operation of the regenerator is at a constant pressure in an ideal state. The gas turbine with a regenerator results in an increase in the efficiency of the cycle, while the specific work output remains unchanged by the addition of the heat exchanger. A brief description of the recuperator has been already given in Section 2.1.3.3. Further, the components of the recuperated gas turbine are shown in Figure 2.7 and the T-S diagram of the respective recuperated gas turbine is depicted in Figure 2.8.

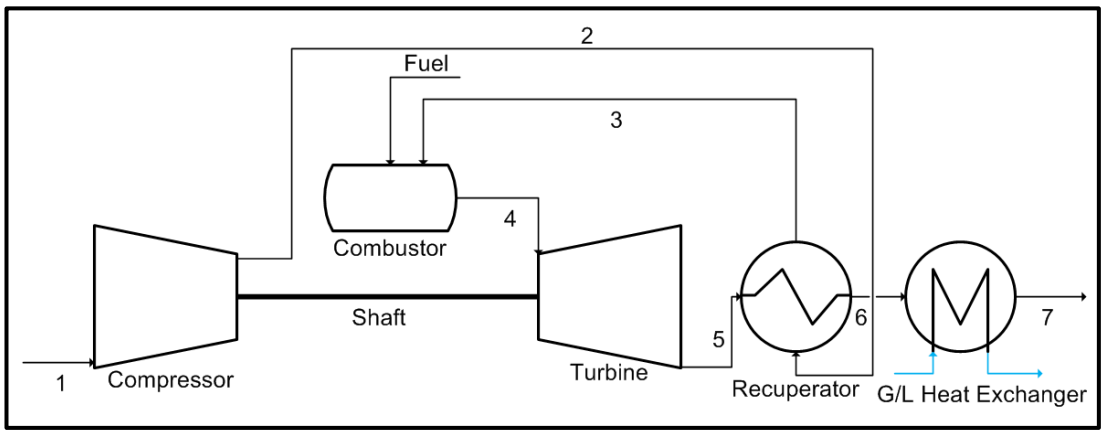

Figure 2.9 Schematic of a cogeneration cycle.

2.2.2 Cogeneration Cycle

The gas turbine exhaust has sufficient energy from which heat can be extracted and used as a means of producing steam or as a heat source for the heating and chilling requirements. The maximum amount of the extractable energy depends on the dew point of the sulphur compounds in order to reduce the corrosion problems as condensed sulphur compounds are acidic in nature and will promote the corrosion in

the heat extractors and exhaust ducts [52, 53]. The steam can be used to run the bottom Rankine cycle, thus generating more electrical power in which a heat recovery steam generator (HRSG) is mostly installed for the generation of the steam.

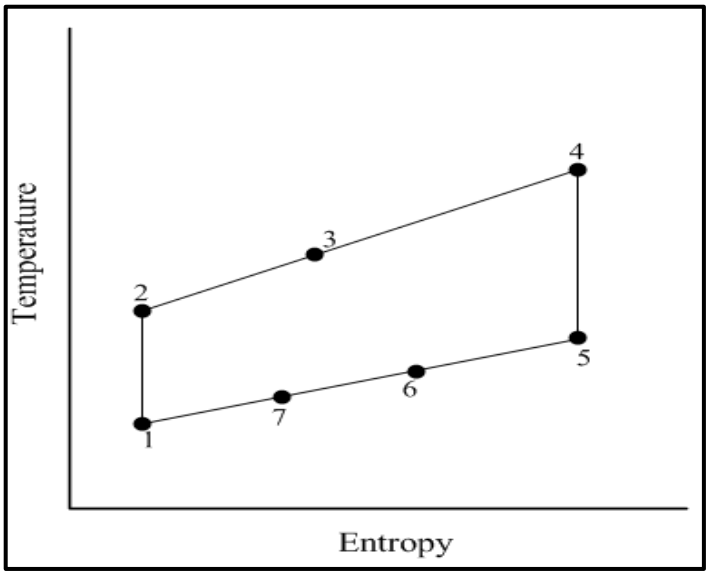

Figure 2.10 TS diagram schematic of a cogeneration cycle.

The extracted heat energy can be utilised for the heating, or the absorption chiller requirements at industrial, residential and commercial sites. These cycles are also known as combined cycles for the bottoming Rankine cycle and/or the combined heat and power (CHP) cycle for the heat extraction systems. A schematic of the combined heat and power cycle is shown in Figure 2.9 and its TS diagram is shown in Figure 2.10.

2.3 Thermodynamic Analysis of Simple Gas Turbine

According to the First Law of Thermodynamics, or the Law of Conservation of Energy, the energy can be converted from one form to another while the total amount of energy always remains the same. The steady state ideal analysis of the gas turbine will help in the prediction of the performance of the components and the complete system of the gas turbine. In this analysis, the working fluid is supposed to be the air having uniform properties and the analysis is with respect to the Figure 2.5 notations. The steady state energy balance is given by [53]:

$$Q = (H_2 - H_1) + \frac{1}{2}(u_2^2 - u_1^1) + W \qquad (2.1)$$

where Q and W are the amount of energy transfer in terms of heat and work, H is the enthalpy, u is the velocity. The subscript "1" indicates the compressor inlet location and "2" indicates the compressor outlet location of Figure 2.5. The component analysis of the simple gas turbine yields the characteristics of each of the component as follows:

$$W_{12} = -(H_2 - H_1) = -c_p(T_2 - T_1) \tag{2.2}$$

$$Q_{23} = H_3 - H_2 = c_p(T_3 - T_2) \tag{2.3}$$

$$W_{34} = H_3 - H_4 = c_p(T_3 - T_4) \tag{2.4}$$

The efficiency of the system can be defined as the ratio of the output to the input. Since in our case the power is the output and the heat added in the combustor is the input, so the efficiency of the cycle is given by [52]:

$$\eta = \frac{\text{net power output}}{\text{heat added}} = \frac{W_{34} - W_{12}}{Q_{23}} = \frac{c_p(T_3 - T_4) - c_p(T_2 - T_1)}{c_p(T_3 - T_2)} \tag{2.5}$$

where η is the efficiency, c_p is the heat capacity at constant pressure, T is the temperature and P is the pressure. The subscript "3" indicates the combustor outlet location and subscript "4" indicates the turbine outlet location of Figure 2.5. The isentropic relation, in terms of P and T will assist in reducing the equation (2.5) [112] and through the definition of the pressure ratio for the compressor or the turbine [113]. By using the following relation:

$$\frac{T_2}{T_1} = \frac{T_3}{T_4} = \left(\frac{P_2}{P_1}\right)^{\frac{\gamma-1}{\gamma}} \tag{2.6}$$

$$r = \frac{P_2}{P_1} = \frac{P_3}{P_4} \tag{2.7}$$

$$\text{i.e., } \frac{T_2}{T_1} = \frac{T_3}{T_4} = (r)^{\frac{\gamma-1}{\gamma}} \tag{2.8}$$

where r is the pressure ratio and $\gamma = \frac{c_p}{c_v}$, is the isentropic coefficient, a property of the gas and it is defined as the ratio of the specific heat at constant pressure to the specific heat at constant volume. So the cycle efficiency is given by,

$$\eta = \left(1 - \frac{1}{r}\right)^{\frac{\gamma-1}{\gamma}} \quad (2.9)$$

The specific power output of the cycle will be,

$$W = W_{34} - W_{12} = c_p(T_3 - T_4) - c_p(T_2 - T_1) \quad (2.10)$$

$$\frac{W}{c_p T_1} = \alpha\left(1 - \left(\frac{1}{r}\right)^{\frac{\gamma-1}{\gamma}}\right) - \left(r^{\frac{\gamma-1}{\gamma}} - 1\right) \quad (2.11)$$

where $\alpha = \frac{T_3}{T_1}$ is the ratio of the maximum cycle temperature to the minimum cycle temperature, where T_3 is the maximum temperature and it depends on the material characteristics and the T_1 is mostly the ambient temperature as the air suction is open to atmosphere.

The equation (2.9) shows that the efficiency of the simple turbine cycle and it depends on the pressure ratio and the nature of the gas. As the value of γ increases, by changing the nature of the gas due to the combustion reaction which results in the change of the composition of the working fluid during the cycle, then the efficiency of the cycle increases. In the same manner, with an increase in the pressure ratio of the cycle, the efficiency of the simple gas turbine cycle increases. In equation (2.11), the specific power output is presented in non-dimensional form, for convenience in its interpretation, while it is evident that the specific power output is a function of the r, α and γ. Further, the specific power output increases with an increase in the pressure ratio and the value of α which is dictated by the metallurgical limits.

2.3.1 Thermodynamic Analysis of the Recuperated Gas Turbine

The recuperated gas turbine is characterised by the addition of the heat exchanger for the preheating of the air before the combustor in order to reduce the specific fuel consumption. However, the specific power output remains the same by the addition of the recuperator. The efficiency of the recuperated gas turbine cycle is given by [52, 53]:

$$\eta = \frac{c_p(T_4 - T_5) - c_p(T_2 - T_1)}{c_p(T_4 - T_3)} \quad (2.12)$$

where T_3 is the temperature of the air at the outlet of the recuperator, as shown in Figure 2.7. The subscript "3" indicates the air-side outlet location of the recuperator,

"4" indicates the combustor outlet location and "5" indicates the turbine outlet location. For the ideal heat transfer in the recuperator, it can be assumed that $T_5 = T_3$ and also, on using the PT isentropic relations, the efficiency of the recuperated gas turbine is given by:

$$\eta = 1 - \frac{r^{\frac{\gamma-1}{\gamma}}}{\alpha} \tag{2.13}$$

This expression indicates that the efficiency of the recuperated gas turbine cycle is not independent of the temperature ratio, α. Further, the efficiency of the recuperated gas turbine cycle increases with a decrease in the pressure ratio and this is in contrast to the simple gas turbine cycle, mainly the efficiency of the recuperated gas turbine cycle increases with an increase in the maximum temperature of the gas turbine. The equation (2.12) reduces to the ideal Carnot efficiency equation, $\eta = 1 - \frac{1}{\alpha}$, when the pressure ratio reaches the limiting value of r = 1 and shows the dependence of the efficiency at the maximum and the minimum temperature for the heat reception and the heat rejection points, respectively [53]. For the considerable improvement in the efficiency of the recuperated gas turbine cycle, the value of the pressure ratio is appreciably less than the optimum for the maximum power output will suffice as it is not necessary to use the maximum pressure ratio as the temperature ratio, α is increased [51]. Therefore, the trade-off between the maximum cycle temperature increasing and the pressure ratio decreasing gives a better performance of the recuperated gas turbine cycle.

2.3.1.1 Recuperator Effectiveness

The simple energy balance across the recuperator heat exchanger, as shown in the Figure 2.8, is given by:

$$Q_{56} = Q_{23} \tag{2.14}$$

$$c_{p_{56}} (T_5 - T_6) = c_{p_{23}} (T_3 - T_2) \tag{2.15}$$

where the subscript "6" indicates the gas-side outlet location of the recuperator. For the ideal system, with the approach temperatures such as T_5 approaching T_4, and also the mean specific heat of the air over the two different temperature ranges either

the air side or the flue gas side is similar [53]. So the effectiveness, ε of the heat exchanger is defined as follows:

$$\varepsilon = \frac{T_3 - T_2}{T_5 - T_2} = \frac{T_{air\_out} - T_{air\_in}}{T_{gas\_in} - T_{air\_in}} \quad (2.16)$$

The effectiveness, ε is not limited to the recuperator, it can be applied to any type of heat exchanger, such as the regenerator, HRSG, etc. This effectiveness is also known as the thermal ratio, or the efficiency of the heat exchanger. The modern heat exchangers are mostly designed with the effectiveness of, or above, 0.9. It must be kept in mind that the specific heat vales $c_{p_{56}}$ and $c_{p_{23}}$ are not approximately constant and similar either on the air side or on the flue gas side but cannot be cancelled with one another, as one is for the combustion air and the other is for the combustor flue gas.

2.3.2 Thermodynamic Analysis of a Real Cycle

In a real cycle, the actual fluid flowing through an expander is the combustion products and the fluid exit into the atmosphere rather than tracing it back to the compressor inlet. Therefore, the real gas turbine cycle is the 'open' cycle rather than the 'closed' cycle and the composition of the working fluid changes during its movement through the cycle due to the combustion reaction in the combustor. There is friction in the movement of the fluid and this causes a pressure drop in the combustor, heat exchangers, inlet, outlet ducts and nozzles. The compression and expansion processes are irreversibly adiabatic and therefore this result in an increase in the entropy and more compression work is required to overcome the fluid friction. The heat exchanger should be of an economic size and the terminal temperature differences are inevitable as the temperature of the air cannot approach that of the exhaust gas that leaves the turbine. The specific heat at constant pressure (cp) and the isentropic coefficient (γ) values vary during the process due to the combustion reactions, changes in the temperature and the changes in the composition of the working fluid. Therefore the losses must be incorporated in the components of the real gas turbine cycle in order to judge the actual performance of the system. More details of the thermodynamic analysis of a real cycle can be found in Section 3.2.

2.3.2.1 Effect of Cp and γ

The specific heat at constant pressure, c_p and the ratio of the specific heat at constant pressure to that at constant volume γ, influences the performance of the gas turbine cycle and this effect must be taken into consideration during a characteristic study of the gas turbine [53]. The c_p and γ are functions of the temperature in the normal range of the temperature and pressure of the cycle [53],

$$\frac{\gamma-1}{\gamma} = \frac{R}{M\, c_p} \tag{2.17}$$

where M is the molecular weight and R is the molar universal gas constant. The calculation of the product analysis is very lengthy when dissociation is taken into account and then the pressure has a significant effect on the amount of dissociation, so c_p and γ become a function of the pressure [53]. Saravanamuttoo et al. [53] have used the approximate vaules for the c_p and γ, such as 1.005 and 1.148 kJ/kg K for air and flue gas specific heats, respectively, and 1.40 and 1.33 for air and flue gas isentropic coefficient, respectively, and then concluded that the numerical differences in the air and product combustion gases, while the reasons why differences in these values of both c_p and γ do not lead to much inaccuracy is due to the opposing variation of the c_p and γ with respect to the temperature variations [53].

When component losses are taken into the consideration, the efficiency of the cycle becomes dependent on the maximum temperature in the cycle and the pressure ratio. In contrast, the lowest possible pressure ratio, which results in an acceptable performance, and it may be slightly different from the optimum value of the pressure ratio [51]. Therefore, the efficiency can be increased by increasing the maximum cycle temperature with an incremental increase in the pressure ratio and this cannot be increased beyond the limiting values [52]. The inclusion of the heat exchanger substantially increases the efficiency and it markedly reduces the optimum pressure ratio for the maximum cycle efficiency [52]. The increase in the effectiveness not only increases the cycle efficiency, however, it also decreases the optimum pressure ratio [52]. The reduction in the efficiency at the higher pressure ratios is due to the reduction in the fuel supply to give a fixed turbine inlet temperature and this result in a higher compressor delivery temperature being offset by the increased work necessary to drive the compressor [68].

2.4 Thermodynamics of Combustor

2.4.1 Combustor Efficiency

The performance of the real cycle can be expressed in a better way in terms of the fuel/air ratio and the specific fuel consumption. The convenient method for allowing the losses in the combustion chamber or burner is the estimation of the combustion efficiency of the burner. The energy balance around the combustor is given by [53]:

$$(1 + \beta)c_{p_g}(T_3 - T_{amb}) + \beta\Delta H_{298} + c_{p_a}(T_{amb} - T_2) + \beta c_{p_f}(T_{amb} - T_f) = 0 \quad (2.18)$$

where β is the fuel/air ratio, subscript "amb" indicates the ambient condition and the subscripts "a", "f", "g" represent the air, fuel, and flue gas, respectively. The specific heat values at constant pressure are the mean specific heat values for the respective stream in the range of the ambient temperature, T_{amb} and the respective stream temperature. The heat of reaction, ΔH_{298} is the enthalpy of the reaction per unit amount of fuel with water in the vapour phase in the product stream. In the gas turbine, it is a convention to use the net calorific value rather than the gross calorific value as it is not possible to use the latent heat of the water vapour of the flue gas [53]. The combustion efficiency, η_b is given by [53]:

$$\text{Combustion Efficiency } (\eta_b) = \frac{\text{theoretical } \beta \text{ for given } \Delta T}{\text{actual } \beta \text{ for given } \Delta T} \quad (2.19)$$

The combustion efficiency gives the details about the loses that occur in the combustion section and in the literature, and in general practice, the most convenient way is to represent the heat rate from the combustion section rather than the combustion efficiency [52, 53].

2.4.2 Thermodynamics of the Gibbs Reactor [112-114]

Both the rate and equilibrium conversion of the chemical reactions depend on the temperature, pressure and the composition of the reactants. However, the equilibrium conversion of the reaction provides a goal by which the improvements in a process can be predicted. The general chemical reaction scheme considered is given by [112]:

$$|v_1|A_1 + |v_2|A_2 + \cdots \rightarrow |v_3|A_3 + |v_4|A_4 + \cdots \quad (2.20)$$

where A_i is the reacting species and $|v_i|$ is the stoichiometric coefficient. When differential amounts of the reaction proceed, then the following relation is used:

$$\frac{dn_1}{v_1} = \frac{dn_2}{v_2} = \frac{dn_3}{v_3} = \frac{dn_4}{v_4} = \cdots = d\varphi \quad (2.21)$$

where n_i is the number of moles of reacting specie. In general,

$$dn_i = v_i d\varphi \quad (2.22)$$

where i = 1,2,3,……N are the number of the species taking part in the reaction and φ is the extent of the chemical reaction. For a multiple set of reactions of any kind, the above equation takes the form,

$$dn_i = \sum_j v_{i,j} d\varphi_j \quad (2.23)$$

where j represents the number of reaction in the chemical reaction set under consideration. The term φ, known as the reaction coordinate or the extent of the reaction, characterises the extent, progress, or degree to which the chemical reaction has proceeded.

The total Gibbs energy of the closed system at constant temperature and pressure must decrease during the course of the reaction. In an irreversible process, at a constant temperature and pressure, the total Gibbs energy attains its minimum value and it is said that the chemical equilibrium is reached, as illustrated in Figure 2.11. Mathematically,

$$d(G^t)_{T,P} = 0 \quad (2.24)$$

where G^t is the total Gibbs free energy, T is the temperature and P is the pressure.

Clearly, the differential displacements of the chemical reaction continue to occur at the equilibrium state without causing changes in the total Gibbs energy of the system. Therefore, for the perfect chemical equilibrium to be established; then either the total Gibbs energy of the chemical reaction system is at the minimum or its differential should be zero. The total Gibbs energy minimization is one means in order to understand the thermodynamics of the chemical reaction system in comparison to the detailed complex stoichiometry and kinetic mechanisms. It must be understood that how the total Gibbs energy minimization predicts the extent of

the reaction. For the extent of the reaction through the minimization of the total Gibbs energy, two ways need to be expressed, either writing the expression of G^t as a function of φ and solve for the value of φ which minimizes the G^t or differentiating the expression and setting it equal to zero and obtaining the value of the φ that satisfies it. The former is applicable to a multiple set of chemical reaction equations, while the latter is applicable to a single chemical reaction equation. The equation (2.24) can be thermodynamically solved for the expression with reaction/rate kinetic terms upon which the extent of the reaction will depend.

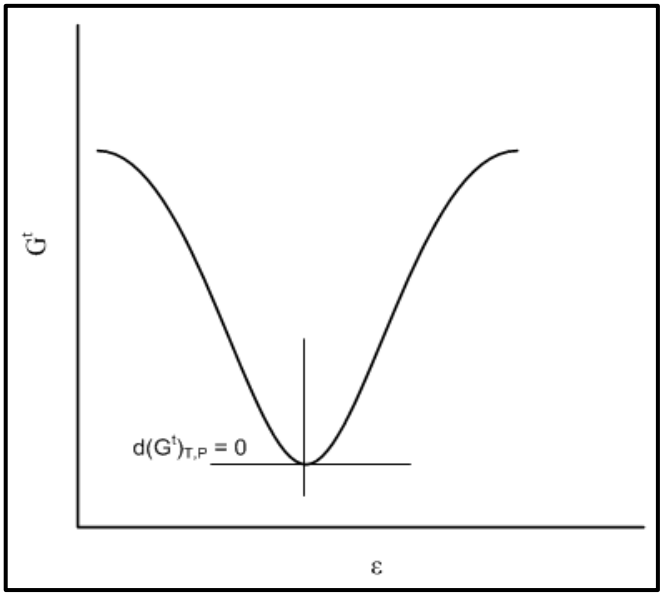

Figure 2.11 Total Gibbs energy as a function of the reaction coordinate.

The thermodynamic expression for the Gibbs energy is the starting point for such derivation, i.e.:

$$d(nG) = (nV)dP - (nS)dT + \sum_i \mu_i dn_i \qquad (2.25)$$

where V is the volume, S is the entropy and μ is the activity coefficient. Expressing in terms of the reaction coordinate,

$$d(nG) = (nV)dP - (nS)dT + \sum_i v_i \mu_i d\varphi \qquad (2.26)$$

As nG is the state function and for the right hand side to be an exact differential, the equation (2.26) becomes:

$$\sum_i v_i \mu_i = \left[\frac{\partial(nG)}{\partial\varphi}\right]_{T,P} = \left[\frac{\partial(G^t)}{\partial\varphi}\right]_{T,P} \qquad (2.27)$$

The expression $\sum_i v_i \mu_i$ represents the rate of change in the total Gibbs energy with respect to the extent of the reaction, φ at constant temperature and pressure. In equilibrium, this quantity tends to be zero, i.e.

$$\sum_i v_i \mu_i = 0 \tag{2.28}$$

The involvement of the fugacity terms will give a more meaningful description of the above expression and help in eradicating the activity coefficient, μ. The definition of the fugacity for a species in a solution, and for a pure specie in a standard state and at standard temperature, is given by the two thermodynamic expressions:

$$\mu_i = \Gamma_i(T) + RT \ln \hat{f}_i \tag{2.29}$$

$$G_i^{\,o} = \Gamma_i(T) + RT \ln f_i^{\,o} \tag{2.30}$$

where f is the fugacity coefficient, Γ indicates the integration constant and the superscript "o" indicates the standard state. The difference in the above two equations yields,

$$\mu_i - G_i^{\,o} = RT \ln \frac{\hat{f}_i}{f_i^{\,o}} \tag{2.31}$$

On combining the equations (2.28) and (2.31) results in the following expression:

$$\sum_i v_i \left[G_i^{\,o} + RT \ln \frac{\hat{f}_i}{f_i^{\,o}} \right] = 0 \tag{2.32}$$

$$\ln \prod_i \left(\frac{\hat{f}_i}{f_i^{\,o}} \right)^{v_i} = - \frac{\sum_i v_i G_i^{\,o}}{RT} \tag{2.33}$$

where $\prod_i$ specifies the product over all species i. The exponential form of the expression is given by,

$$\prod_i \left(\frac{\hat{f}_i}{f_i^{\,o}} \right)^{v_i} = K \tag{2.34}$$

and K is the equilibrium constant of the chemical reaction and it is an important parameter in the chemical reaction kinetics. So,

$$K \equiv \exp\left(\frac{-\Delta G^{o}}{RT}\right) \tag{2.35}$$

and,

$$\ln K = \frac{-\Delta G^{o}}{RT} \tag{2.36}$$

where ΔG^{o} is the standard Gibbs energy change in the reaction. The G^{o} is the property of the pure specie at a fixed pressure in its standard state and it depends only on the temperature. Therefore, the equilibrium constant, K is dependent only on the temperature. The fugacity ratios in equation (2.34), state; that the connection between the equilibrium state of interest and the standard state of the individual specie. The function $\Delta G^{o} \equiv \sum_i v_i G_i^{o}$ is the difference between the Gibbs energies of the products and the reactants weighted by their stoichiometric coefficients when each specie is at standard pressure, and operating temperature and the species are at the standard state as a pure substance. Therefore, the value of ΔG^{o} is fixed for a particular temperature and it is independent of the equilibrium pressure and composition. Values of ΔG^{o} for many chemical formation reactions are tabulated in standard references [112, 113, 115]. However, these values are not measured experimentally; nevertheless these are calculated by subsequent thermodynamic expressions. The values of the other reactions can be calculated by the formation reaction values of the respective specie involved in the chemical reaction.

2.4.2.1 Gas Phase Reactions

Standard state of the gas is the ideal gas state of the pure gas at the standard state pressure P^{o} of 1 bar. Fugacities reflect the non-idealties of the equilibrium mixture and it is a function of the temperature, pressure and composition. So for the gas phase system $f_i^{o} = P^{o}$, the expression becomes,

$$\prod_i \left(\frac{\hat{f}_i}{P^{o}}\right)^{v_i} = K \tag{2.37}$$

This depicts that for a fixed temperature, the composition in equilibrium must change with the pressure in such a way that the $\prod_i \left(\frac{\hat{f}_i}{P^{o}}\right)^{v_i}$ remains constant. The fugacity relation to the fugacity coefficient is given by,

$$\hat{f}_i = \hat{\emptyset}_i \, y_i P \tag{2.38}$$

On inserting the above value into equation (2.37) yields,

$$\prod_i \left(\hat{\emptyset}_i \, y_i\right)^{v_i} = \left(\frac{P}{P^o}\right)^{-v} K \tag{2.39}$$

where $\emptyset$ is the ratio of the fugacity coefficients. This equation shows how the most important three parameters, such as the composition of the components taking part in the chemical reaction, pressure dependent term and the temperature dependent term affect the determination of the chemical equilibrium of the system [112].

2.4.2.2 Multiple Reactions

When the system is composed of multiple reaction systems then the method for the single reaction can be extended to the multiple reaction system by including separate chemical equilibrium constants for each reaction. Therefore, for a multiple reaction system, the following equation can be used:

$$\prod_i \left(\frac{\hat{f}_i}{f_i^{\,o}}\right)^{v_{i,j}} = K_j \tag{2.40}$$

For the gas phase, with multiple reaction systems, the equation is given by:

$$\prod_i \left(\frac{\hat{f}_i}{P^o}\right)^{v_{i,j}} = K_j \tag{2.41}$$

and,

$$\prod_i \left(\hat{\emptyset}_i \, y_i\right)^{v_{i,j}} = \left(\frac{P}{P^o}\right)^{-v_j} K_j \tag{2.42}$$

Here, the last equation (2.42) also represents the combined effect of the composition, pressure and temperature in order to determine the varying chemical equilibrium for the multiple set of reactions.

The above investigation of the free Gibbs energy for determining the kinetic state of the system is best used to investigate those system which lack the complete stoichiometry or if known the mechanisms are too complex or varying to make the processes difficult to model and simulate. The effect of the temperature, pressure, and the composition of the chemical species taking part in the system dictates the

equilibrium conversions of the chemical reactions. The degree of freedom must be specified in order to exactly know the true state of the system and when the system involves the chemical reactions then the simple phase rule is not adequate rather Duhem's theorem for the reacting system should be applied and it can be found in the relevant literatures [112, 113, 115]. The usual problem seems to find the composition of the reaction species at the equilibrium state if the temperature and the pressure at the equilibrium state are specified. The minimization of the total Gibbs free energy provokes a study of those systems with little information in hand and predicts the kinetics of the system. These systems may vary from fuel combustion and gasification to the electrolytic fuel cells. Therefore, the combustion system can be better modelled through the Gibbs free energy mechanism without the need for a detailed rate kinetic mechanism.

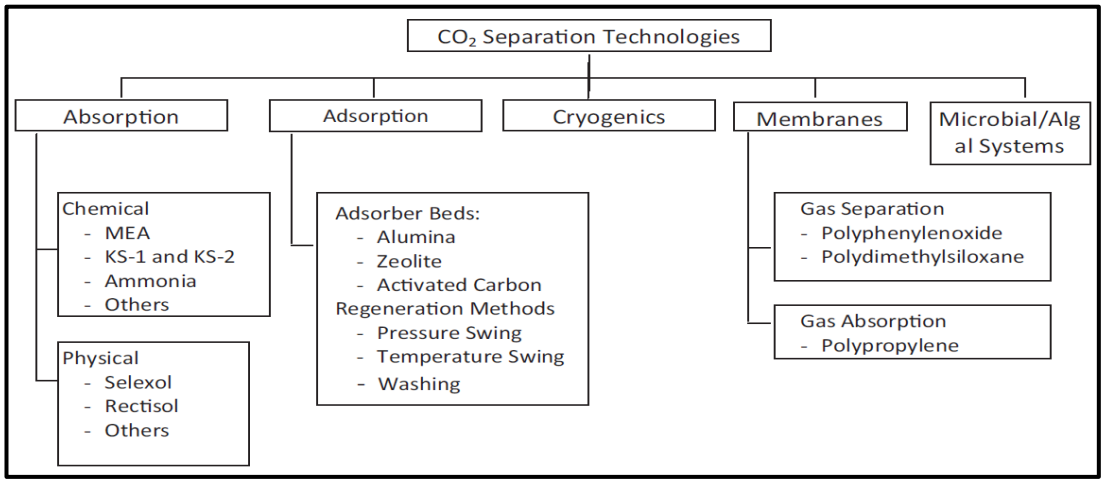

Figure 2.12 Classification of post combustion carbon dioxide capture technologies [45].

2.5 Post-Combustion Carbon Dioxide Capture

Post combustion carbon dioxide capture, as mentioned in Section 1.2.2.1.1, is the downstream technology which removes CO_2 from the flue gas of the power plant. PCC technology is considered to be the most mature technology, that is currently available [116]. The PCC technology is on the edge in comparison to the pre-combustion CO_2 capture and oxy-combustion CO_2 capture technology due to its readiness for retrofitting to the existing power plants. However, integration of the CO_2 capture technologies are energy intensive and results in 75 to 80 % of the total cost of the whole CCS process [117]. The number of CO_2 capture technologies can be employed under the heading of the PCC technology and these can be classified as

listed below [45] and the sub classification of each CO_2 capture technology is provided in the Figure 2.12.

- Absorption
- Adsorption
- Cryogenics
- Membranes
- Microbial/Algal Systems

2.5.1 Absorption

Gas absorption involves the removal of one or more selected components from a mixture of gases due to the higher affinity of the selected components to a suitable liquid. The gas absorption involves the re-distribution of the solute molecules between the gas phase and liquid phase when two phases are brought into intimate contact and finally it results into the equilibrium condition. The regeneration of the absorbate from the absorbent is termed as stripping in which generally heat is applied to release the absorbed components. The system, due to its layout, is also termed as an absorption and stripping process. The absorption is further classified as: physical and chemical absorption.

2.5.1.1 Physical Absorption

In physical absorption, mass transfer takes place purely by diffusion. Further, it is categorised by the absorption of the CO_2 molecules based on Henry's law [45]. The physical absorption is suitable for the system with higher pressure of the stream to be treated with higher partial pressure of the component to be removed. The regeneration of the absorbed components can be achieved either through heat or pressure gradient. The most commonly employed solvents include dimethyl ether of polyethylene glycol (termed as the Selexsol process) and methanol (termed as the Rectisol process) [45, 118]. More details can be found in dedicated literature to this topic [45, 118].

2.5.1.2 Chemical Absorption

In chemical absorption, a true chemical reaction occurs as soon as stream containing a particular component is brought into intimate contact with the liquid solvent. The nature of the chemical bond defines the nature of the reaction and hence the

chemical absorption can be classified as being reversible chemical absorption in which the component of the gaseous stream to be absorbed is loosely bound with the liquid solvent while the other type, termed as irreversible chemical absorption in which the component of the gaseous stream to be absorbed is tightly bound with the solvent and resultant solvent cannot be regenerated [118]. The absorption of the CO_2 and H_2S through aqueous amine is an example of reversible chemical absorption which can be easily regenerated by the application of the heat while absorption of the H_2S through iron chelate is an example of irreversible chemical absorption [118]. The regeneration for reversible chemical absorption results in pure CO_2 stream, thus the process of reversible chemical absorption is more suitable for CO_2 capture from flue gas of power plants and industry [45]. The chemical absorption for CO_2 removal through the flue gas of the power plants is the most preferred choice as it can also remove CO_2 at its low partial pressure [45]. For more details of the reversible chemical absorption for application to CO_2 capture can be found in Section 2.6.

The details of the adsorption, cryogenics, membranes and microbial/algal systems are outside of the scope of this thesis and hence for more details, the dedicated literature can be referred [45, 118-124].

2.6 CO_2 Capture using Alkanolamines

Gas sweeting using alkanolamines is the one of the most widely used methods for the removal of the acid gases, including CO_2, H_2S and COS. However, it was the Bottoms [125, 126] who for the first time used organic bases for the removal of the acid gases. The first alkanolamine used for commercial application was triethanolamine (TEA) [118].

Alkanolamines are one the basic organic compounds which shows considerable basicity having a general formula or RNH_2, R_2NH and R_3N, where R may be alkyl or aryl group [127]. Alkanolamines are classified as primary, secondary and tertiary amines, depending on the number of hydrogen atoms attached to the nitrogen atoms [127]. However, each of the alkanolamine has one hydroxyl and one amino group. The amino group is responsible for its reaction with the acid gases due to its alkalinity while the hydroxyl group results in water solubility and reduction in vapour pressure.

2.6.1 Primary Alkanolamines

Alkanolamines, which have two hydrogen atoms attached to the nitrogen atom of the amine, are termed as primary alkanolamines. They include monoethanolamine (MEA) with chemical formula as $C_2H_4OH\text{-}NH_2$ and diglycolamine (DGA) which is 2-(2-aminoethoxy) ethanol ($HOC_2H_4OC_2H_4\text{-}NH_2$). The primary alkanolamines are categorized by their higher alkalinity and reactivity in comparison to the secondary and tertiary alkanolamines [118, 127].

DGA is commercially employed in the process named as the Flour Econamine Process [118]. DGA has low vapour pressure and permits the higher concentrations up to 60 % to be used for the acid gas removal which results in lower recirculation rates and lower stripping requirements [118, 128].

2.6.1.1 Monoethanolamine

Aqueous solutions of monoethanolamine are widely adopted as the solvent for acid gas removal, including CO_2, H_2S and COS, due to its lower molecular weight, higher alkalinity, and its relative ease to regenerate it [118, 128]. Further, aqueous MEA is still considered a leading solvent for CO_2 capture for testing purposes at pilot-scale systems and commercial-scale applications [45, 129-140]. Due to its lower molecular weight, MEA solutions result in higher solution capacity at moderate solution concentrations [118]. However, MEA encounters several disadvantages during its use, such as solvent degradation due to the oxygen present in the flue gas, solvent losses due to its higher vapour pressure, higher heat of reaction which results in higher regeneration duties and corrosion [45, 141]. It is found that the solvent degradation constitutes 10 % cost of the CO_2 capture system [116]. Further, oxidative degradation is significant in the flue gas containing 3 to 15 % O_2 concentrations [142]. More details of the oxidative degradation of the aqueous amine solutions can be found in the literature [142-145]. The solvent losses due to the higher vapour pressure of the MEA solutions at low operating pressure can be simply avoided by the use of the water wash section at the top of the absorber section. Further, the MEA solvent results in disadvantages due to the higher heat of reaction with CO_2 and H_2S and this result in higher regeneration duty, which is the major focus of the ongoing research to reduce the energy penalty caused by the CO_2 capture plant on its integration with the power plant. Furthermore, MEA solutions

appear more corrosive in comparison to the other alkanolamines, particularly at solvent concentrations exceeding 22 %. [146, 147]. However, the use of the corrosion inhibitors can overcome the issue of the corrosion and permits the MEA solution concentrations as high as 30 %. More details of the corrosion issues in MEA systems can be found in the literature [146-148].

2.6.2 Secondary Alkanolamines

Alkanolamines which have one hydrogen atom attached to the nitrogen atom of the amine are termed as secondary alkanolamines. They include diethanolamine (DEA) with chemical formula $C_2H_4OH\text{-}NH\text{-}C_2H_4OH$ and diisopropanolamine (DIPA) with chemical formula $C_3H_5OH\text{-}NH\text{-}C_3H_5OH$. The secondary alkanolamines are categorized by their higher alkalinity and reactivity in comparison to the tertiary alkanolamines, however, there alkalinity and reactivity is less in comparison to the primary alkanolamines [118, 127].

DEA and DIPA, due to their less reactivity, are favourable for the capturing of the COS, H_2S and CS_2 as it results in less corrosive products at the end in comparison to the primary alkanolamines [118, 128]. Due to their low vapour pressure, the secondary alkanolamines results in low vaporization losses. DEA is not suitable for capturing CO_2 from flue gases containing higher concentrations of the CO_2 due to the corrosive by-products formation [118]. Further, DEA cannot be regenerated by simple stripping process, however, it requires vacuum distillation for its regeneration while DIPA has shown low steam requirements [118].

2.6.3 Tertiary Alkanolamines

Alkanolamines which have no hydrogen atom attached to the nitrogen atom of the amine are termed as tertiary alkanolamines. They include TEA with chemical formula $(C_2H_5O)_3\text{-}N$ and methyldiethanolamine (MDEA) with chemical formula $CH_3\text{-}N\text{-}(C_2H_4OH)_2$. The tertiary alkanolamines are categorized by their low alkalinity and reactivity in comparison to the primary and secondary alkanolamines [118, 127].

TEA is the first alkanolamine which was commercially applied for the removal of the acid gasses [125, 126]. Due to low the alkalinity, reactivity and stability it was replaced by MEA, DEA and MDEA in the gas purification industry [118, 128]. MDEA is suitable for selective absorption of H_2S from the gas containing CO_2 and

H_2S as acid gas impurities [118]. However, in the present scenario of the CO_2 capture from the flue gas at power plants, MDEA has gained importance due to its high capacity, low corrosivity and high stability along with low regeneration duty and vaporization. However, disadvantages of the MDEA solvent include, its low reactivity, difficult regeneration through normal stripping process [149, 150].

2.7 Chemistry of Alkanolamine with CO_2

The choice of solvent for the CO_2 capture depends on three important factors of the solvent, including higher rate of reaction and higher loading capacity along with lower regeneration duty [151]. The MEA shows higher regeneration duties and lower loadings, however, due to the higher reactivity the MEA solvent will be predominantly used as the solvent for the CO_2 capture from power plants [151]. MEA contains one amine group ($-NH_2$), resulting in the basic nature (pKa = 9.5) of the MEA aqueous solution and the alcoholic group (-OH) results in the stability and the lowering of the vapour pressure [152, 153]. The aqueous MEA with concentration 30 wt.% (11.2 molar%) is mostly considered with reasonable loading capacity along limiting solvent degradation and corrosivity [152]. The principal reactions for the primary alkanolamines which occur when aqueous alkanolamine is brought in to contact with the CO_2 (pKa = 6.4) containing stream, are as follows [118]:

$$H_2O \leftrightarrow H^+ + OH^- \quad (2.43)$$

$$CO_2 + H_2O \leftrightarrow HCO_3^- + H^+ \quad (2.44)$$

$$RNH_2 + H^+ \leftrightarrow RNH_3^+ \quad (2.45)$$

$$RNH_2 + CO_2 \leftrightarrow RNHCOO^- + H^+ \quad (2.46)$$

The principal reaction (2.43) is the ionization of water, the reaction (2.44) is the hydrolysis of the dissolved CO_2, the reaction (2.45) results in the protonation of alkanolamines and finally the last reaction (2.46) shows the carbamate formation [118]. If the principal reaction (2.46) dominates, it results in the carbamate ions shifting to alkanolammonium ions through the reaction (2.45) [118]. Therefore, it results in the limited equilibrium of 0.5 mole of CO_2 per mole of alkanolamine, irrespective of the CO_2 concentration in the gaseous stream [118]. Further, if the

reactions (2.45) and (2.46) are combined for the MEA , the combined balanced reaction will be as follows [152]:

$$2(C_2H_4OH)NH_2 + CO_2 \Leftrightarrow (C_2H_4OH)NH_3^+ + (C_2H_4OH)NHCOO^- \quad (2.47)$$

From reaction (2.47), it can be concluded that the CO_2 absorption, which is an exothermic reaction, can be increased by shifting the reaction (2.47) towards the forward direction, while the regeneration of the CO_2, which is the endothermic reaction, can be enhanced by shifting the reaction towards the backward direction [153].

2.8 Kinetics of Alkanolamine with CO_2

There are three mechanisms in the literature [45, 154] which describe the CO_2 absorption into the aqueous MEA, which are as follows:

- Zwitterion mechanism,
- Termolecular mechanism, and
- Base-catalysed hydration mechanism.

However, the absorption of the CO_2 into the alkanolamines is mostly described by the two-step Zwitterion mechanism. In the Zwitterion mechanism, the reaction between CO_2 and amines (AmH) proceeds with the formation of intermediate, termed as Zwitterion, as [151, 154]:

$$AmH + CO_2 \overset{k_1, -k_2}{\Longleftrightarrow} AmH^+COO^- \quad (2.48)$$

This zwitterion reacts with the base (X) undergoing deprotonation, forming carbamate, as [151, 154]:

$$AmH^+COO^- + X \overset{k_X}{\Leftrightarrow} AmCOO^- + XH^+ \quad (2.49)$$

By assuming the Zwitterion concentration at quasi-steady state, the overall reaction rate will be [151],

$$R = \frac{k_1 [CO_2][AmH]}{1 + \frac{k_2}{k_X [X]}} \quad (2.50)$$

where k_1 and k_2 are the rate constants for forward and backward reaction, respectively, shown by reaction (2.48). The k_X is the rate constant for the reaction between Zwitterion and base, shown by reaction (2.49) and R is the apparent rate of

the reaction between CO_2 molecule and alkanolamine. Further, if reaction of the CO_2 with H_2O and OH^- is also considered, there rate expressions will be represented by [154],

$$R' = k_{H_2O}[CO_2][H_2O] \quad (2.51)$$

$$R'' = k_{OH}[CO_2][OH^-] \quad (2.52)$$

where R' and R'' are the apparent rates of reaction between CO_2 with water molecule and hydroxyl ion, respectively. The k_{H_2O} and k_{OH} are the observed rate constants of reactions between CO_2 with water molecule and hydroxyl ion, respectively Combining equations (2.50), (2.51) and (2.52) and summing the reaction rates R, R' and R'' as R_{CO_2} will result in,

$$R_{CO_2} = \left\{ \frac{k_1 [AmH]}{1 + \frac{k_2}{k_X [X]}} + k_{OH}[OH^-] + k_{H_2O}[H_2O] \right\} [CO_2] \quad (2.53)$$

where R_{CO_2} is the observed rate of reaction of CO_2 molecule with alkanolamine. The rate constant with respect to CO_2 can be defined as:

$$k_{CO_2} = \frac{k_1 [AmH]}{1 + \frac{k_2}{k_X [X]}} + k_{OH}[OH^-] + k_{H_2O}[H_2O] \quad (2.54)$$

where k_{CO_2} is the observed rate constant for reaction based on Zwitterion mechanism. Further, defining the rate constant with respect to the alkanolamines, as,

$$k_{AmH} = \frac{k_1}{1 + \frac{k_2}{k_X [X]}} \quad (2.55)$$

where k_{AmH} is the rate constant for reaction between CO_2 and alkanolamine. The equation (2.53), becomes [151, 154],

$$R_{CO_2} = k_{CO_2}[CO_2] \quad (2.56)$$

More details of the chemical kinetics of the CO_2-alkanolamines can be found in the review reported by Vaidya and Kenig [154].

2.9 Literature Review of Amine-based CO_2 Capture Plant

Research and development activities regarding solvent-based post-combustion CO_2 capture, with focus on the reduction of the energy consumption of the system, are being demonstrated worldwide through pilot-scale PCC [129, 131-134, 139]. In addition, PCC technology is near commercialization around the globe;

demonstrations of the integration of the PCC technology to a commercial-scale fossil-fuel power generation system, include the SaskPower Boundary Dam CCS Project, Canada, [155] and the ROAD CCS Project, Netherlands [156].

In addition, most of the reported studies in the literature involve process modelling studies of PCC systems. Process modelling and simulation can save time consuming experimental investigations as it can predict reliable results if the thermodynamic and kinetic packages used in developing the process models are rigorous and of high fidelity [138]. In the literature, there are several studies that discuss the design, operation and optimization of the PCC process using equilibrium-based models [157], rigorous rate-based models [107, 158-160], and simplifications of rate-based models [161]. Yang and Chen [158] have simulated experimental case studies with equilibrium and rate-based models and have demonstrated the superiority of the rate-based model for predicting better results. Canepa and Wang [107] have reported the design of CO_2 capture plants for NGCC, however, economic implications are only considered for the lean loading and reboiler duty. Agbonghae et al. [159] reported the techno-economic process design of commercial-scale CO_2 capture plants for coal and natural gas fired power plants. Berstad et al. [160] have performed a comparative study for the design of the CO_2 capture plant for coal, biomass and natural gas fired power plants, however, it lacks an economic analysis. The exhaust gas from NGCC power plants is lean in CO_2 content, which results in a major penalty when an NGCC power plant is integrated with an amine-based CO_2 capture plant [162-164]. One way of enriching the exhaust gas from a natural gas-fired power plant is through EGR [80]. EGR offers many advantages in terms of enhanced CO_2 content in the exhaust gas and a reduced flue gas flow rate to the PCC system [129, 165]. However, it also has some limitations in terms of the maximum amount of the exhaust gas that can be recirculated without causing oxygen starvation at the combustor inlet, thus resulting in issues with combustion stability as reported in the literature [89, 92]. Following these limitations, the literature reports the design, operation and optimization of an amine-based CO_2 capture system integrated with NGCC in EGR mode and a comparison of the performance of the system without EGR [99, 100, 102, 104, 105, 166].

2.10 Carbon Dioxide Processing and Purity

The CO_2 stream obtained through the top of the stripper column of the reactive absorption-desorption process is dehydrated and compressed. However, the purity of the CO_2 concentrated stream required for sequestration is not yet fully defined and varies depending on the storage [119]. The storage of the carbon dioxide affects the level of the impurities in the carbon dioxide stream as each impurity affects the rock structure and the operation of the storage [119]. There are some issues regarding the storage of the carbon dioxide, such as operation, risk of leakage, health and safety issues, legal concerns and economy, and these must be considered [119]. At present, the option of the co-storage of the CO_2 along with impurities is also considered as the preferred option [122]. The co-storage increases the energy and the storage size requirements and may pose safety risks [46]. The co-storage of the CO_2, along with the SO_2, is considered as having similar properties at the super critical state [122]. The impurities affect the rock structure by forming precipitates, hydrates or different inorganic salts and these may block the further injection into the rock [122].

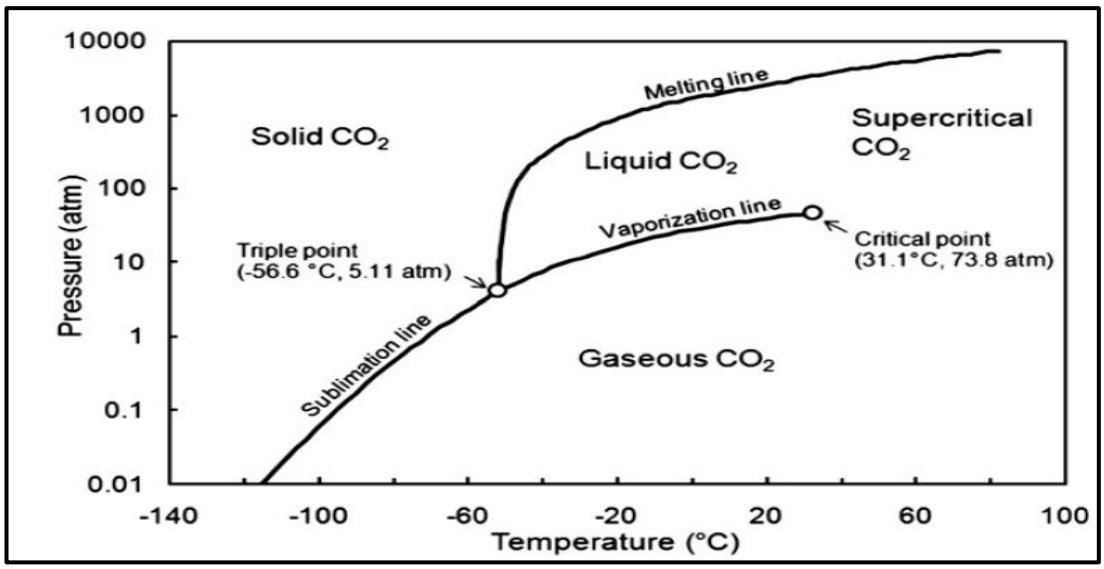

Figure 2.13 The CO_2 phase diagram [46].

The quality or conditions of the CO_2 that needs to be transported or stored in the reservoir must be maintained before it is compressed into pipeline [46]. The quality of the CO_2 must be according to the requirements imposed, also the pressure and the temperature of the carbon dioxide must be such that it may not leak or flash during the transport or storage [46]. The phase diagram, as shown in Figure 2.13, indicates that the pressure must be in the range 100-110 bar and the temperature should be above the critical point (31.1^oC) for the carbon dioxide to remain in the super critical

state [46]. The compression of the carbon dioxide is an energy intensive process and effects the efficiency of the power plant due to the energy consumption and thus results in the decrease of the efficiency of the process by ~2-3 percentage points [46]. The compression of the carbon dioxide is strongly affected by the presence of the impurities, such as water and non-condensable (N_2, O_2 and Ar) impurities [32, 167-170]. These non-condensable impurities come into the carbon dioxide stream through air leaks in the boiler and occurs throughout the boiler and the ESP section which operates at a negative pressure [169, 171, 172].

The carbon processing process consists of the condensation of the water before compression, and during water removal some of the carbon dioxide may dissolve with the condensate and this affect the removal efficiency of the carbon dioxide [170]. As the carbon dioxide forms non-azeotropic mixtures with non-condensable then it depends on the plant configuration, on the transport and storage constraints and the impurity requirements according to the energy and economic perspectives for the final carbon dioxide stream [46].

2.11 Process System Analysis

The modelling and the simulation of the process inform us as to how changes in the system influences or affect the performance of the system. Models are the simplified abstraction of the reality representing the important elements of the process under investigation. Modelling involves the construction of the perspective model in terms of the process language to reproduce the characteristics of the process in order to infer the performance of the process. Simulations involve the initiation of some real processes. The modelling and simulations gain insight into the operation of the process and gives the influence of the suggested disturbances imposed on the system under the limits imposed by the process.

Process modelling and simulations assist in creating the different process alternatives, performing material and heat balances across the system, giving detail design of the process equipment's, estimating the process thermodynamics and the reaction kinetics, evaluating the performance of the process under different scenarios and establishing different control strategies to investigate the dynamic behaviour of the system. Optimizing and integrating the process parameters, with

familiarization to the process safety problems and dealing with the emergency situations.

Three types of the properties for the process which are useful include the thermodynamic properties, the transport properties, and the kinetic properties. A key requirement of the simulation model should be such that it should reproduce these properties to represent the system. Accurate prediction of these properties is important for meaningful simulation analysis. The failure in the accurate prediction through process modelling and simulation are mostly due to the improper selection of the thermodynamic model, inadequate model parameters, and inconsistency in the plant data.

2.11.1 Modelling and Simulation Tools

The process modelling and simulation tool must be able to predict the desired performance of the process with accuracy, reliability, and realism. The process modelling and simulation tool needs to be user friendly, customizable, and take less time and space during the computations [173]. The various process softwares are available for the analysis of the processes which might vary from the nano-scale systems, including molecular processes to the macro level, including complex, integrated production plants and petrochemical complexes. Also tailored black boxes are available for the specific process in order to check the consistency of the process while these customized packages are not able to carry out the complete modelling of the process by understanding the effect of each unit of the model on the other. Thus, the software, with the capability to model process flow diagram by joining each unit and carry the simulation with different operating conditions and then analyse the results, is more diverse. The different simulators available for the modelling and simulation of the processes include, Chemcad, Pro/II, Speedup, gPROMS, Aspen Suite and a number of other software's. The Aspen Suite has the capability of performing both steady state and dynamic simulations of the process under investigation. The Aspen Suite has a mixed simulation and optimization environment that supports sequential, modular and equation oriented approaches for the solution scheme. In addition, it is now equipped with energy, economic and safety analysis to be incorporated in different scenarios for each analysis [173].

Table 2.1 Differences between Aspen Plus and Aspen Hysys for CO_2 capture system.

Aspen Plus	Aspen Hysys
Components: Number of ionic species need to be specified by user for reaction chemistry.	*Components:* Numbers of ionic species are added on its own as soon as the solvent and property package are selected. Physical solvents are also available.
Heat Stable Salts: Add-on not available however can be specified by the user along with reaction chemistry.	*Heat stable salts:* Add-on available with reaction chemistry in the library on just one-click. (NAOH, HCL, HCOOH, CH_3COOH, H_2SO_4, $H_2S_2O_3$, HSCN)
Thermodynamic Property Package: Electrolyte Non Random Two Liquid (ENRTL) method.	*Thermodynamic Property Package:* Acid Gas Property Package (thermodynamically based on ENRTL). *Acid Gas-Physical Solvents* property package is also available.
Reaction Chemistry: Reaction chemistry whether equilibrium or kinetic reactions, need to be specified by the user with respective kinetic and equilibrium parameters.	*Reaction Chemistry:* Reaction chemistry whether equilibrium or kinetic reactions are automatically generated depending on the components and can be altered by the user.
Model: Rate based utilizing mass and heat transfer correlations.	*Model:* Rate based utilizing mass and heat transfer correlations.
Calculation Mode: Rate-based modelling.	*Calculation Mode:* Efficiency mode. (A conventional equilibrium-stage approach to solve the column, but the non-equilibrium behaviour inherent to acid gas systems is taken into consideration). The rate based mass and heat transfer correlations are taken into consideration for efficiency computations.
Acid Gas tabs: Not available.	*Acid Gas tabs:* Dedicated tabs are available in both absorber and stripper for the specific property.
Makeup Block: Not available. User need to specify through mixer.	*Makeup Block:* Dedicated makeup unit is available to cope with the amine and water loss and to avoid the convergence issues.

2.11.2 Why Aspen Software?

McMillan [174] have provided a list for a variety of process modelling and simulation software's from steady state to real time dynamic software's along with their functions and benefits. Each of the software has its own advantages. There are

a number of software's listed in Section 2.10.1 and from these packages the Chemcad, PRO/II and are steady state simulators, while the Aspen tech and gPROMS are steady state and dynamic software's.

The gPROMS is the general purpose process modelling, simulation and optimisation software. It is an equation based system with the ability to perform steady state and dynamic estimations and optimisations [175]. Aspen Technology, Inc., provides the industry-leading process software for the engineering, manufacturing and supply chain problems [176]. The Aspen tech. has the ability to cover a wide range of problems, including the process design side, steady state and dynamic process simulation and modelling and advanced planning, scheduling and blending techniques to deal with supply chain problems [176, 177]. The drag and drop facility for the unit process or operation models of the process industry, along with the number of components and thermodynamic property packages, are enormous in number. This software appears to be more user-friendly and has a number of add-ons and look-up tables [176]. The Aspen Plus supports non-ideal properties and systems with electrolytes and azeotropes, while the Aspen Hysys can perform both forward and backward estimations [177]. Further, the difference between Aspen Plus and Aspen Hysys for the process modelling of the CO_2 capture system is presented in Table 2.1.

2.12 Process System Analysis Algorithm

The simulation and modelling algorithm for the process under study is best illustrated in Figure 2.14. The first step is always the definition of the problem statement and the description of the process under investigation. The accurate description of the process resolves most of the first hand issues regarding the process. The problem statement describes the process entities, along with the silent features of the process. The silent features of the process sets the goals and the objectives to be met during its translation into the process modelling and simulation. The inputs for the process are the operating conditions at which the process parameters are fixed in order to carry out the desired operation. The degree of the freedom analysis of the process informs the user how many of the independent variables must be in hand to completely define the system and this result in the unique solution of the system. The inputs can be found from the design or the operating technical descriptions of the system, the open literature and the inputs can

be obtained by the experimental data for the particular system. Also the experimental data provides the goal for the validation and verification of the model to be implemented in the simulation. For satisfying the degree of the freedom of the process, some intelligent guesses, or valid assumptions based on a rule of thumb process for the process chemistry needs to be taken.

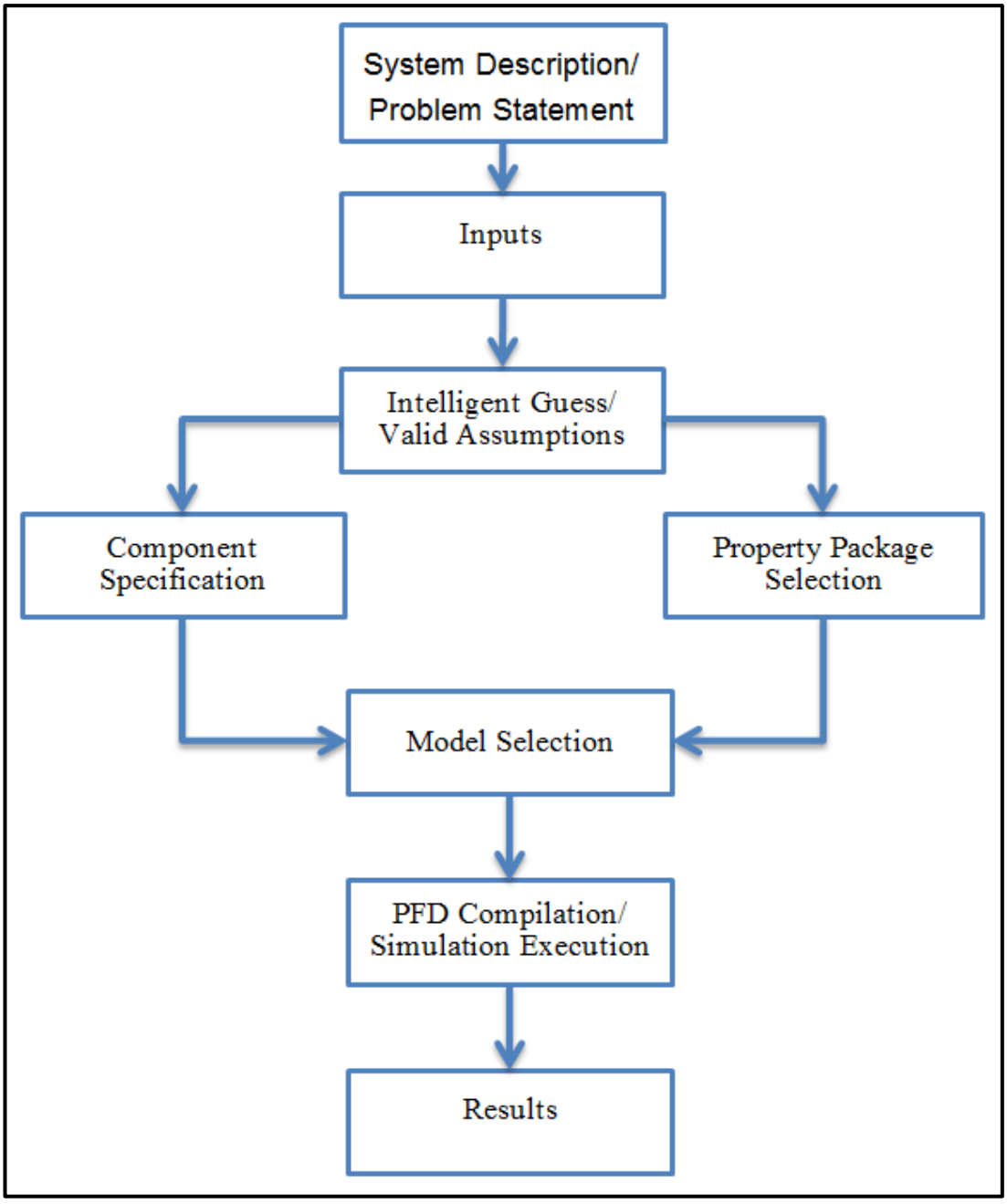

Figure 2.14 Flowchart for the process system analysis algorithm.

The next step is the specification of the species, or the components taking part in the process. The component species are the solid, liquid and gaseous compounds, molecules or the elements taking part in the process. The next parallel step will be

the specification of the relevant property package based on the thermodynamic nature of the process. The property package is the model path or route equipped with a number of equations to determine the thermodynamic, transport and kinetic properties of the system.

After the component specification and the selection of the appropriate property package, the models for each unit involved in the process flow diagram are selected. The unit model might be a unit process or unit operation model and these process models are interconnected with each other through the material, heat or work streams which help in the flow of the mass and energy across the process models. The interconnected process models result in the complete process flow diagram (PFD) model of the system under investigation and after inserting the respective inputs and bounding the system with the required degree of accuracy, convergence and tolerance for the error; it is run for the simulation to precede the respective results for which the model is posed.

The results obtained are compared with the results gained through the experiments and if these results are in good agreement, then further analysis of the results is performed.

2.12.1 Property Package Selection

The composition, temperature, pressure, nature of the properties to be estimated and the availability of the parameters are the most important factors that must be considered before selecting any property package to be suitable for the particular process [178]. Carlson [178] has showed the successive steps and factors which must be carried out or adopted for the selection of the appropriate property package for the particular process and hence adopted in this thesis. Inadequacy in some of the physical property estimations through the respective property package results in an inaccuracy in the results obtained through the simulation [178]. Each property package has its own assumptions and limitations up to the extent that they can be applied.

The pressure and temperature operating conditions describe the range up to which the phase equilibria calculations can be performed through a particular property package [178]. The availability of some specific parameters through the particular

property package might make that property package the ultimate choice due to its ability to estimate the particular parameters.

2.13 Summary

An overview of the literature is provided in the present chapter, with emphasis on the process techniques to be investigated in this thesis. The overview will help in the understanding of the basis for the system under consideration and will set the focus for the subsequent chapters.

The chapter starts with an overview of the gas turbine with emphasis on the micro gas turbine which will be studied in the Chapters 3, 4 and 5. The various modifications proposed in the literature for the gas turbine, in general and the micro gas turbine in particular, has been discussed. Further, the thermodynamics of the gas turbine for simple, recuperated and cogeneration cycles are presented, comprehensively. The Gibbs free energy for the combustion equilibrium simulation is discussed in detail.

The PCC technology to be investigated at the pilot-scale level in Chapter 6 and further its application to commercial-scale level in Chapters 7 and 8 is thoroughly elaborated in this chapter. The numbers of the alkanolamine solvents that can be employed are discussed with special attention on the aqueous MEA solvent. The chemistry and kinetics of the alkanolamines is also presented to have a better understanding of the base process. Further, a general overview of the CO_2 stream obtained through PCC technology, its purity and processing required during CO_2 compression, transport and sequestration is presented in this chapter.

Finally, the process system analysis techniques to be employed in this thesis are explained. The number of process system analysis tools, available, their advantages and disadvantages are discussed. The selection of the appropriate tool is described and the process system analysis algorithm adopted is also presented.

Chapter 3
Process Modelling of a Micro Gas Turbine

In this chapter, the thermodynamic analysis of the ideal and real Brayton cycle is presented. The model of the MGT is developed in Aspen and tested against the set of the experimental data. Further, the sensitivity analysis of the MGT model is performed to investigate the performance of the model at varying boundary conditions. In Sections 3.1 and 3.2, the thermodynamics of the MGT will be given. The process description and simulation strategy will be discussed in Section 3.3 and the base case model is developed in Section 3.4. Based on base case model, the model validation is performed in Section 3.5 and the sensitivity analysis will be performed in Section 3.6. Finally, conclusions are drawn in Section 3.7.

3.1 Thermodynamics of the Ideal Cycle

In the simplest gas turbine, the compressed air absorbs heat in the combustion chamber, which expands in the turbine before going to the atmosphere. The ideal Brayton cycle consists of four steady state steps, including two isentropic steps for compression and expansion; while there are two constant pressure steps for heat addition and rejection. In a simple gas turbine, the exhaust gas from the turbine is at a sufficiently high temperature so that energy would be wasted if it were simply vented to the atmosphere. Therefore, it is used to raise the temperature of the compressed air before the combustor in order to reduce the specific fuel consumption. This is usually achieved by employing a heat exchanger, in the form of a recuperator/regenerator, to preheat the compressor air by the hot exhaust of the turbine. Even after this, the gas turbine exhaust still has sufficient energy from which heat can be extracted and used as a means of producing steam, or as a heat source for the heating and chilling requirements. The maximum amount of the extractable energy depends on the dew point of the sulphur compounds in the flue gas; which are acidic in nature, and it is best to avoid condensation of them in order to reduce corrosion problems in the heat extractors and exhaust ducts. The thermodynamic details of the Brayton cycle are summarized in Figure 2.10. They

consist of the isentropic compression of the air from step 1 to step 2, the preheating of the air from step 2 to 3, the heat addition to the air at constant pressure in the combustor from step 3 to 4, the isentropic expansion in the turbine from step 4 to 5, the heat extraction step is shown from 6 to 7, and the heat rejection at constant pressure from step 7 to back step 1, which completes the closed cycle.

3.2 Thermodynamics of the Real Gas Turbine Cycle

The real gas turbine cycle is an 'open' cycle rather than a 'closed' cycle, and the composition of the working fluid changes during its movement through the cycle due to the combustion reactions in the combustion chamber. The compression and expansion processes are irreversibly adiabatic, and therefore this result in an increase in the entropy, and more compression work is required to overcome the fluid friction. The performance of the real open cycle is expressed or judged by knowing the compressor inlet temperature, turbine inlet temperature and fuel consumption by incorporating the fuel/air ratio and the combustion efficiency [52, 114]. Therefore the losses must be incorporated in the components of the real gas turbine cycle in order to judge the actual performance of the system. The thermodynamic analysis of the compressor and the turbine, in the context of the real cycle and incorporating the isentropic compressor and turbine efficiency, will yield a performance that is close to the actual one [114]. The isentropic compressor efficiency is given by [113-115]:

$$\eta_c = \frac{W_{c\_i}}{W_{c\_a}} = \frac{T_{2\_i} - T_1}{T_2 - T_1} \tag{3.1}$$

where η is the efficiency, w is the net amount of energy transfer in terms of work and T is the temperature. The subscripts "c" indicates the compressor, "i" indicates the isentropic process, "a" indicates the actual process, "1" indicates the inlet of the compressor and "2" indicates the outlet of the compressor.

The isentropic turbine efficiency is given by [113-115]:

$$\eta_t = \frac{W_{t\_a}}{W_{t\_i}} = \frac{T_4 - T_5}{T_{4\_i} - T_5} \tag{3.2}$$

where subscripts "t" indicates the turbine/expander, "4" indicates the inlet of the turbine and "5" indicates the outlet of the turbine.

Using the above definitions, the actual work and the actual efficiency of the turbine cycle is given by [114]:

$$\text{Cycle Work} = W_a = W_{t\_a} - W_{c\_a} \tag{3.3}$$

$$W_a = c_p T_1 \left[\eta_t \frac{T_4}{T_1}\left(1 - \frac{1}{r^{\frac{\gamma-1}{\gamma}}}\right) - \frac{1}{\eta_c}\left(r^{\frac{\gamma-1}{\gamma}} - 1\right)\right] \tag{3.4}$$

$$\eta_a = \frac{\eta_t \frac{T_4}{T_1}\left(1 - \frac{1}{r^{\frac{\gamma-1}{\gamma}}}\right) - \frac{1}{\eta_c}\left(r^{\frac{\gamma-1}{\gamma}} - 1\right)}{\alpha - \frac{1}{\eta_c}\left(r^{\frac{\gamma-1}{\gamma}} - 1\right) - 1} \tag{3.5}$$

where c_p is the heat capacity at constant pressure, r is the pressure ratio, γ is the ratio of the heat capacity at constant pressure to the heat capacity at constant volume, α is the ratio of maximum cycle temperature to the minimum cycle temperature.

The overall actual cycle efficiency is mainly dependent on the pressure ratio, maximum and minimum temperature in the cycle and the component isentropic efficiencies. When the pressure ratio is increased, the isentropic compressor efficiency tends to decrease and the isentropic turbine efficiency tends to increase for which the whole system is designed; and this result in an increase in the overall cycle efficiency.

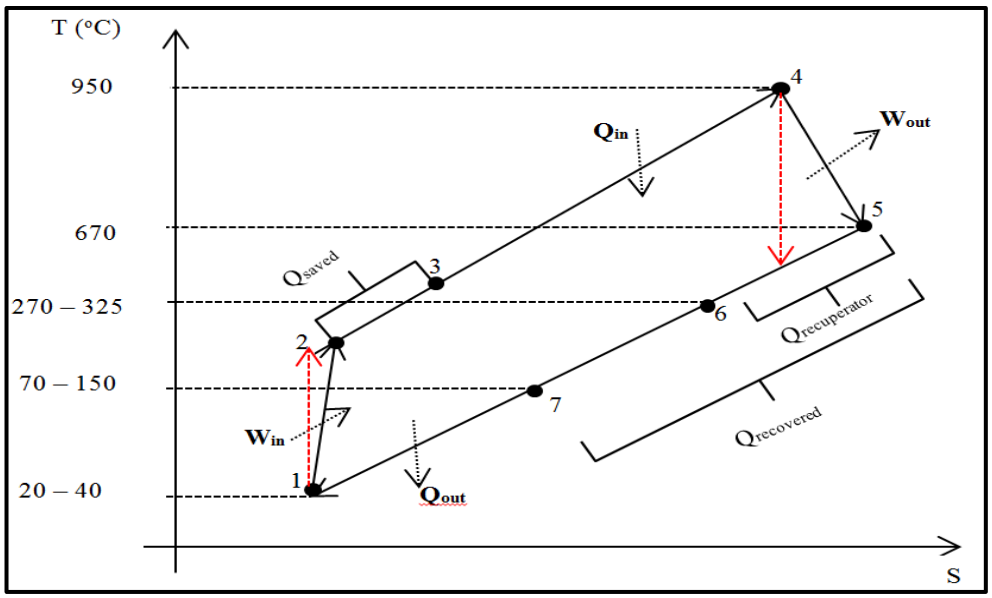

Figure 3.1 A typical T-S diagram for an actual micro gas turbine.

The temperature entropy diagram of the gas turbine is illustrated in Figure 2.10. The compressor is truly isentropic in the ideal case, indicated by the red dashed line, while in an actual system there are loses in the compressor and this is shown by the

black line from point 1 to 2 in Figure 3.1. The process from point 2 to point 3 is the preheating of the compressed air which corresponds to the saving of the heat through recuperating hot exhaust gases from the outlet of the turbine from point 5 to 6. The combustion process causes an increase in the heat content of the gases indicated from point 3 to 4, which drives the turbine from point 4 to 5 and this result in an increase in the entropy as indicated by the black line in contrast to the ideal red dashed line. The section between points 6 and 7 shows the heat recovered in the gas-liquid heat exchanger in combined heat and power (CHP) mode. The section from the points 5 to 7 indicates the heat recovery section either through the air pre-heating in the recuperator which results in the increase in the electrical efficiency or the heat recovery in terms of thermal energy. W_{in} represents the power requirement of the compressor and W_{out} indicates the power produced by the turbine to run the compressor or the generator.

3.3 Process Description and Modelling Strategy

3.3.1 Process Description

The Turbec T100 Series 1 MGT is available at the UKCCS Research Center Pilot-scale Advanced Capture Technology (PACT) National Core Facilities located in Sheffield, UK. The PACT has two MGT's of Turbec; Series 1 and Series 3 which can be coupled with the on-site pilot-scale post-combustion CO_2 capture plant, explored in Chapter 6. The Series 1 MGT at PACT is used for the number of experiments including, base line, CO_2 injection, steam injection and simultaneous injection. The Turbec MGT is a combined heat and power machine with a capability of 100 kW_e of electrical power and 165 kW_{th} of thermal power. The MGT compromises a centrifugal compressor, a radial turbine and a high speed generator, all mounted on the same shaft. The lean premixed emission type combustor is fired with natural gas, and this result in low NO_x, CO and UHC. There are two heat exchangers in the MGT to enhance either the electrical or total efficiency of the MGT. The first heat exchanger is a recuperator, which preheats the compressed air before injecting it to the combustor using the hot exhaust gases from the turbine, and the second heat exchanger is a gas-liquid heat exchanger to generate thermal power by heating the circulated water. The configuration of the MGT components is shown in Figure 3.2. The air at ambient conditions of the temperature and the pressure is

compressed to a pressure ratio of 4.5:1 through the compressor, and then passed through the recuperator for preheating through the exhaust gases of the turbine. The preheated compressed air is mixed and combusted with the natural gas in the combustor. The combustion products at a turbine inlet temperature (TIT) 950 ^{o}C expands through the turbine with the turbine outlet temperature (TOT) to remain fixed at 650 ^{o}C and at near atmospheric pressure.

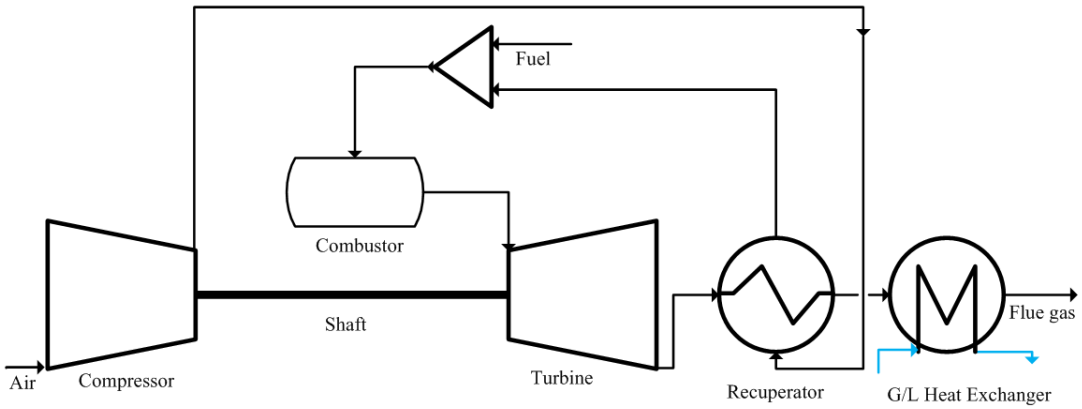

Figure 3.2 Schematic of the Turbec T100 PH combined heat and power micro gas turbine at the PACT Core facility.

Thus, the turbine drives both the compressor and the generator as all are on the same shaft. The exhaust gases pass through the recuperator which boosts the electrical efficiency by preheating the compressed air. Then, the exhaust gases are used to generate the thermal energy by heating the water in the counter-current gas-liquid heat exchanger.

Table 3.1 Natural gas composition for the base case model and its calorific value.

Component	Mole Percentage
CH_4	90.6
C_2H_6	5.1
C_3H_8	1.3
i-C_4H_{10}	0.2
n-C_4H_{10}	0.2
CO_2	1.4
N_2	1.1
Net Calorific Value [kJ/mol]	897.3

Table 3.2 Air composition.

Component	Mole Percentage
N_2	77.3
O_2	20.7
Ar	0.9
CO_2	0.03
H_2O (relative humidity, %)	60

3.3.2 Process Modelling Strategy

The combined heat and power model of the MGT is developed in Aspen. The components of the MGT model are shown in Figure 3.2 which is a schematic of the micro gas turbine. The major model components include the compressor, turbine, reactor, heat exchangers, mixer and splitter. The property package for the estimation of the thermodynamic properties is the Peng-Robinson equation of state. The minimization of the total Gibbs free energy is used as a criterion for the chemical equilibrium in the combustor to estimate the composition of the components of the flue gas. The model is capable of estimating minor species, including carbon monoxide, sulphur dioxide, as well as nitrogen based species, such as nitrogen dioxide, nitrous oxide and nitric oxide. The MGT model is developed in two forms, namely the simplified model and the detailed model. In the simplified MGT model, the efficiency of the compressor and turbine are fixed. Using the equations (3.1) and (3.2), the isentropic efficiency of the compressor and the turbine can be readily estimated. The turbine isentropic efficiency is estimated as 80% while the compressor isentropic efficiency is 75%.

Further, either the compressor outlet temperature or pressure is specified to model the compressor of the MGT. In addition, the simplified MGT model uses the fuel and air inlet conditions and TOT to estimate the performance of the MGT. In the detailed MGT model, the compressor and turbine maps are implemented into the model and the details of the characteristic maps are given in Section 3.3.2.1. The model uses as input parameters the fuel and air inlet conditions and TOT, along with the rotational speed specifications for the compressor and turbine to interpret other variables from the characteristics maps and to estimate the performance of the MGT.

3.3.2.1 Characteristic Maps*

Characteristic maps indicate the performance of the machine in terms of the mass flow rate, pressure ratio or head and isentropic efficiency at various rotational speed levels of the machine. These are available for the Series 2 of the Turbec T100 series, and are incorporated into the MGT model. Due to the same operating conditions and design dimensions of Series 2 of the MGT, the performance maps are applied to the

---

* Professor Mohsen Assadi, University of Stavanger, Norway is acknowledged for providing characteristics maps for the Turbec Series 2 micro gas turbine.

Series 1 of the MGT and may introduce the level of uncertainty in the estimated results. They assist in the estimation of the isentropic efficiency in the MGT model for each operating point, by specifying either the rotational speed or the pressure ratio of the MGT while the other parameters are estimated. They are mostly presented in terms of the non-dimensional and corrected parameters, which assist in the reduction of the number of variables required to specify the operating point of the system. These corrected parameters can be converted to the normal one by the following equations [52, 53, 179, 180]:

$$N_{cr} = \frac{N}{\theta} \tag{3.6}$$

$$\dot{m}_{in,cr} = \frac{\dot{m}_{in}\sqrt{\theta}}{\delta} \tag{3.7}$$

where N is the rotational speed, $\dot{m}$ is the mass flow rate, θ is the temperature ratio defined by equation (3.8) and δ is the pressure ratio defined by equation (3.9). The subscript "cr" indicates the corrected values of the parameter, and "in" indicates the parameter at the inlet of the compressor.

$$\theta = \frac{T_{in}}{T_{ref}} \tag{3.8}$$

$$\delta = \frac{P_{in}}{P_{ref}} \tag{3.9}$$

where T is the temperature, P is the pressure and the subscript "ref" indicates the reference condition which depends on the vendor specification. The performance maps are shown in Figure A. 1 of the Appendix A. The axes' labels for the performance maps are not shown for confidentiality reasons. More details of the performance maps can be found in [181, 182]. However, Aspen uses the head in terms of the pressure ratio for the inclusion of the characteristic maps into the model. The pressure ratio is converted into the head, by the following equation:

$$H' = \frac{\gamma}{\gamma-1} zRT_{in}\left[\left(\frac{P_{out}}{P_{in}}\right)^{\frac{\gamma-1}{\gamma}} - 1\right] \tag{3.10}$$

where H' is the head, the amount of energy required to boost the gas from one pressure level, P_{in} to a higher pressure level, P_{out}; γ is the ratio of the specific heats (c_p/c_v); c_p is the specific heat at constant pressure; c_v is the specific heat at constant volume; z is the compressibility factor; R is the universal gas constant. In addition,

linear interpolation or extrapolation is selected in the software to estimate the data points other than the inputs. Furthermore, to take into account the changing gas properties along the gas turbine path, the three methods available in Aspen are:

- Schultz method [183].
- Huntington method [184].
- Reference/Direct Integration method [184]

By default, the Schultz method is adopted, which introduces new variables to take into account the changes in gas properties into the compressor map due to change in temperature, pressure and composition by adding the f factor termed as the Schultz factor. Schultz equation is also used in Turbo compressors - Performance test code Standard of ISO 5389:2005 [185]. In addition to the Schultz method, the effect of the CO_2 injection on the variables of the performance maps is also tested through equations as mentioned in Section A.1 of the Appendix A. The maximum CO_2 injection of 125 kg/h into the MGT as mentioned in Section 4.2 resulted in 0.7, 1.2, 2.6 % deviations in flowrate, rotational speed and pressure ratio, respectively. The lower deviation of the variables of the performance maps allows the author to use them for the modelling. Furthermore, the default Schultz method is selected into the model to take into account the deviation of the performance maps due to the changes in the gas properties.

Due to the operational variations of the MGT such as, CO_2 injection, steam injection and recirculated exhaust gas, the operation of the MGT might be outside the operating envelope of the characteristic maps for both compressor and turbine. As these operational variation results in an imbalance of the shaft, due to the difference in the flow rate through the compressor and turbine section of the MGT, the operating point of the MGT may move away from the surge curve. This deviation can be estimated through the surge margin and is defined by the following equation [186]:

$$\text{Surge margin} = \left[\frac{r_{\text{at surge}}}{r_{\text{operating point}}} - 1\right] \times 100 \qquad (3.11)$$

where r is the pressure ratio at constant flow rate.

Furthermore, the characteristic maps with a change in working fluid, due to CO2 and/or steam injection exhaust gas recirculation or firing biogas, the fundamental principle is will be, the Mach numbers for all the velocity vectors are the same, the

velocity diagrams are uniform and the Reynolds number is constant. Unique flow conditions will be obtained. Each point on the turbomachinery characteristic curve based on these dimensionless groups should represent a unique flow conditions and the new operational point can be identify in a performance map developed for air combustion. A change in the compressor inlet conditions, pressure or temperature, or a change in the working fluid composition and properties results in a different operational point in the compressor and the turbine.

Table 3.3 Assumptions for the base case MGT model.

Parameter	Value
Ambient temperature [^{o}C]	15
Ambient pressure [bar]	1.013
Relative humidity [%]	60
Turbine outlet temperature [^{o}C]	650
Turbine outlet pressure [bar]	1.06
Recuperator effectiveness [%]	90
Combustor pressure drop [bar]	0.15
Heat exchanger pressure drops [bar]	0.06
Generator loss [%]	0.6
G/L heat exchanger water inlet temperature [^{o}C]	50
G/L heat exchanger water outlet temperature [^{o}C]	70
G/L heat exchanger water pressure [bar]	1.013
G/L heat exchanger gas outlet temperature [^{o}C]	55

3.4 Base Case Model

The base case model of the MGT is developed in steady-state at the ISO conditions [187] with the power output 100 kW_e and at the rotational speed 70000 rpm. The composition of the natural gas, along with the net calorific value, is shown in Table 3.1. The composition of the air is shown in Table 3.2 with the relative humidity 60 %. The assumptions used for the modelling of the base case MGT model are given in Table 3.3. The TOT is fixed by varying the fuel flow rate to the inlet of the combustor, and is kept constant at 650 ^{o}C. For the simplified MGT model, the estimated compressor and turbine efficiencies were used which are given in Section 3.3.2. However, for the detailed MGT model, instead of constant isentropic efficiency of the compressor and the turbine, the characteristic maps have been used in the MGT to reduce the number of assumptions that have to be made for the estimation of the isentropic efficiencies of the compressor and the turbine. The maps help in the reduction of the number of variables required to set the degree of freedom of the detailed model to zero, as compared to the simplified model.

Table 3.4 Comparison of the present model with the published MGT models using different process simulation softwares.

	Parente et al. [87]	Kautz and Hansen [188]	Delattin et al. [85]	De Paepe et al. [182]	Majoumerd et al. [109]	Manufacturer Data [189]	Simplified model	Detailed model
Electrical power [kW_e]	101	100	100 KJ/kg	100	100	100	100	100
Thermal output [kW_{th}]	N/A	N/A	N/A	186.7	170	165	153.3	165
Electrical efficiency [%]	27.8	30	30.8	30.7	31	30	32.1	30.2
Overall efficiency [%]	N/A	N/A	N/A	57.3	84	80	81.2	79.9
CO_2 in flue gas [mol%]	N/A	N/A	N/A	N/A	1.6	N/A	1.6	1.6
O_2 in flue gas [mol%]	N/A	N/A	N/A	N/A	N/A	N/A	17.3	17.5
Flue gas flow rate [kg/s]	N/A	0.79	N/A	0.735	0.771	0.80	0.7	0.8
Fuel consumption [kW]	44 MJ/kg	333	0.8	8.13 g/s	321	333	312	331
Rotational speed [rpm]	N/A	N/A	100%	69679	69675	70000	N/A	70000
Pressure ratio	N/A	4.5	4.3	4.6	4.4	4.5	4.5	4.5
Turbine inlet temperature [^oC]	950	950	930	925.4	948	950	945	948
Turbine outlet temperature [^oC]	N/A	650	640	645	650	650	644	645
Compressor discharge temperature [^oC]	N/A	214	N/A	210.1	N/A	N/A	216.9	212.4
Software Used	In-house Code	Aspen Plus	Aspen Plus	Aspen	IPSEpro	N/A	Aspen Hysys	Aspen Hysys

Table 3.5 Performance summary of the MGT base case model at ISO conditions.

Parameter	Manufacturer data [189]	Simplified model results	Detailed model results
Electrical power [kW_e]	100	100	100
Thermal output [kW_{th}]	165	153	165
Electrical efficiency [%]	30	32.1	30.2
Overall efficiency	80	81.2	79.9
CO_2 in flue gas [mol%]	N/A	1.6	1.6
O_2 in flue gas [mol%]	N/A	17.3	17.5
Flue gas flow rate [kg/s]	0.8	0.7	0.8
Fuel consumption [kW]	333	312	331
Rotational speed [rpm]	70000	N/A	70000
Pressure ratio	4.5	4.5	4.5
Turbine inlet temperature [^oC]	950	945	943
Turbine outlet temperature [^oC]	650	644	650

The details of the characteristic maps can be found in Section 3.3.2.1. The base case model results are summarised in Table 3.5 and they are in good agreement with the manufacturer's reference data [189] as indicated in Table 3.5. The electrical efficiency and overall efficiency presented in Table 3.5 can be defined as:

$$\text{Electrical efficiency} = \left(\frac{\text{Electrical power}}{\text{Fuel consumption}}\right) 100 \tag{3.12}$$

$$\text{Overall efficiency} = \left(\frac{\text{Electrical power+thermal output}}{\text{Fuel consumption}}\right) 100 \tag{3.13}$$

The model results for the simplified and detailed cases are presented in order to have a potential comparison of both the cases along with the manufacturer's reference data [189]. The comparison of the simplified and detailed MGT model results is also done with the literature results of the model developed for the MGT through different process modelling tools [85, 87, 109, 110, 181, 182, 188] is also carried out. The comparison of the present model results with the previously published model results are presented in Table 3.4. The results reported by Parente et al. [87], Kautz and Hansen [188] and De Paepe et al. [182] were based on constant efficiency of the compressor and turbine components of the MGT. The performance results reported by Delattin et al. [85] and Majoumerd et al. [109] were based on the characteristic maps of the compressor and turbine. In addition, none of the reported literature have provided the flue gas composition at the exhaust of the MGT except Majoumerd et al. [109] who has reported the CO_2 composition at the exhaust of the MGT.

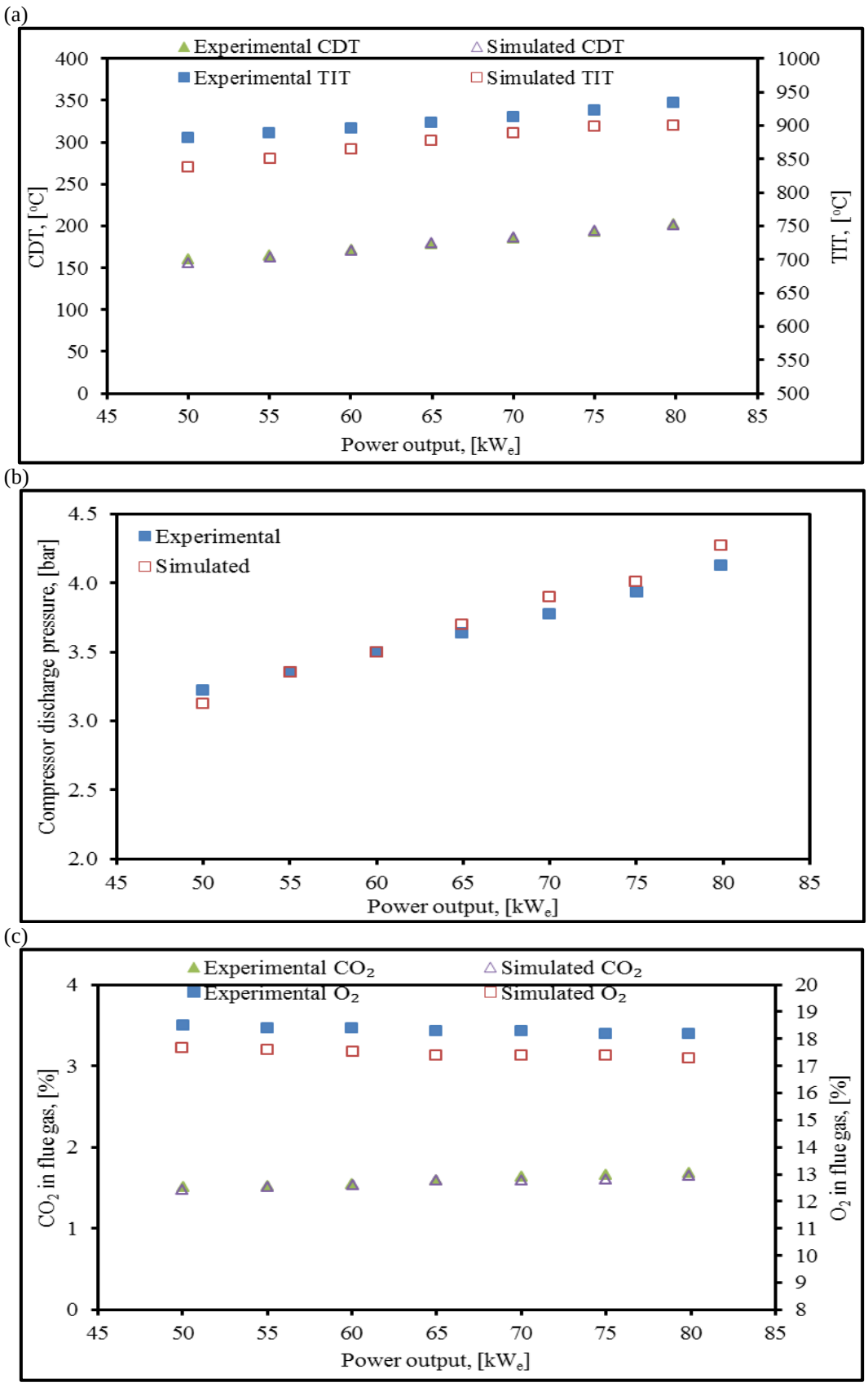

Figure 3.3 Measured and simulated results for MGT (a) Compressor discharge temperature and turbine inlet temperature as a function of power output; (b) Compressor discharge pressure as a function of power output; and (c) CO_2 and O_2 molar composition in the flue gas as a function of power output.

Further, the reported literature has not provided the detailed performance and/or the boundary conditions to reproduce the results and also their results are not fully supported by the extensive experimental data. It is evident from the above discussion that the detailed model predicts performance results closer to the manufacturer reference data. In addition, the detailed model incorporates the characteristics performance maps of the compressor and turbine and thus reducing the number of inputs and hence it is chosen for further analysis.

3.5 MGT Model Validation

The base case model developed is validated against the set of experimental data obtained for the Turbec T100 Series 1 of the MGT through the PACT core facility and the electrical power output is varied from 50 to 80 kW_e to access different operational modes. The details and methodology of the MGT experiments can be found in the literature [190]. These experimental results are performed with substantial additional instrumentation other than the default instrumentation of the MGT in order to better comprehend the behaviour of the MGT at different power outputs. The modelling is performed for each power output to evaluate the performance for each operational scenario and the results obtained from the modelling are compared with the mean values of the experimentally measured data points. The measured versus modelled results for some of the selected parameters are presented in Figure 3.3. The mean percentage absolute deviation for the model results for all the quantities investigated, such as the compressor discharge temperature (CDT), turbine inlet temperature, compressor discharge pressure, flue gas composition for CO_2 and O_2 and power output, in comparison to the measured values are: 1.02, 3.54, 1.97, 1.75, 4.72 and 0.02 %, respectively. As the combustor calculation is based on the minimization of Gibbs free energy rather than kinetics, this result in higher deviations of the turbine inlet temperature. Further, the large deviations of the H_2O composition in the flue gas may be due to condensation of H_2O during the measurement. The tabulated measured and simulated results are presented in Table A.1 and Table A.2 of Appendix A. Figure 3.3 shows that the model results are in good agreement with the experimental data.

The model developed is robust enough to be extended for further analysis and case studies. The model is further tested against the variation of some of the selected parameters by performing a sensitivity analysis in Section 3.6.

3.6 Sensitivity Analysis

The sensitivity analysis provides a useful means to investigate the effect of the process parameters and judge the influence of these parameters on the operation and the performance of the system under investigation. The analysis will provide a reliable operating range for the gas turbine system and will assist in the understanding of the process operation of the gas turbine system at both pilot- and commercial- scale. Operational parameters are varied to better analyse and check the process performance and design of the gas turbine system. The effect of the most important process parameters, such as ambient temperature, ambient pressure, relative humidity of the air, recuperator effectiveness and fuel type or fuel calorific value are varied for a specified range either dictated by a general rule of thumb or observed annually as the atmospheric variation in temperature, pressure and humidity.

Table 3.6 Case studies for the sensitivity analysis of the MGT.

Set No.	Sensitivity Analysis
Set A	Variation of ambient temperature of air ($-20\ ^{o}C \geq T_{amb} \leq 40\ ^{o}C$)
Set B	Variation of ambient pressure of air $0.95\ bar \geq P_{amb} \leq 1.05\ bar$)
Set C	Variation of relative humidity of air ($0 \geq RH \leq 100\ \%$)
Set D	Variation of recuperator effectiveness ($50\ \% \geq \varepsilon \leq 100\ \%$)
Set E	Variation of fuel type (Natural gas, shale gas and bio gas)

The performance parameters are electrical efficiency, compressor discharge temperature and turbine inlet temperature, on which the effect of the aforementioned parameters is checked. Therefore, in total 5 sets of sensitivity analysis case studies are performed and their classification along with the ranges of the variables in which they are varied, is given in Table 3.6. All the case studies are performed for a constant power output of 100 kW_e and the conditions for the 100 kW_e base case are the same as that explored in Section 3.4.

The reported literature lacks an extensive sensitivity analysis of the ambient conditions on the performance and operation of the MGT. Further, only a few

studies can be found in the literature which have evaluated the effect of the ambient temperature alone on the performance of the MGT. Hosseinalipour et al. [191] have reported the effect of the ambient temperature on the turbine inlet temperature and fuel flow variation for the MGT. Jun et al. [77] have reported the variation of the ambient temperature and its effect on the performance of the MGT and as a remedy for its effect, the steam and hot water injection to the MGT is analysed. Further, the effect of the ambient temperature on the MGT, humidified MGT and exhaust gas recirculated MGT in the range of -5 ^{o}C to 35 ^{o}C can be found [109, 110]. Nikpey et al. [181] have reported the effect of the ambient temperature on the performance of the natural gas- and bio gas- fired MGT.

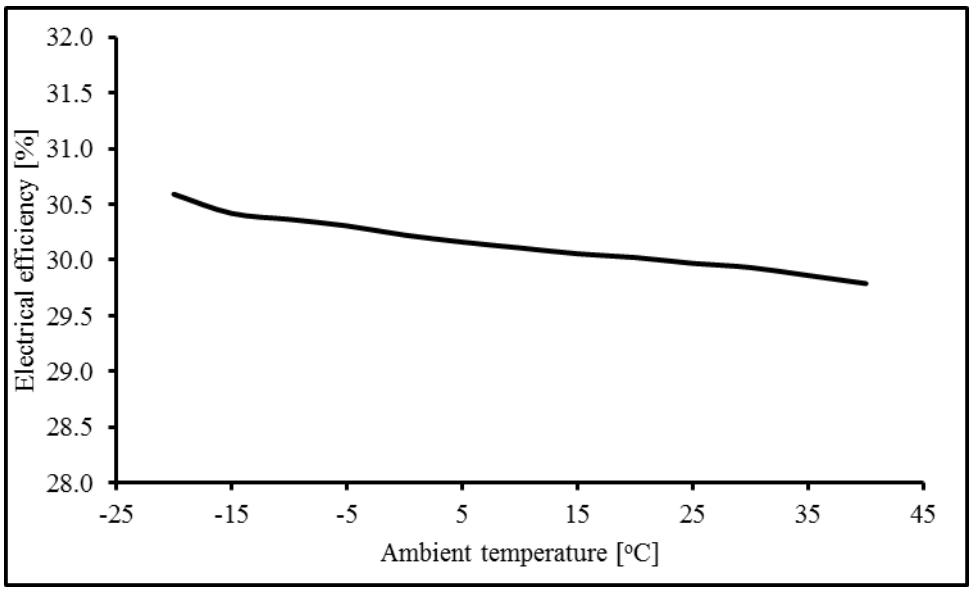

Figure 3.4 The variation of the electrical efficiency of the MGT as a function of the ambient temperature of the air, at fixed ambient pressure of the air 1.013 bar, relative humidity of the air 60 %, recuperator effectiveness 90 % and fuel type natural gas.

3.6.1 Variation of the ambient temperature of air – Set A

The ambient temperature of the air is varied from -20 to 40 ^{o}C, and the other parameters such as the ambient pressure of air 1.013 bar, the relative humidity of air 60 %, the recuperator effectiveness 90 % and the fuel type natural gas are maintained. The composition of the air is shown in Table 3.2. With the increase in the ambient temperature of the air the electrical efficiency decreases. The effect of the ambient temperature on the electrical efficiency of the MGT is shown in Figure 3.4. With the increase in the ambient temperature entering the suction side of the compressor of the MGT, the specific volume reduces which results in a smaller flowrate flowing through the MGT cycle, thus resulting in less power output. As the

MGT is constant power machine, and to keep the power constant at 100 kW_e, the fuel flowrate increases and hence the electrical efficiency decreases. Hence, the MGT operation in geographical regions with higher ambient temperature will result in higher fuel requirements and lower efficiency.

The effect of the variation of the ambient temperature of the MGT on the compressor discharge temperature and the turbine inlet temperature is shown in Figure 3.5. With the increase of the fuel requirement due to the higher ambient temperature of the inlet air, the turbine inlet temperature increases.

Further, with the increase of the ambient temperature, the density of the air decreases which means there will be less mass flowing through the compressor. Hence, the compressor needs to do more work to push the same air as that required in the system, thus resulting in a higher compressor discharge temperature.

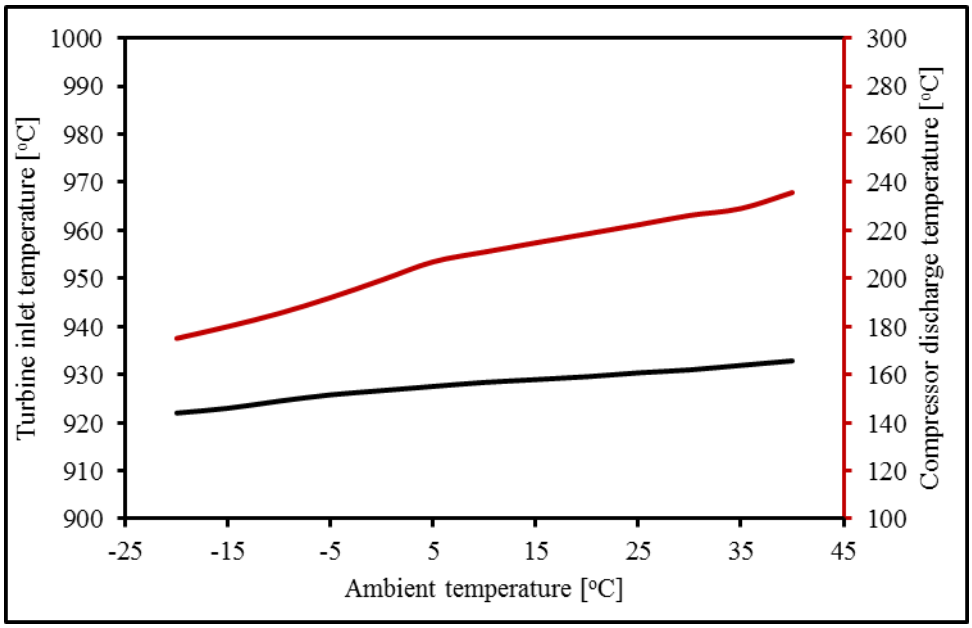

Figure 3.5 The variation of the turbine inlet temperature and compressor discharge temperature of the MGT as a function of the ambient temperature of the air, at fixed ambient pressure of the air 1.013 bar, relative humidity of the air 60 %, recuperator effectiveness 90 % and fuel type natural gas.

3.6.2 Variation of the ambient pressure of air – Set B

The ambient pressure of the air is varied from 0.95 to 1.05 bar, and the other parameters such as the ambient temperature of the air 15 ^{o}C, the relative humidity of the air 60 %, the recuperator effectiveness 90 % and the fuel type natural gas are maintained. The range of the ambient pressure variation of the inlet air is chosen based on the minimum and maximum ambient pressure observed during the year

2015 from January 1 to December 31 as measured by the National Physical Laboratory, UK. The trend of the ambient pressure of the air is shown in Figure 3.6.

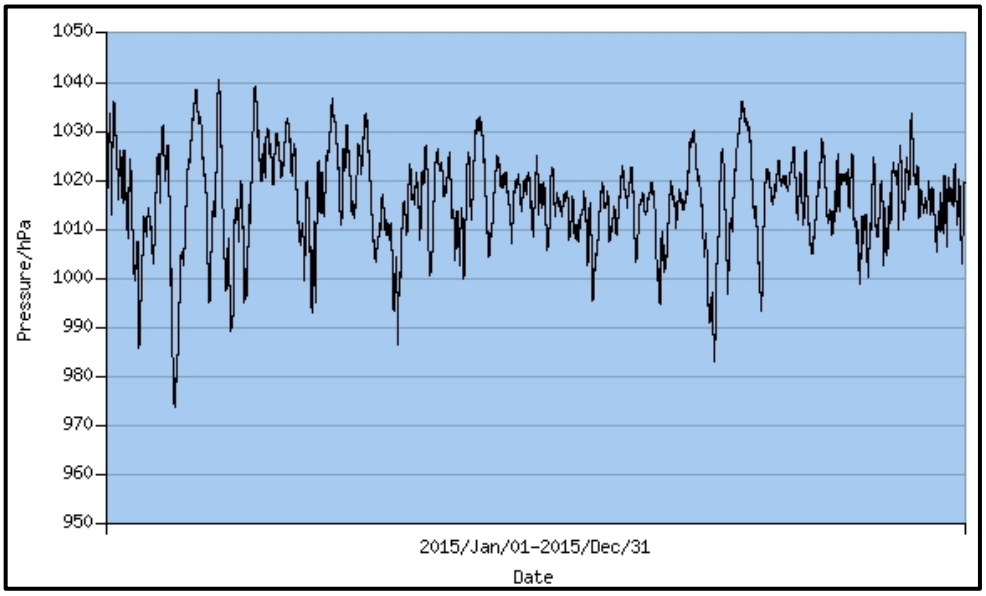

Figure 3.6 Variation of the ambient pressure of the air during January 1 to December 31, 2015 measured by National Physical Laboratory, UK. (Source: http://resource.npl.co.uk/pressure/pressure.html)

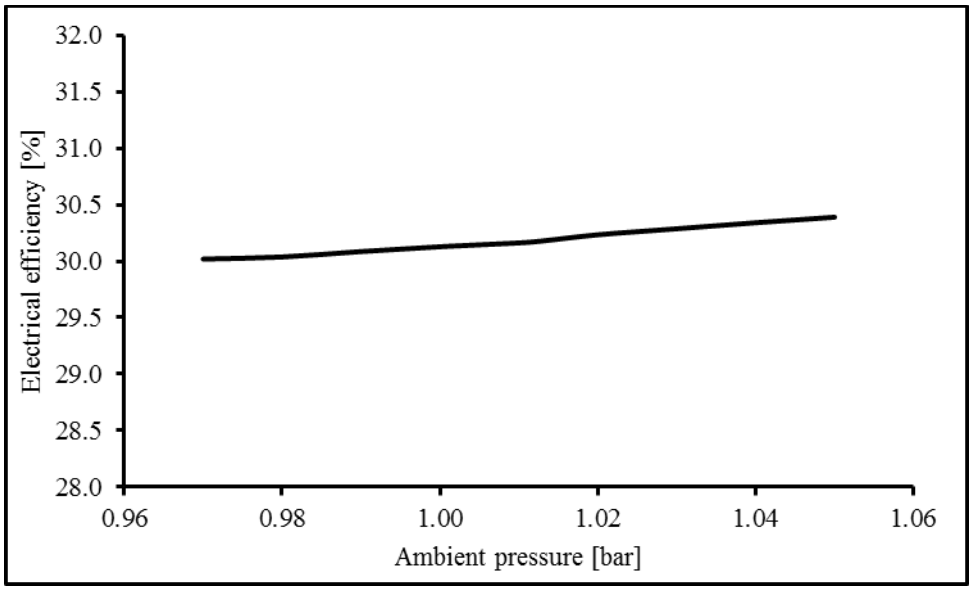

Figure 3.7 The variation of the electrical efficiency of the MGT as a function of the ambient pressure of the air, at fixed ambient temperature of the air 15 ^{o}C, relative humidity of the air 60 %, recuperator effectiveness 90 % and fuel type natural gas.

With the increase in the ambient pressure of the inlet air, the required pressure ratio decreases and hence the compressor has to work less which results in more power output from the MGT. Since the MGT is a constant power machine, and to keep the power output fixed at 100 kW_e, the fuel intake decreases. The decreased fuel flow rate results in increased electrical efficiency at the higher ambient pressure of the inlet air.

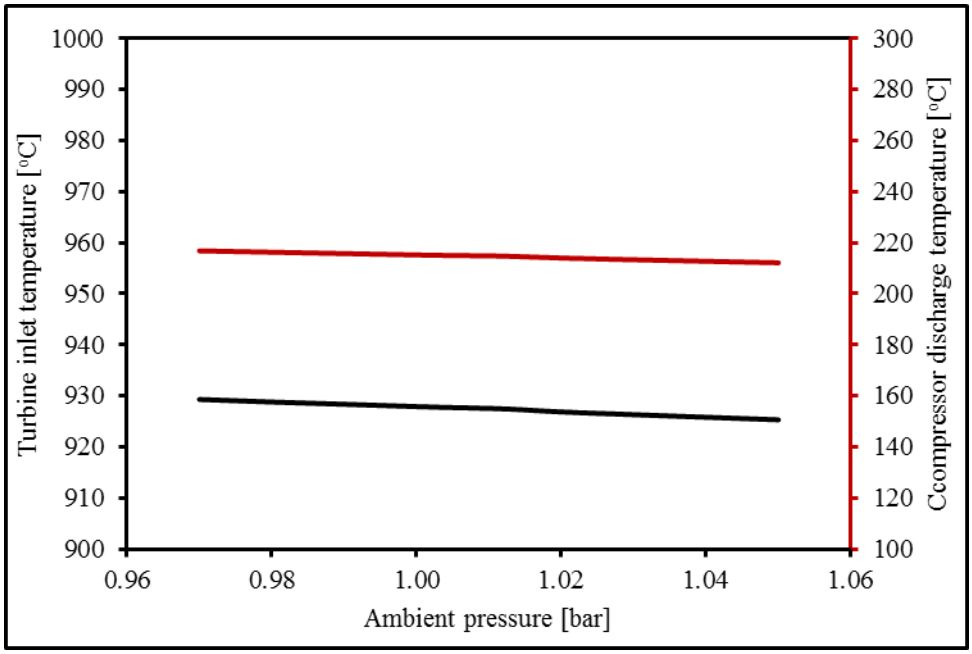

Figure 3.8 The variation of the turbine inlet temperature and compressor discharge temperature of the MGT as a function of the ambient pressure of the air, at fixed ambient temperature of the air 15 ^{o}C, relative humidity of the air 60 %, recuperator effectiveness 90 % and fuel type natural gas.

The effect of the variation of the ambient pressure of the inlet air is shown in Figure 3.7.As stated, due to the higher ambient pressure, the pressure ratio decreases, which results in lower compressor work and hence the compressor discharge temperature decreases. The effect of the variation of the ambient pressure of the inlet air is shown in Figure 3.8. A similar trend in the compressor discharge temperature is observed for the turbine inlet temperature due to the variation of the ambient pressure of the inlet air. Due the low fuel requirements at higher ambient pressure in the combustor of the MGT, the turbine inlet temperature decreases. The effect of the ambient pressure of the inlet air on the turbine inlet temperature is shown in Figure 3.8.

3.6.3 Variation of the relative humidity of the air – Set C

The relative humidity of the air is varied from 0 to 100 %, and the other parameters such as the ambient temperature of the air 15 ^{o}C, the ambient pressure of the air 1.013 bar, the recuperator effectiveness 90 % and the fuel type natural gas are maintained. The relative humidity defines the water content carried by the inlet air. The water content is varied from 0 to 1.66 mol% of the inlet air defining the relative humidity of the air from 0 to 100 %, respectively. The variation of the water content in the inlet air as a function of the relative humidity of the air is shown in Figure 3.9.

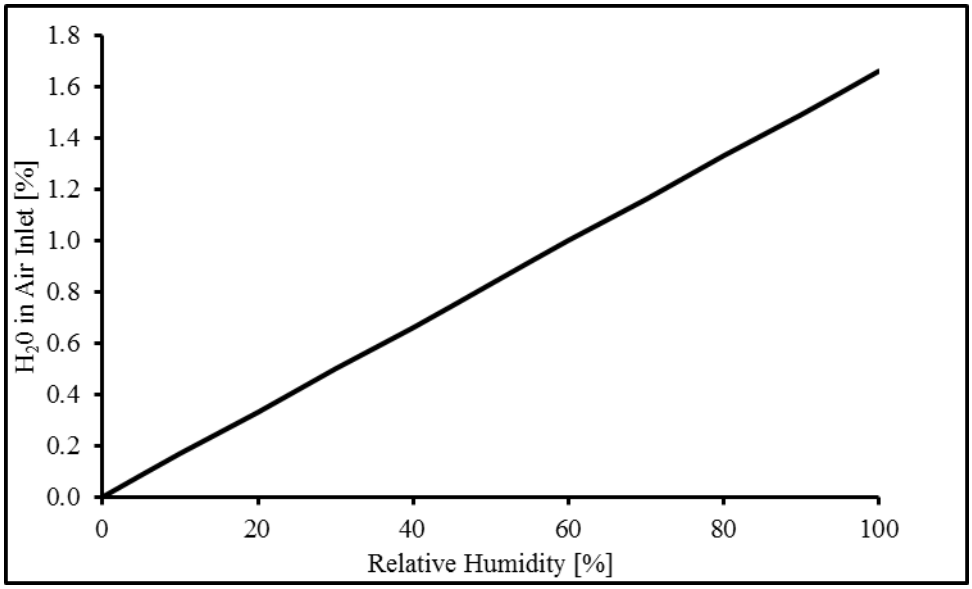

Figure 3.9 The variation of the H_2O content as mole fraction in the inlet air as a function of the relative humidity of the inlet air.

With the increase of the relative humidity the density decreases and the specific volume increases, which results in more compression work and less power output from the MGT. In order to keep the power output constant at 100 kW_e, more fuel is drawn which decreases the electrical efficiency of the MGT. However, the effect on the electrical efficiency is minimal due to the variation of the relative humidity of the air. The effect of the relative humidity of the inlet air on the electrical efficiency is given in Figure 3.10.

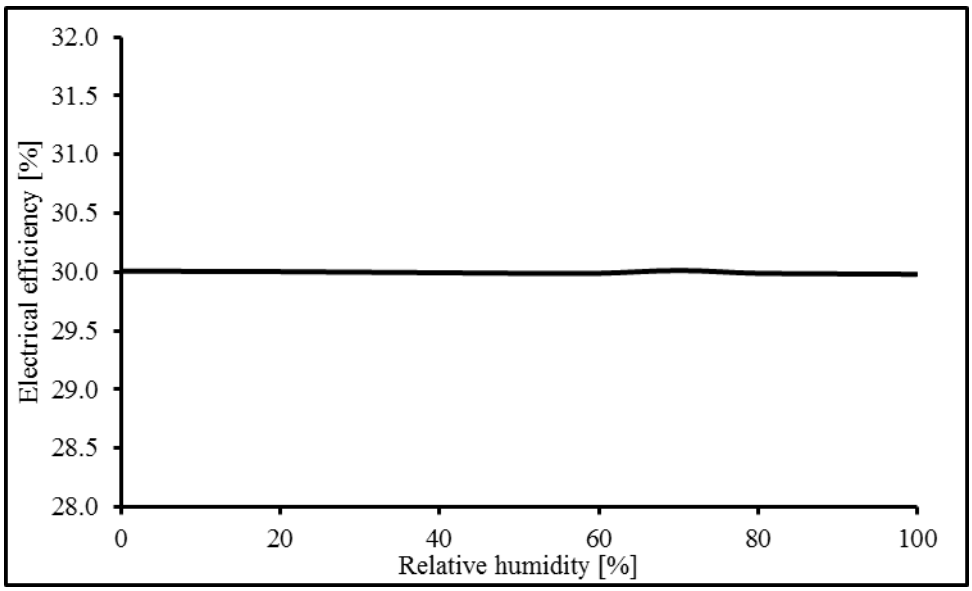

Figure 3.10 The variation of the electrical efficiency of the MGT as a function of the relative humidity of the air, at fixed ambient temperature of the air 15 ^oC, ambient pressure of the air 1.013 bar, recuperator effectiveness 90 % and fuel type natural gas.

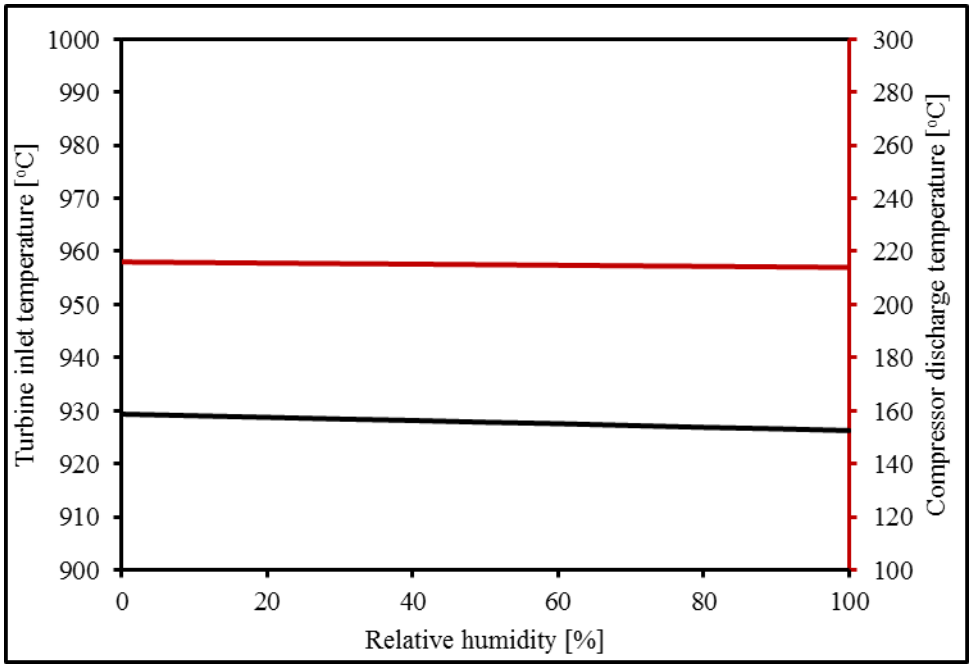

Figure 3.11 The variation of the turbine inlet temperature and compressor discharge temperature of the MGT as a function of the relative humidity of the air, at fixed ambient temperature of the air 15 °C, ambient pressure of the air 1.013 bar, recuperator effectiveness 90 % and fuel type natural gas.

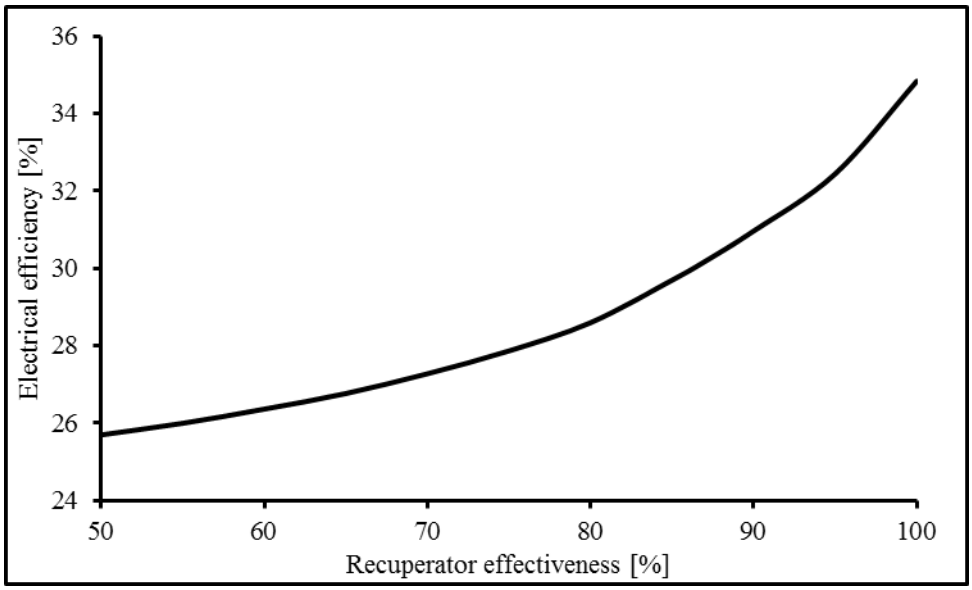

Figure 3.12 The variation of the electrical efficiency of the MGT as a function of the recuperator effectiveness, at fixed ambient temperature of the air 15 °C, ambient pressure of the air 1.013 bar, relative humidity of the air 60 % and fuel type natural gas.

Similarly, the compressor discharge temperature and turbine inlet temperature remain unaffected by the variation of the relative humidity of the air. The effect of the relative humidity on the compressor discharge temperature and turbine inlet temperature is shown in Figure 3.11. There is a small decrease observed which is, as stated earlier, due to the water content which affects the density of the inlet air.

3.6.4. Variation of the recuperator effectiveness – Set D

The recuperator effectiveness is varied from 50 to 100 %, and the other parameters such as the ambient temperature of the air 15 ^{o}C, the ambient pressure of the air 1.013 bar, the relative humidity of the air 60 % and the fuel type natural gas are maintained. Recuperator effectiveness defines the heat transfer from the flue gas exiting the turbine to the air exiting the compressor.

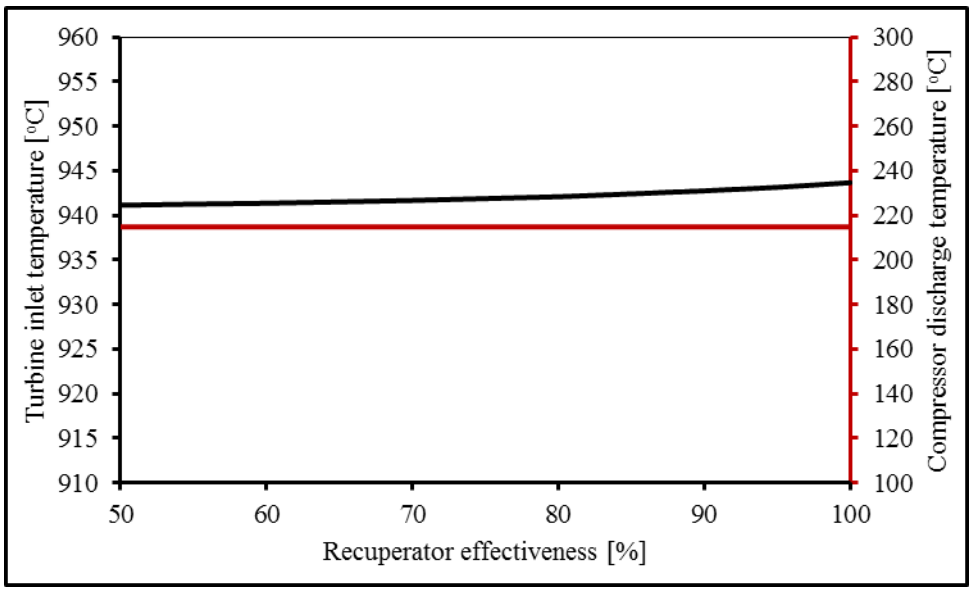

Figure 3.13 The variation of the turbine inlet temperature and compressor discharge temperature of the MGT as a function of the recuperator effectiveness, at fixed ambient temperature of the air 15 ^{o}C, ambient pressure of the air 1.013 bar, relative humidity of the air 60 % and fuel type natural gas.

This results in the pre-heating of the air before it enters the combustor and hence increases the electrical efficiency of the MGT. The higher is the recuperator effectiveness, the hotter will be the air entering the combustor and the higher will be the electrical efficiency of the MGT. The decrease in the recuperator effectiveness defines the ageing, deterioration and erosion of the gas-gas heat exchanger of the MGT. The effect of the recuperator effectiveness on the electrical efficiency of the MGT is shown in Figure 3.12. There is a sharp increase in the electrical efficiency with the increase in the recuperator effectiveness. This increase is due to the more pre-heating of the air, thus reducing the fuel requirement and hence results in the increase in the electrical efficiency of the MGT.

Similarly, due to the more preheating of the incoming air to the combustor, the turbine inlet temperature increases, however, this increase is less pronounced. The effect of the recuperator effectiveness on the turbine inlet temperature of the MGT is

shown in Figure 3.13. However, the compressor discharge temperature remains unaffected since the recuperator is downstream of the compressor. The effect of the recuperator effectiveness on the compressor discharge temperature is shown in Figure 3.13.

Table 3.7 Fuel compositions and calorific values for three different types of the gaseous fuels, including natural gas, shale gas and bio gas.

Component	Mole percentage		
	Natural gas	Shale gas [192]	Bio gas [193]
CH_4	90.6	85.0	64.0
C_2H_6	5.1	4.0	0.0
C_3H_8	1.3	1.0	0.0
i-C_4H_{10}	0.2	0.0	0.0
n-C_4H_{10}	0.2	0.0	0.0
CO_2	1.4	3.0	34.5
N_2	1.1	7.0	1.0
NH_3 [ppmv]	0.0	0.0	100
H_2S [ppmv]	0.0	0.0	4000
Net Calorific Value [MJ/kg]	50.34	40.94	19.87

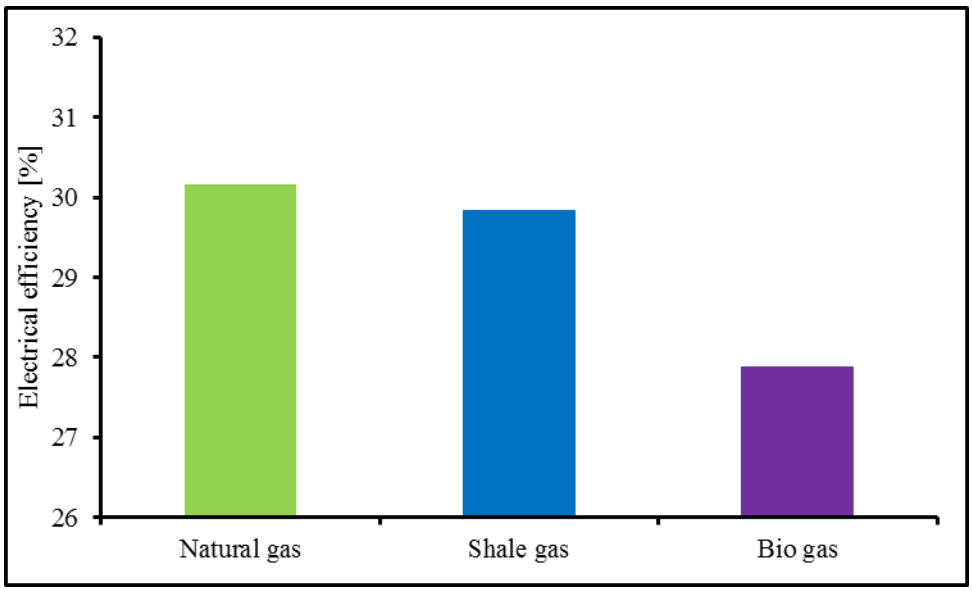

Figure 3.14 The variation of the electrical efficiency of the MGT as a function of the fuel type, at fixed ambient temperature of the air 15 ^{o}C, ambient pressure of the air 1.013 bar, relative humidity of the air 60 % and recuperator effectiveness 90 %.

3.6.5 Variation of the fuel type – Set E

The fuel type is varied from natural gas to shale gas and bio gas, and the other parameters such as the ambient temperature of the air 15 ^{o}C, the ambient pressure of the air 1.013 bar, the relative humidity of the air 60 % and the recuperator effectiveness 90 % are maintained. The molar composition of the three different fuel

types studied, such as natural gas, shale gas and bio gas, and the calorific values are given in Table 3.7. The shale gas results in 6.3 % and bio gas in 29.4 % decrease of the methane content of the fuel in comparison to natural gas. In addition, the CO_2 content increases by 118.6 and 2411 % in shale and bio gas, respectively in comparison to natural gas.

Further, the shale and bio gas results in 18.7 and 60.5 % decrease in the net calorific value of the fuel in comparison to the natural gas. The effect of the fuel type on the electrical efficiency of the MGT is shown in Figure 3.14. The change in fuel type results in a drop in efficiency by 1.1 and 7.6 % for shale and bio gas, respectively in comparison to natural gas. This drop in electrical efficiency was expected as shale and bio gas has a lower calorific value as already stated.

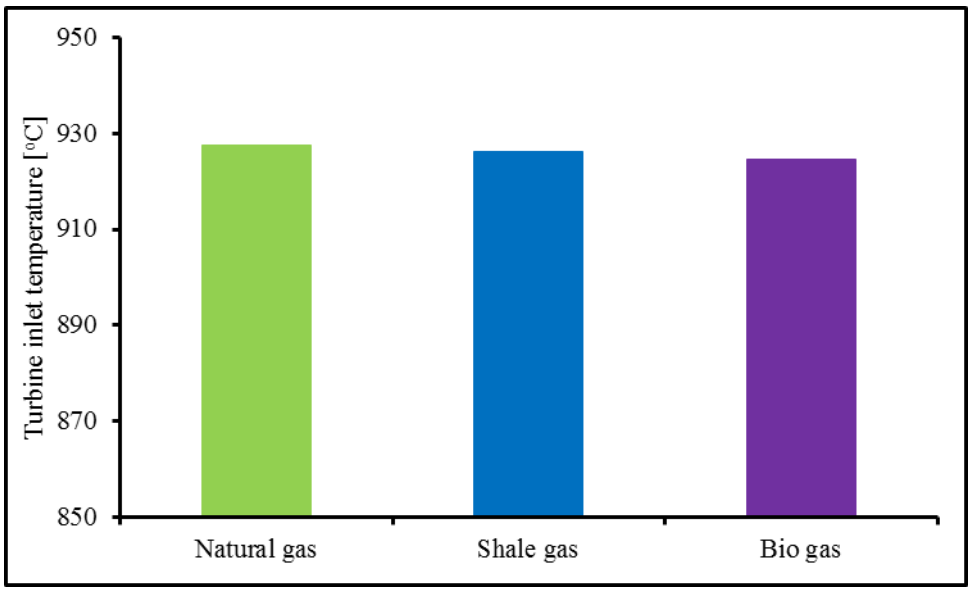

Figure 3.15 The variation of the turbine inlet temperature of the MGT as a function of the fuel type, at fixed ambient temperature of the air 15 °C, ambient pressure of the air 1.013 bar, relative humidity of the air 60 % and recuperator effectiveness 90 %.

Similarly, the turbine inlet temperature decreases by 0.2 and 0.3 % for shale and bio gas, respectively in comparison to natural gas. The effect of the fuel type on the turbine inlet temperature of the MGT is shown in Figure 3.15. The small decrease is due to the constant turbine outlet temperature and the system adjusts itself to attain the required turbine outlet temperature by varying the fuel and air requirements. Also, the compressor discharge temperature decrease is observed when the fuel type is changed. The compressor discharge temperature decreases by 6.5 and 12.1 % for the shale and bio gas, respectively, in comparison to natural gas. This decrease is

observed due to the varying air flow rate through the compressor. The effect of the fuel type on the compressor discharge temperature is shown in Figure 3.16.

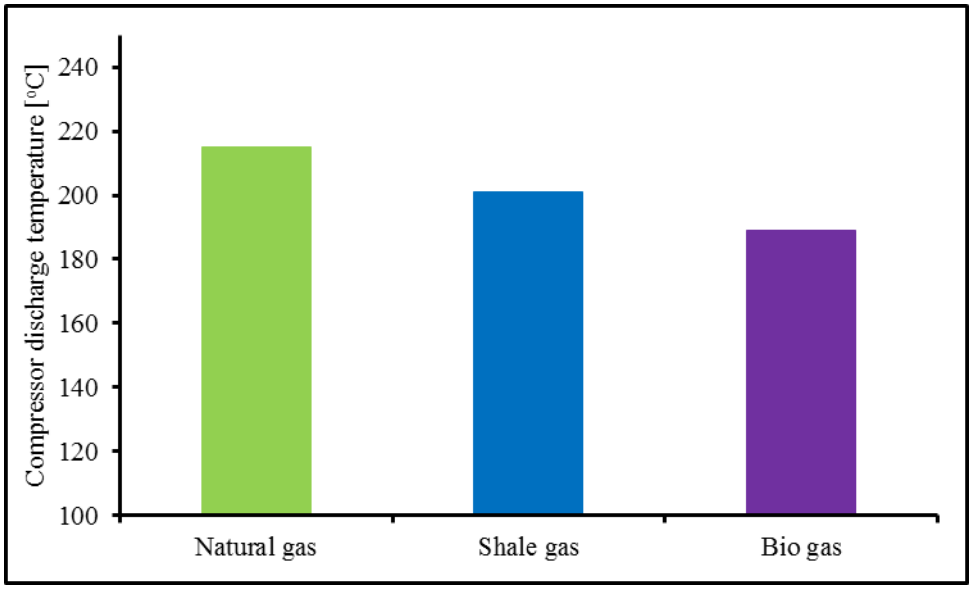

Figure 3.16 The variation of the compressor discharge temperature of the MGT as a function of the fuel type, at fixed ambient temperature of the air 15 ^{o}C, ambient pressure of the air 1.013 bar, relative humidity of the air 60 % and recuperator effectiveness 90 %.

3.7 Conclusions

- The process system analysis assists in the better understanding of the process details of the system under consideration. The detailed analysis, modelling and simulation results in an accurate demonstration for the evaluation of the recuperated CHP micro gas turbine.
- The characteristic maps of the compressor and turbine when included into the MGT model, increases the robustness of the model. Also it results in fewer assumptions and boundary condition specifications in comparison to the model based on the estimated compressor and turbine efficiencies.
- The detailed model validated against an extensive set of part load conditions indicates that the model robustness for its modifications to the base case MGT. The mean percent absolute deviation of the model predicted results, in comparison to the experimental reported results for selected parameters, such as CDT, TIT, CDP, CO_2 molar composition in flue gas and power output are: 1.02, 3.54, 1.97, 1.75 and 0.02 %, respectively.
- The sensitivity analysis indicates that the behaviour of the MGT is affected by the ambient conditions of the air in terms of the ambient temperature,

ambient pressure, and relative humidity; recuperator effectiveness; and/or the type of the fuel.

- The electrical efficiency of the MGT increases at the lower ambient temperature, at higher ambient pressure, at lower humidity of the air. Further, the higher the effectiveness of the recuperator and the heating value of the fuel, higher will be efficiency of the MGT.

In the next Chapter 4, the MGT model is extended to model the exhaust gas recirculation to the MGT and to analyse its performance. In addition, the sensitivity of the MGT-EGR model is performed to optimize the location and operating conditions of the recycled stream. Further, the MGT model is tested and validated against experimental data at different part-load conditions in which the CO_2 is injected at the compressor inlet of the MGT to simulate the real EGR system.

Chapter 4
Effect of CO_2 Enhancement on the Performance of a Micro Gas Turbine

In this chapter, the MGT model developed in Chapter 3 is modified to include the EGR in to the system in order to study the effect of the CO_2 enhancement on the performance of the MGT. The impact of the operating conditions and position of the EGR on the performance of a MGT is also assessed. Further, the MGT model is tested against experimental data for CO_2 injection at the compressor inlet of the MGT at different part load conditions.

4.1 Introduction

Exhaust gas recirculation (EGR) is an innovative mode of gas turbine operation in which the exhaust gas is split: one part being emitted while the other part is dried before being recirculated to the gas turbine inlet. The benefits of EGR are a decreased flow rate with higher concentration of CO_2 in the exhaust gas, which results in a decreased energy penalty when integrated with a CO_2 capture system. The specific flue gas flow rate of the gas turbine system are much higher in the range of 1.5 kg/MW in comparison to a steam boiler system 0.95 kg/MW and the EGR can considerably reduce the flue gas flow rate resulting in a lower load on the amine-based carbon capture system when integrated [100]. The decrease in the mass flow can be accounted for by the changing temperature at the compressor inlet as the recycled stream is at the higher temperature, and to achieve the same combustor temperatures, lower cooler air is required [104]. The application of the EGR results in an increased MACH number at the inlet and outlet tips of the compressor rotor due to the changes in the thermodynamic properties of the fluid stream [100]. However, this increase will not pose severe issues to the turbo machinery [166]. In addition, the increase in the CO_2 concentration in the working stream of the gas

turbine, due to the EGR, results in the change of the thermodynamic properties of the fluid stream, both in the turbo machinery and the combustion section of the gas turbine. Further, in spite of the these advantages, the EGR cycle has various technical problems, including the maximum amount of the exhaust gas to be recirculated, for maintaining the required level of flame stability, UHC and CO emissions. Moreover, the experimentation with a DLN F-class gas turbine combustor shows the stable operation for EGR up to 35 % [91]. From the reported literature [89-92], it is recommended that the O_2 concentration at the combustor inlet should be higher than about 16 % for efficient and stable combustion. Higher levels of UHC and CO are observed at 14 %. Further, modifications recommended in the literature for an EGR applicability include; changes in the premixedness, control system and variation in the design of the pilots for the burners to reach higher levels of the EGR percentage [91]. Technical modifications to the combustor design may result in more oxidant injection or pure oxygen stream with different distribution levels which will result in a higher EGR percentage and much higher CO_2 levels in the flue gas. In addition, the guarantee issues from the gas turbine manufacturers should be the top priority for the safe operation and redesign of the combustor and/or the whole gas turbine structure.

The more detailed literature review can be found in Section 2.1.6.1. Further, the literature reports the varying optimum EGR from 40 to 50 % through different process modelling tools. However, in most of the reported literature the location of the EGR injection back to the MGT is pre-assumed to be the compressor inlet of the MGT. Similarly, the condition of the EGR in terms of the condensation temperature, which in turn defines the dryness of the recycled stream, is still undefined. As a result, most of the reported literature has overlooked the location and operating conditions of the EGR which needs to be defined.

Therefore, due to the limited literature found in this field, more work needs to be done to better understand the thermodynamic performance of EGR for the MGT, along with the effect of the operating conditions and location of the EGR. Studying the behaviour of the MGT along with EGR in full detail is necessary to fully comprehend the optimum performance of the MGT in the innovative mode of the EGR operation.

The EGR cycle is relatively new, especially in the present scenario of targets for reducing CO_2 emissions, and its limits needs to be defined as it results in CO_2 enhancement with reduced flow rate. The change of the fluid nature due to the exhaust gas recycle will affect the stream thermodynamic properties at different points of the MGT and results in varying performance of the MGT. Further, this effect needs to be studied in detail for key parameters, such as density, heat capacity, and γ as they will disturb the behaviour at large due to their contribution in compressor and turbine performance equations.

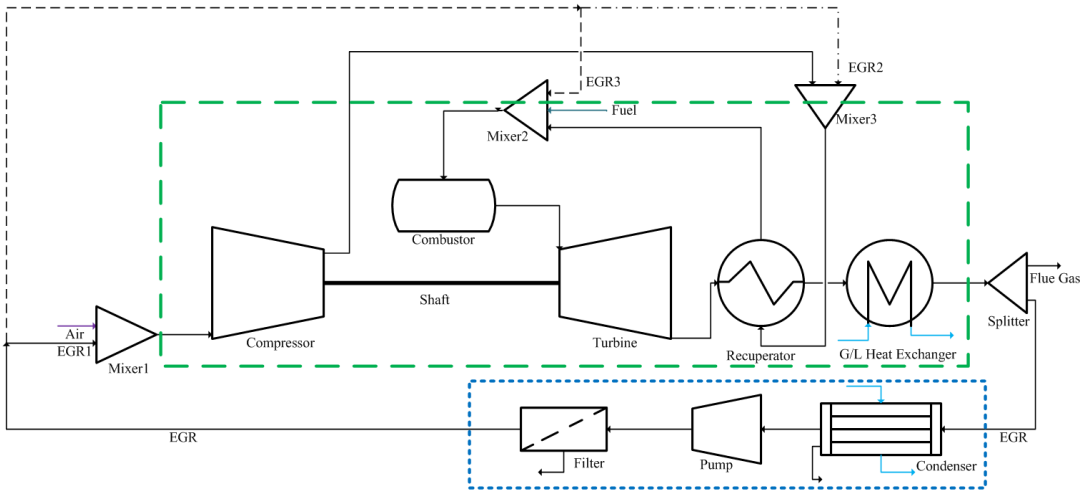

Figure 4.1 Schematics of a micro gas turbine (green dashed rectangle) along with exhaust gas recirculation loop (blue dotted rectangle) and representing EGR at different locations; Location (i) at Mixer1 by stream EGR1, Location (ii) at Mixer2 by stream EGR2 and Location (iii) at Mixer3 by stream EGR3.

4.2 CO_2 Enhancement Modelling

Due to the lower CO_2 concentration in the exhaust gas of the MGT, as indicated in Table 3.5 which implies that the exhaust gas of the MGT needs to be enhanced in terms of the CO_2 concentration. The most viable method is through either injection of CO_2 at the compressor inlet or through exhaust gas recirculation in which part of the exhaust gas is split through the splitter; dried through the condenser and recirculated back to the compressor inlet of the MGT. The recycle loop consists of the splitter, condenser, booster fan and filter. The condenser acts in two ways: to decrease the temperature of the recycled stream and remove the water from the recycled stream depending on the temperature specified. The recycled stream can only be injected back to the system if its pressure is slightly higher than the live

pressure of the stream, and this is achieved by the booster fan which increases the pressure from the condenser pressure back to the live pressure of the stream. The filter assists in the removal of any of the solid contaminants present in the recycle stream. A schematic of the EGR cycle model developed is shown in Figure 4.1. The amount of the exhaust gas recirculated can be defined by the following expression:

$$\text{EGR ratio} = \frac{\text{Amount of recirculated exhaust gas}}{\text{Amount of exhaust gas}} \quad (4.1)$$

The Turbec T100 Series 1 MGT is studied for the EGR system located at the UKCCS research center PACT facility and the models are developed in Aspen. The components of the MGT are same as shown in Figure 3.2 and the MGT-EGR model components are shown in Figure 4.1. The additional components of the EGR loop as described above are indicated by blue dotted rectangles in Figure 4.1. The property package for the estimation of the thermodynamic properties is the Peng-Robinson equation of state. The minimization of the total Gibbs energy is used as a criterion for the chemical equilibrium in the combustor. More details for the process modelling specification can be found in Section 3.3.2.

For the location of the EGR stream, three potential locations can be chosen, which are defined as follows:

- Location (i): At the compressor inlet.
- Location (ii): After the compressor or before the recuperator in the air side stream.
- Location (iii): In the combustor or after the recuperator in the air side stream.

The schematics of the EGR models with varying position for the locations (i), (ii), and (iii) are shown Figure 4.1 by Mixer1, Mixer2 and Mixer3, respectively. The EGR operating conditions are studied by varying the condensation temperature of the condenser, which defines how cool or hot the recycled stream is in terms of the temperature, and also how wet or dry is the recycled stream by the content of the water in the recycled stream, which is dictated by the water removed in the condenser.

In addition, the thermodynamic properties of the working stream for the EGR are investigated at different locations of the MGT, namely:

i. Compressor inlet.
ii. Compressor outlet/recuperator air side inlet.
iii. Combustor outlet/turbine inlet.
iv. Turbine outlet/recuperator gas side inlet.

The thermodynamic properties investigated include; mass density, heat capacity and isentropic co-efficient ($\gamma = c_p/c_v$); to better apprehend the effect of the EGR on the performance of the MGT for recycling the exhaust gas other than just injecting CO_2 in the MGT.

This chapter deals with process modelling and simulation analysis of the MGT integrated with a pilot-scale amine-based CO_2 capture plant. The experimental data obtained through the PACT facility is used only to validate the MGT base case and the MGT with CO_2 injection models. Similarly the experimental data of the pilot-scale amine-based CO_2 capture plant is used to validate the model of the pilot-scale amine-based CO_2 capture plant as presented in Chapter 6. However, the exhaust gas recirculation to the MGT is analysed only through modelling and simulation in Section 4.4, after testing the MGT against extensive validation in Sections 3.5 and 4.3. Further, the integrated case of the MGT with the pilot-scale amine-based CO_2 capture plant is analysed through modelling and simulation for varying rates of CO_2 injection as presented in Section 4.7. In conclusion, the effect of CO_2 enhancement on the performance of the MGT integrated with pilot-scale amine-based CO_2 capture plant is analysed in this chapter.

4.3 MGT Model Validation with CO_2 Injection

The CO_2 concentration at the exhaust of the MGT is lean and in the range 1.51 to 1.69 mol% as illustrated in Figure 3.3 (c) and this will cause a major energy penalty when integrated with the CO_2 capture system. As explained earlier, this drawback is avoided either by injecting CO_2 into the MGT or by recycling the exhaust gas back to the gas turbine, which results in the enrichment of CO_2 for improved CO_2 capture efficiency.

The steady state model of the MGT developed in Chapter 3 is extended to study the effect of the CO_2 enrichment. The MGT model is also validated against the set of experimental data for CO_2 injection at the compressor inlet of the MGT at different part load conditions for varying injection rates of CO_2 injection. The CO_2 flow rate is varied for each part load condition from 0 to 125 kg/hr to access the behaviour of the CO_2 injection for different operational modes.

(a)

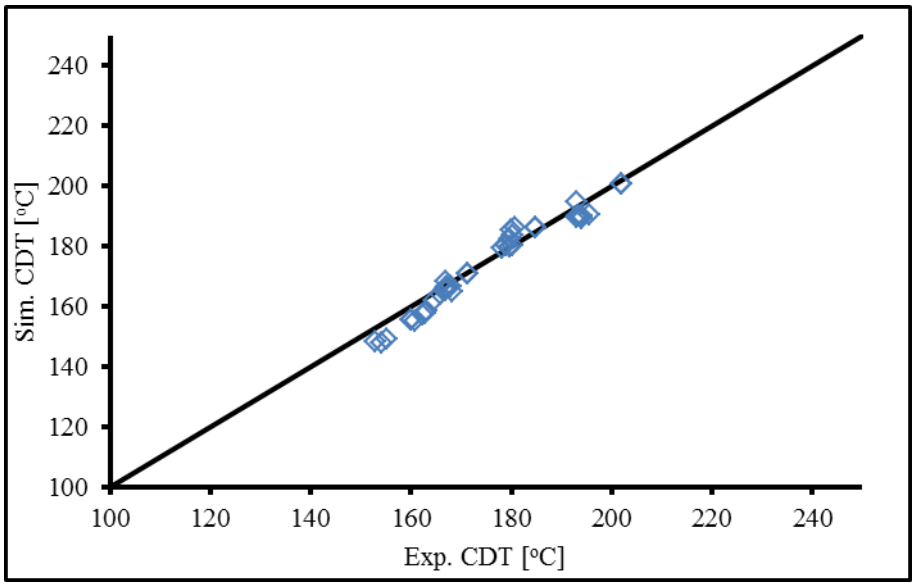

(b)

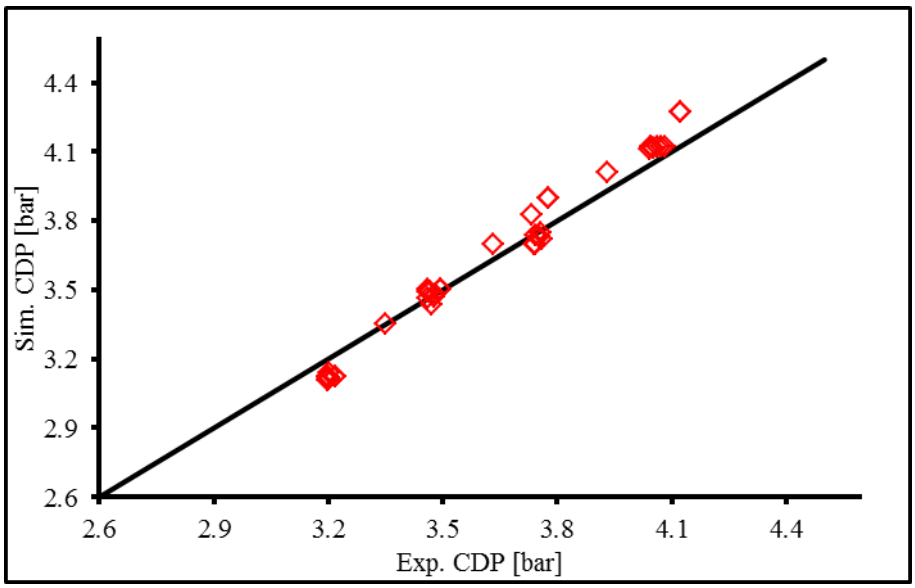

Figure 4.2 Model results as a function of the experimental results (a) Parity plot for compressor discharge temperature; and (b) Parity plot for compressor discharge pressure.

(a)

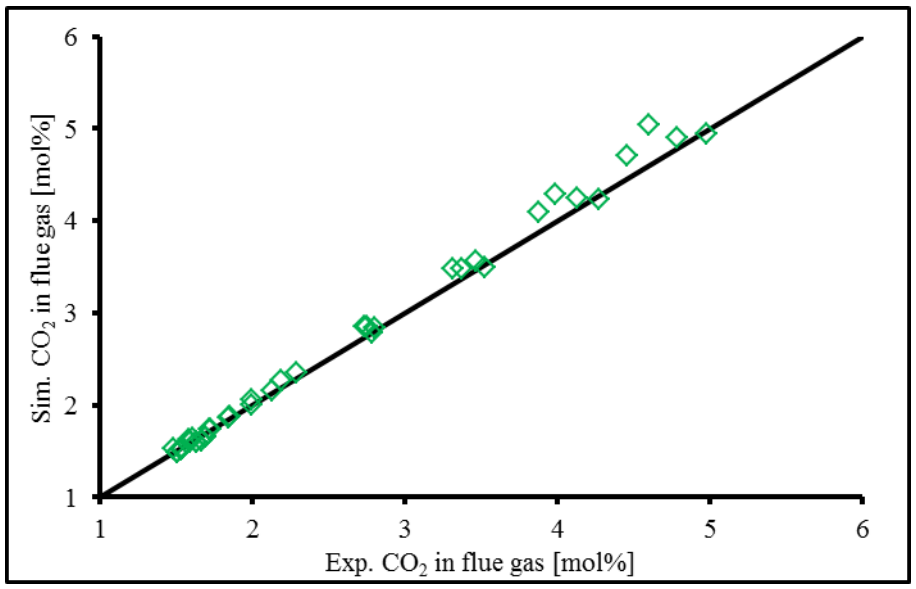

(b)

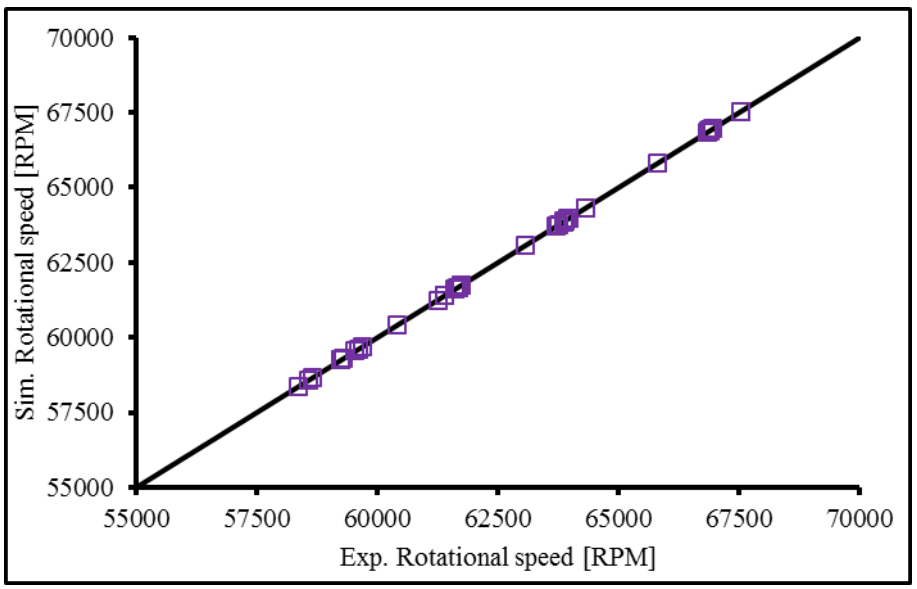

Figure 4.3 Model results as a function of the experimental results (a) Parity plot for CO_2 composition in flue gas; and (b) Parity plot for rotational speed.

The process modelling is performed for various CO_2 injections for each part load condition to evaluate the process performance of the different operational scenarios and the results obtained from the process modelling are compared to the mean values of the experimentally measured data points. The measured versus modelled results for some of the selected parameters are shown in Figures 4.2 and 4.3. The mean percentage absolute deviation for the parameters investigated are within the acceptable range, such as the compressor discharge temperature, compressor

discharge pressure, flue gas composition for CO_2 and O_2 and power output, in comparison to the measured values are: 1.81, 1.54, 2.73, 2.29 and 0.02 %, respectively. Figures 4.2 and 4.3, show that the model results are in good agreement with the experimental data. As the combustor calculation is based on the minimization of Gibbs free energy rather than kinetics, this result in higher deviations of the turbine inlet temperature. Further, the large deviations of the H_2O composition in the flue gas may be due to condensation of H_2O during the measurement. The tabulated measured experimental and model predicted results are presented in Tables A. 3 to A. 10 of Appendix A for various part load power outputs of 80, 70, 60 and 50 $kW_{e.}$

In addition, detailed results are presented for a number of variables including, turbine inlet temperature, flue gas temperature, and rotational speed and H_2O molar composition in the flue gas; other than the variables reported in Figures 4.2 and 4.3. The minimum and maximum CO_2 observed during the modelling of the CO_2 injection in the MGT is 1.48 and 5.04 mol% in comparison to the mean experimental values of 1.48 and 4.98 mol%, respectively.

The minimum O_2 observed in the flue gas is 17.60 and 17.11 mol% for the measured and modelled cases at the CO_2 injection rate of 125 kg/hr, respectively, with the O_2 content at the combustor inlet of 19.96 mol%. The O_2 content at the combustor inlet is much higher than the limited oxygen present at the combustor inlet as reported in the literature [89-92].

4.4 Effect of the EGR Ratio

The more realistic application is to recycle part of the exhaust gas back to the compressor inlet which is termed as EGR. The EGR ratio is varied to check its impact on the system performance through the splitter in the model in order to adjust the amount of the EGR ratio defined by Equation (4.1). The steady state model developed is extended to include the exhaust gas recirculation mode to the MGT in order to study the effect of CO_2 enrichment. The modelling is done at the ISO conditions [187] and the electrical power output is maintained at 100 kW_e and the

TOT is fixed at 650 ^{o}C. The natural gas and air composition are the same as reported in Tables 3.2 and 3.3, respectively.

Table 4.1 Performance of the EGR cycle at ISO conditions.

Parameter	Model results
Electrical power [kW_e]	100
Thermal output [kW_{th}]	185
Electrical efficiency [%]	29.5
Overall efficiency [%]	84
Booster fan efficiency [%]	85
CO_2 in flue gas [mol%]	3.5
O_2 in flue gas [mol%]	14.2
Flue gas flow rate [kg/s]	0.35
EGR percentage [%]	55
Rotational speed [rpm]	70000
Pressure ratio	4.5
Turbine inlet temperature [^{o}C]	930
Turbine outlet temperature [^{o}C]	650

The increase in the EGR ratio increases the CO_2 in the exhaust gas with a decrease in O_2 concentration both at the combustor inlet and exhaust gas, as shown in Figure 4.4 (a). The decrease in O_2 concentration at the combustor inlet causes O_2 starvation, which will affect the combustion stability with higher UHC and CO emissions at the outlet. The decreasing trend of the O_2 at the combustor inlet and outlet is shown in Figure 4.4 (b). The modelling suggests that EGR $\leq$ 55 % should be maintained to remain within the oxygen levels recommended for efficient combustion [90-92], and this results in CO_2 enrichment from 1.6 mol% in the base case MGT cycle to 3.5 mol% in the MGT-EGR cycle. Further, the EGR system decreases the total mass flow of the flue gas, which will influence the performance of the CO_2 capture system. The results of the EGR model at 55 % EGR are given in Table 4.1. The electrical and overall efficiency presented in Table 4.1 are defined by equations (3.12) and (3.13), respectively in Section 3.4. The increase in CO_2 composition in the exhaust gas is almost by a factor of 2.2 of the CO_2 composition without EGR and is approximately the same as that reported in the literature [100, 106, 108] for EGR equipped commercial scale natural gas-fired power plants.

(a)

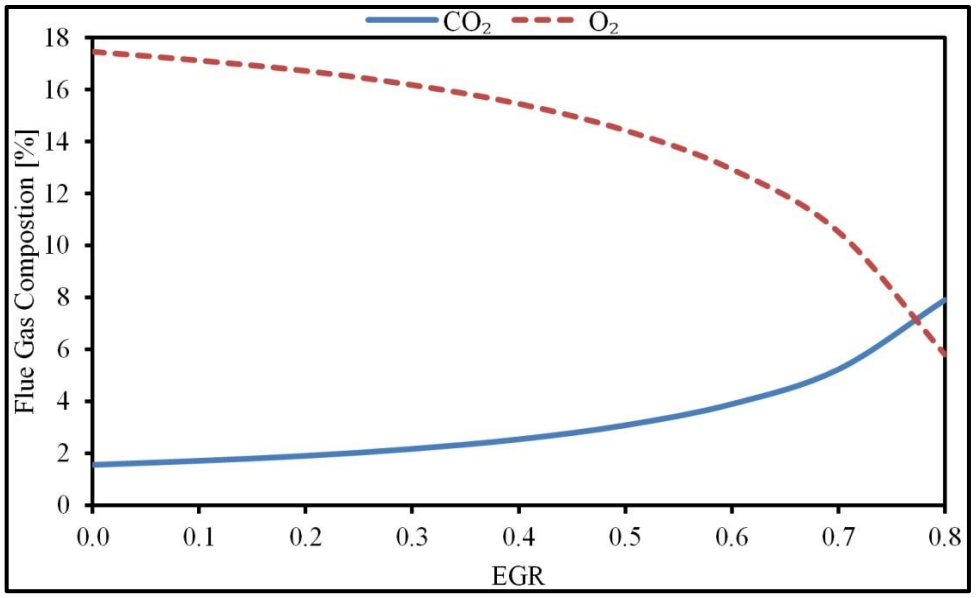

(b)

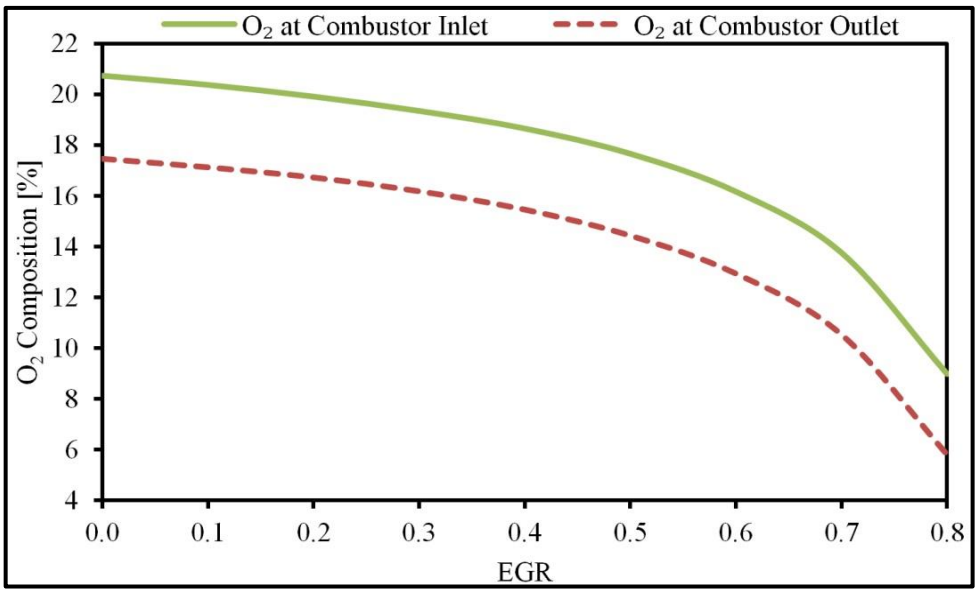

Figure 4.4 Effect of the EGR ratio on (a) CO_2 and O_2 molar composition in the flue gas; and (b) O_2 molar composition at the combustor inlet and outlet.

The electrical efficiency decrease is 2.3 % for the EGR cycle in comparison to the base case MGT cycle, however, the overall efficiency increases by 5.1 % in comparison to the MGT without EGR. The efficiency for the EGR cycle is decreased to 29.5 % from 30.2 % of the base case MGT cycle. This decrease is due to the blower power recirculating the exhaust gas from the condenser pressure back to the compressor inlet. The booster fan used in the model is 85 % efficient as given in Table 4.1. The effect of the EGR ratio on the decrease of electrical efficiency is

shown in Figure 4.5. The enhanced thermal output of the EGR cycle, in comparison with the MGT cycle, will result in the improved performance of the bottom Rankine cycle in commercial-scale gas turbines. The effect of the EGR on the flue gas composition profile of all the components present, for the MGT with EGR is shown in Figure A. 2 of Appendix A. The flue gas flow rate decrease of 55 % will result in a better performance for the CO_2 capture plant. This, along with enhanced CO_2 concentration, will benefit the economics of the system when integrated with a smaller-size CO_2 capture system.

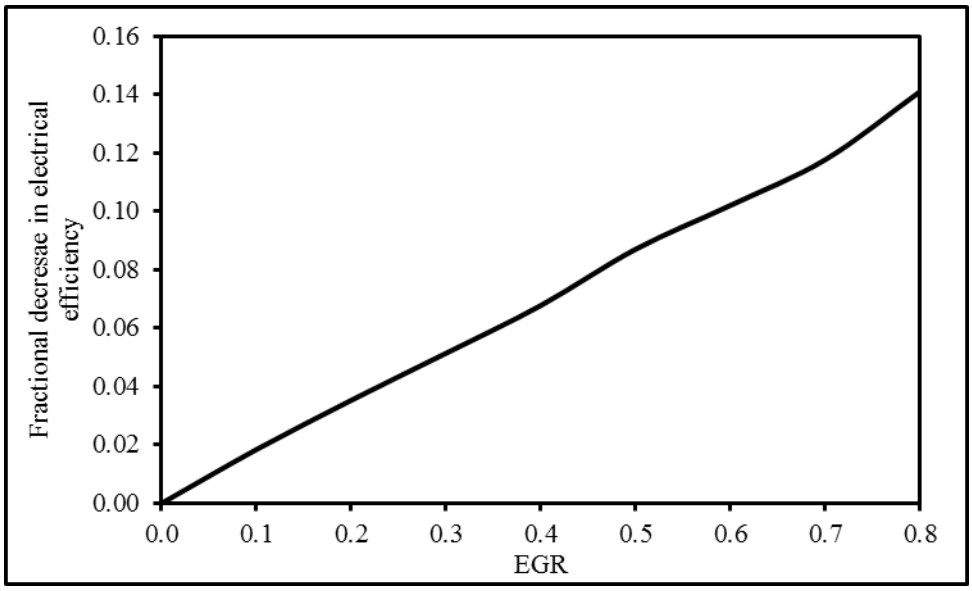

Figure 4.5 Impact of the EGR ratio on the electrical efficiency of the MGT.

Further, EGR also impacts on the thermodynamics of the MGT streams due to the change in composition of the fluid. The effect of the EGR on the thermodynamic properties of the fluid at different locations in the MGT, as mentioned in Section 4.2, is explored in Section 4.4.1.

4.4.1 Thermodynamic Comparative Potential

The change in the composition of the stream affects the thermodynamic properties of the working stream, which affects the performance of the MGT. As defined in Section 4.2, three thermodynamic properties are chosen to check the performance of the MGT for the changed composition of the working stream at different locations.

(a) (b)

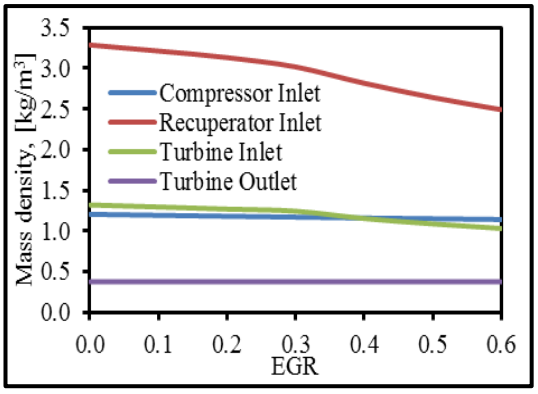

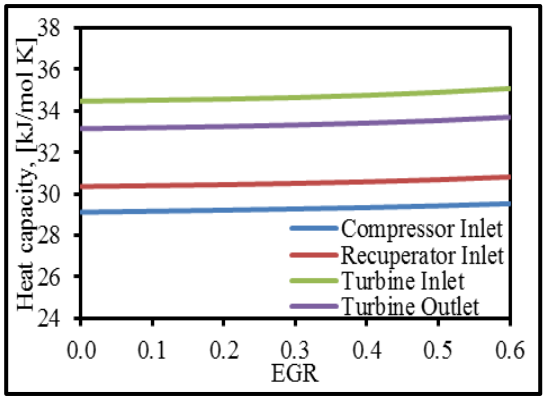

(c)

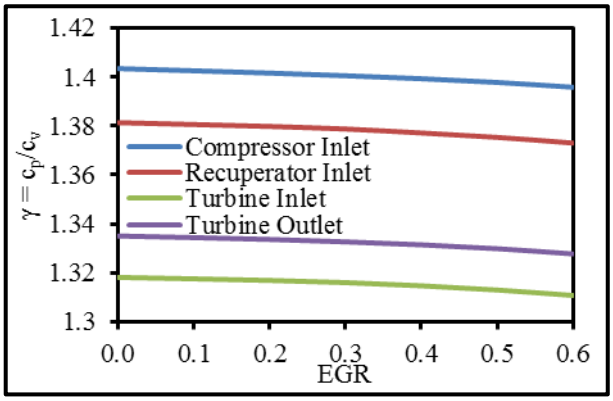

Figure 4.6 Effect of the EGR on the thermodynamic properties of working stream at different locations of the MGT (a) Mass density versus EGR; (b) Heat capacity versus EGR; and (c) Isentropic coefficient versus EGR.

The thermodynamic properties for different locations of the MGT are shown in Figure 4.6. The mass density of the fluid decreases with an increase in the EGR as shown in Figure 4.6 (a) at all locations due to the increased content of CO_2 in the fluid. However, this effect is more pronounced at higher temperatures and pressures. This effect also depends on the concentration of the other participating constituent's in the fluid at the particular location. As it is observed, for the EGR of 55 %, the mass density of the fluid decreases by 5 and 0.2 % at the compressor inlet and turbine outlet, respectively, however, the decrease is up to 22 and 20 % at the recuperator inlet and the turbine inlet, respectively. The effect of the increased CO_2 content on the heat capacity of the fluid at different locations of the MGT is less pronounced. As, an increase of 1.5 % is observed at the gas turbine inlet for the heat capacity for the MGT with EGR, further, this increased heat capacity results in the higher heat duty of the recuperator and G/L heat exchanger for MGT with EGR. The effect of the EGR on the heat capacity for the different locations of the MGT is

shown in Figure 4.6 (b). Further the isentropic coefficient of the fluid at different locations of the MGT decreases due to an increase of EGR as shown in Figure 4.6 (c). The decrease of the isentropic coefficient is less pronounced and an average 0.5 % decrease from MGT without EGR.

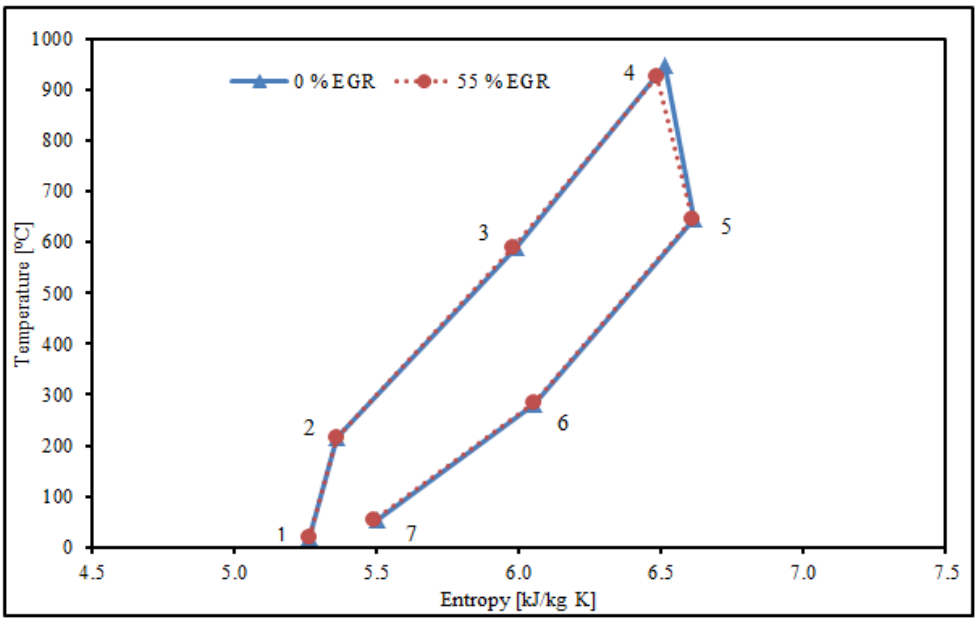

Figure 4.7 The TS diagram of the MGT with EGR at different locations of the MGT.

The impact of the EGR on the TS diagram of the Brayton cycle is also analysed and the TS diagram of the MGT when the EGR percentage of 55 % is shown in Figure 4.7 and compared with the TS diagram of the MGT without EGR. The locations indicated by the numerical numbers in the Figure 4.7 are the same as those explored in Section 3.2. Due to the heat capacity effect, the temperature at different locations of the MGT decreases as a results of the EGR when compared with the MGT without EGR. Hence, the entropy being a function of temperature also decreases. Further, this decrease is more pronounced at higher temperatures and pressures as shown in Figure 4.7. Thus, it can be concluded that the performance of the MGT for the EGR cycle can be better comprehended by understanding the behaviour of the fluid for the increased CO_2 content in the working fluid of the MGT.

4.5 Effect of the Position of the EGR

As already defined in Section 4.2 and illustrated in Figure 4.1; the three different positions for the EGR injection into the MGT were evaluated and there were the

locations (i), (ii), and (iii). These three EGR locations have different conditions and will require varying the thermos-physical nature of the fluid. The pressure of the EGR stream should be kept the same, or above, the live pressure of any of the aforementioned injection locations, and therefore the pressure specified at the booster fan is slightly higher than the pressure at the injection point. The modelling for the injection at different locations is performed at an EGR percentage of 55% and at ISO conditions. The process modelling indicates that the EGR injection at these different locations will have a distinctive effect on the system performance in terms of the process control, operation and design. The effect of the change in the EGR position on the electrical efficiency, overall efficiency, O_2 molar composition at the combustor inlet and flue gas composition are shown in Figure 4.8.

At location (i), the pressure of the recycle stream should be slightly above atmospheric, however for locations (ii) and (iii) the pressure at the injection locations is nearly the discharge pressure of the compressor. The efficiency decrease shown in Figure 4.8 (a) in comparison to the base case MGT is only 7.6 % for the EGR cycle at location (i); while it is 25 % and 20 % for the locations (ii) and (iii) of the EGR cycles, respectively.

The lowest decrease in the electrical efficiency, as shown in Figure 4.8 (a), is for the recycle at location (i), since the recycle pressure at the booster fan is less and therefore less work is required by the booster fan. The drop in efficiencies at locations (ii) and (iii) are much higher due to the booster fan work that pushes the exhaust gas to higher pressures at locations (ii) and (iii). The same behaviour is observed for the overall efficiency for the recycle at the three different locations. In terms of CO_2 enrichment, all three cases result in an equal increase in CO_2 concentration in the flue gas, as shown in Figure 4.8 (b). The O_2 concentration at the combustor inlet for EGR at location (iii) appears to be maintained high as observed in Figure 4.8 (b), however, the internal kinetics of the combustor needs to be studied in detail and this may be affected by the higher EGR ratios. In terms of the additional equipment requirements, the condenser is required for all three of the EGR locations. While the recycle back to location (i) will require a blower/fan for boosting the condenser pressure back to the compressor inlet.

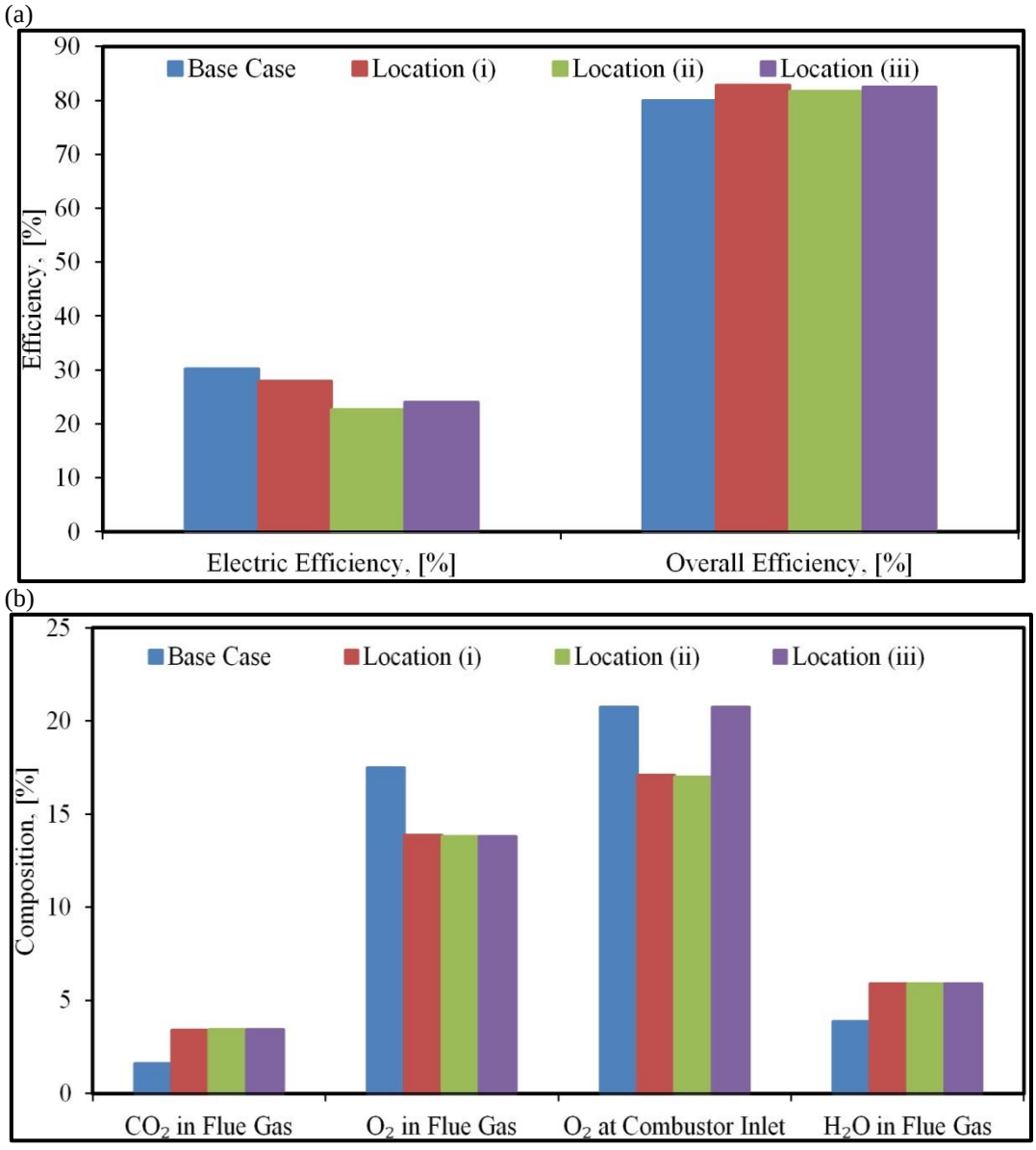

Figure 4.8 Effect of the EGR location on (a) the electrical and overall efficiency; and (b) flue gas composition, and O_2 composition at the combustor inlet.

However, the recycle to locations (ii) or (iii) will require a new compressor in the recycle loop in addition to the inherent compressor of the MGT. The same requirement is the reason for the lowering of the efficiencies for the EGR cases at locations (ii) and (iii). There are no surge problems when the exhaust gas is recycled at location (i). The surge issues arise when the exhaust gas is recycled at locations (ii) and (iii), due to the mismatch in the flow through the inherent compressor and turbine of the MGT. As the inherent compressor and turbine of the MGT are on the same shaft, any imbalance will affect the MGT default control, which needs to be overridden for these locations in order to converge the respective models.

Therefore, the EGR at location (i) will result in a better performance than in the other two locations due to the operational and control difficulties encountered. The EGR at location (i) will be evaluated as a function of the EGR ratio, and the condenser variables are varied to select the operating condition of the EGR for the MGT.

(a)

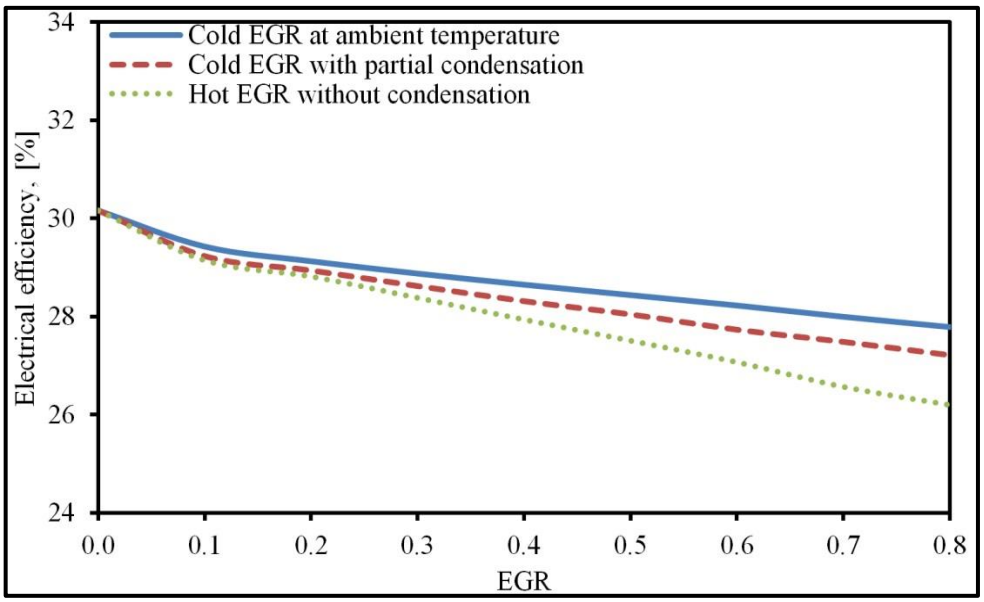

(b)

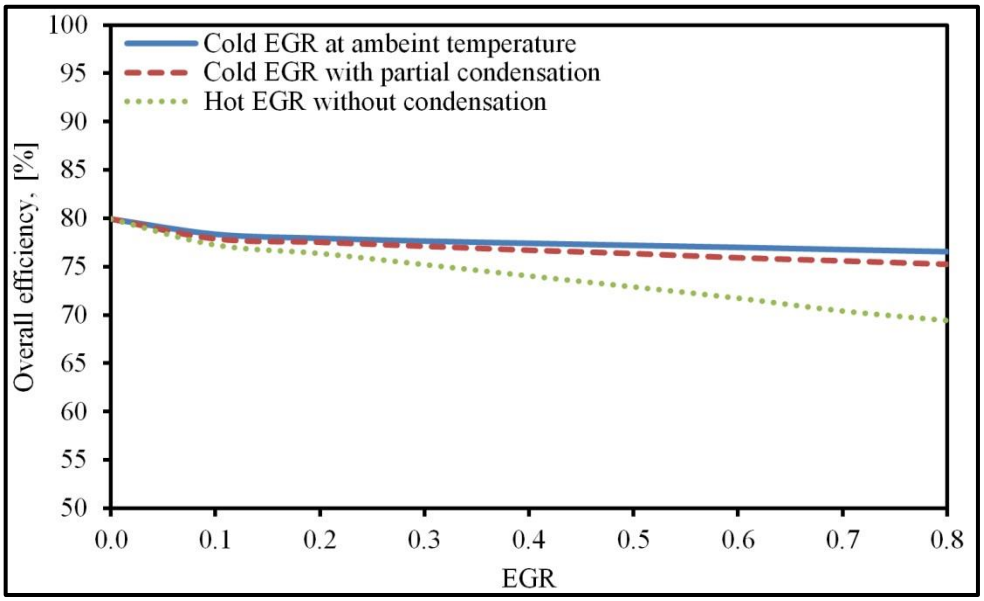

Figure 4.9 Effect of the EGR conditions on (a) the electrical efficiency, and (b) the overall efficiency.

4.6 Effect of the EGR Conditions

After defining the EGR location the other thing to define properly is the physical condition of the recycled stream and the H_2O content in it. The condensation temperature is an important parameter which affects the performance of the MGT equipped with the EGR at location (i). This defines the dryness of the EGR, and the temperature and water level in the EGR, which will affect the power requirement for the compressor due to density effects. Three cases are defined in order to assess the impact of the EGR condition:

- Cold EGR at ambient temperature.
- Cold EGR with partial condensation.
- Hot EGR without condensation.

The first two cases are realized by varying the condensation temperature while for the last case there is no condenser in the recycle loop. The cold EGR at ambient temperature is maintained at the temperature of 15 ^{o}C, the cold EGR with partial condensation is maintained at 40 ^{o}C and the hot EGR is at 70 ^{o}C. Also, the cold EGR at ambient temperature is in dry condition as most of the water content is removed while the hot EGR without condensation is the wet EGR. It is important to mention that the cold EGR at ambient temperature may not be possible in applications due to the higher utility requirement and/or sulphur deposition at such low temperatures, however, this case is only analysed through modelling for comparison with other cases.

The modelling of these conditions is performed by changing the condenser temperature and varying the EGR ratio for each condensation temperature at ISO conditions. It is observed that the electrical efficiency drop is higher as the temperature of the EGR stream increases as shown in Figure 4.9 (a). This is due to more compressor work and higher fuel feeding requirements as the EGR stream temperature increases and the temperature of the recycled stream is controlled mainly by the condenser. The overall efficiency follows the same trend by keeping the thermal output of the MGT constant and at the same level as in the base case as shown in Figure 4.9 (b). As a result, the flue gas temperature increases due to the

heat capacity change of the resulting flue gas and the increased amount of water content as the temperature and condensation rate increase. The increased water content in the exhaust gas is depicted in Figure 4.10, and will affect the performance of the compressor as it may condense at or before the compressor.

The increased water content will also dilute the CO_2 concentration in the exhaust gas after the EGR, which in turn will affect the performance of the CO_2 capture system if integrated. As predicted by the modelling, the electrical efficiency drop for the dry EGR is less as compared to the wet EGR. In addition, the water content in the wet EGR is the highest as there is no condenser in the recycle loop.

The lower is the condensation temperature; the better will be the performance of the MGT in EGR mode as the EGR stream becomes drier. However, the decrease in the condensation temperature may lead to sulphur deposition which will affect the recirculating ducts and the blower or compressor material depending on the sulphur content in the fuel to be burnt, and this situation must be taken into consideration.

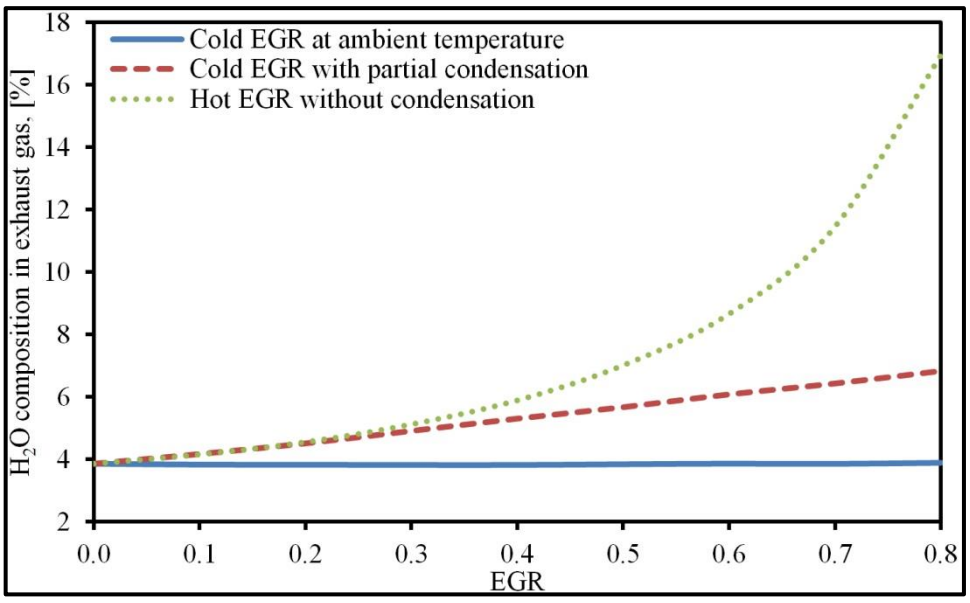

Figure 4.10 The H_2O composition in the exhaust gas at different EGR conditions.

4.7 Effect of CO_2 Enrichment on the Validated Pilot-scale CO_2 Capture Plant

The PACT core facility also houses a pilot-scale CO_2 capture plant with a capacity of 1 ton per day of CO_2 capture based on MEA as solvent. The pilot-scale CO_2

capture plant model is developed in Aspen and is validated against the extensive set of experimental data. The process details and model validation will be explored in full details in Chapter 6, and therefore it is not reported in this section. However, the effect of the CO_2 enrichment on the performance of the pilot-scale CO_2 capture plant is analysed.

The slip stream of the micro gas turbine is sent to the pilot-scale CO_2 capture plant for the removal of CO_2 from the flue gas. The CO_2 injection in MGT is varied from 0 to 125 kg/hr, as elaborated in Section 4.3, and its effect through the slip stream on the performance of the pilot-scale CO_2 capture plant is investigated through modelling. The MGT with CO_2 injection is considered for integration with the pilot-scale CO_2 capture plant which also covers the CO_2 concentration range of the MGT with EGR, since, the maximum CO_2 concentration for CO_2 injection in the MGT results in 4.91 mol%, which is higher than the CO_2 concentration of 3.5 mol% observed during the MGT with the EGR case. The flow rate of the flue gas entering the absorber is fixed at the value of 400 kg/hr and the CO_2 capture rate is fixed at 90 % and the solvent employed is MEA with 30 wt. % aqueous solution. The lean loading is fixed at 0.2 mol CO_2/mol MEA for all the cases. The solvent flow rate was estimated based on the 90 % CO_2 capture rate, and also it is verified by the literature [159]. Further, the solvent flow rate varies from 404 kg/hr at no injection of the CO_2 to 600 kg/hr at CO_2 injection of 125 kg/hr. It must be kept in mind that the solvent flow rate cannot be decreased below about 400 kg/hr due to the operational limit of the pilot-scale CO_2 capture plant.

The effect of the CO_2 enrichment is clear from the results as shown in Figures 4.11 and 4.12. The effect of the CO_2 injection on the specific reboiler duty is shown in Figure 4.11 and it is observed that the specific reboiler duty decreases with an increase in the CO_2 concentration in the flue gas. The CO_2 concentration increases by a factor 3.5 in comparison to the CO_2 concentration without injection, which results in the specific reboiler duty decreasing by 20.5 % for the CO_2 injection at the rate of 125 kg/hr. The effect of the CO_2 injection on the specific reboiler duty, along with the CO_2 content in flue gas, for the pilot-scale CO_2 capture plant coupled with MGT is shown in Figure 4.11. The specific reboiler duty decreases from 10.2 to 8.1

GJ/tCO_2 for the CO_2 concentration increase from 1.42 to 4.91 mol%, respectively. This results in a drop of 5.9 % in the specific reboiler duty per unit percentage increase in CO_2 concentration, based on a linear fit equation. Also the drop in the specific reboiler duty was observed during experimentation for similar pilot-scale CO_2 capture plants. The drop of 7.1 % per unit percentage increase in CO_2 concentration was observed when the CO_2 concentration was increased from 5.5 to 9.9 mol% as reported in Section 6.5. Similarly, the drop of 7.5 % per unit percentage decrease in CO_2 concentration was observed when the CO_2 concentration was increased from 4.5 to 11.5 mol% [194]. In addition, the drop of only 2.93 % per unit percentage decrease in CO_2 was observed when CO_2 concentration increases from 5.46 to 13.37 mol% with decreases in specific reboiler duty from 5.01 to 3.85 GJ/tCO_2, respectively, as reported by Notz et al. [139] and in Section 6.4. Also, the specific reboiler duty of 8.3 GJ/tCO_2 at 4.5 mol% CO_2 concentration in the literature [194] through experimentation validates the estimated specific reboiler duty of 8.1 GJ/tCO_2 at 4.91 mol% CO_2 concentrations in the present study. Further, the present sharp drop in specific reboiler duty is in line with the literature reported trend [104] and far higher than the reported drop in Table C.1 of Appendix C in the specific reboiler duty for a commercial-scale natural gas fired power plant coupled with a CO_2 capture plant with EGR.

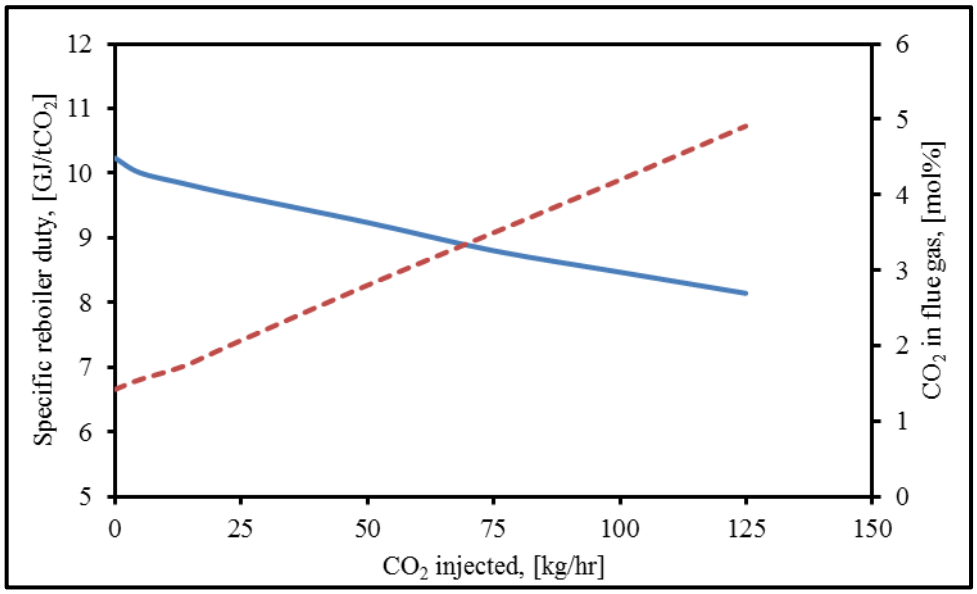

Figure 4.11 Effect of CO_2 injection on the specific reboiler duty (solid line) along with CO_2 in flue gas (dashed line) of the pilot-scale CO_2 capture plant.

The specific reboiler duty decreases due to the higher partial pressure of the CO_2 for the higher CO_2 injection rate of 125 kg/hr. Since the flowrate of the flue gas remains constant, the amount of the CO_2 in the constant flue gas increases which results in a large driving force, thus resulting in more CO_2 to be absorbed by the solvent and then regenerated at lower specific reboiler duty. Therefore, the higher CO_2 partial pressure results in higher driving force with higher CO_2 loading in the solvent, hence favouring the capture reaction [104]. Since, the present pilot-scale CO_2 capture facility is of 8 m packing height with a random type, the specific reboiler duty estimated for such a low range of the CO_2 concentration is the same as that predicted in Chapter 6 and in the literature [137, 139, 140, 195] for similar kinds of facilities keeping in mind their variable operating conditions, including the L/G ratio, packing height, absorber inlet temperatures, lean solvent loading and strength and stripper pressure.

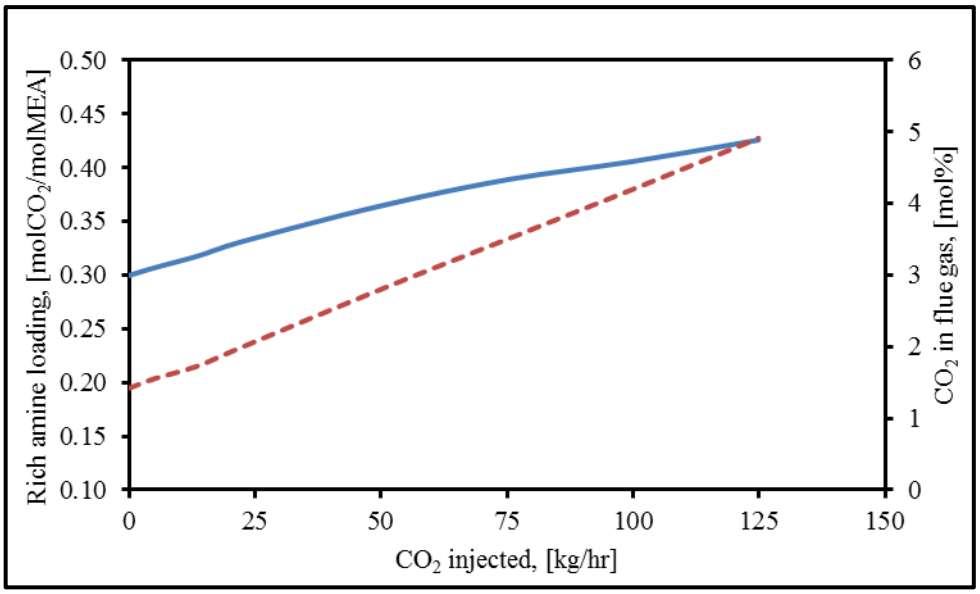

Figure 4.12 Effect of the CO_2 injection on the rich amine loading (solid line) along with the CO_2 in flue gas (dashed line) for the pilot-scale CO_2 capture plant.

With the increase in CO_2 composition, the amine loading increases and also the difference between the rich and lean loading increases. This indicates that the amount of the CO_2 absorbed also increases. The increased loading results in less steam being required in the stripper, so the regeneration in the stripper becomes easier with the reduced energy requirement in the reboiler for the increased CO_2

composition. The increased rich loading results in the increased cyclic capacity and with it the specific reboiler duty decreases. The rich amine loading increases by 42 % for maximum CO_2 injection of 125 kg/hr. The effect of the CO_2 injection on the rich loading, along with the CO_2 content in flue gas, for the pilot-scale CO_2 capture plant coupled with the MGT is shown in Figure 4.12.

Furthermore, the US Department of Energy Report [196] has reported a number of case studies for different commercial-scale gas turbines both with and without EGR coupled with a CO_2 capture system. They found approximately 0.5 % point improvement in efficiencies when EGR is applied. Further, NGCC with a CO_2 capture system results in 8.1 % reduction in total energy consumption when EGR is applied [105]. It is found that the whole system efficiency is always higher by 2 to 3 % points than without the EGR system [103].

4.8 Conclusions

- The results in this Chapter show that the effect of the location and conditions for the EGR stream of the MGT is worthy to be considered for the assessment of the behaviour of the MGT with EGR.
- The increased CO_2 content, either due to the EGR or CO_2 injection, affects the thermodynamic properties of the fluid at different locations of the MGT. The application of the EGR results in a decrease of the mass density and isentropic coefficient of the fluid at any particular stream location of the MGT. However, the heat capacity of the fluid increases for the fluid stream at any particular stream location of the MGT, with the application of the EGR.
- The process system analysis assists in the selection of the best configuration, the EGR recycle back to the compressor inlet, i.e. location (i) defined as the recycle back at the compressor inlet, is the optimum location for the EGR operation with MGT.
- In terms of the EGR stream conditions, the partial condensation, which results in a dry recycle stream and condensation temperature at the minimum to operate, is the optimum condition for the EGR to work.

- The application of the EGR results in the CO_2 concentration enhancement to 3.5 mol% from 1.6 mol% in the base case with a 55 % decrease in the exhaust gas flow, which would benefit its integration with the PCC technology. The higher EGR percentage is due to the fact that the MGT combustion is lean with higher excess air as compared to the commercial-scale gas turbines.
- The increase in CO_2 composition in the exhaust gas is almost by a factor 3.5 and 2.2 times for CO_2 injection in MGT and EGR, respectively. The CO_2 injection results in the CO_2 concentration increase to 5.04 mol% from 1.48 mol%.
- The enhancement of the CO_2 concentration due to the injection of CO_2 in MGT results in 20.5 % lower specific reboiler duty for the pilot-scale CO_2 capture plant, at maximum CO_2 injection rate of 125 kg/hr.

In the next chapter, the validated MGT developed in Chapter 3 is further tested against experimental data for steam injection and simultaneous steam and CO_2 injection into the MGT at different part load power outputs for varying steam and CO_2 injection rates. After validating the MGT model against steam injection and simultaneous steam and CO_2 injection, the MGT model is altered to auto generated steam injected MGT and humidified air turbine MGT models. The performance of the MGT, MGT-EGR, steam injected MGT and humidified air turbine MGT are compared. Further, the thermodynamic analyses of the developed models are performed and the thermodynamic properties of the selected parameters at different locations of the MGT are estimated and compared for the different models developed.

Chapter 5
Process System Comparison of Exhaust Gas Recirculated, Steam Injected and Humidified Micro Gas Turbine

In this chapter, the MGT model developed in Chapter 3 is further validated against the experimental data for steam injection and the simultaneous injection of steam and CO_2 in the MGT; and further the effect of the injection on the performance of the MGT is studied. The auto generated steam injected MGT and humidified air turbine MGT models are developed to check the behaviour of the MGT for these altered models. Finally, a process system comparison is performed for the MGT for the different modified models, including the base case MGT, MGT with EGR, steam injected MGT and humid air turbine MGT model.

5.1 Introduction

Stringent environmental emission regulations and continuing efforts to reduce carbon dioxide from the energy sector, in the context of global warming, have promoted interest in improving the efficiency of power generation systems whilst reducing emissions. Further, this has led to the development of innovative gas turbine systems which either result in higher electrical efficiency or reduction of CO_2 emissions. These innovative gas turbine technologies include exhaust gas recirculated gas turbines, steam injected gas turbine (STIG) and humidified air turbine (HAT). The details of the exhaust gas recirculated gas turbines can be found in Chapter 4. The waste heat after the expansion of the working fluid can be used to raise the steam or to humidify the compressed air; which are then injected into the combustion chamber [70]. This result in an increased mass flow through the expander hence increased system efficiency. The different configurations of the STIG and HAT cycles can be found in the literature [64, 71]. Belokon et al. [197] observed inefficient combustion if the steam to air ratio is higher than 7 % from the experiments performed in the LM5000 combustor. The humidification of the VT40

combustor from 0 to 33 % of water experimentally injection reduced the NO_x emissions [198].

The steam injection in the MGT, along with its thermodynamic analysis, showed an efficiency increase of 5 % [85] while the validation with the experimental data and perturbation analysis indicated an efficiency rise of 2.2 % [182]. The heat exchanger network design for the water injection in the MGT also results in an efficiency increase of 2 % [199]. The HAT cycle configuration for the MGT, along with its thermodynamic assessment indicates a 4 % efficiency increase [87] and the techno-economic assessment of the micro HAT cycle improved the economic performance [88]. An exergy analysis, along with the effect of the pressure ratio, on the specific power and efficiency indicated an improved performance for different cycle configurations for water and steam injection at different locations [84]. The spray saturator is designed for the micro HAT cycle by a parametric analysis of the co-, counter- and cross- current saturators [200]. The volume of the spray saturator in [200] is approximately the same as that reported by [87] for the humidifier with packing. The MGT with HAT when integrated with an amine-based CO_2 capture plant resulted in higher carbon capture efficiency due to higher CO_2 content [109]. De Paepe et al. [201] have performed the first experimental runs for the MGT with humid air operation.

In spite of the work performed on commercial scale gas turbines, more work needs to be done to better understand the thermodynamic performance of the three novel cycles, including the EGR, STIG and HAT cycle for the MGT. However, none have compared the MGT for different alterations as performed in this work for the electrical and total efficiency improvements, emissions reduction, and the changing properties of the streams at different levels of the MGT. Due to the limited literature found on this topic, an extensive study needs to be performed in this regard. The change of the fluid nature, either due to the exhaust gas recycle or water and steam injection, will affect the stream properties at different points of the MGT and results in varying performance of the MGT. Further, this effect needs to be studied in detail for key parameters, such as density, heat capacity, and isentropic co-efficient (γ) as they will disturb the behaviour at large of the MGT due to their contribution in the

compressor and turbine performance equations. Therefore, in this chapter the process system comparison of the aforementioned cycles with MGT is presented.

5.2 Steam Injection Modelling

As illustrated in Sections 2.1.4 and 5.1, the steam injection or humidification can result in increased cycle efficiency which will be beneficial on integration with a CO_2 capture system. The steam and/or water can be injected in the MGT at three different locations:

- Compressor inlet.
- Compressor outlet/recuperator inlet.
- Recuperator outlet/combustor inlet.

Each point has its own technical problems and benefits and further details can be found in the literature [77]. However, before developing the detailed steam injected MGT model and humidified air turbine MGT model; the steam injection MGT and simultaneous steam and CO_2 injection model validation is performed in Sections 5.2.1 and 5.2.2, respectively.

5.2.1 MGT Model Validation with Steam Injection

The base case model is developed and tested against the set of experimental data at different part load power outputs in Chapter 3 and validation is also performed against the set of experimental data with varying CO_2 injection rates at different part load power outputs in Chapter 4. Now, the MGT model is tested against the steam injection rates of 20 and 40 kg/hr for part load power outputs of 50, 55, 60 and 65 kW_e to access the behaviour of the MGT for different operational modes at variable steam injections. The process modelling is performed for steam injection at 20 and 40 kg/hr for each part load condition to evaluate the process performance of the different operational scenarios and the results obtained from the process modelling are compared with mean values of the experimentally measured data points obtained through the MGT rig available at the PACT facility, UK.

(a)

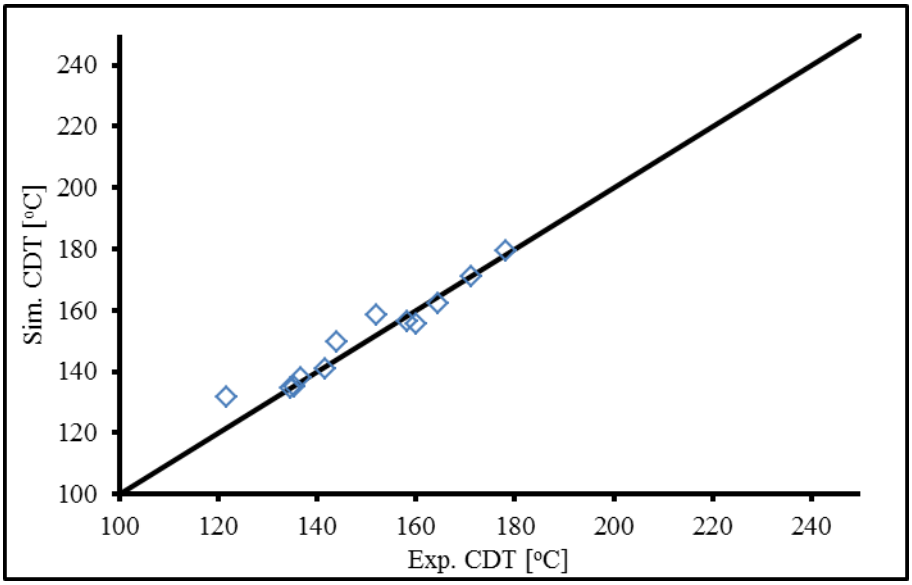

(b)

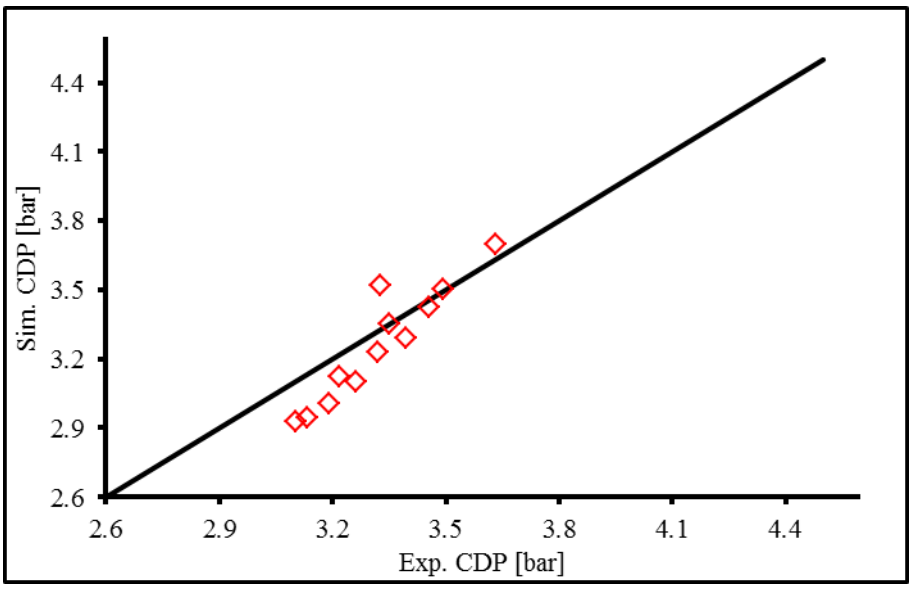

Figure 5.1 Model results as a function of the experimental results (a) Parity plot for compressor discharge temperature; and (b) Parity plot for compressor discharge pressure.

The saturated steam is injected at the compressor outlet/recuperator inlet of the MGT at a pressure higher than the compressor discharge pressure in order to allow proper injection and mixing with the air. For the steam streams, the NBS property package was used for the thermodynamic property estimation in the modelling. The measured versus modelled results for some of the selected parameters are shown in Figures 5.1 and 5.2. Measured and modelled results for the compressor discharge temperature and pressure are shown in Figure 5.1 and the CO_2 and O_2 composition in the flue gas is shown in Figure 5.2. The mean percentage absolute deviation for all the parameters investigated are within the acceptable range, in particular the compressor discharge temperature, compressor discharge pressure, flue gas

composition for CO_2 and O_2 and power output, in comparison to the measured values are: 2.44, 4.37, 2.31, 2.57 and 0.02 %, respectively. Figures 5.1 and 5.2 show that the model results are in good agreement with the experimental data. As the combustor calculation is based on the minimization of Gibbs free energy rather than kinetics, this result in higher deviations of the turbine inlet temperature. Further, the large deviations of the H_2O composition in the flue gas may be due to condensation of H_2O during the measurement.

(a)

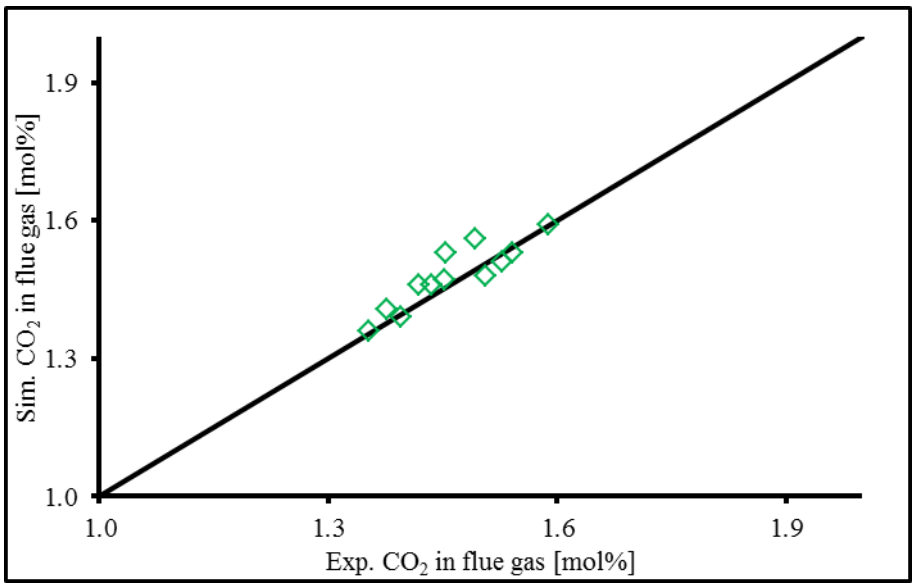

(b)

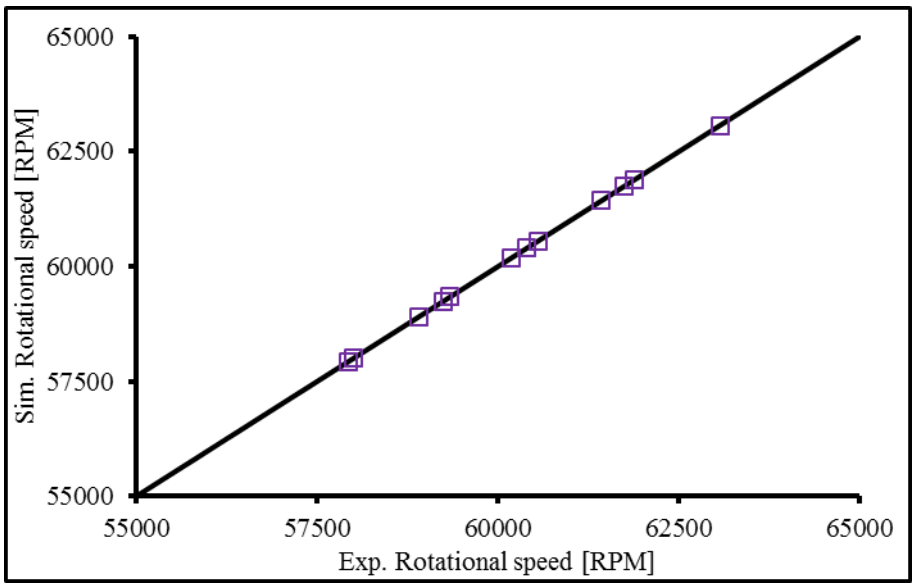

Figure 5.2 Model results as a function of the experimental results (a) Parity plot for CO2 composition in flue gas; and (b) Parity plot for rotational speed.

The tabulated measured experimental and model predicted results are presented in Tables A. 11 and A. 12 of the Appendix A for various part load power outputs of 50,

55, 60 and 65 kW_e. In addition, detailed results are presented for a number of the variables including, turbine inlet temperature, flue gas temperature, rotational speed and H_2O molar composition in the flue gas; other than the variables reported in Figures 5.1 and 5.2. Steam injection results in a decrease in the temperature at different locations of the MGT, as is clear through Tables A.11 and A.12 in the Appendix A. The modelling predicts that the temperatures decline by an average 14 and 2 % for the CDT and TIT during the steam injection in the MGT. Similarly, the compressor discharge pressure decreases by an average 7 % during the steam injection into the MGT though modelling. The CO_2 concentration in the flue gas decreases by an average 5%, however, this can be attributed to an average of 52 % increase in the H_2O concentration in the flue gas. However, if the H_2O content in the flue gas is condensed and/or maintained at the same level as without any injection, then the CO_2 concentration matches that of the MGT without any injection.

5.2.2 MGT Model Validation with Simultaneous Steam and CO_2 Injection

The MGT model developed in Chapter 3 is also tested against the simultaneous steam and CO_2 injection into the MGT. The steam injection is varied for 20 and 40 kg/hr for each part load power output. For each steam injection input, and for each part load power output, the CO_2 injection rate is varied from 0 to 125 kg/hr. The part load power output considered during the experimental campaign was 50, 55, 60 and 65 kW_e. The saturated steam is injected at the compressor outlet/recuperator inlet of the MGT at a pressure higher than the compressor discharge pressure in order to allow proper injection and mixing with the air. The CO_2 is injected at the air-line to the compressor inlet of the MGT at a pressure higher than atmospheric. The process modelling is performed for each variation study and for each part load condition in order to evaluate the process performance of the different operational scenarios and the results obtained from the process modelling are compared with the mean values of the experimentally measured data points obtained through the MGT rig that is available at the PACT facility, UK. The measured versus modelled results for some of the selected parameters are shown in Figures 5.3 and 5.4. Figure 5.3 indicates the compressor discharge temperature and pressure while Figure 5.4 shows the CO_2 and O_2 concentrations in the flue gas of the MGT. The mean percentage absolute deviation for the parameters investigated are within the acceptable range, such as the

compressor discharge temperature, compressor discharge pressure, flue gas composition for CO_2 and O_2 and power output, in comparison to the measured values are: 4.13, 4.59, 3.66, 3.04 and 0.03 %, respectively. Figures 5.3 and 5.4 show that the model results are in good agreement with the experimental data. As the combustor calculation is based on the minimization of Gibbs free energy rather than kinetics, this result in higher deviations of the turbine inlet temperature. Further, the large deviations of the H_2O composition in the flue gas may be due to condensation of H_2O during the measurement.

(a)

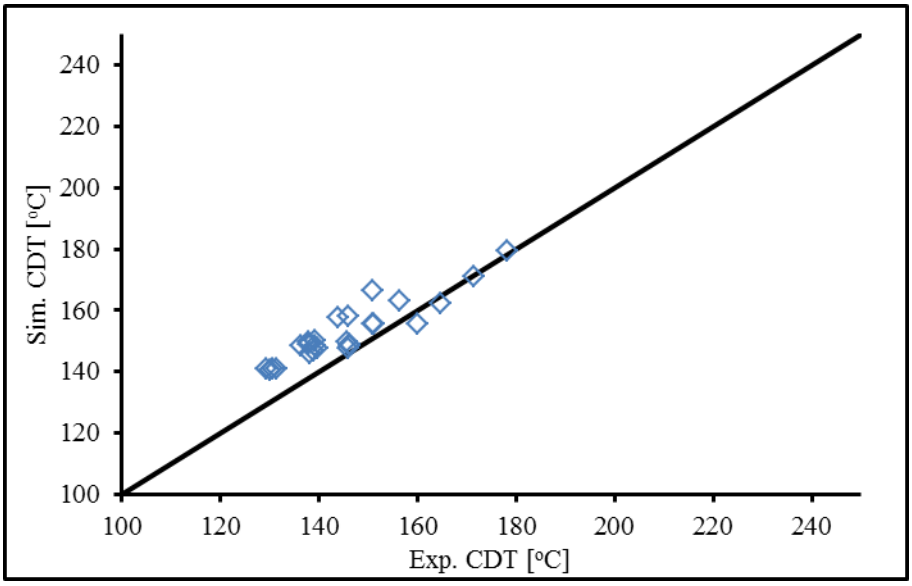

(b)

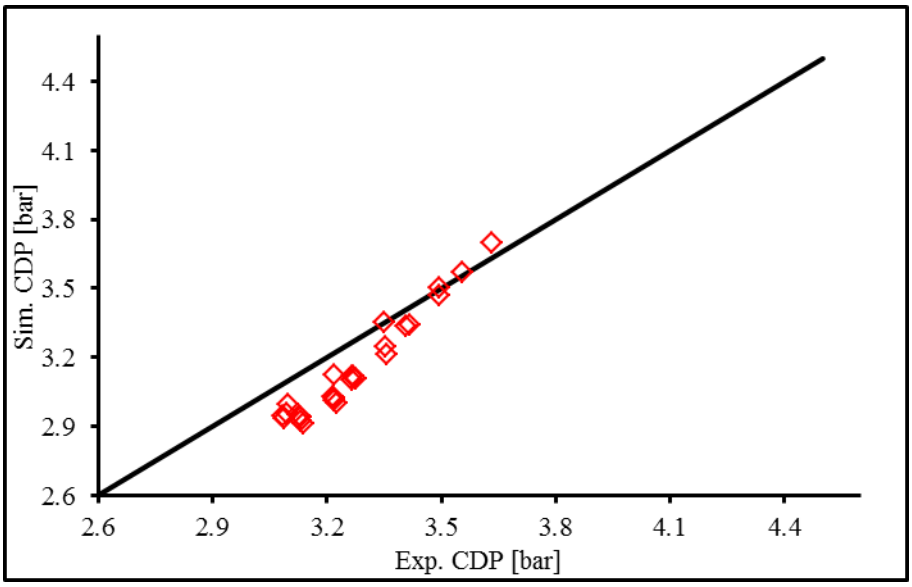

Figure 5.3 Model results as a function of the experimental results (a) Parity plot for compressor discharge temperature; and (b) Parity plot for compressor discharge pressure.

(a)

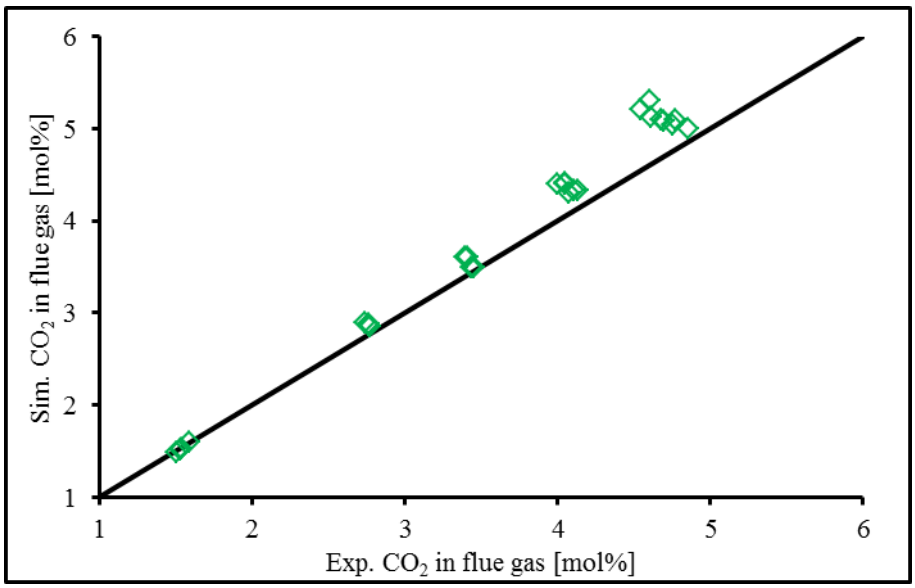

(b)

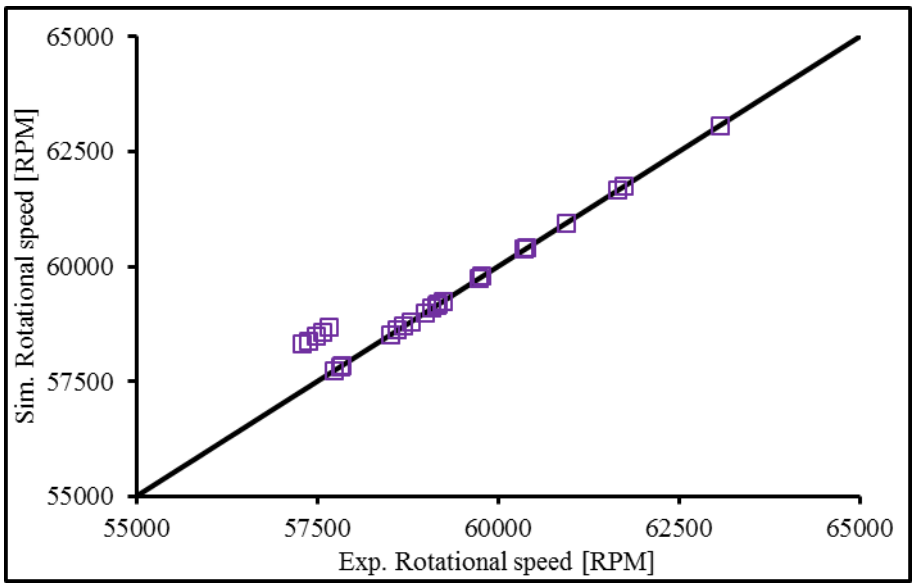

Figure 5.4 Model results as a function of the experimental results (a) Parity plot for CO2 composition in flue gas; and (b) Parity plot for rotational speed.

The tabulated measured experimental and model predicted results are presented in Tables A. 13 and A. 16 of the Appendix A for various part load power outputs of 50, 55, 60 and 65 kW_e. In addition, detailed results are presented for a number of variables that include, turbine inlet temperature, flue gas temperature, rotational speed and H_2O molar composition in the flue gas; other than the variables reported in Figures 5.3 and 5.4. Simultaneous steam and CO_2 injection also results in a decrease in the temperature at different locations of the MGT as is clear in Tables A.13 and A.16 of the Appendix A. The modelling predicts that the temperatures

decline by an average 8 and 2 % for CDT and TIT during the simultaneous injection into the MGT. Similarly, the compressor discharge pressure decreases by an average of 7 % during the simultaneous injection into the MGT. However, the CO_2 concentration in the flue gas increases by 3.4 times that of the CO_2 concentration without any injection. Also, the maximum CO_2 concentration observed is 5.30 mol% due to the simultaneous steam and CO_2 injection into the MGT.

5.3 Process Configuration and Modelling Strategy

The more practical application is to develop the model with auto generated steam injection to the MGT and/or humidification of the compressed air which are termed as a steam injected MGT (MGT-STIG) model and humid air turbine MGT (MGT-HAT) model, respectively. The process system configuration of the MGT-STIG and MGT-HAT will be discussed in detail in Sections 5.3.1 and 5.3.2, respectively. The injection of the steam and water are defined in terms of their ratio to the air flow rate as the steam to air ratio and water to air ratio, respectively. The steam to air and water to air ratios are varied to check their impact on the system performance of the MGT and later the thermodynamic parameters for the developed model are compared with the MGT-EGR developed in Chapter 4 and the MGT base case model developed in Chapter 3.

The steady state models are developed for the MGT-STIG and MGT-HAT in order to study the effect of steam/water injection on the MGT performance. The modelling is done at ISO conditions [187] and the electrical power output is maintained at 100 kW_e and the TOT is fixed at 650 ^oC. The natural gas and air composition are the same as that reported in Tables 3.1 and 3.2, respectively. The property package for the estimation of the thermodynamic properties is the Peng-Robinson equation of state. The minimization of the total Gibbs energy is used as a criterion for the chemical equilibrium in the combustor. More details for the process modelling specification can be found in Section 3.3.2. As discussed in Section 5.2.1, the NBS Steam property package is implemented for the water loop in the STIG cycle and it gives better results in comparison to the ASME 1967 steam property package.

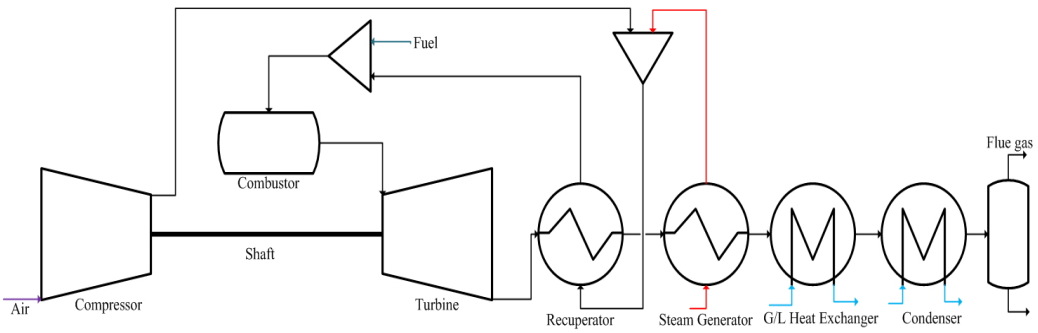

Figure 5.5 Schematic of the micro gas turbine with an auto generated steam injection.

5.3.1 MGT-STIG Model

An option to increase the efficiency of the system is the injection of steam into the MGT. A schematic of the auto generated steam is shown in Figure 5.5. In this work, the steam is injected at the recuperator inlet as discussed in Section 5.2. The steam is auto generated by utilizing the waste heat available after the recuperator through the heat exchanger, termed the steam generator, as shown in Figure 5.5. In order to inject steam smoothly, the injection pressure of the steam should be higher than the live stream pressure at the injection point. The steam is generated at the saturation pressure corresponding to the saturation temperature of 150 ^{o}C. The steady state base case model was altered in such a way to study the degradation of the thermal power due to the addition of the steam generator for auto steam generation. The three heat exchangers, namely recuperator, steam generator and gas-water heat exchanger are arranged in series as shown in Figure 5.5, in order to extract as much heat as possible from the exhaust of the turbine whilst keeping the pinch point of each heat exchanger.

5.3.2 MGT-HAT Model

The problems of the steam injection in terms of the pinch point limitation can be overcome by altering the MGT to a MGT-HAT cycle. The steam generator limitations can be avoided by the implementation of the humidification system, so that the exhaust gas temperatures closely match, in a reversible manner. In the humidification tower, the water evaporates below the boiling point corresponding to the partial pressure of the water in the mixture at the prevailing total pressure in the tower.

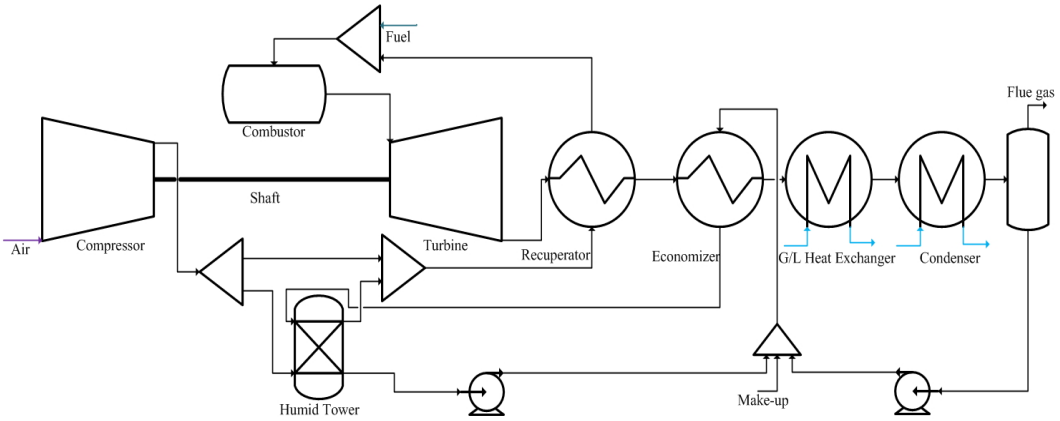

Figure 5.6 Schematic of the micro gas turbine with a humidification system.

The pinch point limitation of the boiler, plus the problem of not utilizing the low grade heat to evaporate the water limits the steam injection process. In contrast, in the humidified tower the air is saturated with water, so that the water stream evaporates across the height of the tower at different saturation temperatures that prevail at the corresponding pressure and the process of humidification is non-isothermal in comparison to the isothermal boiling. The MGT-HAT model is schematically shown in Figure 5.6. In a MGT-HAT cycle, the compressed air passes through the humidification tower and the saturated air from the top of the tower passes through the recuperator and then to the combustor. The water coming into the humidification tower is preheated close to the saturation temperature through an economizer installed after the recuperator in series. In the humidification tower, the air and water contact each other counter currently and thus results in an increase in the evaporation temperature as the air moves up the tower. The major components added to the MGT for the HAT cycle include, the humidification tower for air humidification, the heat exchanger as an economizer for water heating, the condenser to remove water from the exhaust gas, two pumps (one for the condensate water that recirculates back to the economizer, while the second is for the recirculation of the water from the bottom of the humidification tower back to the economizer), splitters and mixers. The splitter after the compressor is for the bypass of the humidification tower when the MGT is to be operated dry or on partial HAT. The water recirculation reduces the water make-up; however, due to the water quality issues, regular make-ups of water are necessary.

5.4 MGT Performance under Steam and Water Injection

The MGT modelling details for steam injection through the MGT-STIG process model are discussed in Section 5.3.1 and the water injection using humidification of the compressed air through MGT-HAT process model are discussed in Section 5.3.2. The process performance for the different alterations to the MGT, including; MGT-EGR from Chapter 4, MGT-STIG and MGT-HAT are presented in Table 5.1. The base case MGT model details and its performance results are presented in Section 3.4 while the MGT-EGR model details and its performance results are presented in Section 4.4. The model performance results discussion for the MGT-STIG and MGT-HAT is provided in the Sections 5.4.1 and 5.4.2, respectively.

Table 5.1 Performance of different MGT models at ISO condition.

Parameter	MGT model	MGT-EGR model	MGT-STIG model	MGT-HAT model
Electrical power [kW_e]	100	100	100	100
Thermal output [kW_{th}]	165	185	100	50
Electrical efficiency [%]	30.2	29.5	32.4	32.1
Overall efficiency [%]	79.9	84	64.8	48.1
Recuperator duty [kW]	310	315	247	400
CO_2 in flue gas [mol%]	1.6	3.5	1.9	1.7
O_2 in flue gas [mol%]	17.5	14.2	17.4	17.6
NO_x in flue gas [ppm]	2.1	1.8	1.9	1.7
Flue gas flow rate [kg/s]	0.8	0.35	0.6	0.65
Fuel consumption [kW]	331	339	309	311
Rotational speed [rpm]	70000	70000	70000	70000
Pressure ratio	4.5	4.5	4.6	4.6
Turbine inlet temperature [^oC]	943	930	950	921
Turbine outlet temperature [^oC]	650	650	650	650
EGR percentage [%]	-	55	-	-
Steam/water injected [g/s]	-	-	17.7	40
Condensation temperature [^oC]	-	15	15	15
G/L heat exchanger water side range [^oC]	20	20	20	20

5.4.1 Impact of Steam Injection

The auto generated saturated steam at 150 ^oC is injected into the MGT at the compressor outlet/recuperator air side inlet which results in an increased electrical efficiency. For more details of the STIG model developed refer to Section 5.3.1. The fractional increase in the electrical efficiency with the increase in the steam to air ratio is shown in Figure 5.7, and the performance of the steam injected MGT is

given in Table 5.1, keeping the amount of the steam injected in the range as reported in the literature [85, 87, 182] for an MGT. The increase in the electrical efficiency is due to the increased mass flow through the turbine section. The steam injection leads to an increase in the electrical efficiency of 2.2 % absolute, and this is the same as reported by De Paepe et al. [182]. The condenser installed at the exit of the G/L heat exchanger, as shown in Figure 5.5 results in the enrichment of the CO_2 in the flue gas, which will be useful for the carbon capture plant as the increased partial pressure of the CO_2 aids in its capture. The CO_2 in the flue gas is increased to 1.9 mol% for the STIG cycle in comparison to 1.6 mol% with no steam injection. Also the condenser reduces the make-up water demand; however due to water quality issues, the condensate is not recirculated in the model developed. The steam injection results in the degradation of the thermal output when steam is auto generated from the MGT.

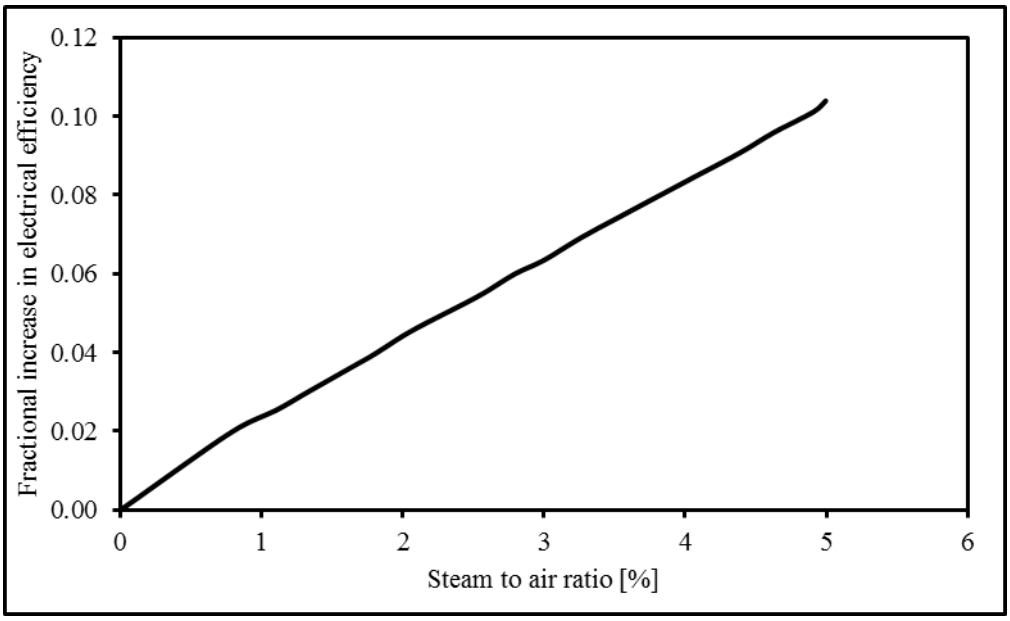

Figure 5.7 Impact of steam injection on the electrical efficiency.

It may be concluded that the thermal mode needs to be disabled for the auto generation of the steam from the MGT due to the higher exergy destruction in the steam generator. The thermal output decreased by 39.4 % in comparison to the base case MGT and hence the overall efficiency also decreased to 64.8 % from 79.9 %. For commercial-scale gas turbine systems, steam injection may lead to the omission of the bottom Rankine cycle. Further, steam injection may lead to combustion problems in terms of flame instability with higher UHC and CO emissions, which

may need combustor modifications to mitigate such effects. As the steam injected is much less than that reported by [197], it will not result in severe combustion instabilities in the MGT.

5.4.2 Impact of Humidified Air Injection

The MGT cycle is altered to check the behaviour of the system when humidified air is used for the combustion and further expansion through the turbine. The details of the HAT cycle can be found in Section 5.3.2. The compressed air is passed through the humidification tower with the same dimensions as in [87, 200] and the humidified air is injected once it is saturated at the outlet. If any carryover of the droplets occurs through the humidification tower, these can be evaporated by heating the air through the recuperator before the combustion section. The HAT cycle increases the electrical efficiency in a similar manner to the STIG cycle. The fractional increase in the electrical efficiency as a function of the water injection into the air is shown in Figure 5.8 and the performance of the HAT cycle is listed in Table 5.1.

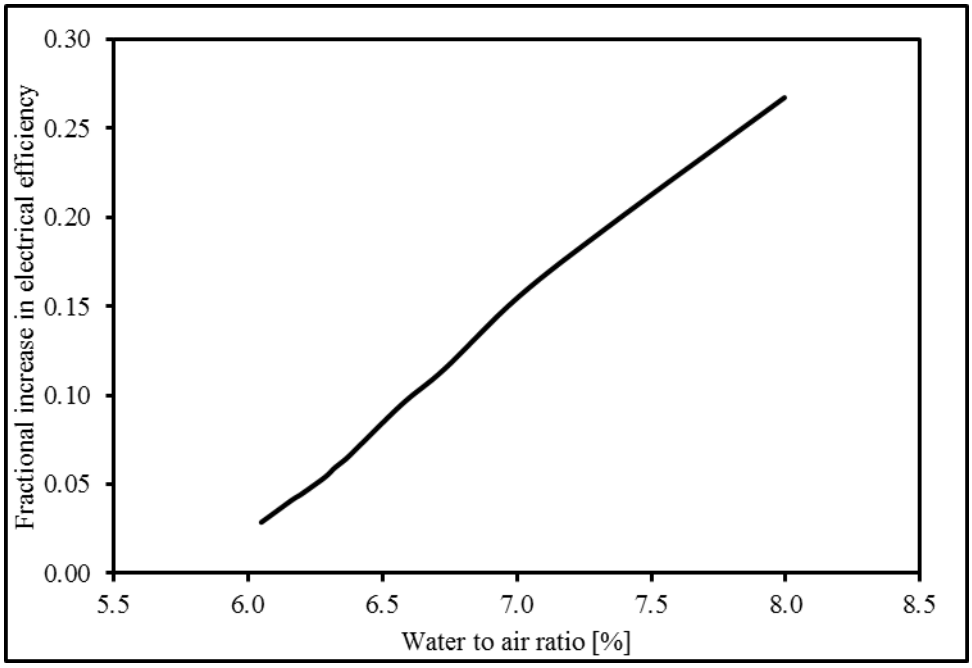

Figure 5.8 Impact of HAT on the electrical efficiency.

The amount of water injected is limited, as reported in the literature [87], for an MGT. The HAT cycle increases the electrical efficiency by approximately 2.1 % absolute, this being approximately the same as that reported by [87, 199]. The HAT

cycle decreases by about 70 % the thermal output and the overall efficiency is limited to 48.1 % in comparison to 79.9 % for the base case MGT. Part of the thermal duty is consumed by the economizer for the preheating of the water before injecting it into the humidification tower. Due to the disabling of the thermal mode, the HAT cycle will also omit the bottom Rankine cycle in a commercial-scale gas turbine system similar to the STIG cycle. The condenser will result in the negative make-up due to the extra water condensed and then injected due to the higher H/C ratio of natural gas. The extra water comes from the natural gas combustion due to the higher H/C ratio. The condenser also contributes to the enrichment of CO_2 from 1.6 to 1.7 mol% in the flue gas. The injected water may cause combustion instabilities and flame fluctuations, which can be implied by the decrease of the TIT and TOT. The NO_x emissions are lowest for the HAT cycle in comparison to the other alterations, and this has been reported by [198]. Hence, the HAT cycle needs combustor modifications in order to cope with the changes in the stream properties.

Further, both the MGT-STIG and MGT-HAT models predict the lower NO_x in comparison to the MGT base case and the MGT-EGR, as presented in Table 5.1.

5.5 Comparative Potential

The changes in the thermodynamic properties of the fluid at different locations in all the aforementioned cycles are listed in Table 5.2. The changes in the thermodynamic properties are due to the change in the composition of the streams unpaid to either the exhaust gas recycle or the injection of water or steam. The thermodynamic properties estimated are the mass density, heat capacity and isentropic co-efficient (γ) at different locations discussed in Section 4.2 and/or Section 5.1. In Table 5.2, the thermodynamic properties are presented for, the MGT base case model discussed in Section 3.4, the MGT-EGR model discussed in Section 4.4, the MGT-STIG model discussed in Section 5.4.1, and the MGT-HAT model discussed in Section 5.4.2.

The mass density of the fluid follows the trend of HAT>MGT>STIG>EGR at the recuperator inlet and turbine inlet, while at the turbine outlet the trend is HAT>MGT>EGR>STIG. The heat capacity of the EGR cycle at the recuperator inlet, turbine inlet and turbine outlet is higher than in the other three cycles. While at

the recuperator inlet the trend of STIG>MGT>HAT is observed. On the other hand, at the turbine inlet and outlet, the heat capacity varies in the order of STIG>HAT>MGT. Similar trends can be traced for the isentropic co-efficient (γ) value. Due to the increased density, the heat duty of the recuperator is higher for the HAT cycle, as presented in Table 5.1. However, for the EGR cycle, the increased heat duty of the recuperator and G/L heat exchanger is due to the increased heat capacity. It can be concluded that the performance of the MGT with its different modifications, including the MGT base case, MGT-EGR, MGT-STIG and MGT-HAT can be judged by understanding the thermodynamic properties of the fluid at the different locations.

Table 5.2 Thermodynamic properties of the fluid at different locations due to the different alterations of the MGT.

	Mass density, [ρ]	Heat Capacity, [c_p]	$\gamma = c_p/c_v$
Units	kg/m^3	kJ/mol K	-
	MGT model		
Compressor inlet	1.21	29.1	1.403
Recuperator inlet	3.18	30.4	1.381
Turbine inlet	1.27	34.6	1.317
Turbine outlet	0.376	33.2	1.335
	MGT-EGR model		
Compressor inlet	1.15	29.5	1.397
Recuperator inlet	3.05	30.9	1.373
Turbine inlet	1.26	35.2	1.310
Turbine outlet	0.372	33.7	1.328
	MGT-STIG model		
Compressor inlet	1.21	29.1	1.403
Recuperator inlet	3.15	30.6	1.378
Turbine inlet	1.25	35.0	1.312
Turbine outlet	0.369	33.5	1.330
	MGT-HAT model		
Compressor inlet	1.21	29.1	1.403
Recuperator inlet	4.31	30.1	1.398
Turbine inlet	1.33	35.0	1.312
Turbine outlet	0.390	33.4	1.331

Despite the technical challenges for the each alternative cycle presented, combustion instability is the issue of concern because it might result in flame instability along with higher UHC and CO emissions due to the changes in the fluid properties. Therefore, modifications in the combustor might be needed for these three novel cycles. The injection of steam and water in the STIG and HAT cycles, respectively, may also result in an imbalance on the shaft as the mass flow of the fluid is different,

which is expanding through the turbine section, in comparison to the fluid which is compressed.

5.6 Conclusions

- The thermodynamic performance of three novel cycles, namely EGR, STIG and HAT cycles are compared with the base case MGT cycle. The thermodynamic and process system analysis provided thorough information on the performance of the novel cycles and results in an accurate demonstration of the MGT applicability and flexibility for these modifications.
- The MGT model is validated against variable steam and simultaneous steam and CO_2 injection at different part load conditions. The steam injection results in a decrease in the values of the process conditions at different locations of the MGT. However, this decrease is less when simultaneous injection of steam and CO_2 is assessed. The CO_2 concentration in the flue gas increases by 3.4 times to the CO_2 concentration without injection. Further, if the water in the flue gas is condensed then the CO_2 concentration will be enhanced.
- The process system analysis for different modifications of the MGT showed that the CO_2 enrichment varies from the 1.6 mol% in the base case MGT cycle to 3.5, 1.9 and 1.7 mol% in the MGT-EGR, MGT-STIG and MGT-HAT cycle, respectively. The increased CO_2 content in the flue gas of all the novel cycles show a potential advantage when integrated with a PCC technology. Moreover, for the EGR cycle the flue gas flow rate decreases by 55 %, which will require a smaller PCC plant with lower specific reboiler duty as found in Chapter 4.
- The results show that the electrical efficiency increases by 7.3 and 6.3 % for the MGT-STIG and MGT-HAT cycle and decreases by 2.3 % for the MGT-EGR cycle in comparison to the base case MGT cycle with 30.2 % electrical efficiency.
- Due to the higher total efficiency, the MGT-EGR cycle is superior to the other two modifications, especially for integration with a CO_2 capture system as a result of lower load and higher CO_2 enrichment. However, at a

distributive level of power generation, where the sole purpose is to have the highest electrical power output, the MGT-STIG and MGT-HAT cycle will be the preferred choices due to the higher electrical efficiencies.

- Therefore, in spite of the technical challenges to the modifications, the innovative cycles show the potential to improve the performance in terms of either efficiency or CO_2 capture readiness due to CO_2 enrichment. There is a trade-off between CO_2 enhancement and increase in electrical efficiency and the choice of MGT cycle modifications should depend on the adopted criteria.

In order to assess the impact of the CO_2 enhancement on the CO_2 capture plant, the amine-based CO_2 capture plant model is developed in Chapter 6. The developed model is tested against the extensive set of pilot-scale amine-based CO_2 capture plant facilities with the focus on the flue gas over a wider range of CO_2 concentrations. Further, the sensitivity analysis was performed for the developed process model of the pilot-scale amine-based CO_2 capture in order to check the behaviour of the amine-based CO_2 capture plant against variables process operating parameters.

Chapter 6
Process Modelling of Pilot-Scale Amine-Based CO_2 Capture Plant

In this chapter, a reactive absorption stripping process model of a CO_2 capture system is developed. The process modelling is performed using a rate-based thermodynamic property package incorporating the chemical reactions involved in the amine-based CO_2 capture plant. The developed model is tested against two sets of extensive experimental data for the model validation using monoethanolamine as the liquid solvent. The model is further tested through a sensitivity analysis to understand the effect of the varying operating conditions over wide range of parameters.

6.1 Introduction

From the available options as discussed in Section 1.2.2.1, the PCC technology is a readily available option to integrate with the existing power plants and/or new power plants based on fossil fuels. The present chapter focuses on the model development for the PCC technology; amine-based CO_2 reactive absorption system and the model is validated against the extensive experimental data. The model validation at the pilot-scale is performed in order to ascertain if the model is capable of representing the performance of the system under consideration, and the model results are compared with the experimental results. Further, a sensitivity analysis of the pilot-scale amine-based CO_2 capture plant is presented to understand the process performance of the system for variable operating parameters.

A basic schematic of the CO_2 capture process is shown in Figure 6.1. It consists of an absorber, stripper, water wash column, cross heat exchanger, solvent tanks for spent and fresh solvents, reboiler and condenser for the stripper column. Also, the CO_2 capture plant is equipped with a flue gas desulphurization unit and direct contact cooler which are emitted from Figure 6.1 for simplicity. The flue gas; from the facility, which may be coal, gas, biomass fired power plant; is passed through

the direct contact cooler in which it is cooled in a counter current manner. The cooled flue gas is passed through desulphurization section to remove any traces of the SO_2 for the flue gas coming from coal/biomass-fired facility. However, for the gas-fired facility, the desulphurization section is bypassed. The flue gas then enters the bottom of the packed absorber which is in contact with the absorbent solution in a counter current manner. The treated gas from the absorber top enters the water wash section to remove traces of the solvent carried by the treated gas before being released to the atmosphere. The rich solution containing CO_2 is pumped through the cross heat exchanger into the packed stripper column for solvent regeneration, releasing a high concentration CO_2 stream at the top of the stripper. The lean solvent runs down the stripper and is cooled through the rich solvent. Further, the regenerated solvent after further cooling through lean cooler is recirculated back to the top of the absorber.

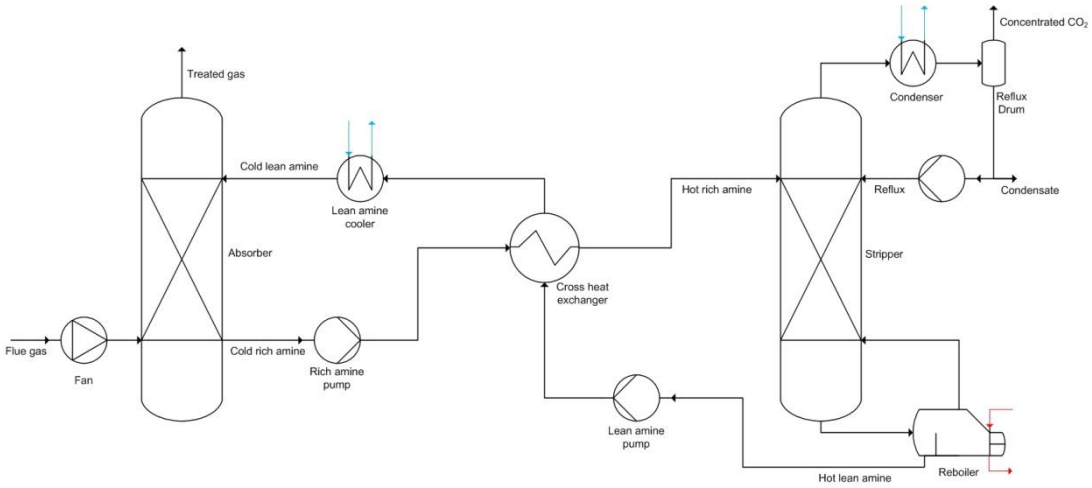

Figure 6.1 Basic schematic of the CO_2 capture plant.

6.2 Modelling Details

The modelling of the pilot-scale amine capture plant is realised in Aspen Hysys by incorporating the new Acid Gas property package rather than equilibrium based Amine package. The Acid Gas property package is the integral functionality of Aspen and it is based on the Electrolyte Non-Random Two Liquid (Electrolyte NRTL) thermodynamic model for liquid phase electrolyte properties. The model used for the vapour phase properties is the Peng-Robison Equation of State [202]. In the open literature, the model is extensively validated against the set of experimental data [118]. The principal reactions involving equilibrium, chemistry of CO_2 and

MEA solution, along with kinetic reactions involving formation of carbamates and bicarbamates, are given in Table 6.1 [118, 158, 202].

The expression for the kinetically governed chemical reactions is expressed as follows:

$$R_i = k_i f(\alpha) - k_i^j f^j(\alpha) \tag{6.8}$$

where the R_i is the rate of the reaction for i^{th} reaction, k_i is the reaction rate constant for forward reaction while k_i^j is the reaction rate constant for the backward reaction and the α is the base component for the chemical reaction. The expressions for the reaction rate constants are given as follow:

$$k_i = A_i \exp\left[\frac{-E_i}{RT}\right] T^{x_i} \tag{6.9}$$

$$k_i^j = A_i^j \exp\left[\frac{-E_i^j}{RT}\right] T^{x_i^j} \tag{6.10}$$

where A_i and A_i^j are the pre exponential factors for forward and reverse reactions, respectively; E_i and E_i^j are the activation energies for forward and reverse reactions, respectively; R is the ideal gas constant, T is the absolute temperature, and x_i and x_i^j are the extended reaction rate constants for the forward and reverse reactions, respectively, and their values are zero for all the reactions. The kinetic data for the kinetically governed chemical reactions is listed in Table 6.2.

Table 6.1 Principal equilibrium and kinetic reactions [118, 158, 202].

Reactions	Reaction Type	Reaction Number
$H_2O + MEAH^+ \leftrightarrow MEA + H_3O^+$	Equilibrium	(6.1)
$2H_2O \leftrightarrow H_3O^+ + OH^-$	Equilibrium	(6.2)
$HCO_3^- + H_2O \leftrightarrow CO_3^{2-} + H_3O^+$	Equilibrium	(6.3)
$CO_2 + OH^- \rightarrow HCO_3^-$	Kinetic	(6.4)
$HCO_3^- + \rightarrow CO_2 + OH^-$	Kinetic	(6.5)
$MEA + CO_2 + H_2O \rightarrow MEACOO^- + H_3O^+$	Kinetic	(6.6)
$MEACOO^- + H_3O^+ \rightarrow MEA + CO_2 + H_2O$	Kinetic	(6.7)

The correlations used for the mass transfer, interfacial area, pressure drop are built-in Aspen. The Bravo-Fair correlation [203] was used for the mass transfer and interfacial area estimation. For the pressure drop, the built-in vendor correlation for the particular packing was used. The model components include; two packed columns; one for the absorber with the upper portion acting as a water-wash section and the other for the stripper; two heat exchangers as the cross heat exchanger and lean amine cooler; two pumps for the lean and rich amine circulation; reboiler and condenser across the stripper column and make-up units. The model replicates the flowsheet schematic shown in Figure 6.1.

Table 6.2 Kinetic data for the kinetically governed reactions [158].

Species	Reaction Direction	Activation Energy [kJ/mol]	Pre-exponential Factor [kmol/m^3 s]
HCO_3^-	Forward	5547	1.33E+17
HCO_3^-	Reverse	107420	6.63E+16
$MEACOO^-$	Forward	41264	3.02E+14
$MEACOO^-$	Reverse(absorber)	69158	5.52E+23
$MEACOO^-$	Reverse(stripper)	95384	6.50E+27

Two process performance bounds are recommended in the literature [204, 205] when estimating the diameter of packed column for the specific liquid and the gas flow rates. The pressure drop across the height of the packing in the columns should not exceed 20.83 mm of H_2O per meter of the packing for amine systems [204, 205], and the approach to the maximum capacity should not exceed 80 % of the flooding velocity [204, 205]. These process performance bounds are designed to achieve 90 % separation of the CO_2 and the column height is estimated for achieving this amount of separation.

6.3 Experimental Data

In the literature, there are various pilot-scale CO_2 capture plant studies reported with the MEA as solvent [129, 139, 194, 206-208]. Most of the reported data lacks complete disclosure of the information to be used for the modelling purposes. Dugas [208] reported data is majorly focused on the mass transfer performance of the absorber and stripper. However, the experimental results reported by Notz et al.

[139] is a set of comprehensive case studies incorporating a variety of the variables for a number of the operable ranges.

The pilot-scale amine-based CO_2 capture plant model is validated against the two sets of experimental data for the pilot-scale study of the PCC technology by reactive absorption. The 1st set of experimental data for the pilot-scale amine-based CO_2 capture plant was reported by Notz et al. [139] who carried out the investigation at the Laboratory of Engineering Thermodynamic, Technical University of Kaiserslautern, Kaiserslautern, Germany. The 2nd set of experimental data for the pilot-scale amine-based CO_2 capture plant was reported by Akram et al. [129] who carried out the investigation at the PACT facilities, the UKCCS Research Center, Sheffield, UK. Both of the studies reported results for an aqueous solution of MEA with strength of 30 wt. %.

Table 6.3 Boundary conditions in terms of packing and dimensions for the pilot-scale amine-based CO_2 capture plant for both sets of experimental data.

Packing and dimensions for the Amine Capture plant.		
	1st Set [139]	2nd Set [129]
Absorber		
Packing Type	Sulzer Mellapak	IMTP
Packing Dimensions [mm] / Type	250Y	25
Packing Height [m]	4.2	8
Diameter [mm]	125	303
Sections	5	2
Water Wash Section		
Packing Type	Sulzer Mellapak	IMTP
Packing Dimensions [mm]	250Y	25
Packing Height [m]	0.42	1.2
Diameter [mm]	125	303
Sections	1	1
Stripper		
Packing Type	Sulzer Mellapak	IMTP
Packing Dimensions [mm]	250Y	25
Packing Height [m]	2.52	8
Diameter [mm]	125	303
Sections	3	2

The 1st set of experimental data used for model validation consisted of 13 variation studies with a total of 47 associated experiments for the pilot-scale CO_2 capture plant. All the process performance indicators are indicated for each of the experiments at different locations in the pilot-plant. The flue gas from the gas-fired burner was used for pilot-scale CO_2 capture plant. To study the behaviour of the coal-fired power plant, either the CO_2 from the stripper top is recycled and/or the CO_2 is injected in the flue gas from the CO_2 storage bottles. To perfectly simulate the behaviour of the flue gas from coal-fired power plant, traces of NO_x and SO_2 were also added. The columns of the CO_2 capture plant are filled with the structured Sulzer Mellapak packing. The process layout of the plant is the same as that reported in Section 6.1 and more specific details can be found in literature [139]. The boundary conditions for the 1st set of experimental data for the pilot-plant can be found in the Table 6.3.

The 2nd set of experimental data used for model validation is reported for the 1 ton per day of the CO_2 capture facility based on an aqueous solution of MEA for a flue gas from the gas-fired facility. The Solvent based Carbon Capture Plant (SCCP) can accommodate a variety of solvents and is equipped with a flue gas desulphurization unit, for the pre-treatment of the flue gas depending on the sulphur content of the flue gas, through a carbonate wash. The plant is equipped with temperature and deferential pressure sensors and sampling ports and it is controlled and monitored by a dedicated control system. The plant can be integrated with a 250 kW air-fired combustion plant, 300 kW micro gas turbine and/or gas mixing facility. This results in the incorporation of the real plant flue gas from coal, biomass, natural gas, synthetic gas or co-firing. However, for the present study the pilot-scale amine-based CO_2 capture plant is integrated with the slip stream of the exhaust gas of the 100 kW_e micro gas turbine. To enhance the CO_2 concentration of the exhaust gas, the CO_2 is injected into the slip stream of the micro gas turbine before entering the absorber. The columns of the CO_2 capture plant are filled with random INTALOX Metal Tower Packing (IMTP). The process layout of the plant is the same as that reported in Section 6.1 and more specific details can be found in the literature [129]. The boundary conditions for the 2nd set of experimental data pilot plant can be found in the Table 6.3.

6.4 Model Validation against the 1st Set of Experimental Data

The pilot-scale amine-based CO_2 capture plant model is validated against the extensive pilot-scale experimental results reported by Notz et al. [139]. The model was tuned and ran for the input conditions for all the 47 experiments and the model results for the selected parameters are presented in Table B.1 in Appendix B. The boundary conditions for the model are given in Table 6.3. The mean percent absolute deviation for rich and lean loadings, specific reboiler duty and CO_2 capture rate are 2.8, 2.6, 5.0 and 0.6 %, respectively.

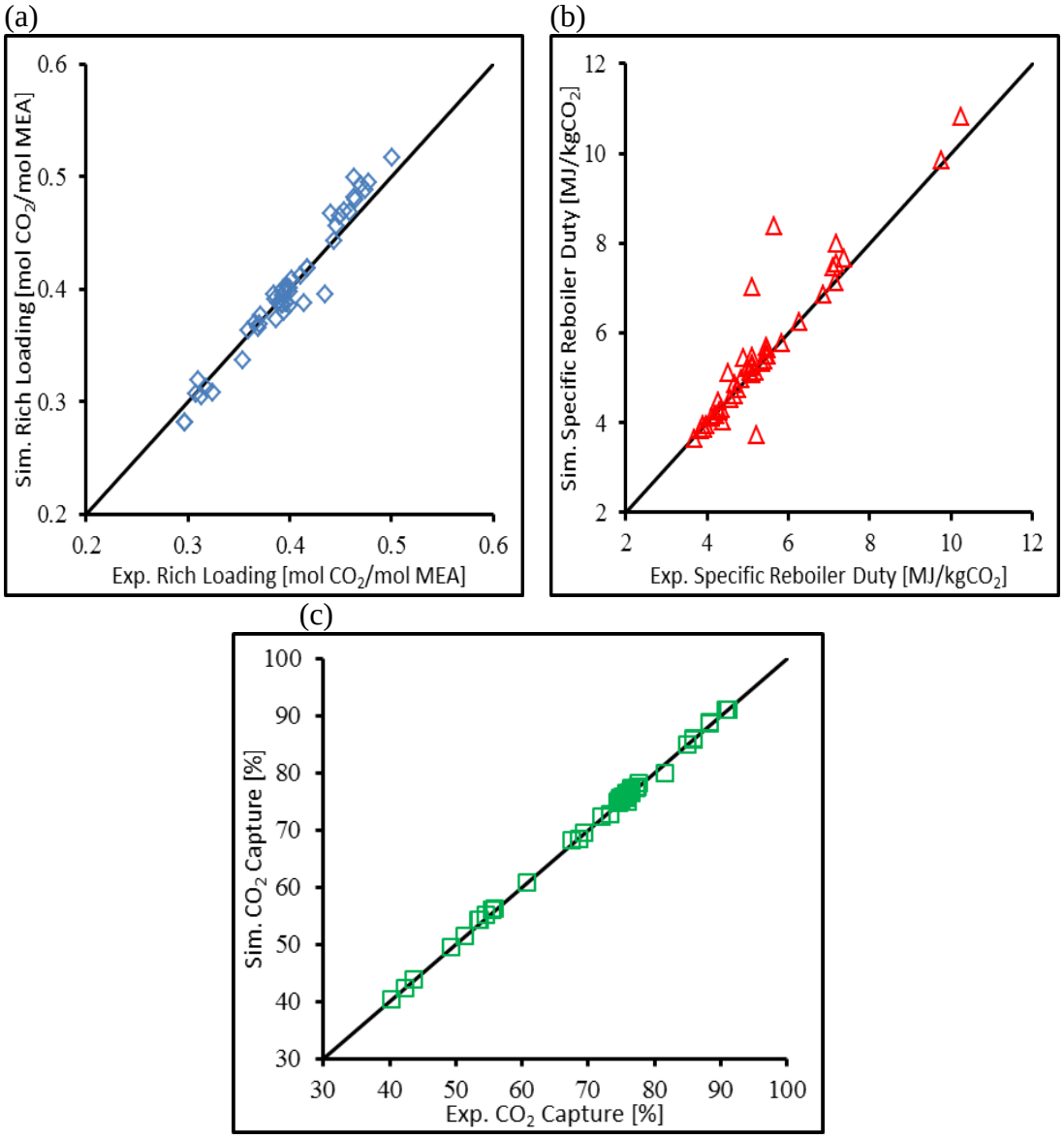

Figure 6.2 Model results as a function of the experimental results reported by Notz et al. [139] (a) Parity plot for rich loading; (b) Parity plot for specific reboiler duty; and (c) Parity plot for CO_2 capture.

These indicate that the model results are in good agreement with the reported experimental results. The model results are summarised in Figure 6.2 as parity plots for rich CO_2 loading, specific reboiler duty and CO_2 capture rate. Some of the outliers in Figure 6.2 (b) are due to the experimental uncertainty which is 6 % for the reboiler duty as reported by Notz et al. [139]. As one of the case studies reported is for the variation of the CO_2 partial pressure in the flue gas and this is of major interest to the understanding of the behaviour of the CO_2 enhancement on the performance of the pilot-scale amine-based CO_2 capture plant.

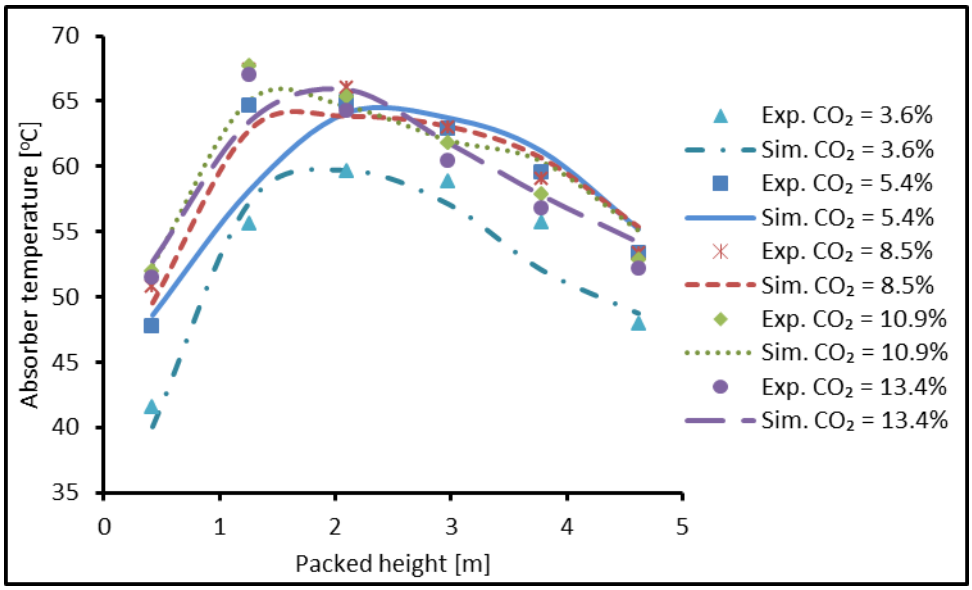

Figure 6.3 Model and experimental results for the absorber temperature profiles reported by Notz et al. [139] for the set of experiments designated as Set E, reporting the variation of the CO_2 composition in the flue gas.

The case is studied in detail to implement the performance of the exhaust gas recirculation to the commercial-scale power plant and study the effect on the integrated amine-based CO_2 capture plant. Therefore, the absorber and stripper temperature profiles, as shown in Figure 6.3 and Figure 6.4, respectively, for the set of experiments designated as Set E, and this variation study is focused on the variation of the CO_2 composition in the flue gas, ranging from 3.6 to 13.4 mol% with the liquid to gas ratio maintained at 2.8. This range of the CO_2 composition in the flue gas represents the wider range from commercial-scale natural gas fired power plants to coal fired power plants and also covering the intermediate range of exhaust gas recirculation to the natural gas fired power plant. It is evident from Figure 6.2, Figure 6.3 and Figure 6.4, that the model results are in good agreement with the reported experimental results. Having validated the model results against

the experimental results for the two pilot-scale experimental investigations, especially with emphasis on the results for the CO_2 enhanced flue gas from the gas-firing, the process model can be used with confidence to predict the design and/or scale-up of the amine-based CO_2 capture plant.

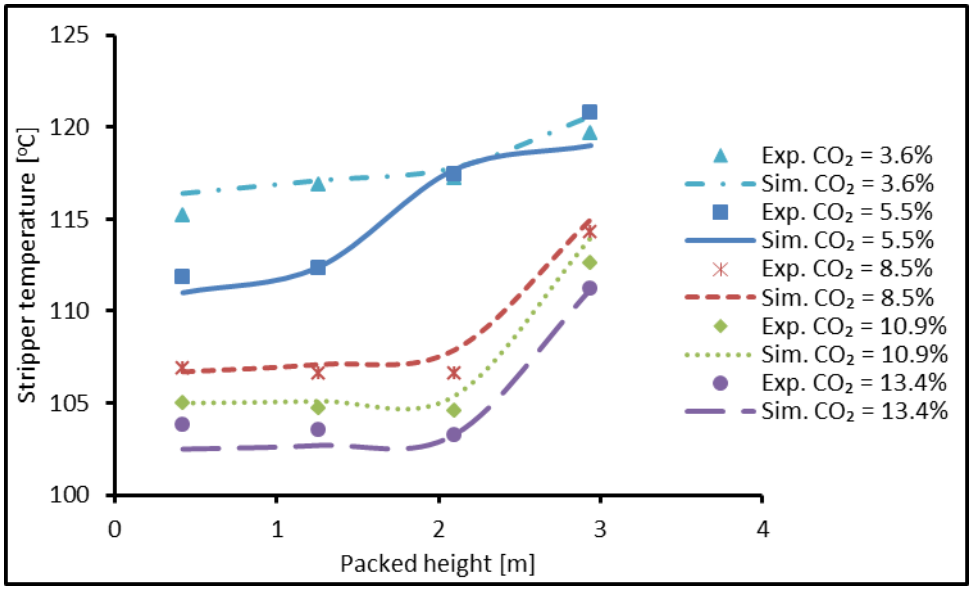

Figure 6.4 Model and experimental results for the stripper temperature profiles reported by Notz et al. [139] for the set of experiments designated as Set E, reporting the variation of the CO_2 composition in the flue gas.

6.5 Model Validation against the 2nd Set of Experimental Data

The pilot-scale amine-based CO_2 capture plant model was also validated against the in-house experimental results reported by Akram et al. [129]. The model was tuned and ran for the input conditions for all the experiments and the model results for the selected parameters are presented in Table 6.4. The boundary conditions for the model are given in Table 6.3. The experimental details have been presented by Akram et al. [129] and therefore are not discussed here. The experimental investigation performed was focused on the exhaust gas recirculation for the micro gas turbine and the capture of CO_2 from the CO_2-enriched flue gas. The CO_2 stream is injected into the slip stream of the exhaust gas of the micro gas turbine to enhance the CO_2 concentration at the absorber inlet. The range of the CO_2 composition in the flue gas investigated varies from 5.5 mol% to 9.9 mol% which covers the wider operating range for commercial-scale NGCC with EGR, and the packing employed in the absorber and stripper is the random IMTP 25.

Table 6.4 Pilot-scale Amine-based CO_2 capture plant model validation against the 2nd set of experimental data.

Case	1		2		3		4		5	
	Exp.	Sim.	Exp.	Sim.	Exp.	Sim.	Exp.	Sim.	Exp.	Sim.
CO_2 composition (after CO_2 injection) [mol%]	5.5	5.5	6.6	6.6	7.7	7.7	8.3	8.3	9.9	9.9
Lean solvent concentration [wt.%]	31.9	31.9	29.9	29.9	31.7	31.7	29.8	29.9	30.5	30.5
Rich solvent concentration [wt.%]	30.8	30.8	27.8	28.8	30.6	30.6	27.5	28.9	29.1	29.4
Lean solvent loading [mol CO_2/mol MEA]	0.165	0.165	0.172	0.172	0.183	0.183	0.18	0.181	0.204	0.203
Rich solvent loading [mol CO_2/mol MEA]	0.388	0.379	0.399	0.398	0.411	0.396	0.417	0.410	0.443	0.425
Degree of regeneration [%]	57.5	56.5	56.9	56.8	55.5	53.8	56.8	55.9	54	52.3
Mass flow of flue gas [kg/h]	242.1	242.1	245.8	245.8	246.4	246.4	247.9	247.9	248.4	248.4
Liquid to Gas ratio (L/G)	1.7	1.7	2	2	2.3	2.3	2.4	2.4	2.9	2.9
Solvent to CO_2 ratio [kg/kg]	19.9	20.0	20.6	20.1	21.1	20.1	20.7	19.8	21.7	20.0
Specific reboiler duty [GJ/tCO_2]	7.1	6.9	7.4	7.2	6	6.0	6.1	5.9	5.3	5.2
Stripper bottom temperature [^oC]	110.4	109.0	108.8	108.7	109.7	109.7	108.8	108.8	108.8	108.7
Absorber inlet gas temperature [^oC]	37.0	37.0	39.0	39.0	38.0	38.0	38.0	38.0	40.0	40.0
Wash column circulating liquid [^oC]	46.4	46.4	48.5	48.5	50.7	50.7	51.0	51.0	52.7	52.7
Wash column exit gas [^oC]	42.6	42.4	44.3	43.1	45.5	43.5	46.7	46.0	48.9	47.9
Absorber exit gas [^oC]	40.6	40.5	41.4	41.3	45.5	44.3	43.5	42.9	44.9	44.2

The mean percentage absolute deviation for the specific reboiler duty, rich and lean loadings and rich and lean solvent concentrations are 2.0, 2.4, 0.2, 1.9 and 0.1 %, respectively. The maximum uncertainty in the MEA concentration and CO_2 loading during experimental campaign were 0.3 and 3.1 %, respectively. The methodology adopted for the measurements of MEA concentration and CO_2 loadings can be found in the Akram et al. [129]. These indicate that the model results are in good agreement with the experimental results.

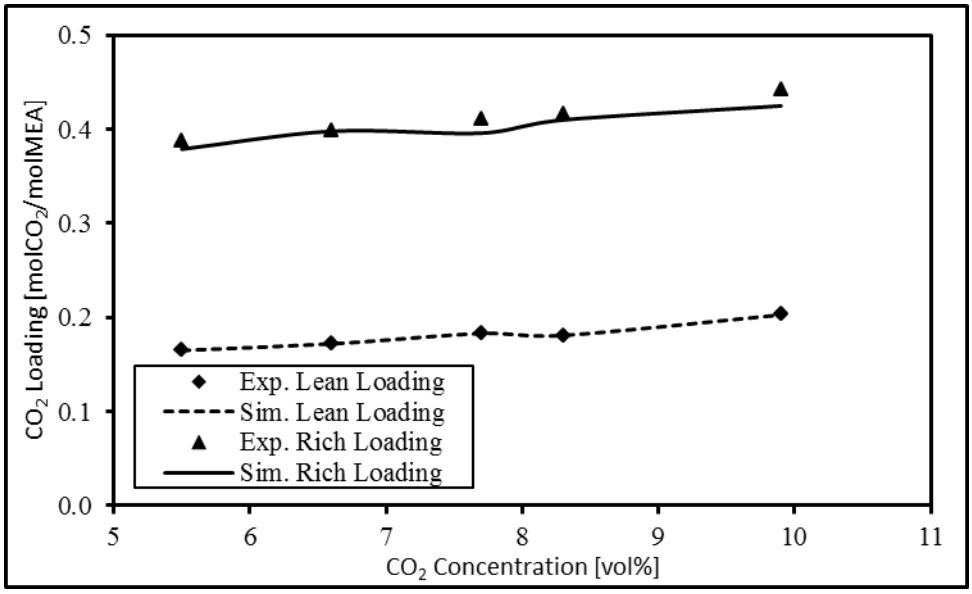

Figure 6.5 Model and experimental results for the lean and rich solvent loading as a function of the CO_2 concentration in flue gas.

The variation of the CO_2 loadings, both lean and rich, for the variation of CO_2 concentration in the flue gas entering the absorber column is shown in Figure 6.5 and the variation of the specific reboiler duty as a function of the CO_2 concentration of the flue gas is shown in Figure 6.6. The reboiler duty consists of the three contributions for the stripping of the CO_2 from the rich solvent, including sensible energy to raise the temperature, vaporization energy to raise the stripping agent steam and desorption energy to liberate CO_2 out of the solvent. It is observed that from the total reboiler duty, 25 % is being used for the steam raising. The more details of the impact of the CO_2 enhancement on the stripper and more especially the reboiler can be found in Akram et al. [129]. The absorber column temperature profile along the height of the absorber column, for various CO_2 concentrations as reported in Table 6.4, is plotted in Figure 6.7 in order to understand the effect of the CO_2 concentration on the performance of the column.

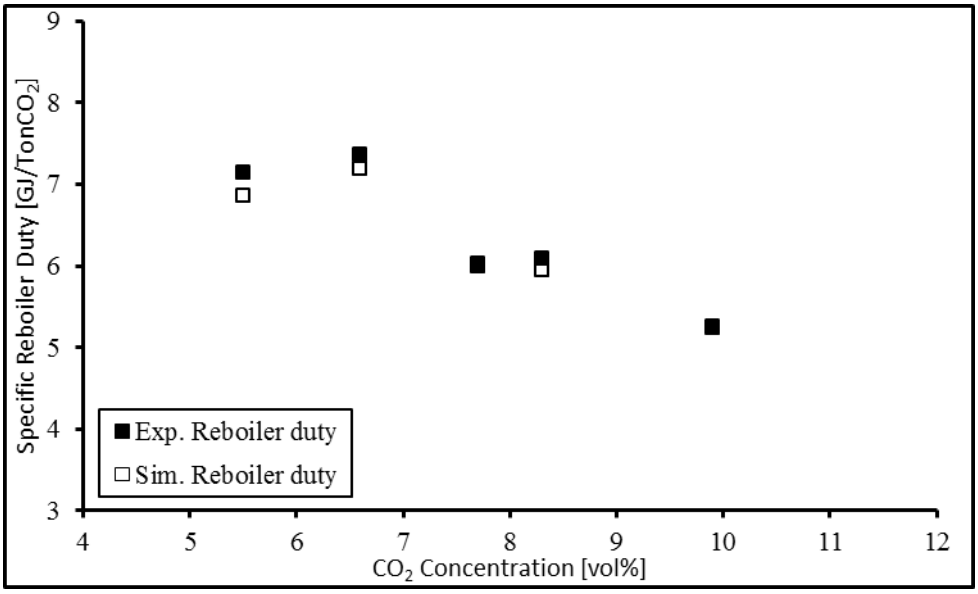

Figure 6.6 Model and experimental results for the specific reboiler duty as a function of the CO_2 concentration in flue gas.

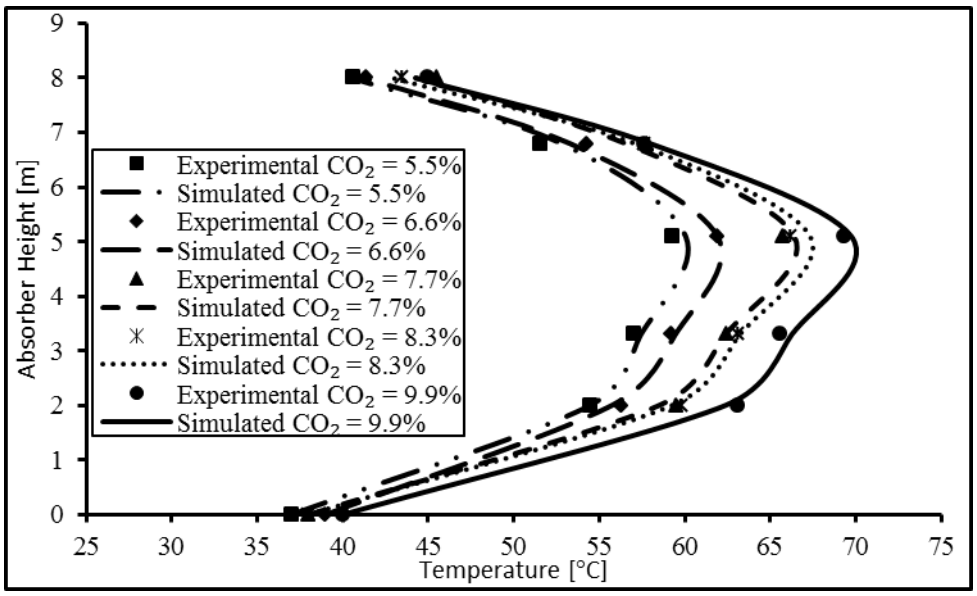

Figure 6.7 Model and experimental results for the absorber temperature profile along the height of the absorber column for various the CO_2 concentrations in flue gas.

Similarly, the stripper temperatures at various locations of the stripper column, as a function of the CO_2 concentration of the flue gas, are plotted in Figure 6.8. From the above discussion and the validation results of the amine-based CO_2 capture plant model against the extensive experiment investigations reported by Notz et al. [139] and Akram et al. [129] have confirmed the robustness of the model. Especially the validation results indicate the effect of the CO_2 enhanced flue gas from the gas-fired turbine and/or burner on system. Hence, the process model developed can be used

with confidence to predict the design and/or scale-up of the amine-based CO_2 capture plant.

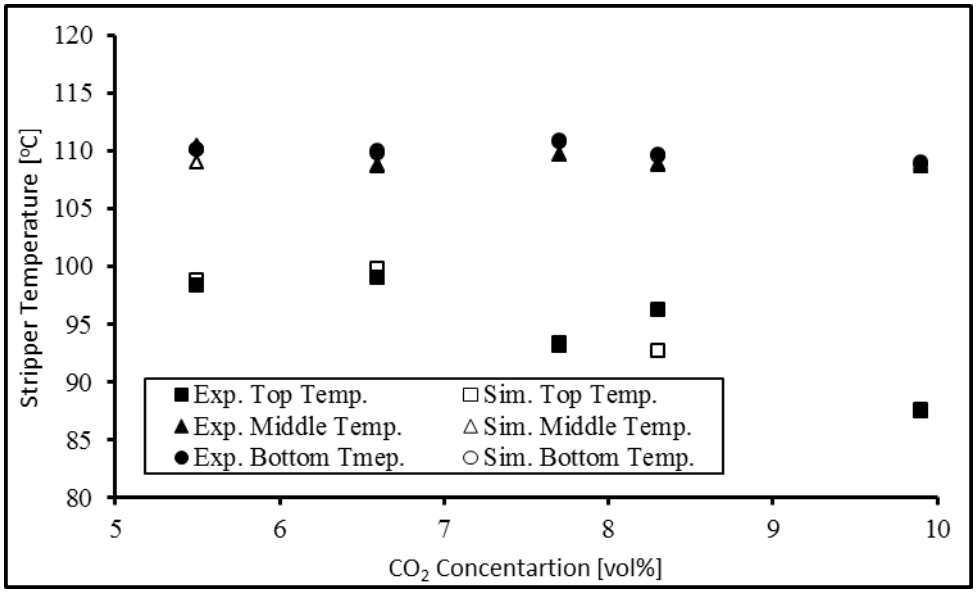

Figure 6.8 Model and experimental results for the stripper temperature profile for various the CO_2 concentrations in flue gas.

6.6 Sensitivity Analysis

The sensitivity analysis provides a useful means to investigate the effect of the process parameters and judge the performance of the system under investigation. The analysis will provide a reliable operability range for the PCC technology and will assists in the understanding of the process operation of the PCC technology at an industrial level. Operational parameters are varied to check the effect of these variables, and to better analyse the process performance and design of the PCC technology. The effect of the most important parameters, such as the temperature of the flue gas and the solvent circulated, CO_2 composition in flue gas, solvent concentration, L/G ratio by varying the solvent flow rate, lean loading, CO_2 capture rate and operating pressure, are varied for a specified range. The specified range for a specific parameter is either dictated by a general rule of thumb or the restrictions due to corrosion of material of construction. The performance parameters are specific reboiler duty, lean and rich CO_2 loadings, absorber and stripper temperature profiles; on which the effect of the aforementioned parameters is checked. So, in total 8 sets of sensitivity analysis case studies are performed and their classification along with ranges of the variables in which they are varied is given in Table 6.5.

Table 6.5 Case studies for the sensitivity analysis of the pilot-scale amine based CO_2 capture plant.

Set No.	Sensitivity Analysis	Type
Set A	Variation of CO_2 composition in flue gas ($5.5\ mol\% \geq y_{CO2} \leq 9.9\ mol\%$)	Experimental and Modelling
Set B	Variation of CO_2 capture rate ($60\% \geq \psi \leq 95\%$)	Modelling
Set C	Variation of liquid flow rate ($0.6 \geq L/G \leq 2.6$)	Modelling
Set D	Variation of amine strength ($20wt\% \geq \omega \leq 36wt\%$)	Modelling
Set E	Variation of lean amine loading ($0.10 \geq \alpha \leq 0.35$)	Modelling
Set F	Variation of flue gas temperature ($30^oC \geq T_G \leq 50^oC$)	Modelling
Set G	Variation of liquid temperature ($30^oC \geq T_L \leq 50^oC$)	Modelling
Set H	Variation of stripper pressure ($1.2bar \geq P_s \leq 2.2bar$)	Modelling

The type of the case study either performed through modelling only or is supported through an experimental sensitivity analysis is given in Table 6.5. The sensitivity analysis is performed for the PACT solvent-based CO_2 capture plant model developed and validated in Section 6.6. The variation case studies as listed in Table 6.5, is discussed in detail in the subsequent subsections.

6.6.1 Variation of the CO_2 Composition in the Flue Gas – Set A

The composition of the CO_2 in the flue gas which is assisted towards the absorber of the pilot-scale amine-based CO_2 capture plant is varied from 5.5 mol% to 9.9 mol%, and other parameters, such as solvent concentration 30 wt.%, CO_2 capture rate 90 %, temperature of the flue gas and lean solvent 40 ^oC and stripper pressure 1.2 bar, are maintained. The effect of the CO_2 composition on the lean and rich solvent loading and specific reboiler duty are shown in Figure 6.5 and Figure 6.6, respectively. With the increase of CO_2 content in the flue gas, both loadings; lean and rich CO_2 loadings increases, also the difference between rich and lean CO_2 loadings increase. This indicates that the amount of the CO_2 absorbed in the rich solvent flowing towards the bottom of the absorber column is increasing. Moreover, with the increase of the CO_2 content in the flue gas, the number of molecules of the CO_2

increases; which results in the enhanced driving force and hence the mass transfer also increases [139]. The increased lean loading results in the lower steam requirements in the stripper, hence the regeneration in the stripper is becoming easier with the reduced energy requirement in the reboiler for the increased CO_2 content in the flue gas. Also, the minimum specific energy requirement would be achieved if the maximum rich CO_2 loading is achieved, which depends on the thermodynamic equilibrium solubility of the CO_2 at the prevailing conditions.

The absorber and striper temperature profiles are given in Figure 6.7 and Figure 6.8, respectively. The mean percent absolute deviations for the temperature measurements at different locations across the absorber column are 1.0, 0.5, 0.9 and 1.6 % for T_1, T_2, T_3, and T_4, respectively. With the increase in the CO_2 composition, the absorber temperature bulge should moves towards the top of the absorber. Since, the increased CO_2 concentration increases the mass transfer, however, the increased temperature bulge results due to the reduced absorption rates which in turn suggests the installation of the inter cooler across the absorber. However, these are not observed or clear in Figure 6.7, due to only 4 measurement points during the experimental campaign. The temperature bulge in the model results and as obtained through the measured ones are approximately the same. The simulated stripper temperatures were also measured at the same locations as in the experimentation. The mean percent absolute deviation for the stripper temperatures are 1.0, 0.3 and 0.1 % for the top, middle and bottom temperature measurements, respectively. Further, the decreased specific reboiler duty is also evident from the decreased temperatures across the stripper column with the increase of the CO_2 content in the flue gas. In conclusion, the increase in the CO_2 composition in the flue gas results in the decrease in the specific reboiler duty by approximately 7.7 and 6.6 %, through experimentation and modelling, respectively.

6.6.2 Variation of the CO_2 Capture Rate – Set B

The CO_2 capture rate is varied from 60 to 95 %, and the other parameters, such as the CO_2 composition 4.5 mol%, solvent concentration 30 wt. %, flue gas and lean solvent temperature 40 ^oC and the stripper pressure 1.2 bar are maintained. As the CO_2 capture rate varies, the specific reboiler duty decreases. It is observed that with the increase in the capture rate, the difference between lean and rich loadings

increase and the lean loading increases which results in a difficulty in regeneration, and therefore the specific reboiler duty increases.

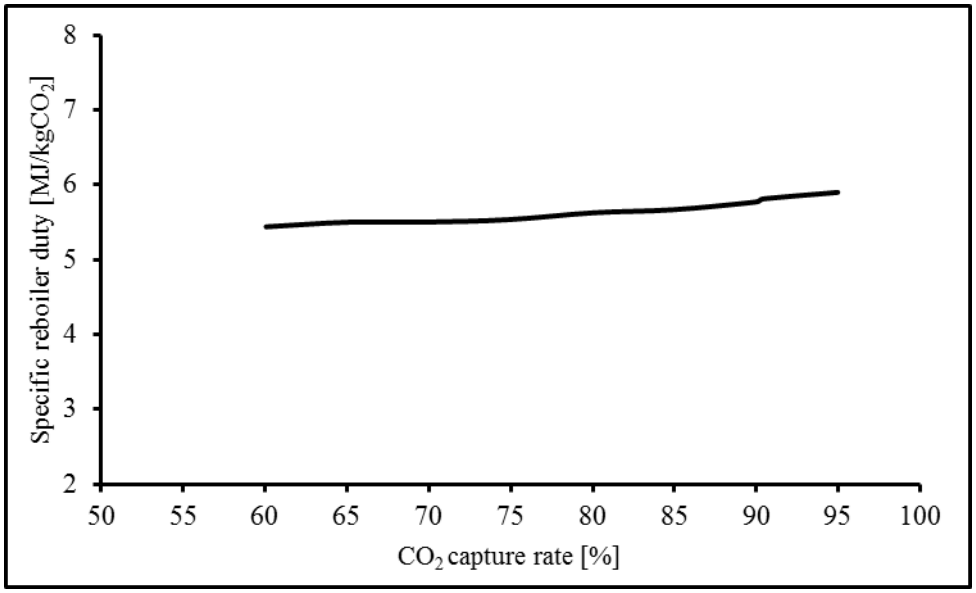

Figure 6.9 The variation of the specific reboiler duty as a function of the CO_2 capture rate, at a fixed CO_2 composition in the flue gas 4.5 mol%, solvent concentration 30 wt.%, flue gas temperature 40 ^oC, lean solvent temperature 40 ^oC and stripper pressure 1.2 bar.

The variation of the specific reboiler duty as a function of the CO_2 capture rate is given in Figure 6.9. It is observed that the specific reboiler duty increases slightly for the CO_2 capture level increase up to about 90 %. However, the increase in the specific reboiler duty becomes more pronounced for the increase of the CO_2 capture level beyond 90 %. In conclusion, the higher the CO_2 capture rate, the higher is the specific reboiler duty.

6.6.3 Variation of the Liquid Flow Rate – Set C

The liquid flow rate is varied to have a variation in the liquid to gas (L/G) ratio which is an important parameter for the optimization of the specific reboiler duty. The liquid flow rate is varied in such a way to give the L/G ratio variation from 0.6 to 2.6, while keeping all the other parameters as the CO_2 composition 4.5 mol%, solvent concentration 30 wt.%, CO_2 capture rate 90 %, flue gas and lean solvent temperature 40 ^oC and the stripper pressure 1.2 bar fixed. Experimentally, the L/G ratio cannot be less than 1.0 because of the maximum and minimum gas and liquid flowrates, respectively restriction of 400 kg/h.

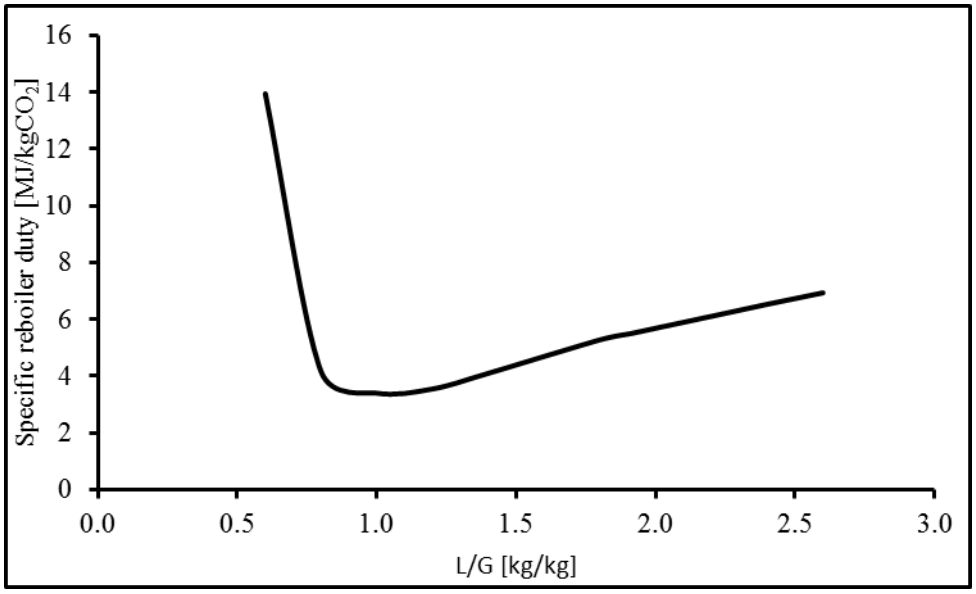

Figure 6.10 The variation of the specific reboiler duty as a function of the liquid to gas (L/G) ratios, at fixed CO_2 composition in the flue gas 4.5 mol%, CO_2 capture rate 90 %, solvent concentration 30 wt.%, flue gas temperature 40 ^{o}C, lean solvent temperature 40 ^{o}C and stripper pressure 1.2 bar.

The effect of the change in liquid to gas ratio on the specific reboiler duty is given in Figure 6.10. As the absorbed amount of the CO_2 remains the same, so by varying the liquid flow rate below a certain optimum point results in a sharp increase in the specific reboiler duty. However, by increasing the liquid to gas ratio beyond a certain optimum point, results in a gradual increase in the specific reboiler duty.

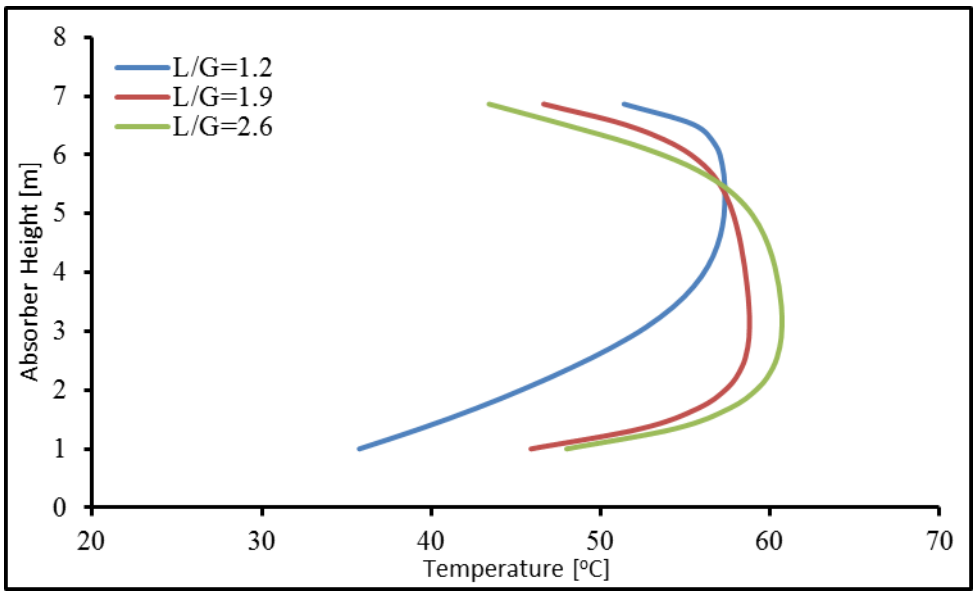

Figure 6.11 The absorber column temperature profile along the height of the column for various liquid to gas (L/G) ratios, at fixed CO_2 composition in flue gas 4.5 mol%, CO_2 capture rate 90 %, solvent concentration 30 wt.%, flue gas temperature 40 ^{o}C, lean solvent temperature 40 ^{o}C and stripper pressure 1.2 bar.

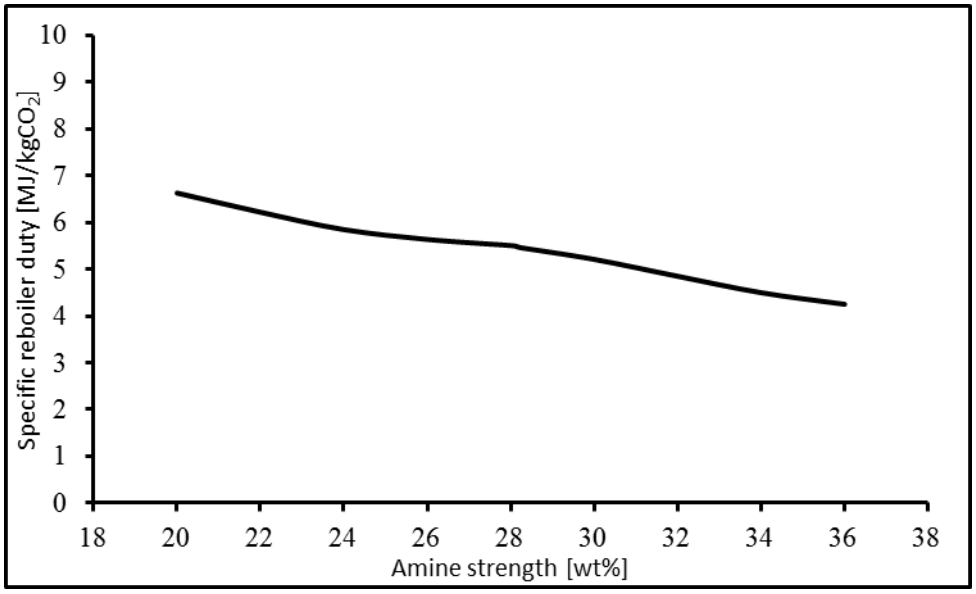

Figure 6.12 The variation of the specific reboiler duty as a function of the amine strength, at fixed CO_2 composition in the flue gas 4.5 mol%, CO_2 capture rate 90 %, flue gas temperature 40 ^oC, lean solvent temperature 40 ^oC and stripper pressure 1.2 bar.

The difference between the rich and lean loading decreases with an increase in the solvent flow rate. With the decreased lean loadings, the amount of the steam requirement drastically increases to achieve that low lean loading. Also, with the increased solvent flow rate, the energy required to regenerate larger amounts of the solvent increases. In conclusion, the optimum liquid to gas ratio becomes 1.0 for the present fixed conditions and under the experimental constraints. The absorber temperature profile across the height of the column is shown in Figure 6.11. With the increase in the liquid to gas ratio, by increasing the solvent flowrate, then the temperature bulge in the absorber column moves towards the bottom of the absorber as the reaction kinetics becomes more active at the bottom of the column.

6.6.4 Variation of the Amine Strength – Set D

The solvent strength of the amine solution is varied from 20 to 36 wt. %, while keeping the other parameters constant as the CO_2 composition 4.5 mol%, CO_2 capture rate 90 %, flue gas and lean solvent temperature 40 ^oC and the stripper pressure 1.2 bar fixed. The effect of the variation of the amine strength on the specific reboiler duty is given in Figure 6.12. The increased strength of the amine solvent results in higher solubility of the CO_2 and an increased mass flow of the absorbed CO_2 is observed. Hence, the increased rich loadings with decreased stripping requirements are observed. It is observed that the change in the amine strength has less effect on the absorption heat as is clear through the temperature

profiles of the absorber column as shown in Figure 6.13. It must be kept in mind that the increased amine strength will result in higher corrosivity and this will affect the material of construction. However, this effect can be reduced by the use of the corrosion inhibitors. In conclusion, the higher the amine strength, the lower is the specific reboiler duty.

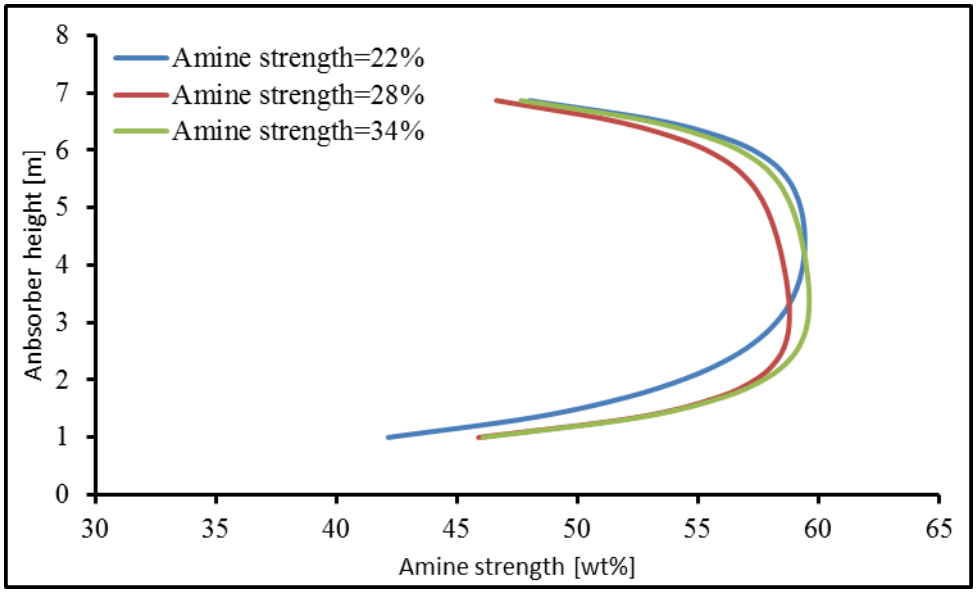

Figure 6.13 The absorber column temperature profile along the height of the column for various amine strengths, at fixed CO_2 composition in the flue gas 4.5 mol%, CO_2 capture rate 90 %, flue gas temperature 40 ^{o}C, lean solvent temperature 40 ^{o}C and stripper pressure 1.2 bar.

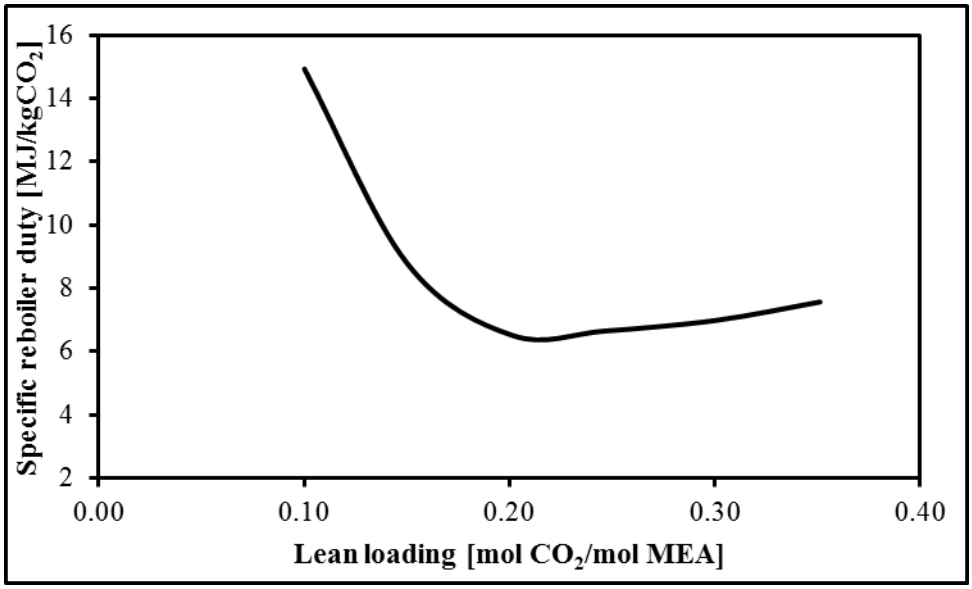

Figure 6.14 The variation of the specific reboiler duty as a function of the lean loading, at fixed CO_2 composition in the flue gas 4.5 mol%, amine strength 30 wt. %, CO_2 capture rate 90 %, flue gas temperature 40 ^{o}C, lean solvent temperature 40 ^{o}C and stripper pressure 1.2 bar.

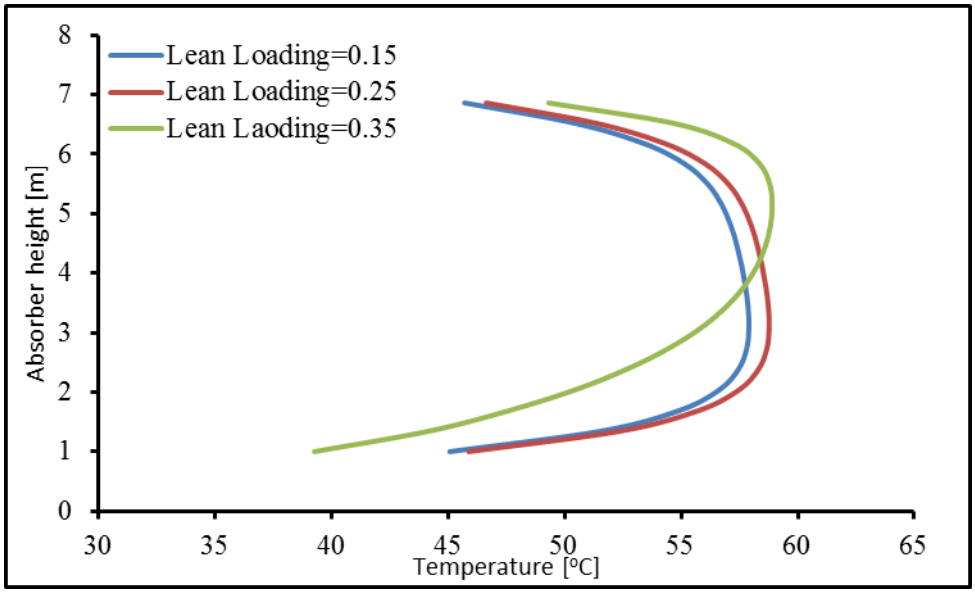

Figure 6.15 The absorber column temperature profile along the height of the column for various lean loadings, at fixed CO_2 composition in the flue gas 4.5 mol%, amine strength 30 wt. %, CO_2 capture rate 90 %, flue gas temperature 40 ^{o}C, lean solvent temperature 40 ^{o}C and stripper pressure 1.2 bar.

6.6.5 Variation of the Lean Amine Loading – Set E

The lean loading of the amine solvent is varied from 0.10 to 0.35 mol CO_2/mol MEA while keeping all the other parameters constant as the CO_2 composition 4.5 mol%, amine strength 30 wt. %, CO_2 capture rate 90 %, flue gas and lean solvent temperature 40 ^{o}C and stripper pressure 1.2 bar fixed. The effect of the lean loading on the specific reboiler duty is shown in

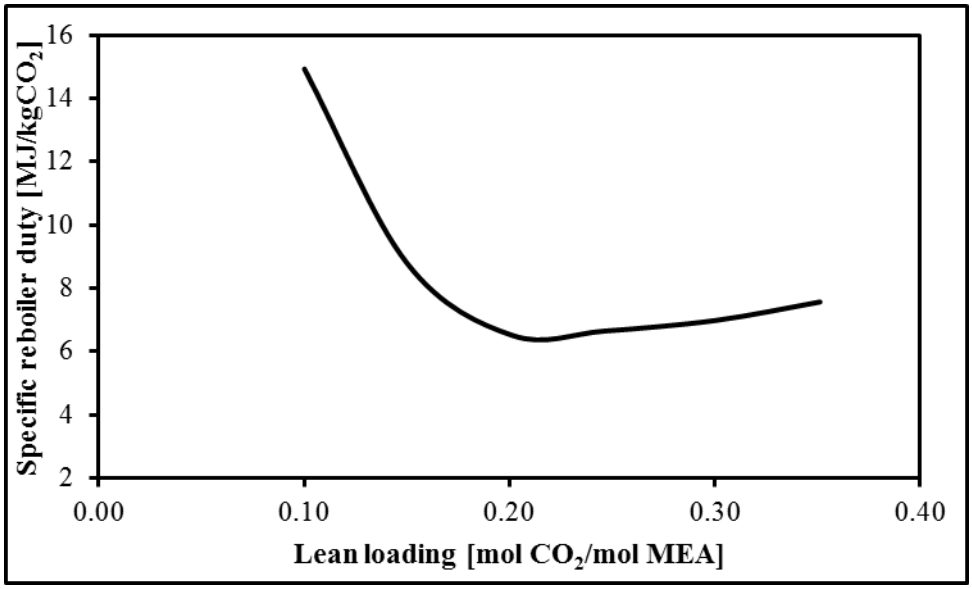

Figure **6.14**. The variation of the lean loading drastically affects the specific reboiler duty. The increased lean loading results in a higher rich loading with increased cyclic capacity. Further, with the increase in the lean loading, the specific reboiler

duty decreases and it decreases drastically below a certain optimum point. The effect of the lean loading of the amine solvent on the temperature profile of the absorber is shown in Figure 6.15. It is observed that the variation of the lean loading affects the absorption rates. As with the increase in the lean loadings, the absorption rate increases and the temperature bulge in the absorption column increases. In conclusion, with the decrease of the lean amine loading, the cyclic capacity decreases and hence the degree of regeneration also decreases.

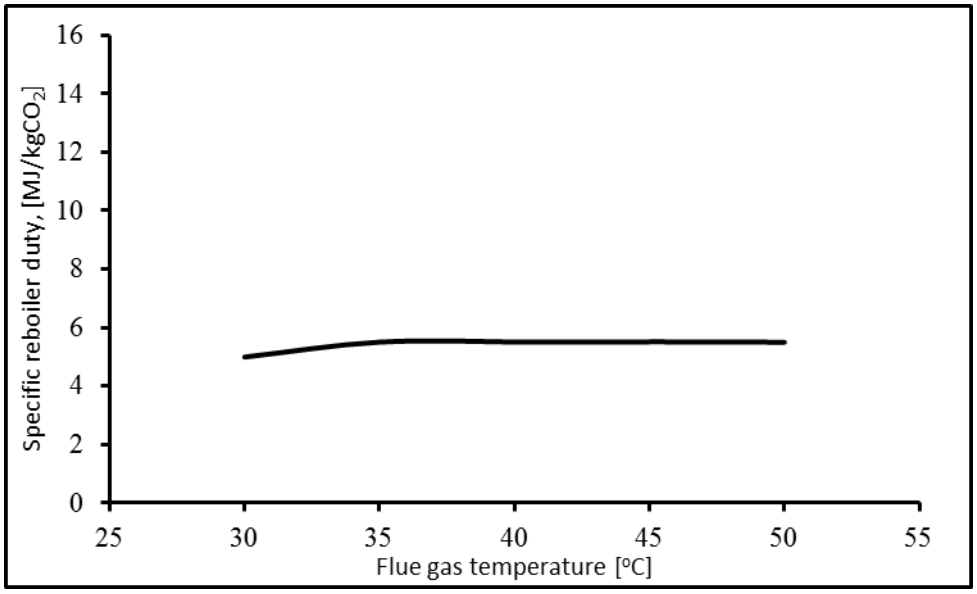

Figure 6.16 The variation of the specific reboiler duty as a function of the flue gas temperature, at fixed CO_2 composition in flue gas 4.5 mol%, amine strength 30 wt. %, CO_2 capture rate 90 %, lean solvent temperature 40 ^{o}C, and stripper pressure 1.2 bar.

6.6.6 Variation of the Flue Gas Temperature – Set F

The temperature of the flue gas entering the absorber is varied from 30 to 50 ^{o}C while keeping all the other parameters constant as the CO_2 composition 4.5 mol%, amine strength 30 wt. %, CO_2 capture rate 90 %, lean solvent 40 temperature ^{o}C and stripper pressure 1.2 bar fixed. It is observed that there is no evident effect of the flue gas temperature on the specific reboiler duty, also on the lean and rich loadings. This may be due to the opposing behaviours of the chemical reaction kinetics and the physical solubility of the CO_2. The impact of the flue gas temperature on the specific reboiler duty is shown in Figure 6.16 and the effect of the flue gas inlet temperature on the absorber temperature profile is given in Figure 6.17. Also, it is evident from Figure 6.17 that the absorber temperature profile is slightly affected by the variation of the flue gas temperature, since only the bottom section of the

absorber temperature profile varies due to the changing flue gas temperature at the absorber inlet.

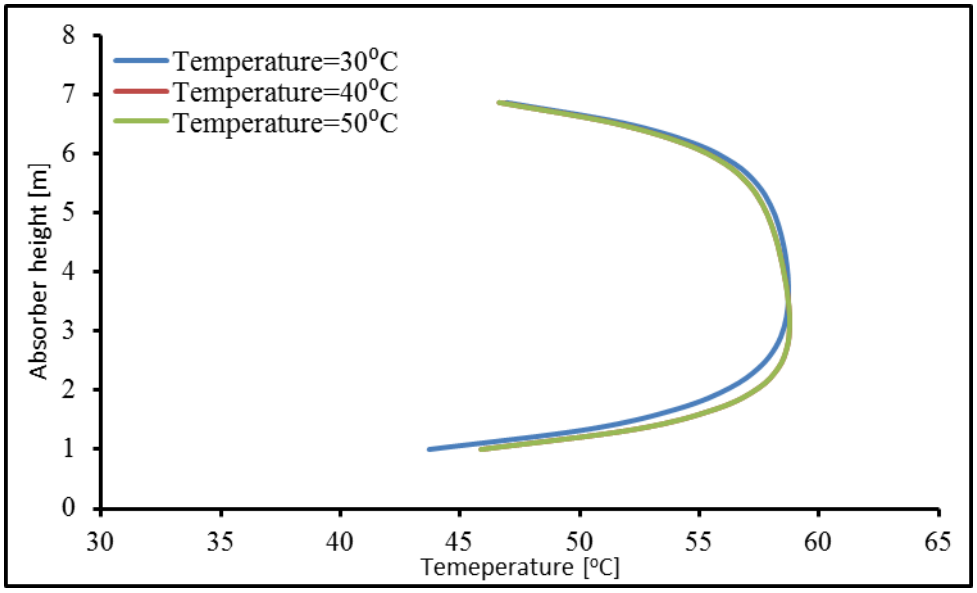

Figure 6.17 The absorber column temperature profile along the height of the column for various flue gas inlet temperatures, at fixed CO_2 composition in the flue gas 4.5 mol%, amine strength 30 wt. %, CO_2 capture rate 90 %, lean solvent temperature 40 °C, and stripper pressure 1.2 bar.

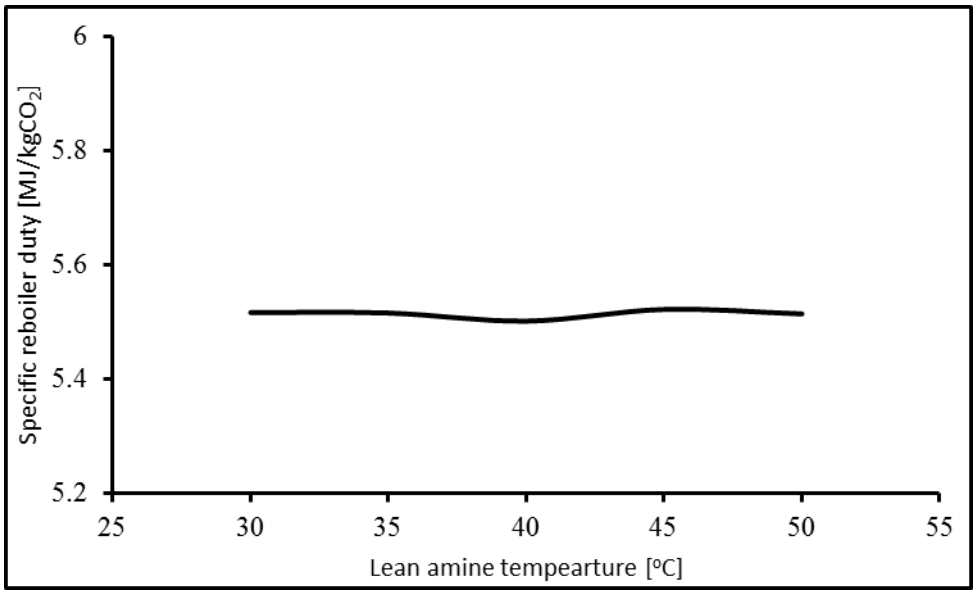

Figure 6.18 The variation of the specific reboiler duty as a function of the lean solvent temperature, at fixed CO_2 composition in the flue gas 4.5 mol%, amine strength 30 wt. %, CO_2 capture rate 90 %, flue gas temperature 40 °C and stripper pressure 1.2 bar.

The effect of the flue gas temperature is not significant and this has been observed in the literature as reported by Notz et al. [139]. No comprehensive conclusion can be drawn from the variation of the flue gas temperature, due to the opposing influence of the temperature on the equilibrium solubility and absorption kinetics.

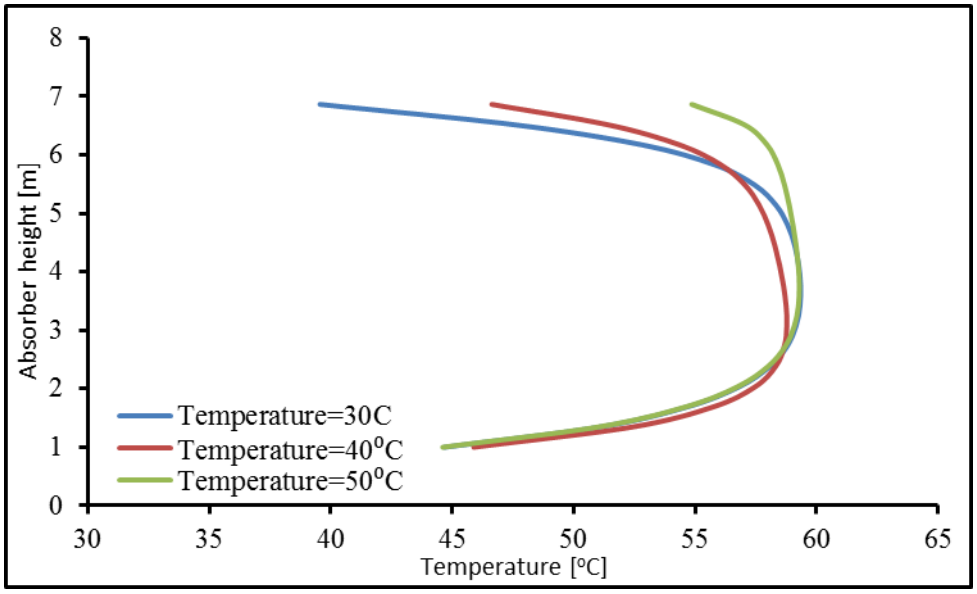

Figure 6.19 The absorber column temperature profile along the height of the column for various lean solvent temperatures, at fixed CO_2 composition in the flue gas 4.5 mol%, amine strength 30 wt. %, CO_2 capture rate 90 %, flue gas inlet temperature 40 ^{o}C and stripper pressure 1.2 bar.

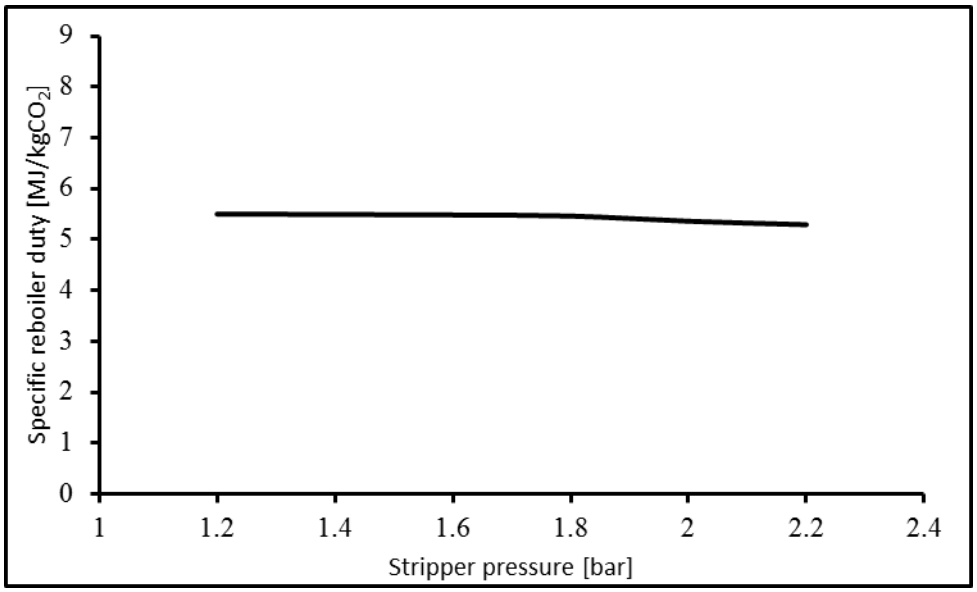

Figure 6.20 The variation of the specific reboiler duty as a function of stripper pressure, at fixed CO_2 composition in flue gas 4.5 mol%, amine strength 30 wt. %, CO_2 capture rate 90 %, flue gas temperature 40 ^{o}C and lean solvent temperature 40 ^{o}C.

6.6.7 Variation of the Liquid Temperature – Set G

The temperature of the lean solvent entering the absorber is varied from 30 to 50 ^{o}C while keeping the other parameters constant as CO_2 composition 4.5 mol%, amine strength 30 wt. %, CO_2 capture rate 90 %, flue gas temperature 40 ^{o}C and stripper pressure 1.2 bar fixed. Similar, to the effect of the flue gas temperature; the effect of the lean temperature is not evident. The effect of the lean solvent temperature on the specific reboiler duty, lean and rich loading is minimal and less noticeable. The

effect of the liquid solvent temperature on the specific reboiler duty is shown in Figure 6.18. Also, it is evident from Figure 6.19 that the temperature profile of the absorber is not affected and the only affect visible is at the top section of the absorber where the liquid solvent with varying temperature enters.

6.6.8 Variation of the Stripper Pressure – Set H

The pressure of the stripper column is varied from 1.2 to 2.2 bar while keeping all the other parameters constant as CO_2 composition 4.5 mol%, amine strength 30 wt. %, CO_2 capture rate 90 %, flue gas temperature 40 ^oC and lean solvent temperature 40 ^oC fixed.

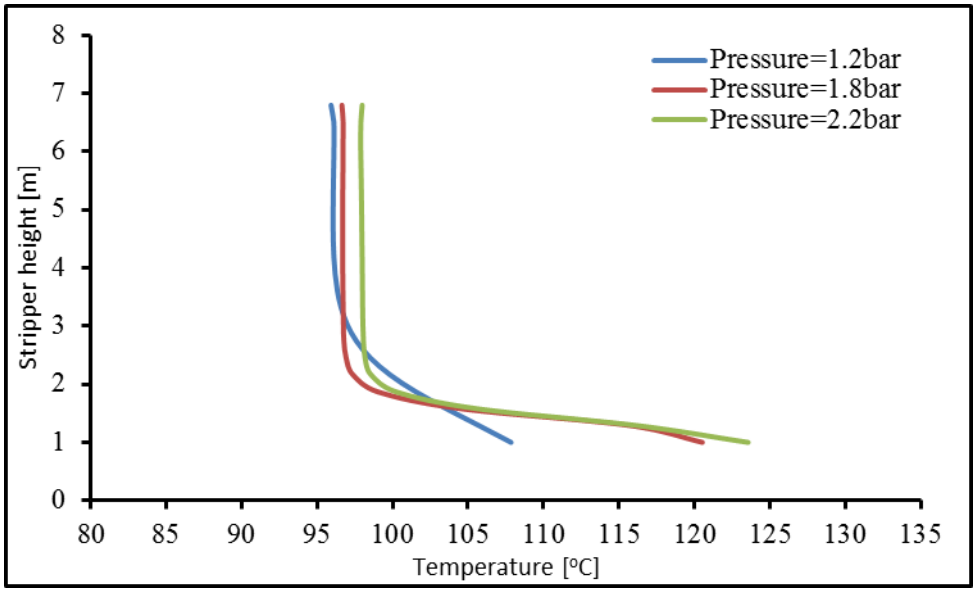

Figure 6.21 The stripper column temperature profile along the height of the column for various stripper pressure, at fixed CO_2 composition in flue gas 4.5 mol%, amine strength 30 wt. %, CO_2 capture rate 90 %, flue gas inlet temperature 40 ^oC and lean solvent temperature 40 ^oC.

With the increase in the stripper pressure, the difference between the lean and rich loadings increases and hence the specific reboiler duty decreases. This indicates that the stripping of CO_2 from liquid is easier for an increased stripper pressure. The effect of the variation of the stripper pressure on the specific reboiler duty is shown in Figure 6.20.With the increase in the stripper pressure, the stripper temperatures also increases as is evident from the stripper temperature profile as shown in Figure 6.21. With the increase in stripper temperatures, the larger amount of the CO_2 gets stripped out of the solvent, thus resulting in the regeneration becoming easier. Therefore, with the increase of the stripper pressure, the specific reboiler duty decreases and the reboiler temperature increase. However, the stripper pressure

cannot be increased beyond a certain limit as issues such as solvent degradation must be kept in mind.

6.7 Conclusions

- The rigorous rate based model developed for the MEA-based CO_2 capture plant shows robustness for extensive experimental data for the two pilot-scale MEA-based CO_2 capture plants. The maximum mean percent absolute deviation observed was 5 % for the number of variables compared from the model reported and experimental reported values.
- For both sets of the reported experimental data, the model is particularly investigated and validated against CO_2 enhanced flue gas at a variable range to analyse the impact of the EGR on the performance of the CO_2 capture plant.
- The sensitivity analysis assists in the understanding of the behaviour of the CO_2 capture plant for the number of operating conditions which are simultaneously affecting its performance. Its helps in estimating the optimum operating envelope for the particular pilot-scale CO_2 capture plant.
- It is observed that the higher the CO_2 composition, the lower will be the specific reboiler duty.
- Further, by increasing the amine strength, the stripper pressure, and by decreasing the amine loading, the specific reboiler duty decreases.
- However, by increasing the CO_2 capture rate, the specific reboiler duty increases.
- No comprehensive conclusions can be drawn for the effect of the flue gas and lean amine solvent inlet temperatures due to the opposing nature of the reaction kinetics and absorption chemistry.

The validated model is used to scale-up and/or design the commercial-scale amine-based CO_2 capture plant in Chapter 7. The commercial-scale amine-based CO_2 capture model is integrated with the NGCC and the NGCC with EGR and a techno-economic analysis is carried out in Chapter 7 for various EGR percentages. Based on the techno-economic analysis, the optimum design of the commercial-scale amine-based CO_2 plant is presented which can service the NGCC with and without EGR.

Chapter 7
Techno-Economic Process Design of a Commercial-Scale Amine-Based CO_2 Capture System for Natural Gas Combined Cycle Power Plant with Exhaust Gas Recirculation

In this chapter, a techno-economic process design of a PCC model is presented based on the validated amine-based CO_2 capture plant model as presented in Chapter 6. Further, the commercial-scale NGCC power plant model, both with and without EGR, is also validated before integrating it into the amine-based CO_2 capture plant model. Finally, the optimum design and/or scale-up of four different cases, is presented based on process and economic variables.

7.1 Introduction

Reactive absorption using alkanolamines, as one of the PCC technologies, is gaining more importance as the baseline technology for CO_2 capture due to its maturity [126, 138]. Currently, the major focus of the ongoing research is to reduce the amount of energy consumed in the regeneration of the solvent.

In the literature there are various studies [99, 100, 102, 104, 105, 166] that report the integration of an amine-based CO_2 capture plant with NGCC at 40 and 50 % EGR with little or no information about the actual design of the amine-based CO_2 capture plant. These studies report the heat exchanger network design [100, 102, 166] for various options for the steam extraction, the effect of the EGR on the thermodynamic properties of the turbo machinery, [100, 166] cost savings, [102] and a comparison of the process system performance with a humidification system, the supplementary firing and the external biomass fired boiler [99, 104, 105].

The process design of an amine-based CO_2 capture system for a commercial-scale NGCC in EGR mode and its comparison with a system without EGR, but without explicitly considering the techno-economics during the process design, can be found in the literature [101, 103, 106, 108, 209]. Sipöcz and Tobiesen [108] reported that a

single absorber and a single stripper with heights 26.9 m and 23.5 m, respectively, can service a NGCC plant 410.6 MW_e (gross) without EGR. For a NGCC plant with a capacity 413.5 MW_e (gross) and with an EGR 40 %, they reported absorber and stripper heights 23.6 m and 21.2 m, respectively, and with a reduced specific reboiler duty 3.64 MJ/kgCO_2 for the NGCC with EGR compared to 3.97 MJ/kgCO_2 for the NGCC without EGR. They also reported the comparative plant economics for different cases, without considering it during the design stage. As reported by Agbonghae et al. [159], their design dimensions appear unrealistic as they cannot accommodate the quoted amount of flue gas. Also, as discussed by Agbonghae et al. [159], the reported design results by Biliyok and Yeung [106] and Biliyok et al. [101] of 4 absorbers with 10 m dimeter and 15 m height; and a single stripper with 9 m diameter and 15 m height was most likely based on the design for an off-shore application as reported in the literature [162, 210]. For a 40 % EGR, with a corresponding 40 % reduction in the flue gas flow rate, they reduced the number of absorbers to 3 without explicitly mentioning their design dimensions. Furthermore, Canepa et al. [103] reported that 2 absorbers with 9.5 m diameter and 30 m height, and a single stripper with 8.2 m diameter and 30 m height as the design results of an amine-based CO_2 capture plant for a NGCC power plant 250 MW_e (gross). When Canepa et al. [103] applied an EGR 40%, with a reduced flue gas flowrate, the height of both the absorber and stripper remained unchanged, although the specific reboiler duty was reduced. Also, the design results reported by Luo et al. [209] did not explicitly mention the reduction in the height of the absorber and stripper when an EGR 38 % was applied to the NGCC plant with a capacity 453 MW_e (gross). Table C.1 in the Appendix C, reports the design results for the different cases both with and without EGR as elaborated in the above discussion.

It is clear from the above discussion that the work presented in the open literature lacks a detailed techno-economic process design of the amine-based CO_2 capture plant for an on-shore based commercial-scale natural gas-fired power plant, both with and without EGR. Also, the effects of the EGR on the process design results need to be investigated by varying the EGR ratio on the same basis as that of the NGCC power plant. The already published literature have mostly presented the design results of the CO_2 capture system for an EGR percentage 40 %, [101, 103, 106, 108] with the exception of the paper by the Luo et al. [209]. Therefore, this chapter is focused on an amine-based CO_2 capture plant which can service an on-

shore based commercial-scale natural gas-fired power plant in EGR mode. Further, the theme is to optimally design an amine-based CO_2 capture plant for the NGCC without EGR and NGCC with EGR at varying EGR percentages. Also, the sensitivity of the EGR percentage has been checked for the design and/or scale-up of the commercial-scale amine-based CO_2 capture plant for NGCC. The philosophy is to implement the rigorous rate-based process model for the process design of the amine-based CO_2 capture plant by considering both the process variables and economic parameters during the process design.

7.2 Process Layout and Modelling Strategy

7.2.1 Process Layout

A 650 MW_e (gross) NGCC plant is modelled in Aspen and the process model results are compared with the results published in the 2013 Report of the US Department of Energy [211]. This report investigated the NGCC plant in three different configurations: NGCC without CO_2 capture, NGCC with CO_2 capture, and NGCC in EGR mode with CO_2 capture. The gas turbine modelled in this paper is an F-frame GE gas turbine (GE 7FA.05) with a gas turbine inlet temperature 1359 ^oC, a gas turbine outlet temperature 604 ^oC and a pressure ratio 17. The bottom Rankine cycle is a triple pressure level single reheat cycle with steam cycle specification of 16.5/566/566 MPa/^oC/^oC. Further, the heat recovery steam generator (HRSG) generates both the main and the reheat steam for the steam cycle. The natural gas and air composition, along with input parameters used in the model are given in Table **7.1**, and the basic schematic of the NGCC is shown in Figure 7.1. The various sections of the NGCC, including the gas turbine, steam turbine and HRSG, are indicated by bounded rectangles in Figure 7.1. For the NGCC with EGR, part of the exhaust gas is recirculated back to the compressor inlet to enhance the CO_2 concentration in the flue gas that is directed towards the CO_2 capture system in the present study. As previously stated, the EGR results in a reduced flue gas flow rate with an increased CO_2 concentration, which is of two-fold benefit for the integration of the NGCC in the EGR mode with the amine-based CO_2 capture system. The EGR loop consists of the condenser and the recirculation fan to boost the pressure of the recycle stream to the compressor inlet pressure.

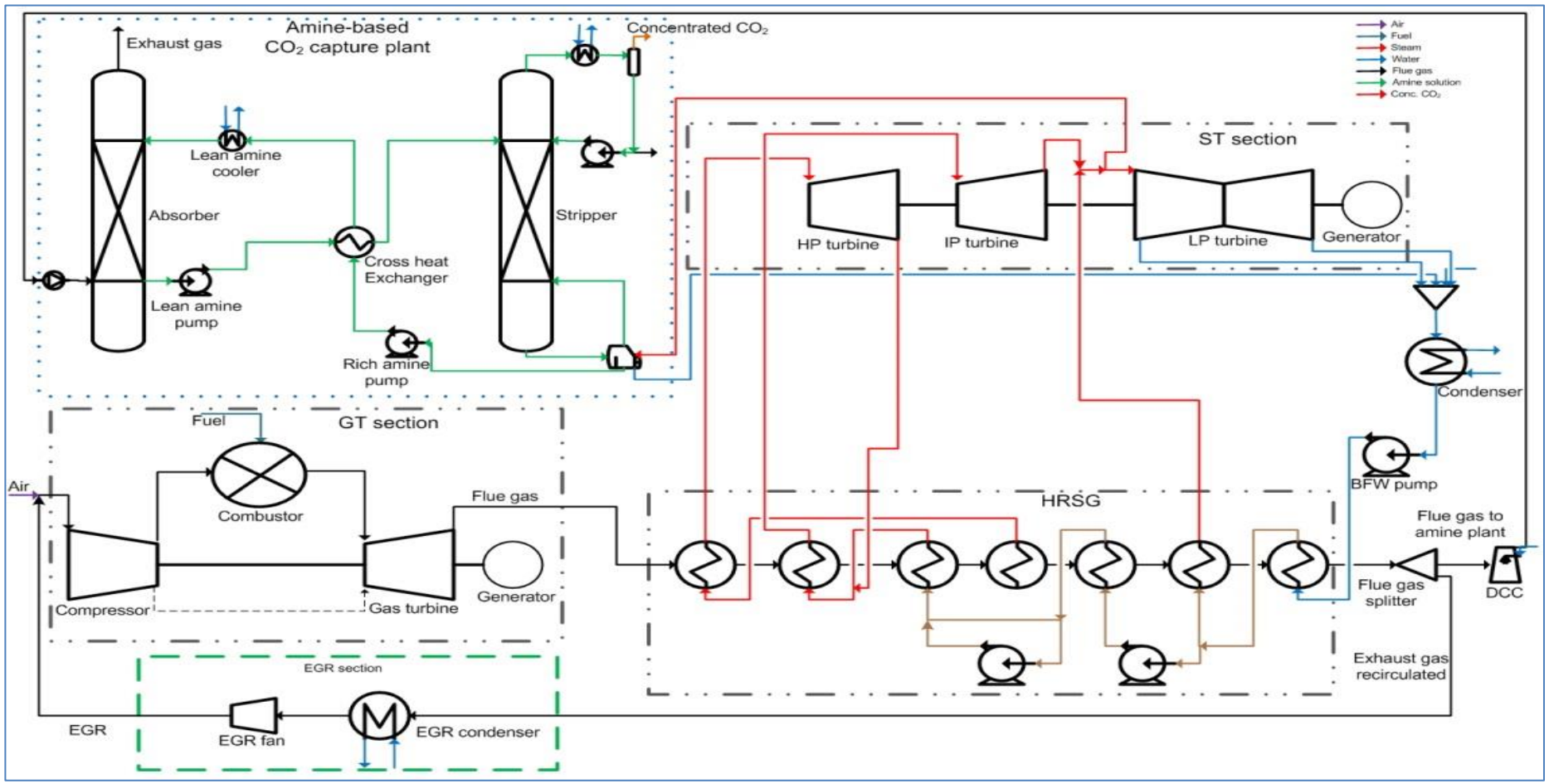

Figure 7.1 Basic schematic of the NGCC with EGR integrated with an amine-based CO_2 capture plant.

Table 7.1 Input specifications for the NGCC models [211].

Parameter	Without EGR	With EGR
Gas turbine inlet temperature [^{o}C]	1359	1363
Gas turbine outlet temperature [^{o}C]	604	615
Air inlet temperature [^{o}C]	15	15
Flue gas temperature at HRSG exit [^{o}C]	88	107
Exhaust gas recirculation rate [%]	0	35
Pressure ratio	17	17
Compressor efficiency [%]	85	85
HP[a] steam turbine efficiency [%]	88	88
IP[b] steam turbine efficiency [%]	92.4	92.4
LP[c] steam turbine efficiency [%]	93.7	93.7
Fuel inlet temperature [^{o}C]	38	38
Fuel inlet pressure [MPa]	2.76	2.76
Natural gas calorific value [MJ/kg]	47.22	47.22
Natural gas molar composition [%]		
CH_4	93.1	
C_2H_6	3.2	
C_3H_8	0.7	
iso-C_4H_{10}	0.4	
CO_2	1.0	
N_2	1.6	
Air molar composition [%]		
N_2	77.32	
O_2	20.74	
Ar	0.92	
CO_2	0.03	
H_2O	0.99[d]	

[a]HP - high pressure.

[b]IP - intermediate pressure.

[c]LP - low pressure.

[d]Relative humidity of ~60 %.

The exhaust gas from the HRSG exit is split and a portion of the exhaust gas is recirculated and the remainder is sent to the amine-based CO_2 capture system. In the US Department of the Energy Report [211], the total capacity of the NGCC in EGR mode was 615 MW_e (gross) at an EGR percentage of 35 %. The decreased capacity is due to the auxiliary loads of the EGR loop and the amine-based CO_2 capture process. For the NGCC in EGR mode, the gas turbine inlet temperature 1363 ^{o}C and gas turbine outlet temperature 615 ^{o}C is maintained. The flue gas temperature at the HRSG exit is 107 ^{o}C and the configuration of the three pressure levels with a single reheat of the steam cycle remains the same. The input parameters for the NGCC in EGR mode are summarised in Table 7.1 and the basic schematic of the NGCC with EGR is shown in Figure 7.1 where the EGR section is indicated by the green dashed

rectangle. The higher temperatures observed in NGCC with EGR in comparison to the NGCC without EGR, are due to the higher heat capacity of the working gas stream as a result of the increased CO_2 concentration in it.

A schematic of the amine-based CO_2 capture plant shown in Figure 7.1 and it is bounded by the dotted blue rectangle. The CO_2 capture plant consists of the two columns; absorber and stripper, cross heat exchanger, cooler and pumps. The flue gas enters the bottom of the packed column absorber and it is contacted in a counter current manner with the downward flowing monoethanolamine (MEA) solvent. The resulting treated gas is low in CO_2 content and it passes through the water-wash section to remove traces of entrained MEA. The CO_2 loaded solvent from the bottom of the absorber is pumped and further heated in the cross heat exchanger with the lean amine coming from the stripper reboiler. The rich solvent is heated in the stripper by the upward flowing steam, leading to its regeneration to the lean amine solution; the lean amine solution is cooled down by heat exchange with the rich amine solution in the cross heat exchanger and by the lean amine cooler before re-entering the top of the absorber. The concentrated CO_2 from the condenser of the stripper is dried, compressed and sent to a CO_2 storage site.

7.2.2 Modelling Details

For the NGCC, the gas turbine is modelled using the Peng-Robinson equation of state and the combustor is modelled on the basis of the Gibbs free energy minimization. The steam cycle is modelled using the NBS steam property package. Further, the HRSG is modelled as a multi-stream heat exchanger. For the present study, the EGR percentage is not only fixed at 35 %; rather two more cases of the NGCC in EGR mode with ±15 % of the reported EGR percentage of 35 % are modelled and the design of the amine-based CO_2 capture system is done for an EGR percentage of 20, 35 and 50 %. It is assumed that combustion stability issues do not arise when the EGR percentage is 50 %, and technical modifications of the combustor are available to deal with those issues already mentioned in Section 5.1. Some of these modifications as suggested in the literature are mentioned in Section 4.1. The EGR cycle is modelled by including the condenser and booster fan in to the model of the gas turbine as shown by the EGR loop in Figure 7.1. The details of the modelling of the EGR loop are the same as reported in Section 4.2. The EGR

percentage of 50% is selected to study the behaviour and design of the capture system at this higher EGR at which literature lacks.

The power output of the gas turbine is considered as the basis for the techno-economic process design of the amine-based CO_2 capture plant. For the EGR cases, the steam turbine power is also fairly constant for the three cases investigated. Although there is a drop in the flue gas flowrate with an increase in EGR, this is compensated by the increase in the flue gas temperature. Thus the total enthalpy of the flue gas will be about the same for all the cases and hence the steam generated in the HRSG will be almost the same.

The amine-based CO_2 capture plant is modelled using the Acid Gas thermodynamic property package. This is an integral functionality of Aspen and it is based on the Electrolyte Non-Random Two Liquid (Electrolyte NRTL) thermodynamic property package for the liquid phase properties. The Peng-Robinson thermodynamic equation of state was used for the vapour phase properties.

In addition, the correlations used for the mass transfer and interfacial area estimation is the Bravo-Fair correlation [203] which is built-in into Aspen. Similarly, for the pressure drop estimation the vendor correlation for the particular packing are used.

7.2.3 Modelling Strategy

In general, the design of absorber and stripper columns is well described in the literature [204, 205, 212]. However, the process design of packed absorber and stripper is not a straightforward process. It is a hit and miss trial procedures until the optimum design variables that can meet the specific design conditions and/or targets are arrived at. These design targets are defined by the hydrodynamic parameters of the packed column, specifically the maximum pressure drop that can be tolerated and the approach to the maximum capacity of the column [204, 205, 212]. The design and scale-up optimization of the amine-based CO_2 capture plants for the base case NGCC, with a power output of 650 MW_e, and NGCC with EGR percentage at 20, 35 and 50 %, are designed and optimised by the procedures defined by Agbonghae et al., [159] which can be referred to for more details. The design and/or scale-up strategy, with a process simulation tool, can be described by the following interlinked steps:

i. Model validation at the pilot-scale level.

ii. Selection of the process and economic parameters.

iii. Process performance bounds/criteria.

iv. Techno-economic process sensitivity analysis.

The model validation at the pilot-scale is performed in order to ascertain if the model is capable of representing the performance of the system under consideration. The model of the amine-based CO_2 capture plant is validated against two set of experimental data as reported in Chapter 6. and are presented in Sections 6.4 and 6.5.

Table 7.2 Input specifications [159] for the amine-based CO_2 capture plant.

Parameter	Value
MEA concentration [kg/kg]	0.3
Lean amine loading [mol CO_2/mol MEA][16]	0.2
CO_2 capture rate [%]	90
Flue gas temperature at absorber inlet [^oC]	40
Lean MEA temperature at absorber inlet [^oC]	40
Rich amine pump efficiency [%]	75
Lean amine pump efficiency [%]	75
Rich amine pump discharge pressure [bara]	3.0
Lean amine pump discharge pressure [bara]	3.0
Cross heat exchanger hot side temperature approach [^oC]	10
Cross heat exchanger pressure drop [bar]	0.1
Lean amine cooler pressure drop [bar]	0.1
Condenser temperature [^oC]	35
Stripper condenser pressure [bara]	1.62
Cooling water temperature rise [^oC]	5

Table 7.3 Economic analysis assumptions [159] used for techno-economic design of an amine-based CO_2 capture plant in Aspen.

Parameter	Value
Costing template	U.K.
Steam cost [£/ton]	17.91
Cooling water cost [£/m^3]	0.0317
Electricity cost [£/MWh]	77.5
Service life, s [yrs]	20
Interest rate, i [%]	10
Equipment material	316L stainless steel

The process and economic variables selected for the present study are presented in Table 7.2 and Table 7.3, respectively. These process and economic variables remain fixed during the sensitivity analysis. The present design is for MEA strength of 30 weight % aqueous solution and the CO_2 capture rate is fixed of 90 %, a common basis for these types of study. In most of the reported studies in the open literature, 30 wt. % aqueous MEA was taken as the base line solvent for comparison with

various blends and/or new solvents; therefore it is generally considered as the benchmark solvent for the PCC technology. The lean loading is fixed at an optimum value of 0.2 mol CO_2/mol MEA [159], and the absorber inlet temperatures are fixed at 40 ^{o}C. The lean loading is already being optimized by Agbonghae et al. [159] hence not reiterated in this work. The amine section pump efficiencies are fixed at 75 % and the maximum pressure for the amine solution around the circuit is 3 bara. The costing is performed with the Aspen Economic Analyzer, which is an integral part of Aspen, through the economic analysis tab. It is important to mention here that the cost estimated in terms of capital expenditure of the plant (CAPEX), and operating expenditure of the plant (OPEX) do not include ancillary equipment costs which may be part of the actual system based on hazard and operability studies [159]. However, if recommendations in the literature [213, 214] are properly applied for the economic analysis; the associated uncertainty with the economic analysis results will be reduced. It is believed that CAPEX estimated will consists of the total plant cost along with the pre-production fixed and variable cost, inventory cost, royalty and interest fee cost during construction. While the total plant cost will include the total process equipment costs, total facilities costs, project and process contingency costs, engineering and general facilities costs.

The optimum design variables are those which result in the least OPEX. Further, to confirm the optimum point for each variable, the total annualized expenditure is estimated with a scale-up in the CAPEX and a scale-down in the OPEX. The total expenditure (TOTEX) is given by the following equation [159]:

$$\mathrm{TOTEX} = \mathrm{X_1(OPEX)} + \mathrm{X_2(CAPEX)}\left[\frac{\mathrm{i\,(i+1)^s}}{\mathrm{(i+1)^s-1}}\right] \qquad (7.1)$$

where i is the interest rate and s is the service life of the plant, already defined in Table 7.3. Further, X_1 and X_2 are the scaling factors used to define the three cases:

- Case A: X_1 =1.0 and X_2 = 1.0
- Case B: X_1 =1.0 and X_2 = 1.5
- Case C: X_1 =0.5 and X_2 = 1.0

The scale-up of the CAPEX is included to account for the additional equipment, if required due to HAZOP and any uncertainty in the CAPEX estimation. The case of the scale-down of the OPEX is to account for the cheaper utilities or for better integration of the CO_2 capture plant with the power plant and/or utilities available

from the same power plant. The cases B and C will also account for uncertainties which may be present in the cost analysis. In addition, the interest rate is fixed at 10 % for the service life of 20 years and the equipment material selected is stainless steel. The utilities cost for steam, electricity and cooling water for the estimation of the economic parameters are listed in Table 7.3. The utilities cost as mentioned in Table 7.3 are based on the independent source rather than derived from the same power plant. Two process performance bounds are recommended in the literature when estimating the diameter of packed column for the specific liquid and the gas flow rates. The pressure drop across the height of the packing in the columns should not exceed 20.83 mm of H_2O per meter of the packing for amine systems, [204, 205] and the approach to the maximum capacity should not exceed 80 % of the flooding velocity [204, 205]. These process performance bounds are designed to achieve 90 % separation of the CO_2 and the column height is estimated for achieving this amount of separation.

The main question that requires an answer is the following: in order, to implement the techno-economic process analysis for the design and/or scale-up of the validated pilot-scale amine-based CO_2 capture plant to a commercial-scale amine-based CO_2 capture plant, which can service on-shore based validated NGCC of 650 MW_e (gross) capacity. In addition, the design and/or scale-up of the above case are extended to the NGCC with EGR for three different EGR percentages of 20, 35 and 50 %. In total four case studies are investigated, each consisting of a commercial-scale CO_2 capture plant which can service NGCC. The first case of a commercial-scale CO_2 capture plant is for NGCC without EGR. For the other cases, the design and/or scale-up of a commercial-scale CO_2 capture plant are obtained for 20, 35 and 50 % EGR operated NGCC. The design and/or scale-up of these cases are obtained provided the above mentioned process performance bounds are met for the specified process and economic parameters.

7.3 Model Validation

7.3.1 NGCC and NGCC with EGR

As stated in Section 7.2.1, the model results of the NGCC were compared with the results obtained from the Report of the US Department of Energy [211]. Also, the results for the NGCC with an EGR percentage of 35 % are available in the same

report and hence they are also compared. The model results are summarised in. Table 7.4. Further, the model results for the NGCC with EGR percentages at 20 and 50 % are also presented in Table 7.4. The percentage absolute deviation for any of the variables presented in Table 7.4 is less than 3.2 and 4.1 %, for NGCC without EGR and NGCC with 35 % EGR percentage, respectively.

Table 7.4 Validation of the model results for NGCC without EGR and NGCC with EGR percentage at 35 % and extended model results for the NGCC with EGR percentages at 20 and 50 %.

Parameters	NGCC without EGR			NGCC with EGR		
EGR	0 DoE [211]	0 Model	35 % DoE [211]	35 % Model	20 % Model	50 % Model
Gas turbine power output [MW_e]	420.8	418.1	418.6	418.7	419.9	419.9
Steam turbine power output [MW_e]	229.6	232.6	196.6	202.6	202.6	202.6
Total gross power output [MW_e]	650.7	650.7	615.2	621.3	622.5	622.5
Exhaust gas recirculation [%]	-	-	35	35	20	50
Condensate pump load [kW_e]	416	420	268	270	268	271
Boiler feed water pumps load [MW_e]	4.5	4.5	4.5	4.5	4.5	4.5
EGR auxiliary loads [kW_e]	0	0	677	684	452	905
Other auxiliary loads [39] [MW_e]	11.5	11.5	14.3	14.3	14.3	14.3
Total net power output [MW_e]	634	634	595	602	603	603
Turbine inlet temperature [^oC]	1359	1368	1363	1366	1360	1387
Turbine outlet temperature [^oC]	604	608.6	615	617	612	637
Recirculated gas flow rate [kg/s]	-	-	347.5	351.7	196.0	499.2
Flue gas flow rate [kg/s]	1029.7	1029.7	667.6	652.8	783.9	499.2
Flue gas molar composition [%]						
CO_2	4.04	3.91	6.07	6.20	5.12	8.19
O_2	12.09	12.38	8.29	7.95	9.9	4.33
N_2	74.32	74.42	74.96	74.87	74.38	75.87
Ar	0.89	0.88	0.90	0.89	0.89	0.90
H_2O	8.67	8.42	9.78	9.94	9.52	10.58

Thus, the model results are in good agreement with the data in the Report of US Department of Energy. Hence, the flue gas can be confidently linked with the

amine-based CO_2 capture plant for its design and scale-up. The CO_2 composition in the flue gas for the NGCC with EGR is increased by a factor 1.3, 1.6 and 2.1 in comparison to the CO_2 composition in NGCC without EGR for an EGR percentage of 20, 35 and 50 %, respectively. The flue gas flow rate, which is to be treated in the amine-based CO_2 capture system, is also decreased by the same percentage when the exhaust gas recirculation is applied. In addition to the above, the authors have reported in the literature [165, 215] a sensitivity analysis for the EGR stream on the performance of the gas turbine.

Details are also provided in Table 7.4 of the auxiliary loads in order to show the losses in different sections of the system. Thus, allowing the estimation of the total net power output of the power plant. For the estimation purposes, the auxiliary loads are divided into two classes; one which can be directly measured and the other which are fixed based on the Report of the US Department of Energy [211] and are termed as other auxiliary loads in Table 7.4. The measurable auxiliary losses consist of the condensate pump and boiler feed water pump loads. The other fixed losses consist of the pumps load for water circulation, cooling tower fan loads, selective catalytic reduction losses, gas turbine and steam turbine auxiliaries loads and miscellaneous loads. For the NGCC with EGR, the additional loads of the EGR recirculation fan and the EGR coolant recirculation pump losses are also included in the above mentioned auxiliary loads. The difference between literature reported and model predicted value of the net power output for 35 % EGR case, is due to the fact that the literature reported value consider losses in CO_2 capture plant for that particular case.

7.3.2 Amine-based CO_2 Capture Plant Model Validation at Pilot-scale

The process model validation of the pilot-scale amine-based CO_2 capture plant has been already done and presented in Sections 6.4 and 6.5 of Chapter 6 and is not repeated here.

7.4 Design and/or Scale-up for a Commercial-scale Amine-based CO_2 Capture Plant

The design and/or scale-up of the amine-based CO_2 capture plant is performed for the four cases already discussed in Section 7.2.2; one for the base case, the NGCC without EGR and with NGCC capacity 650 MW_e, and three cases for the NGCC

with an EGR percentage of 20, 35 and 50 %. The conditions of the flue gas in terms of the process parameters, flow rates and composition for all these four cases for which the amine-based CO_2 capture plant is to be designed and/or scaled-up, is tabulated in Table 7.4. The input specification for the commercial-scale amine-based CO_2 capture plant in terms of the process parameter inputs and techno-economic variables are listed in Table 7.2 and Table 7.3, respectively. The commercial-scale amine-based CO_2 capture plant is modelled and optimized for the Mellapak 250Y and the lean amine loading is fixed at 0.2 mol CO_2/mol MEA [159]. The summary of the design results for the amine-based CO_2 capture plant for the four different scenarios is shown in Table 7.5 and the detailed process design results and process economic results can be found in Table C. 2.

Table 7.5 Design results summary for the amine-based CO_2 capture plant for four different scenarios of the NGCC.

Parameter	NGCC without EGR	NGCC with 20 % EGR	NGCC with 35 % EGR	NGCC with 50 % EGR
Gross power plant size [MW_e]	650.7	621.1	621.3	622.5
Gas turbine power output [MW_e]	418.1	419.9	418.7	419.9
Exhaust gas recirculation Rate [%]	-	20	35	50
CO_2 in flue gas [mol%]	3.91	5.12	6.2	8.19
Flue gas flow rate [kg/s]	1029.7	783.8	652.8	499.1
Optimum liquid/gas ratio [kg/kg]	0.96	1.22	1.46	1.9
Optimum rich CO_2 loading [molCO_2 /mol MEA]	0.480	0.485	0.487	0.489
Absorber				
Number of absorber	2	2	2	2
Absorber packing	Mellapak 250Y	Mellapak 250Y	Mellapak 250Y	Mellapak 250Y
Absorber diameter [m]	15.00	13.61	12.75	11.39
Optimum absorber Height [m]	16.47	15.75	15.43	15.31
Stripper				
Number of stripper	1	1	1	1
Stripper packing	Mellapak 250Y	Mellapak 250Y	Mellapak 250Y	Mellapak 250Y
Stripper diameter [m]	9.20	9.06	9.02	9.00
Optimum stripper height [m]	29.73	29.46	28.67	27.88

7.4.1 Commercial-scale Amine-based CO_2 Capture Plant for NGCC without EGR

The process design results for the amine-based CO_2 capture plant for the commercial-scale NGCC without EGR are given in Figure 7.2. The design results are estimated for the liquid to gas ratio in the range from 0.94 to 1.04 at the CO_2

capture rate of 90 % and lean amine loading of 0.2 mol CO_2/mol MEA. The selected parameters presented here, which are affected by the liquid to gas ratio variation, are the packed heights of the absorber and stripper, the specific reboiler duty, the steam flow rate to the reboiler and the cooling water flow rate to the condenser and the lean amine cooler in the amine-based CO_2 capture plant. It is evident from Figure 7.2 (a) that the absorber packed height varies mainly as a function of the liquid to gas ratio. The variation of the absorber packed height around the optimum point varies both with increasing and decreasing the liquid to gas ratio around that point. The absorber packed height increases sharply as a function of the liquid to gas ratio when the liquid to gas ratio is decreased below an optimum point of the liquid to gas ratio. Also, there is a gradual decrease in the absorber packed height as a function of the liquid to gas ratio when this increases beyond the optimum point of the liquid to gas ratio. However, this decrease is less distinct and cannot be considered for the selection of the optimum point. Further, the stripper packed height is less affected by the variation of the liquid to gas ratio as seen from Figure 7.2.

In addition, the specific reboiler duty decreases with the reduction of the liquid to gas ratio without identifying the optimum location and this is observed for the absorber packed height as a function of the liquid to gas ratio. Also, the decrease in the steam requirement and cooling water requirement for the amine-based CO_2 capture plant, as shown Figure 7.2 (b), is observed with the reduction of the liquid to gas ratio. However, this decrease is not sharp and does not result in the location of the optimum design parameters alone. Also, the steam requirement is directly dependant on the specific reboiler duty, and hence does not result in the optimum design parameters for the relevant minimum specific reboiler duty. However, from Figure 7.2 (a), it is clear that the optimum point appears to be at the liquid to gas ratio of about 0.95.

However, if the process economic results for the same range of liquid to gas ratio is considered then the optimum location for the process design of the amine-based CO_2 capture plant can be better assessed. The economic results are presented in Figure 7.3, including the CAPEX, OPEX and TOTEX for different liquid to gas ratios. The TOTEX is estimated for three different cost scenarios as discussed in Section 5.2.2. It is evident from Figure 7.3(a) that the CAPEX increases abruptly with the reduction of the liquid to gas ratio below a certain optimum value, and this increase

is due to the sharp increase in the absorber packed height. Similarly, the OPEX also increases with the decrease in the liquid to gas ratio below a certain optimum point, and this is due to the increased CAPEX associated with the maintenance cost.

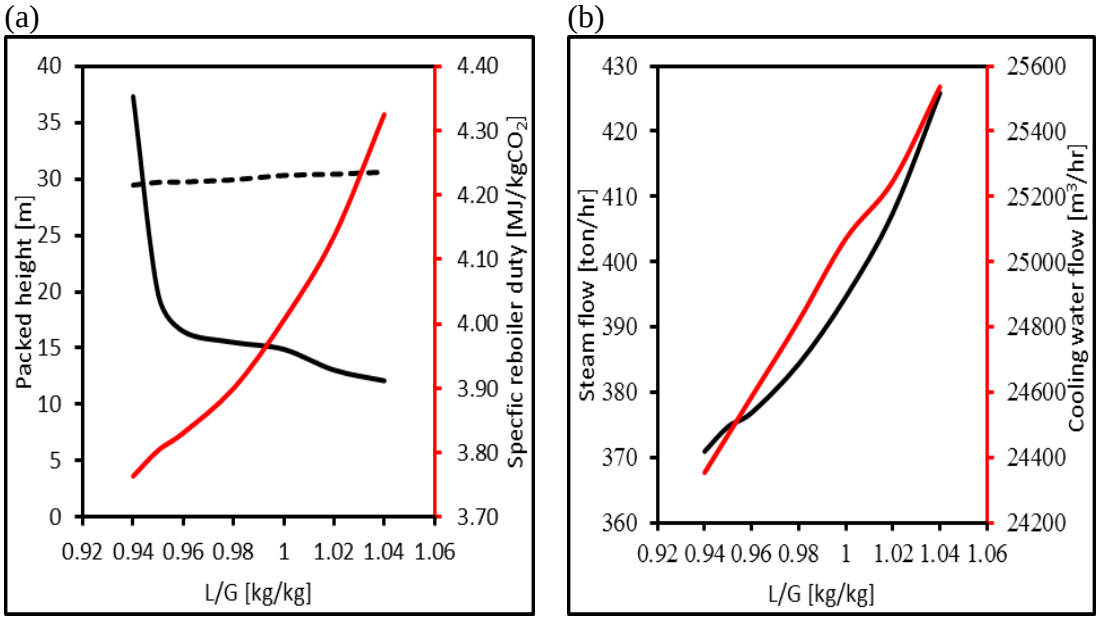

Figure 7.2 Process design results for the amine-based CO_2 capture plant for the NGCC without EGR. (a) Variations of absorber packed height (black solid line), stripper packed height (black dashed line) and specific reboiler duty (red solid line) as a function of the liquid to gas ratio; and (b) Variations of steam flow requirement (black line) and cooling water requirement (red line) as a function of the liquid to gas ratio.

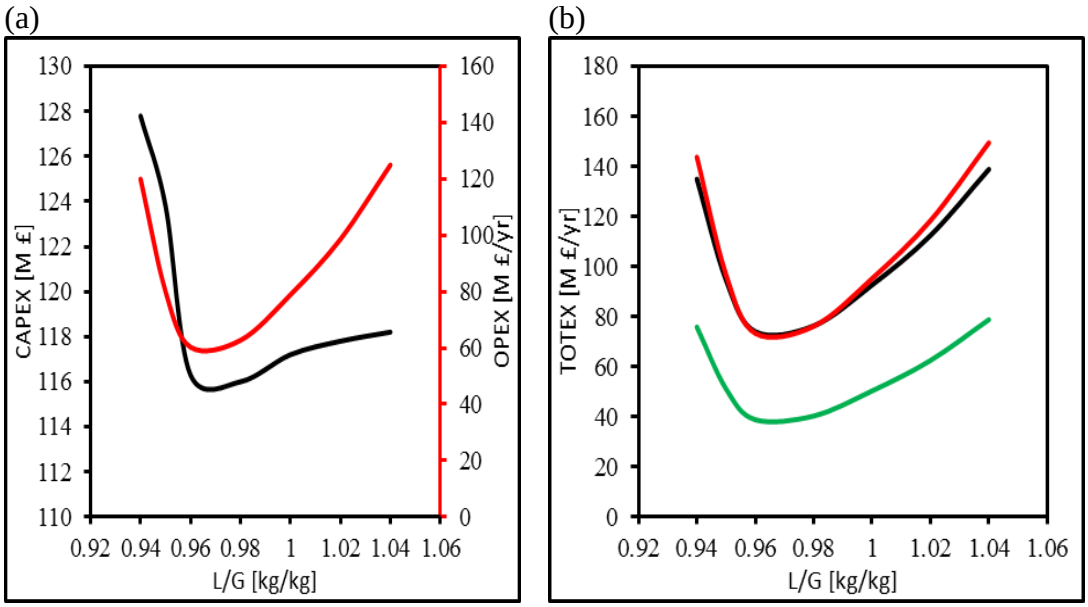

Figure 7.3 Process economic results for the amine-based CO_2 capture plant for the NGCC without EGR. (a) Variations of the CAPEX (black line) and OPEX (red line) as a function of the liquid to gas ratio; and (b) Variation of the TOTEX as a function of the liquid to gas ratio for three different cases as Case A (black line), Case B (red line) and Case C (green line).

Further, the OPEX increases with the increase in the liquid to gas ratio, beyond an optimum point, and this is due to the increased utilities requirement. The optimum

location of the liquid to gas ratio from the minima of the OPEX is 0.96 and this results in the absorber packed height 16.47 m, stripper height 29.73 m and specific reboiler duty 3.83 MJ/kgCO_2. This optimum point is also verified by the minima of the TOTEX for the three different cases of the TOTEX as shown in Figure 7.3 (b). A summary of the optimum design results can be found in Table 7.5 and the detailed optimum process design is presented in Table C. 2 in the Appendix C. However, the literature [108] reported a minimum liquid to gas ratio of 0.68, with an absorber height of 26.9 m and stripper height of 23.5 m. Further, it should be kept in mind that Sipocz and Tobiesen [108] reported that the design is for the NGCC power plant with a capacity of 410.6 MW_e. Conversely, the design results reported by Biliyok et al. [101] and Biliyok and Yeung [106] are of constant absorber height 15 m, with the number of absorbers as 4. In addition, the maximum NGCC power plant capacity is 453 MW_e as reported by Luo et al. [209], with absorber height 25 m and the specific reboiler duty 4.54 MJ/kg CO_2. It can be concluded that the economic analysis is also an important parameter to reach the optimum design dimensions for the design and/or scale-up of commercial-scale amine-based CO_2 capture plant.

7.4.2 Commercial-scale Amine-based CO_2 Capture Plant for NGCC with EGR

The process design results for the amine-based CO_2 capture plant for the commercial-scale NGCC with EGR at three different EGR percentage cases, 20, 35 and 50 %, are presented in Figure 7.4. The results for the EGR cases are similar to those reported for the amine-based CO_2 capture plant for the commercial-scale NGCC without EGR. The design results are estimated for the CO_2 capture rate 90 %, lean amine loading 0.2 mol CO_2/mol MEA and liquid to gas ratio in the range 1.20 to 1.25 for 20 % EGR percentage, 1.40 to 1.60 for 35 % EGR percentage, and 1.80 to 2.00 for 50 % EGR percentage. The selected parameters presented here, which are affected by the liquid to gas ratio variation, are the same as those in the NGCC without EGR which includes; packed heights of the absorber and stripper, specific reboiler duty, steam flow rate to the reboiler and cooling water flow rate to the condenser and lean amine cooler in the amine-based CO_2 capture plant. From Figure 7.4 (a), it is clear that the absorber packed height increases abruptly with the reduction of the liquid to gas ratio below an optimum point for different cases of the EGR ratio. In addition, there is a less distinct decrease in the absorber packed height with the increase of the liquid to gas ratio beyond an optimum point of the liquid to

gas ratio. Further, the stripper packed height and specific reboiler duty follows the same general trend as discussed for the NGCC without EGR. The steam flow requirement and cooling water requirement are shown in Figure 7.4 (b).

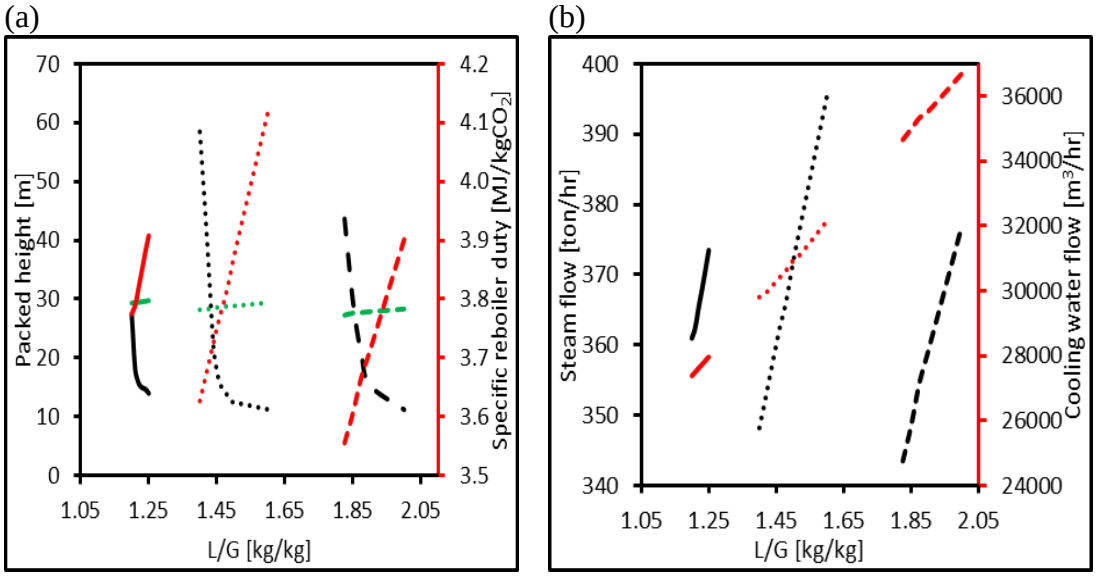

Figure 7.4 Process design results for the amine-based CO_2 capture plant for the NGCC with EGR (20 % EGR: Solid lines; 35 % EGR: Dotted Lines; and 50 % EGR: Dashed Lines). (a) Variations of absorber packed height (black lines), stripper packed height (green lines) and specific reboiler duty (red lines) as a function of the liquid to gas ratio; and (b) Variations of steam flow requirement (black lines) and cooling water requirement (red lines) as a function of the liquid to gas ratio.

In addition, the steam flow requirement and cooling water flow requirement follow the same general trend as discussed for the NGCC without EGR. Hence, the optimum point for the liquid to gas ratio, based on the process analysis alone for different EGR cases, is 1.21, 1.45 and 1.88 for the 20, 35 and 50 % EGR percentages, respectively. Nevertheless, if the process economic analysis is performed for a similar range of liquid to gas ratio for each of the EGR ratios, then the optimum location can be better estimated.

The CAPEX and OPEX variation as a function of the liquid to gas ratio is presented in Figure 7.5 (a) and the TOTEX variation as a function of the liquid to gas ratio is presented in Figure 7.5(b) for varying EGR ratios. It is evident from Figure 7.5 that the true optimum for the amine-based CO_2 capture plant can be better approximated by considering the process economic analysis. Based on the minima of the OPEX, the optimum liquid to gas ratio for different EGR ratios are 1.22, 1.46 and 1.90 for the 20, 35 and 50 % EGR percentages, respectively.

A summary of the optimum design results can be found in Table 7.5 and the detailed optimum process design is presented in Table C. 2. However, for the reported literature design dimensions, the minimum absorber height as mentioned by Sipocz and Tobiesen [108] is 23.6 m for a single absorber at the EGR percentage of 40 % for NGCC operating at 413.5 MWe. Although, the absorber heights reported by Biliyok et al. [101] and Biliyok and Yeung [106] are 15 m, however, the number of absorbers are 3 for both of the studies at 40 % EGR percentage for the 440 MWe NGCC power plant. Similarly, the minimum specific reboiler duty reported is 3.64 MJ/kg CO_2 which is at 40 % EGR percentage for the 440 MWe NGCC power plant [108]. A comparison of the design results for amine-based CO_2 capture plant as reported in the literature for NGCC, both with and without EGR, is presented in Table C.1 in the Appendix C.

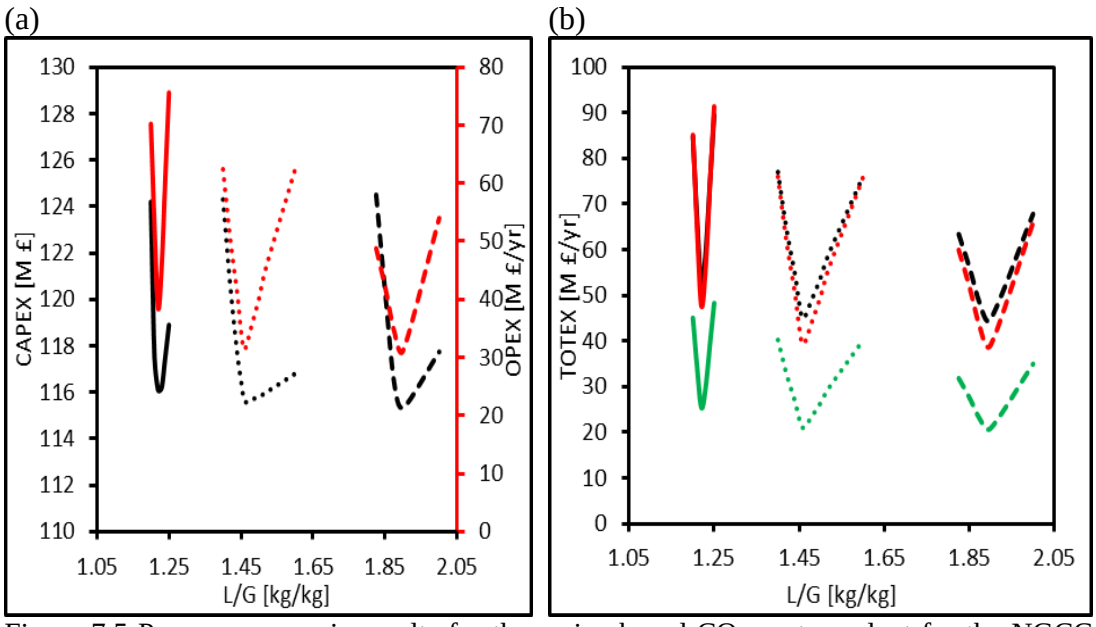

Figure 7.5 Process economic results for the amine-based CO_2 capture plant for the NGCC with EGR (20 % EGR: Solid lines; 35 % EGR: Dotted Lines; and 50 % EGR: Dashed Lines). (a) Variations of the CAPEX (black lines) and OPEX (red lines) as a function of the liquid to gas ratio; and (b) Variation of the TOTEX as a function of the liquid to gas ratio for three different cases as Case A (black lines), Case B (red lines) and Case C (green lines).

Finally, it is observed that with an increase in the EGR ratio, the absorber and stripper packed height, specific reboiler duty and associated steam flow requirement, CAPEX, OPEX and TOTEX decreases, as can be observed from Table C. 2 in the Appendix C.

It must be mentioned here that this chapter deals with design and/or scale-up of the commercial-scale amine-based CO_2 capture system which can service commercial-scale natural gas power plants with and without EGR. The aim of this design and/or scale-up was to use the conventional process flow diagram as shown in Figure 6.1 rather than any modified configurations such as absorber intercooling, condensate heating and evaporation, stripper overhead compression, lean amine flashing, multi-pressure stripping, split-amine and modified heat and mass integrations as mentioned in the literature [267]. These modified configurations and integrations are outside the scope of this research work.

However, effect of the EGR on the design variables, operating variables and cost of the commercial-scale amine-based CO_2 capture plant is reported. The application of EGR results in 1.6 % and 3.1 % decreases in specific reboiler duty due to the application of the EGR as reported in Table C.2 of the Appendix C. The breakdown of the reboiler duty and how CO_2 enhancement affects the reboiler duty can be found in chapter 6.

7.5 Conclusions

- Instead of employing a process design analysis alone, a combined process economic analysis is an essential requirement for reaching the optimum design variables for commercial-scale amine-based CO_2 capture plants.
- The optimum design results for the commercial-scale amine-based CO_2 capture plant are reported for an onshore commercial-scale NGCC with and without EGR for a gross power output of 650 MW_e.
- The application of EGR results in lower specific reboiler duty, reduced design dimensions and cost of the commercial-scale CO_2 capture plant.
- This resulted in the optimum liquid to gas ratio being 0.96 for the structured Mellapak 250Y packing with a CO_2 capture rate of 90 % and CO_2 composition of 3.91 mol% in the flue gas.
- When a 20 % EGR percentage is applied to the same plant, the optimum liquid to gas ratio is 1.22 for the same packing and CO_2 capture rate. However, the CO_2 composition of the flue gas is increased to 5.13 mol%.
- The optimum liquid to gas ratio for the NGCC with 35 % and 50 % EGR are 1.46 and 1.90, respectively, with the CO_2 composition in the flue gas now

being 6.20 and 8.19 mol%; provided that any modification in the combustor if required of the gas turbine is available for the 50 % EGR percentage equipped NGCC power plant.

- The carbon capture from the existing or new natural gas-fired power plants will work to reduce greenhouse gases by minor variations to the present cycle in the form of EGR, which will result in fewer penalties in terms of the energy consumption and the cost incurred in comparison to a natural gas-fired power plant without EGR. The wide adoption of carbon capture, especially for fossil-fuelled power plants, will result in a better energy mix for the future low carbon economy.

The design and/or scale-up strategy implemented in this chapter is used to further design the CO_2 capture plant which can service subcritical and supercritical coal and biomass fired power plants and thus is presented in Chapter 8. Further, the CO_2 compression system is included in the analysis and the process performance of the whole energy system. In addition, the process comparison of the subcritical and supercritical coal and biomass fired power plants is done with the NGCC, both with and without EGR for the whole system carbon capture.

Chapter 8
Comparative Potential of Natural Gas, Coal and Biomass Fired Power Plant with CO_2 Capture and Compression

In this chapter, a process system analysis is performed for commercial-scale standalone coal and biomass fired, subcritical and supercritical type power plants and the key performance and overall energy results are compared with NGCC with and without EGR power plant results. Further, the co-firing of coal and biomass for the supercritical type power plant is also assessed and compared. In addition, the MEA-based CO_2 capture plant and CO_2 compression system is also integrated for each of the power plants studied. Finally, the comparative potential of each of the above mentioned power plants is discussed in detail.

8.1 Introduction

As discussed in Section 1.1, the thermal power generation system is the major source of CO_2 emissions. The application of CCS to the thermal power plants or carbon neutral techniques should be adopted to a faster rate in order to mitigate the effect of global warming and to reduce the level of CO_2 emissions [13]. The technologies or techniques that can remove and/or reduce the large amount of CO_2 from the atmosphere should be a considerable part of the present energy mix in order to limit the global temperature rise to 2 ^{o}C [216]. In the past, biomass was not used abundantly for large scale power generation systems rather than fossil fuels due to the low energy density, scarcity, considerable cost of transportation and its environmental impact [217]. However, environmental concerns have renewed the interest towards the use of biomass as an energy source for power generation [27, 218, 219]. It is agreed that the most efficient and inexpensive means of reducing CO_2 emissions is replacing coal with biomass and/or co-firing coal with biomass [30]. The factors that influence the selection of suitable biomass as an energy source and the conversion techniques of biomass to energy through suitable

processes is widely discussed in literature [27, 220]. Sustainably-grown biomass emits the same amount of CO_2 during combustion, which it consumes during its growth [26, 221], which makes biomass a CO_2 neutral fuel. Although, it is needed to reduce the time lag between the instantaneous release of the CO_2 due to the biomass burning and the eventual consumption of the released CO_2 by the newly grown biomass [27]. However, if CCS is applied to sustainably-grown biomass, it would effectively result in negative CO_2 emissions [222] which is commonly termed as bio energy carbon capture and storage (BECCS). Therefore, biomass results in no net CO_2 emissions when coal is replaced by sustainably-grown biomass and/or results in a reduction of the net CO_2 emissions when co-firing of coal with biomass is done. To attain the projected biomass contribution to the electricity generation market, and further to reduce CO_2 emissions, biomass will contribute a considerable proportion towards commercial-scale power generation systems as discussed in the literature [223, 224]. Baxter [30] has discussed major barriers in the deployment of biomass and/or co-firing for the thermal power generation system with focus on fireside issues. However, the major barriers to the demonstration and deployment are economics and sustainable biomass availability, rather than being technical in nature [216, 225].

For commercial-scale power generation, two alternatives can be considered in the existing commercial-scale coal fired power plants, such as commercial-scale standalone biomass fired power plants, or co-firing coal with biomass [226] instead of commercial-scale standalone coal fired power plants and commercial-scale NGCC power plants. There is a widespread understanding that the co-firing of coal and biomass to the existing commercial-scale coal-fired power plants will result in a reduction of the net CO_2 emissions and will be a prospective option to combat global warming [227-229]. Co-firing coal with biomass is considered as a well proven technology [230] as co-firing is demonstrated worldwide in 150 plants through a combination of installations [231].

Use of biomass in thermal power generation systems may affect the system performance and efficiency due to the low heating value of the biomass [232]. However, biomass will result in additional benefits other than negative emissions if CCS is applied. The combustion behaviour of the pulverised coal and biomass has been widely discussed by Williams et al. [233]. As biomass is less volatile and

contains less fuel bound nitrogen, therefore its results in less NO_x during combustion [234]. The lower emissions of SO_2 due to lower sulphur content in biomass have made biomass co-firing more economical rather than installing SO_2 control systems [234]. Combustion behaviour, fireside issues and minor components pollutant gas emissions have been widely discussed in the literature [30, 235, 236]. Sebastián et al. [226] and Mann and Spath [234] have performed the life cycle assessment of co-firing of coal and biomass in a coal fired power plant to estimate the potential emissions and economic savings. The techno-economic assessment and specific reduction in the CO_2 emissions for co-firing of coal and biomass in different types of technologies, including pulverized fuel firing, pressurized fluidised firing and atmospheric pressure circulating fluidised bed firing using the process simulator ESCIPSE have been reported in the literature [217, 232, 237]. Energy analysis is performed for the co-firing of the biomass with coal to analyse the impact of the biomass co-firing on the system performance through process system analysis [238]. Similarly, cost analysis and optimum plant size for co-firing of the coal with biomass has been reported by Kumar et al. [239] and De and Assadi [240]. However, none of the above mentioned literature has reported the impact of biomass firing and/or co-firing of coal and biomass on the carbon capture technology. Al-Qayim et al. [241] have reported a techno-economic assessment of a standalone biomass fired power plant with two different kinds of CCS technologies, including PCC and oxy-fuel system, and have compared the cost and emissions incentives to that of a coal fired power plant. IEA [242] have reported the different case studies for the co-firing of biomass with coal for different technologies, including pulverised fuel firing, circulating fluidised bed firing and bubbling fluidised bed firing. Similarly, same results as that of the IEA [242] have been reported by Domenichini et al. [243]. Benchmarking comparison of NGCC, coal and biomass fired power plants integrated with a MEA-based CO_2 capture plant has been reported by Berstad et al. [160] with emphasis on the efficiency losses and specific CO_2 emissions for varying stripper operating pressure.

As, CO_2 compression will be an integral part of the CO_2 capture process from a power plant, therefore the penalty introduced due to the CO_2 compression system must be accounted for. There are studies being reported in the literature [244-248] reporting the integration of the coal fired power plant with CO_2 capture system with parametric studies. In addition, the literature [249-261] also reports the integration

of the CO_2 capture and CO_2 compression system to the coal fired power plant. The integration is based on comparing the parametric and sensitivity effects on the performance of the whole system. Heat integration studies and various options of steam tapping to optimise the integration of the CO_2 capture and CO_2 compression to the coal fired power plant has been discussed [250, 254-256, 261] in order to make coal based power plants as a favourable approach to be adopted for carbon capture and storage. The integration of the CO_2 capture with NGCC operated with and without EGR is widely discussed in Chapter 7; hence it is not repeated here. Therefore, NGCC due to the higher efficiency is the most attractive option to be adopted for integration into CO_2 capture and CO_2 compression system in the present scenario of interest towards gas-CCS.

However, none of the reported literature have compared the potential of the different power plant systems, including natural gas firing, pulverised subcritical coal firing, pulverised supercritical coal fired, pulverised subcritical biomass firing, pulverised supercritical biomass fired, and co-firing of coal and biomass; integrated with CO_2 capture and compression system. It is clear from the above discussion that very limited work has been presented in the literature about the application of CCS towards the standalone biomass fired power plant and co-fired power plant. Further, the comparison of coal and biomass fired power plants with a NGCC power plant integrated with CO_2 capture and CO_2 compression system is rarely found in the literature except for the parametric comparison reported by Berstad et al. [160] without explicitly mentioning the detailed performance results of each process.

Therefore, the aim of this chapter is to investigate the potential comparison of natural gas, coal and biomass fired power plants integrated with CO_2 capture and CO_2 compression system and analyse the process performance, in terms of efficiency, pollutant emissions and potential losses. In addition, different types of each of the natural gas, coal and biomass fired power plants integrated with CO_2 capture and CO_2 compression system are discussed and compared. The different types of each of the power plants discussed are elaborated in Section 8.2.1. Therefore, the focus of this chapter is to evaluate the overall energy performance, penalty and losses of the different power plant systems on their integration to the CO_2 capture and CO_2 compression system.

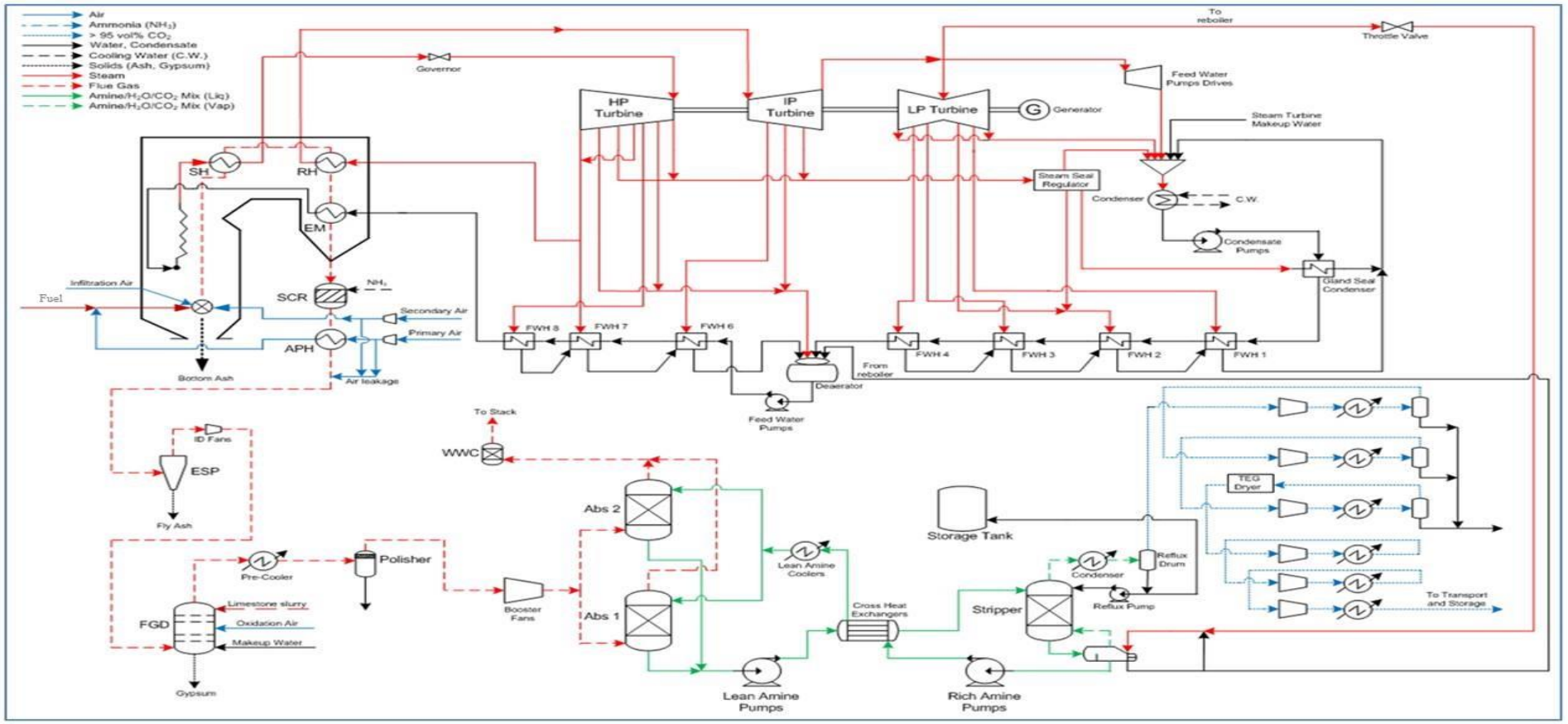

Figure 8.1 Basic schematic of the solid fuel fired power plant integrated with an amine-based CO_2 capture plant and CO_2 compression system (adopted with changes from Agbonghae [262]).

8.2 Process Configuration and Case Studies

Each of the natural gas, coal and biomass fired power plants can be sub divided into different case studies which are investigated in this chapter. Each of the types is integrated with a CO_2 capture system and CO_2 compression system and details of each type is discussed in the relevant subsections. The numbers of power plant cases performed are as follows:

- Natural gas fired power plant
  - NGCC without EGR
  - NGCC with EGR
- Solid fuel fired power plant
  - Supercritical type
    - Constant heat input
      - Coal fired
      - Biomass fired
    - Constant fuel flow rate
      - Coal fired
      - Biomass fired
    - Co-firing coal and biomass
  - Subcritical type
    - Constant heat input
      - Coal fired
      - Biomass fired
    - Constant fuel flow rate
      - Coal fired
      - Biomass fired

8.2.1 Natural Gas Fired Power Plant

The natural gas fired power plant modelled in this chapter is based on Siemens 8000H frame gas turbine with ISO output of 275 MW from the gas turbine section as reported in the 2013 Report of the US Department of Energy [211]. A schematic of the natural gas fired power is similar to that shown in Figure 7.1 that indicates the different sections of the NGCC power plant bounded by rectangles as mentioned in Section 7.2.1. Except for the H frame gas turbine; there is a fuel gas heating system

to enhance the system performance. The pressure ratio of the compressor is 20 with a gas turbine inlet temperature 1487 ^{o}C and a gas turbine outlet temperature 619 ^{o}C. The bottom Rankine cycle is the same as that elaborated in Section 7.2.1, consisting of triple pressure level single reheat cycle with steam cycle specification of 16.5/566/566 MPa/^{o}C/^{o}C. The HRSG generates both main and reheat steam for the steam cycle. The flue gas temperature is 88 ^{o}C at the HRSG exit and it is then directed to the CO_2 capture system and the captured CO_2 stream is compressed through a CO_2 compression system. The specifications of the NGCC power plant modelled in this chapter are given in Table 8.1. The natural gas and air compositions are the same as those reported in Table7.1.

Table 8.1 Input specifications for the NGCC models [211].

Parameter	Without EGR	With EGR
Gas turbine inlet temperature [^{o}C]	1487	1487
Gas turbine outlet temperature [^{o}C]	619	619
Air inlet temperature [^{o}C]	15	15
Flue gas temperature at HRSG exit [^{o}C]	88	106
Exhaust gas recirculation rate [%]	0	35
Pressure ratio	20	20
Compressor efficiency [%]	85	85
HP[a] steam turbine efficiency [%]	88.9	88.9
IP[b] steam turbine efficiency [%]	92.6	92.6
LP[c] steam turbine efficiency [%]	94.0	94.0

[a]HP - high pressure.
[b]IP - intermediate pressure.
[c]LP - low pressure.

For NGCC with EGR, 35 % of the exhaust gas is recirculated to the compressor inlet of the gas turbine. The reminding 65 % of the flue gas is sent to the MEA-based CO_2 capture plant and the captured CO_2 is sent for compression through CO_2 compression system. The effect of the EGR on the performance of the gas turbine has already been explored in Chapters 4, 5 and 7 and therefore is not discussed here. For NGCC with EGR, the gas turbine inlet and outlet temperatures are the same as that of the NGCC without EGR; however, the flue gas exit temperature is 106 ^{o}C at the HRSG exit. The specifications of the NGCC with EGR are listed in Table 8.1. A schematic of the NGCC with EGR is the same as that shown in Figure 7.1, except the fuel gas heating system at the fuel line to the combustor. The EGR loop of the NGCC power plant is indicated by green dashed rectangle in Figure 7.1. The details of the CO_2 capture system for NGCC can be found in Sections 7.2.1 and 8.2.2.4 while the details of the CO_2 compression system is discussed in Section 8.2.3.

8.2.2 Coal Fired Power Plant

The pulverised coal fired power plant modelled in this chapter is based on subcritical and supercritical pulverised coal cases reported by the 2010 Report of the US Department of Energy [263]. The pulverised coal fired power plant is based on the gross power output of 800 MW_e. A schematic of the coal fired power plant is shown in Figure 8.1 and it is integrated with a CO_2 capture unit and CO_2 compression unit. For the subcritical case, the steam cycle specification is 16.5/566/566 MPa/^oC/^oC and for the supercritical case, the steam specification is 24.1/593/593 MPa/^oC/^oC. For the subcritical case, the steam generator is drum type, natural circulation with super-heater, re-heater, economizer and air preheater while for the supercritical case, the steam generator is once-through with super-heater, re-heater, economizer and air preheater [263]. The coal fired is bituminous type Illinois No. 6 coal, and its proximate and ultimate analysis with heating value is given in Table 8.2 with as-received and dry analysis. The air composition used for combustion is same as given in Table 3.2 and/or Table 7.1.

Table 8.2 Proximate, ultimate and heating value of coal [263] and biomass.

	Coal		Biomass Pellets	
Proximate Analysis	As-received (wt. %)	Dry (wt. %)	As-received (wt. %)	Dry (wt. %)
Moisture	11.12	0.00	6.69	0.00
Volatile Matter	34.99	39.37	78.10	83.70
Ash	9.70	10.91	0.70	0.75
Fixed Carbon	44.19	49.72	14.51	15.55
Total	100	100	100	100
Ultimate Analysis	As-received (wt. %)	Dry (wt. %)	As-received (wt. %)	Dry (wt. %)
C	63.75	71.72	48.44	51.87
S	2.51	2.82	<0.02	0.02
H_2	4.50	5.06	6.34	6.79
H_2O	11.12	0.00	6.69	0.00
N_2	1.25	1.41	0.15	0.16
O_2	6.88	7.75	37.69	40.37
Ash	9.70	10.91	0.70	0.75
Cl	0.29	0.33	<0.01	0.01
TOTAL	100	100	100	100
Heating Value	As-received	Dry	As-received	Dry
HHV (kJ/kg)	27113	30506	19410	20802
LHV (kJ/kg)	26151	29444	18100	19398

In addition, to the primary and secondary air, infiltration air and/or air leakages are also accounted for as indicated in Figure 8.1.The Rankine cycle consists of three levels of steam turbines; high pressure, intermediate pressure and low pressure turbines. There are 8 feed water heaters, 3 upstream of the deaerator; heating the boiler feed water from the HP and IP turbines steam bleeds. The remaining 4 feed water heaters are at the downstream of the deaerator and LP turbine bleed steam is used for the boiler feed water heating. The condenser operates at a condensing pressure of 7 kPa with a corresponding saturation temperature 38 ^{o}C. In addition, the steam required by the MEA-based CO_2 capture plant is extracted from IP-LP cross-over and the condensate return from the MEA-based CO_2 capture plant is returned to the steam cycle at the deaerator.

Further, the pulverised coal fired power plant is equipped with emission control technologies, including, the selective catalytic reduction (SCR) unit for the NO_x removal, the fabric filters for particulate removal, the flue gas desulfurization (FGD) for the SO_2 removal and the CO_2 capture unit for CO_2 removal. The flue gas from the economizer enters the SCR unit before preheating the air in the air preheater and then comes the fabric filters for removing the solid contaminants. Then the flue gas enters the FGD unit for SO_2 removal before it enters the CO_2 capture assembly. The SCR, fabric filter and FGD units are shown in Figure 8.1 and their details are given in the next subsections.

8.2.2.1 Selective Catalytic Reduction Unit

The SCR unit uses ammonia with catalysts for the conversion of the NO_x pollutant into nitrogen and water. The SCR unit removes 86 % of the NO_x released during combustion with 2 ppmv of the ammonia slip at the end of the catalyst life. The number of active metals can be used as catalyst which along with temperature ranges can be found in the literature [263, 264]. The SCR unit is located at the downstream of the economizer as shown in Figure 8.1. The principal reactions involved in the SCR unit are as follows [262, 264]:

$$4NO + 4NH_3 + O_2 \rightarrow 4N_2 + 6H_2O + \text{heat} \quad (8.1)$$

$$2NO_2 + 4NH_3 + O_2 \rightarrow 3N_2 + 6H_2O + \text{heat} \quad (8.2)$$

8.2.2.2 Fabric Filter

The fabric filter removes any solid particulate contaminant carried away beyond the boiler assembly by the flue gas. It works on 99.8 % efficiency. The same ratio of 80/20 percent split is applied between the fly ash and the bottom ash as reported in the 2010 Report of the US Department of Energy [263]. The fabric filter, as an electrostatic precipitator (ESP), is shown between the air preheater and the induced draft fan in the coal fired power plant schematically shown in Figure 8.1.

8.2.2.3 Flue Gas Desulphurization Unit

The FGD unit is a wet limestone forced oxidation process with gypsum as a by-product. The removal efficiency of the FGD unit is 98 % and it reduces the SO_2 content up to 10 ppmv [263]. The FGD unit is shown at the downstream of the induced draft fan of the coal fired power plant schematic in Figure 8.1. The principal reactions involved in the FGD unit are as follows [262, 264]:

$$CaCO_3(s) + SO_2(g) + 0.5H_2O \rightarrow CaSO_3 \cdot 0.5H_2O + CO_2(g) \quad (8.3)$$

$$CaCO_3(s) + SO_2(g) + 0.5O_2 + 2H_2O \rightarrow CaSO_4 \cdot 2H_2O + CO_2(g) \quad (8.4)$$

8.2.2.4 CO_2 Capture Unit

The MEA-based reactive absorption and desorption is considered for the CO_2 capture from the flue gas at the CO_2 capture rate of 90 %. The flowsheet of the CO_2 capture unit is shown in Figure 8.1. The CO_2 capture unit consist of 2 absorbers and one stripper. The flue gas from the FGD unit is sent to the booster fan for the pressure increase before it is split into two streams and then each stream is fed at the bottom of the packed absorber column. The flue gas is contacted with the lean amine solution in a counter-contact manner which is introduced from the top of each absorber. The rich amine solution from the bottom of both absorbers is collected and pumped to the top of the stripper as a single stream. The rich amine solution is heated through a cross lean/rich heat exchanger before entering the packed stripper column. The CO_2 is stripped from the amine solution and the uncondensed CO_2 stream from the condenser is sent to the CO_2 compression unit. The lean amine solution flows down the stripper column and is pumped back for recirculation to the top of the absorber. The lean amine solution is cooled initially through the cross lean/rich heat exchanger and then through the lean amine cooler. Further, there is a

water wash section at the top of the absorbers to remove entrained droplets of the amine solution in the treated gas exiting the absorber columns.

8.2.3 Biomass Fired Power Plant

The standalone pulverised biomass fired power plant is modelled based on the model developed for the coal fired power plant as mentioned in Section 8.2.2. The pulverised biomass fired plant model is also based on the 800 MW_e of the gross power output. The air composition is the same as that given in Table 3.2 and/or Table 7.1. The components and details of the subcritical and supercritical cases of the pulverised biomass fired plant are the same as that of the coal fired plant model explored in Section 8.2.2. The boiler, steam cycle and emission control configuration is kept the same in order to have a thorough comparison of the coal and biomass firing systems. The biomass used is US forestry residue, and it is shipped in pellet form. The proximate, ultimate analysis of the biomass used along with heating value is reported Table 8.2 in the form of as-received and dry basis analysis. There is about 40, 93 and 67 % decrease in the moisture content, ash and fixed carbon, respectively of the biomass when compared with the coal for proximate analysis. However, there is 123 % increase in volatile matter in the case of biomass. Similarly, for the ultimate analysis, there is about 24 and 88 % decrease in carbon and nitrogen, respectively while there is 41 and 448 % increase in hydrogen and oxygen, respectively of the biomass in comparison to that of the coal. Further, there is approximately 28 % decrease in calorific value of the biomass when compared with the coal as reported in Table 8.2.

Due to these varying properties of the biomass, two case studies are performed for both subcritical and supercritical cases of the solid fuel fired power plants, one based on constant heat input and the other based on constant fuel flow rate. In the constant heat input cases, the flow of the fuel varies to maintain the same heat transfer from flue gas to the water/steam in the super-heater, re-heater and economiser while for the cases based on the constant fuel flow rate, the fuel flow rate to the boiler is kept constant irrespective of the fuel type, whether coal or biomass, which results in varying heat transfer to the super-heater, re-heater and economiser. The cases with constant heat input, results in a large increase in the fuel flow rate with lower heating value. The cases with constant fuel flow rate results in degradation of the total power output from the power plant due to the lower heating value of the fuel.

Further, in order to judge the better performance of the biomass use in power plant, the co-firing of coal with biomass is also performed for a number of varying fractions of the coal and biomass as explored in Section 8.3. The co-firing of coal and biomass is performed for supercritical, constant heat input case of the solid fuel power plant. The co-firing of coal and biomass cases modelled are classified and given in Table 8.3 where the portion of coal and biomass is specified as a percentage of the fuel feed stream. The power plant model based on the co-firing of coal and biomass is also based on the 800 MW_e of the gross power output. The power plant characteristics for the co-firing coal with biomass are similar to those for the standalone coal or biomass fired power plants.

Table 8.3 Pulverised supercritical Co-firing of coal and biomass cases classification*.

Cases	Coal/Biomass percentage in fuel feed stream
Coal	100/0
C80/B20	80/20
C60/B40	60/40
C40/B60	40/60
C20/B80	20/80
Biomass	0/100

*where ‘C’ represents coal and ‘B’ represents biomass.

Table 8.4 Summary of the input specifications for solid fuel fired power plant.

Parameters	Value
Gross power output [MW_e]	800
Boiler efficiency [%]	88
Turbine thermal input [MW_{th}]	1705
Fabric filter efficiency [%]	99.8
SCR unit efficiency [%]	86
FGD unit efficiency [%]	98
Percent excess air [%]	15
Primary to secondary air split	0.235/0.765
Infiltration air to that of the total air [%]	2
Flue gas temperature at ESP inlet [^oC]	169

8.3 Modelling Strategy

The modelling of natural gas and solid fuel fired power plants are realized using the Aspen Plus process modelling software. The NGCC with and without EGR models are based on the modelling details as explored in Section 7.2.2. The NGCC power plant model validation with and without EGR can be found in Section 7.3.1. The input specifications for the H frame gas turbine and steam turbine section of the

NGCC model with and without EGR are given in Table 8.1. The EGR percentage applied is 35 %.

For solid fuel fired subcritical and supercritical power plants, the models developed by Agbonghae [262] are used and from which more information can be referred. The theoretical air, excess air, air leakages and infiltration air for the constant boiler efficiency of 88 % are calculated based on recommendations found in the literature [264-266]. The properties of the coal and biomass used are given in Table 8.2. The ammonia required in the SCR unit is estimated based on the principal reactions given in Section 8.2.2.1, which shows that ammonia required will be theoretically equal to the number of the moles of NO_x present in the flue gas at the economiser outlet while keeping 2 ppmv of the ammonia slip into account. The limestone, O_2 and make-up water required in the FGD unit are estimated based on the principal reactions mentioned in Section 8.2.2.3. The assumptions made during the process modelling of the different parts of the solid fuel fired power plant, including the boiler, SCR, FGD, and steam cycle section can be found in the quality guidelines for energy process system studies provided by the US Department of Energy [265, 266]. However, a summary of the input specifications irrespective of the solid fuel fired power plant type can be found in Table 8.4.

Table 8.5 Optimal design data for an amine-based CO_2 capture plant [159, 262].

Parameter	Value
Flue Gas Flowrate (kg/s)	821.26
Optimum Lean CO_2 loading (mol/mol)	0.2
Optimum Liquid/Gas Ratio (kg/kg)	2.93
Absorber	
Number of Absorbers	2
Absorber Packing	Mellapak 250Y
Diameter (m)	16.13
Optimum Height (m)	23.04
Stripper	
Number of Stripper	1
Packing	Mellapak 250Y
Diameter (m)	14.61
Optimum Height (m)	25.62
Specific Reboiler Duty (MJ/kg CO_2)	3.69

The MEA-based CO_2 capture plant model is based on second generation, rigorous rate based models. The process details of the CO_2 capture plant can be found in Sections 6.1 and 8.2.2.4. The model has been extensively validated against the experimental data as reported in Sections 6.4 and 6.5. The design and/or scale-up of the model to the commercial-scale amine-based CO_2 capture plant model are explored in Sections 7.2.3 and 7.4 which are based on the optimization of both process and economic parameters. The input specification for the amine-based CO_2 capture plant can be found in Table 7.2. However, the design data applied for the commercial-scale amine-based CO_2 capture plant used in this study is given in Table 8.5 and it is based on the optimal design data reported by Agbonghae et al. [159, 262] for the commercial-scale coal fired power plant.

The CO_2 compression system modelled is a multiple-stage compression system with inter-stage coolers and knock out drums with the total stages being 6. The final CO_2 compression pressure is set at 153 bar. The CO_2 compression system data for the inter-stage pressure is given in Table 8.6. The CO_2 compression system is modelled based on the assumptions mentioned by the quality guidelines for energy process system studies provided by the US Department of Energy [265, 266]. The CO_2 stream cooling temperature is set at 30 ^{o}C and at the third-stage the CO_2 stream is dried with a tetra ethylene glycol (TEG) unit with a H_2O specification in the CO_2 stream specified at 20 ppmv [262]. The pressure drop of 2 % is specified in the knock-out drums of the CO_2 compression system [265, 266].

Table 8.6 CO_2 compression unit data [263].

Stage	Outlet Pressure (bar)
1	3.6
2	7.8
3	17.1
4	37.6
5	82.7
6	153.0

8.4 Results and Discussion

In the following sections, the comparative potential of the different power plant cases as explored in Section 8.2 are discussed. The each power plant case is integrated with CO_2 capture and compression section. The gross power output is

kept constant at 800 MW_e in order to provide a meaningful comparison of the all the integrated cases of the power plant with CO_2 capture and compression.

8.4.1 NGCC with and Without EGR Results

The NGCC power plants with and without EGR integrated with the CO_2 capture and CO_2 compression units, and the key performance results are shown in Table 8.7. The model is developed based on the model parameters indicated in Tables 8.1, 8.5 and 8.6. Further, during application of the EGR to the NGCC power plant, the steam cycle configuration and parameters are kept the same. The effect of the application of the EGR on the performance of the NGCC is clear through the results in Table 8.7. The EGR application results in 35 % decrease in air and flue gas flow rate. The EGR percentage of 35 % is selected based on the recommendation made by the 2013 Report of US Department of Energy [211].

Table 8.7 Summary of the key performance results for the NGCC with and without EGR integrated to CO_2 capture and CO_2 compression units.

Case	NGCC	NGCC with EGR
Natural gas [kg/s]	29.2	29.5
Air [kg/s]	1177.1	771.1
EGR percentage [%]	0	35
Recirculated gas [kg/s]	-	398.8
Main steam [kg/s | bar | ^oC]	135 | 166.5 | 566	135 | 166.5 | 566
Reheat from furnace/boiler [kg/s | bar | ^oC]	98.5 | 24.8 | 566	98.5 | 24.8 | 566
Steam to stripper reboiler [kg/s | bar | ^oC]	110 | 5.2 | 338	108 | 5.2 | 338
Flue Gas Composition		
CO_2 [mol%]	4.16	6.53
H_2O [mol%]	8.90	9.22
N_2 [mol%]	74.23	75.76
O_2 [mol%]	11.83	7.59
Ar [mol%]	0.88	0.90
CO_2 Capture Plant	NGCC	NGCC with EGR
Flue gas, absorber inlet [kg/s]	1206.3	779.6
Lean MEA solution, absorber inlet [kg/s]	1193.8	1166.6
Rich CO_2 loading [mol/mol]	0.476	0.478
CO_2 captured [kg/s]	69.95	70.50
Specific reboiler duty [MJ/kg CO_2]	3.933	3.841
CO_2 Compression System	NGCC	NGCC with EGR
Total compression duty [MW_e]	20.76	20.94
Total intercooling duty [MW_{th}]	35.50	35.81

The EGR results in 1 % increase in the fuel flow requirements which are due to the varying properties of the working fluid owing to the EGR as explored in Section 4.4.1. Further the EGR results in a 57 % increase in the CO_2 molar composition in the exhaust gas. The increased CO_2 composition in the flue gas with its reduced flow rate, results in less solvent requirements, lower specific reboiler duty for the CO_2 capture plant. The solvent flow rate and specific reboiler duty decrease by 2.3 % in comparison to the values obtained when there is no EGR. However, the amount of the CO_2 captured increases, which results in more CO_2 compression work as shown in Table 8.7. Detailed key performance results of the NGCC with and without EGR power plants integrated with CO_2 capture and CO_2 compression systems are shown in Table D.1 of Appendix D.

Table 8.8 Summary of the energy performance results for the NGCC with and without EGR integrated to CO_2 capture and CO_2 compression units.

Case	NGCC	NGCC with EGR
Fuel heat input, HHV [MW_{th}]	1528	1543
Total power, without steam extraction [MW_e]	800	800
Gas turbine power, with steam extraction [MW_e]	551	550
Steam turbine power, with steam extraction [MW_e]	163	160
Total power, with steam extraction [MW_e]	714	665
Power output without CO_2 capture and compression [MW_e]	785	782
Power output with CO_2 capture only [MW_e]	670	672
Power output with CO_2 capture and compression [MW_e]	650	651
Efficiency without CO_2 capture and compression [%]	51.40	50.60
Efficiency with CO_2 capture only [%]	43.89	43.50
Efficiency with CO_2 capture and compression [%]	42.53	42.15
Efficiency penalty with CO_2 capture only [%]	7.5	7.1
Efficiency penalty with CO_2 capture and compression [%]	8.9	8.5
Specific CO_2 emissions from power plant [g/kWh]	431	435
Specific CO_2 compression work [MJ/kg]	0.2968	0.2970
Specific losses per unit of CO_2 captured [%/kgs^{-1}]	0.11	0.10

The summary of the energy performance of the NGCC with and without EGR power plants integrated with CO_2 capture and CO_2 compression is shown in Table 8.8. Specific CO_2 compression work per unit of the CO_2 captured increases as the amount of the CO_2 captured also increases. It is evident that the net efficiency of the NGCC with EGR without CO_2 capture and compression systems decreases in comparison to the NGCC without EGR. This decrease is due to higher fuel flow rate requirements. Similarly, the net efficiency of the NGCC with an EGR power plant

with CO_2 capture only and net efficiency of the NGCC with an EGR power plant with CO_2 capture and compression also decreases. However, the efficiency penalty of the NGCC with EGR is less in comparison to the NGCC without EGR due to the increased specific CO_2 emissions from the NGCC with an EGR power plant. Similarly, the specific efficiency losses per unit of the CO_2 captured decreases as more CO_2 is captured. This decrease is 9 % of the specific efficiency losses per unit of the CO_2 captured obtained through the NGCC power plant without EGR. Detailed energy performance results in the NGCC with and without EGR power plants integrated with CO_2 capture and CO_2 compression system are shown in Table D. 2 of Appendix D.

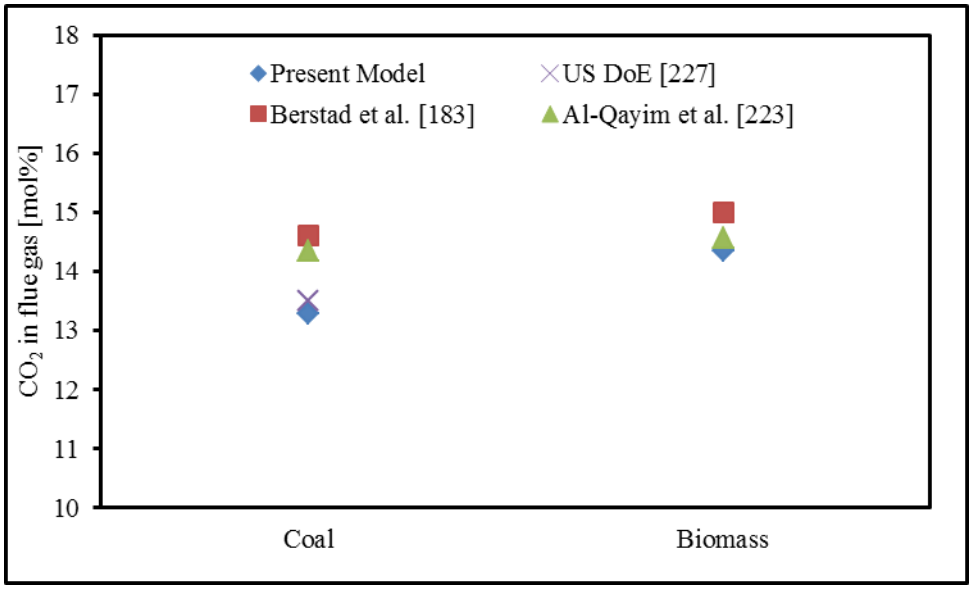

Figure 8.2 Comparison of molar composition of CO_2 in the flue gas of pulverised supercritical coal and biomass fired power plant with a constant heat input model with literature reported values.

8.4.2 Solid Fuel Power Plant Results

The pulverised fuel subcritical and supercritical power plants are modelled for both coal and biomass firing based on the details provided in Sections 8.2 and 8.3. Both constant heat input and constant fuel flow rate cases are considered for supercritical and subcritical systems as discussed in Section 8.2.3. Further, the addition of the CO_2 capture and CO_2 compression to each model is also considered. The properties of the coal and biomass fired are given in Table 8.2 and a summary of the input specifications for the power plants is given in Table 8.1. The gross power output for each of the power plant models is set at 800 MW_e in order to have a meaningful comparison.

Table 8.9 Summary of the key performance results for the pulverised coal and biomass fired subcritical and supercritical power plants integrated with CO_2 capture and CO_2 compression systems with constant heat input and constant fuel flow rate cases.

	Supercritical			Subcritical		
Case	Constant heat input	Constant heat Input	Constant fuel flow rate	Constant heat input	Constant heat input	Constant fuel flow rate
Fuel type	Coal	Biomass	Biomass	Coal	Biomass	Biomass
Coal [kg/s]	71.3	99.6	71.3	74.1	108.7	74.1
Total air [kg/s]	729	702	502	774	768	522
NH_3 injected [kg/s]	1.7	1.1	0.8	1.9	1.3	0.9
Slag + Fly Ash [kg/s]	6.9	0.7	0.5	6.2	0.8	0.5
Main steam [kg/s | bar | ^oC]	630 |242.3 |593	630 |242.3 |593	452 |242.3 |593	641 |166.5 |566	641 |166.5 | 566	419|166.5 | 566
Reheat from furnace/boiler [kg/s | bar | ^oC]	514 |45.2 |593	514 |45.2 |585	367 |45.2 |593	606 |39 |566	606 |39 |566	394 |39 |566
Steam to stripper reboiler [kg/s | bar | ^oC]	223 |5.07 |296	230 |5.07 |296	163 |5.07 |296	243 |5.07 |294	241 |5.07 |294	172 |5.07 |293
Gypsum, moisture-free [kg/s]	9.6	0.1	0.1	10.0	0.1	0.1
Flue Gas Composition						
CO_2 [mol%]	13.28	14.35	14.35	13.58	14.37	14.36
H_2O [mol%]	15.48	14.17	14.18	15.47	13.71	14.2
N_2 [mol%]	68.05	68.28	68.28	68.04	68.66	68.28
O_2 [mol%]	2.37	2.38	2.37	2.10	2.45	2.35
Ar [mol%]	0.81	0.81	0.81	0.81	0.82	0.81
CO_2 Capture Plant						
Flue gas, absorber inlet [kg/s]	832	803	574	884	876	597
Lean MEA solution, absorber inlet	2403	2470	1743	2605	2694	1816

[kg/s]						
Rich CO_2 loading [mol/mol]	0.479	0.480	0.480	0.479	0.480	0.480
CO_2 captured [kg/s]	152.0	157.1	112.1	164.9	170.9	116.7
Specific reboiler duty [MJ/kg CO_2]	3.686	3.673	3.634	3.685	3.683	3.638
CO_2 Compression System						
Total compression duty [MW_e]	44.90	46.46	33.18	48.75	50.52	34.53
Total intercooling duty [MW_{th}]	76.90	79.64	56.83	83.58	86.61	59.14

Table 8.10 Summary of the energy performance results for the pulverised coal and biomass fired subcritical and supercritical power plants integrated with CO_2 capture and CO_2 compression systems with constant heat input and constant fuel flow rate cases.

	Supercritical			Subcritical		
Case	Constant heat input	Constant heat input	Constant fuel flow rate	Constant heat input	Constant heat input	Constant fuel flow rate
Fuel type	Coal	Biomass	Biomass	Coal	Biomass	Biomass
Fuel heat input, HHV [MW_{th}]	1933	1933	1384	2010	2010	1371
Steam turbine power, without steam extraction [MW_e]	800	800	574	800	800	548
Steam turbine power, with steam extraction [MW_e]	664	656	473	664	658	410
Power output without CO_2 capture and compression [MW_e]	758	758	536	757	757	510
Power output with CO_2 capture only [MW_e]	602	596	421	601	595	396
Power output with CO_2 capture and compression [MW_e]	557	549	388	556	544	361
Efficiency without CO_2 capture and compression [%]	39.22	39.30	38.70	37.67	37.67	37.20
Efficiency with CO_2 capture only [%]	31.16	30.82	30.40	29.91	29.59	28.87
Efficiency with CO_2 capture and compression [%]	28.84	28.41	28.01	27.67	27.08	26.35
Efficiency penalty with CO_2 capture only [%]	8.1	8.5	8.3	7.8	8.1	8.3
Efficiency penalty with CO_2 capture and compression [%]	10.4	10.9	10.9	10.0	10.6	10.7
Specific CO_2 emissions from power plant [g/kWh]	1092	1142	1293	1138	1258	1158
Specific CO_2 compression work [MJ/kg]	0.2954	0.2957	0.2959	0.2956	0.2956	0.2960
Specific losses per unit of CO_2 captured [$\%/kgs^{-1}$]	0.053	0.054	0.071	0.047	0.047	0.074
Electricity output penalty [kWh/tCO_2]	257	262	228	247	237	272

The key performance results for standalone coal and biomass fired subcritical and supercritical power plants integrated with CO_2 capture and compression system with constant heat input and constant fuel flow rate cases are reported in Table 8.9. The energy performance results for standalone coal and biomass fired subcritical and supercritical power plants integrated with CO_2 capture and compression systems with constant heat input and constant fuel flow rate cases are reported in Table 8.10.

8.4.2.1 Constant Heat Input Results

Constant heat input cases are performed for both subcritical and supercritical; coal and biomass fired power plants integrated with CO_2 capture and CO_2 compression systems. A comparison of the CO_2 molar composition in the flue gas of the supercritical coal and biomass fired power plants with the literature reported [160, 241, 263] CO_2 molar composition, is presented in Figure 8.2. The comparison indicates that the CO_2 composition matches well with the literature reported [160, 241, 263] values within the permitted range of errors. Due to the lower sulphur content in the biomass, the FGD unit may not be required for the biomass-fired power plant with a CO_2 capture system and the requirement of the reduction of the SO_2 content before the CO_2 capture system can be met by a SO_2 polisher using an alkali wash. Similarly, due to the low ash content, the slag and fly ash produced by the biomass fired power plant is minimal, however, the true nature and properties of the slag and fly ash cannot be predicted by the present model. Detailed key performance results for pulverised coal and biomass fired subcritical and supercritical power plants integrated with CO_2 capture and CO_2 compression systems with constant heat input cases are given in Tables D. 3 and D. 4 of Appendix D. In addition, the flue gas composition at different locations of the pulverised coal and biomass fired subcritical and supercritical power plants integrated with CO_2 capture and CO_2 compression systems with constant heat input cases are given in Table D. 5 of Appendix D.

Due to the lower heating value of the biomass as discussed in Section 8.2.3 the fuel requirements for the subcritical and supercritical power plant cases increases by 46 and 40 %, respectively. However, due to more injection of fuel in the case of the biomass, the CO_2 composition in the flue gas also increases by approximately 6 and 8 % for the subcritical and supercritical cases, respectively, with approximately 4 % decrease in the flue gas flow rate. Further, the biomass results in more CO_2 captured

due to the increased CO_2 content in the flue gas, which results in the increased CO_2 compression auxiliary loads for both subcritical and supercritical cases. The net power output with CO_2 capture and CO_2 compression systems decrease by 3 and 1.5 % for the subcritical and supercritical cases, respectively. A similar behaviour is observed for the net efficiency for the subcritical and supercritical system and thus results in a slight increase in the efficiency penalty. Due to the higher specific CO_2 emissions from biomass fired power plants, there is a slight increase in the specific CO_2 compression work per unit of the CO_2 captured and specific losses per unit of the CO_2 captured as given in Table 8.10. Detailed energy performance results for pulverised coal and biomass fired subcritical and supercritical power plants integrated with CO_2 capture and CO_2 compression system with constant heat input cases are given in Table D. 5 of Appendix D.

8.4.2.2 Constant Fuel Flow Rate Results

Constant fuel flow rate input cases are performed for both subcritical and supercritical; coal and biomass fired power plants integrated with CO_2 capture and CO_2 compression systems. The constant flow rate cases results in substantial de-rating of the gross and net power output from the power plants both sub critical and supercritical when fuel is switched from coal to biomass. The biomass firing results in approximately 35 and 30 % de-rating of the power output in comparison to the cases for subcritical and supercritical, respectively. However, if de-rating of the power plant is adoptable to the system, there still is a substantial decrease in the net efficiency of the power plant integrated with CO_2 capture and CO_2 compression system by approximately 9 and 3 %, for subcritical and supercritical cases respectively. The efficiency penalty of the constant fuel flow rate cases is the same as that observed for constant heat input cases as the base power output considered for comparison is the de-rated power output and not 800 MW_e. Detailed key performance results for pulverised coal and biomass fired subcritical and supercritical power plants integrated with CO_2 capture and CO_2 compression systems with constant fuel flow rate cases are given in Tables D. 3 and D. 4 of Appendix D. In addition, the detailed flue gas composition at different locations of the pulverised coal and biomass fired subcritical and supercritical power plants integrated with CO_2 capture and CO_2 compression system with constant fuel flow rate cases are given in Table D. 6 of Appendix D.

The firing of the biomass results in an increase in CO_2 content by 6 and 8 % for the subcritical and supercritical cases, respectively, with approximately 31 % decrease in the flue gas flow rate. The solvent requirement to scrub the decreased flow rate flue gas also decreases by 30 and 27 % for the supercritical and subcritical cases, respectively. Due to decreased flow rate of the flue gas, the amount of the CO_2 captured also decreases. Thus results in a considerable increase in specific CO_2 compression work per unit of the CO_2 captured and specific losses per unit of the CO_2 captured. Due to the lower sulphur content in the biomass, and in addition due to the lower biomass flow rate in comparison to what is required; the FGD unit may not be required for the biomass-fired power plant with a CO_2 capture system and the requirement of the reduction of the SO_2 content before the CO_2 capture system can be met by a SO_2 polisher using an alkali wash. As a result, the amount of the by-product, gypsum decreases enormously for the constant fuel flow rate cases when the fuel is switched to biomass. Similarly, due to the low ash content, the slag and fly ash produced by the biomass fired power plant is minimal, however, the true nature and properties of the slag and fly ash cannot be predicted by the present model. Detailed energy performance results for pulverised coal and biomass fired subcritical and supercritical power plants integrated with CO_2 capture and CO_2 compression systems with constant fuel flow rate cases are given in Table D. 5 of Appendix D.

8.4.3 Co-firing Coal and Biomass Results

The pulverised fuel supercritical co-firing coal and biomass power plant models are developed based on details provided in Section 8.2.3. Further, integration of the CO_2 capture and CO_2 compression systems is also considered for each of the case studied. The classifications of the co-firing coal and biomass cases are presented in Table 8.3 based on the fraction of coal or biomass present in the fuel feed stream. The gross power output for each of the co-firing coal and biomass power plant models is set at 800 MW_e in order to have a meaningful comparison. The key performance results for supercritical co-firing coal and biomass power plants integrated with CO_2 capture and CO_2 compression systems cases are reported in Table 8.11. The energy performance results for supercritical co-firing coal and biomass power plants integrated with CO_2 capture and CO_2 compression systems cases are reported in Table 8.12. .

Table 8.11 Summary of the key performance results for the pulverised supercritical co-fired coal and biomass power plants integrated with CO_2 capture and CO_2 compression systems.

Fuel type	Coal	C80/B20	C60/B40	C40/B60	C20/B80	Biomass
Coal [kg/s]	71.3	75.6	80.4	85.9	92.3	99.6
Total air [kg/s]	729	726	723	720	712	702
NH_3 injected [kg/s]	1.7	1.6	1.5	1.4	1.3	1.1
Slag + Fly Ash [kg/s]	6.9	6.0	4.9	3.7	2.3	0.7
Main steam [kg/s | bar | ^oC]	630 |242.3 |593	630 |242.3 |593	630 |242.3 |593	630 |242.3 |593	630 |242.3 |593	630 |242.3 |593
Reheat from furnace/boiler [kg/s | bar | ^oC]	514 |45.2 |593	514 |45.2 |593	514 |45.2 |593	514 |45.2 |593	514 |45.2 |593	514 |45.2 |593
Steam to stripper reboiler [kg/s | bar | ^oC]	233 |5.07 | 296	225 |5.07 |296	226 |5.07 |296	228 |5.07 |296	230 |5.07 |296	230 |5.07 |296
Gypsum, moisture-free [kg/s]	9.6	8.2	6.5	4.7	2.6	0.1
Composition						
CO_2 [mol%]	13.28	13.42	13.56	13.73	13.93	14.35
H_2O [mol%]	15.48	15.48	15.48	15.50	15.40	14.17
N_2 [mol%]	68.05	67.94	67.80	67.64	67.53	68.28
O_2 [mol%]	2.37	2.35	2.35	2.34	2.34	2.38
Ar [mol%]	0.81	0.81	0.80	0.80	0.80	0.81
CO_2 Capture Plant						
Flue gas, absorber inlet [kg/s]	832	830	829	827	819	804
Lean MEA solution, absorber inlet [kg/s]	2403	2414	2403	2453	2464	2470
Rich CO_2 loading [mol/mol]	0.479	0.479	0.479	0.480	0.480	0.480
CO_2 captured [kg/s]	152.0	153.0	154.4	155.7	156.5	157.1
Specific reboiler duty [MJ/kg CO_2]	3.686	3.679	3.677	3.675	3.674	3.673

CO_2 Compression System						
Total compression duty [MW_e]	44.90	45.26	45.03	46.04	46.29	46.46
Total intercooling duty [MW_{th}]	76.90	77.57	77.18	78.92	79.35	79.64

Table 8.12 Summary of the energy performance results for the pulverised supercritical co-fired coal and biomass power plants integrated with CO_2 capture and CO_2 compression systems.

Fuel type	Coal	C80/B20	C60/B40	C40/B60	C20/B80	Biomass
Fuel heat input, HHV [MW_{th}]	1933	1933	1933	1933	1933	1933
Steam turbine power, without steam extraction [MW_e]	800	800	800	800	800	800
Steam turbine power, with steam extraction [MW_e]	664	662	659	658	657	656
Power output without CO_2 capture and compression [MW_e]	758	758	758	758	758	758
Power output with CO_2 capture only [MW_e]	602	600	598	597	596	596
Power output with CO_2 capture and compression [MW_e]	557	554	553	551	550	549
Efficiency without CO_2 capture and compression [%]	39.22	39.30	39.30	39.30	39.30	39.30
Efficiency with CO_2 capture only [%]	31.16	31.02	30.94	30.86	30.83	30.82
Efficiency with CO_2 capture and compression [%]	28.84	28.68	28.61	28.48	28.43	28.41
Efficiency penalty with CO_2 capture only [%]	8.1	8.3	8.4	8.4	8.5	8.5
Efficiency penalty with CO_2 capture and compression [%]	10.4	10.6	10.7	10.8	10.9	10.9
Specific CO_2 emissions from power plant [g/kWh]	1092	1106	1117	1133	1139	1142
Specific CO_2 emissions from power plant due to coal [g/kWh]	1092	885	670	453	228	0
Specific CO_2 compression work [MJ/kg]	0.2954	0.2958	0.2959	0.2957	0.2958	0.2957
Specific losses per unit of CO_2 captured [%/kgs^{-1}]	0.053	0.054	0.054	0.054	0.054	0.054

The co-firing of coal and biomass results in more fuel requirement as the fraction of the biomass in the fuel stream increases. However, the amount of the flue gas decreases and the CO_2 content in the flue gas increases, for the increased fraction of the biomass in the fuel. This also results in higher specific CO_2 emissions from power plants when the biomass share in the fuel feed stream increases; however, it results in more specific CO_2 capture from the power plant. Further, if the biomass used is sustainably-grown biomass, it will result in more negative emissions from the system. The detailed key performance results for the different cases of the co-firing of the coal and biomass can be found in Tables D. 7 and D. 8 of Appendix D. The lower flow rate of the flue gas with higher CO_2 concentration, results in the decrease of the specific reboiler duty. The effect of co-firing coal and biomass on the CO_2 composition in the flue and specific reboiler duty is given in Figure 8.3. A more detailed flue gas composition at different locations of the power plant for each co-firing case can found in Table D. 10 of Appendix D.

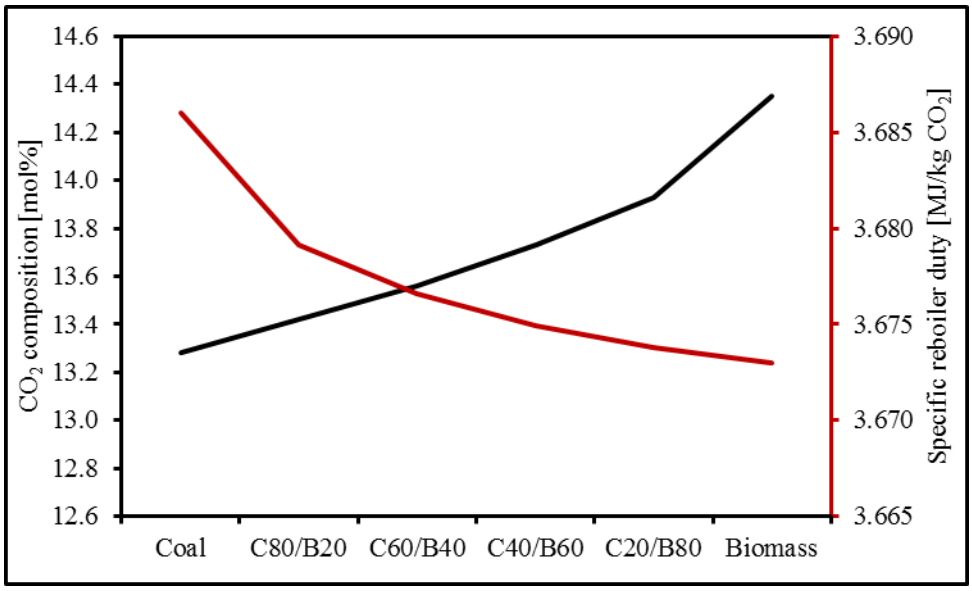

Figure 8.3 Effect of co-firing coal and biomass on the CO_2 composition in the flue gas and specific reboiler duty.

The net power output and net efficiency decreases when the biomass fraction in the feed stream increases due to a larger auxiliary load on the system. It is observed that the efficiency penalty with CO_2 capture and compression systems increases by approximately 4.8 % when coal is totally replaced by biomass. However, there is a slight increase in specific CO_2 compression work per unit of the CO_2 captured and specific losses per unit of the CO_2 captured.

The detailed energy performance results for the different cases of the co-firing of the coal and biomass can be found in Table D. 9 of Appendix D. Due to the low sulphur content in the biomass, as reported in Table 8.2, the amount of gypsum produced decreases with the increased share of biomass in the fuel feed stream. Due to this trend, the FGD unit may not be required in the standalone biomass power plant when integrated with a CO_2 capture system as discussed in Section 8.4.2. Also, the slag and fly ash amounts decrease substantially when coal is replaced by biomass.

8.5 Comparative Potential

The results and discussion presented in Section 8.4 for the different power plant cases modelled with CO_2 capture and CO_2 compression systems show that the standalone NGCC and/or NGCC with CO_2 capture and CO_2 compression system results in a higher net efficiency with the least CO_2 emissions. However, the least efficiency penalty due to the integration of the power plant with CO_2 capture and CO_2 compression systems is observed for the NGCC with an EGR power plant. This is due to the fact that for the NGCC with an EGR power plant, the auxiliary load of the CO_2 capture system decreases due to the lower flue gas flow rate. The net efficiency of different power plants modelled, along with the efficiency penalty due to integration of the CO_2 capture and CO_2 compression systems, is shown in Figure 8.4.

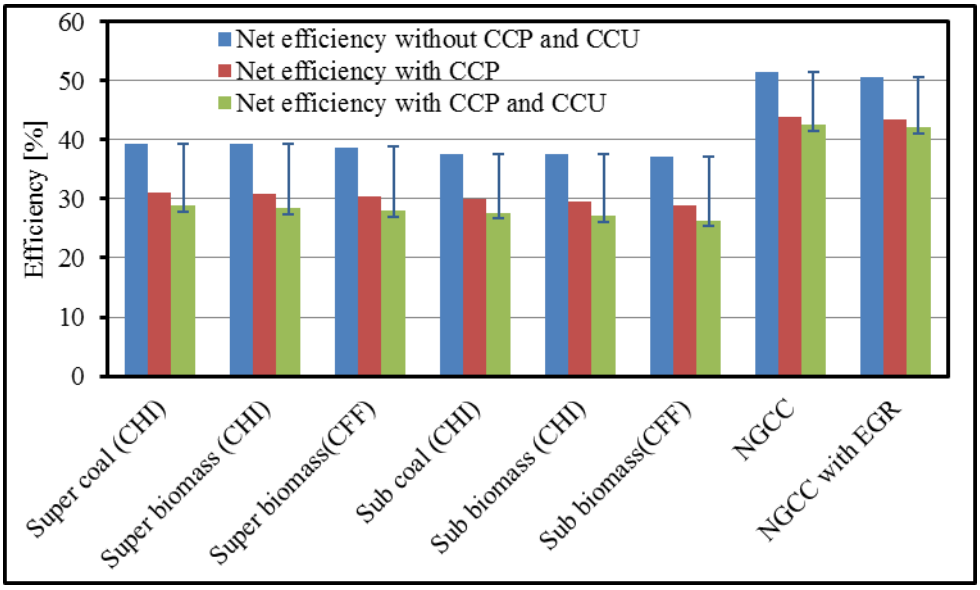

Figure 8.4 Net efficiencies and efficiency penalty of different power plant models integrated with CO_2 capture and CO_2 compression systems (where vertical bars indicate the efficiency penalty; CCP: CO_2 capture plant; CCU: CO_2 compression unit; CHI: Constant heat input; and CFF: Constant fuel flow rate).

Biomass fired power plants result in higher efficiency penalty along with higher specific CO_2 emissions from standalone biomass fired power plant. Due to higher specific CO_2 emissions, the specific CO_2 captured is also higher for the biomass fired power plants. The specific CO_2 captured for different power plant models is shown in Figure 8.5. The coal fired power plants also shown higher specific CO_2 captured in comparison to NGCC and NGCC with EGR power plants. However, if the biomass considered is sustainably-grown biomass then it will result in negative emissions which will be the benefit of using biomass. It is also interesting to note that the specific CO_2 emissions represented in Table 8.12 represents a gradual increase in content, however, the contribution of the these emissions to the greenhouse gases is decreasing. Depending on a one to one relationship, the co-firing of coal and biomass results in 80, 60, 40, 20 and 0 % CO_2 emissions from C8B2, C6B4, C4B6, C2B8 and Biomass cases. From these emissions, the 90 % of them are captured by the CO_2 capture system and hence the biomass case results in negative emissions towards the atmosphere.

Further, coal and biomass power plants show the least specific losses per unit of the CO_2 captured. The specific losses per unit of the CO_2 captured for coal and biomass fired power plants with CO_2 capture and CO_2 compression systems are approximately half in comparison to the NGCC and NGCC with EGR integrated with CO_2 capture and CO_2 compression system.

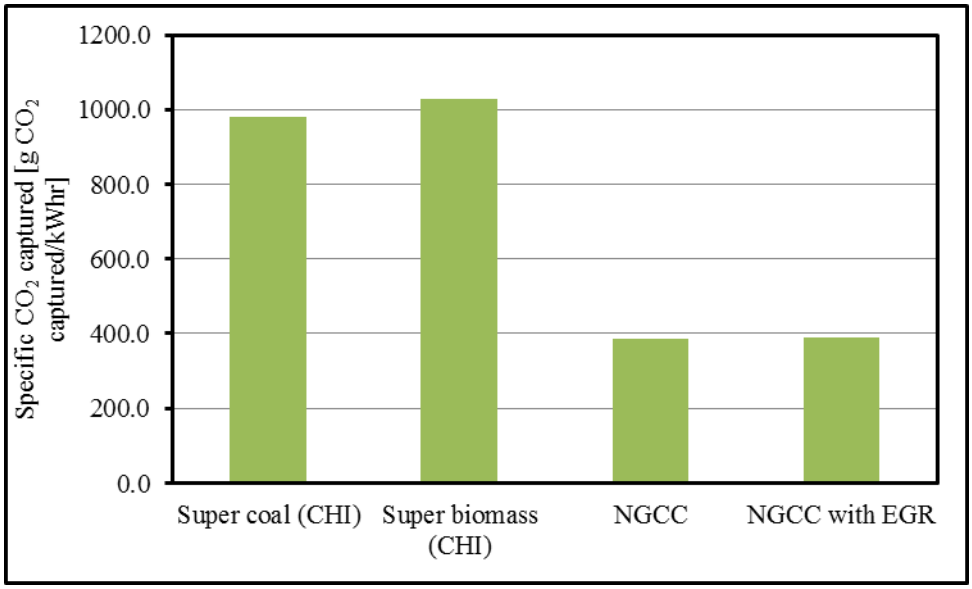

Figure 8.5 Specific CO_2 captured for different power plants through a CO_2 capture plant (where CHI is constant heat input).

The power plant cases with constant fuel flow rate results in substantial power de-rating, which makes them an unattractive option to adopt. From the specific CO_2 captured and specific losses per unit of CO_2 captured, the coal and biomass fired power plant with CCS is the most favourable options provided the changes required in the power plant due to fuel switch to standalone biomass and/or co-firing of coal and biomass are ready to be adopted. However, in the present scenario of the gas-CCS interest, NGCC with EGR coupled to CO_2 capture and CO_2 compression systems will be an attractive option to adopt due to the lower efficiency penalty.

8.6 Challenges of CO_2 Capture from Biomass

It is important to mention here that both coal and biomass contains light metals and inorganic ions in their flue gas which will affect the operation and performance on the CO_2 capture system. The degradation, corrosion and stability of the MEA will be strongly affected by the presence of these light metals and inorganic ions in the flue gas. The white wood pellet biomass considered in this research work contains about 0.3, 2.2, 2.6, 0.7, 0.6 and 10.2 ppm of Ar, Cr, Cu, Pb, V and Zn, respectively in it. The lack of the underpinning knowledge in the open literature can be judged by the tittle of the one of the research publication, "*Do we underestimate the impact of particles ... on amine-based CO_2 capture processes?*" by Schallert et al. [268]. These light metals and inorganic ions will affect the performance of the MEA in terms of the pH, and CO_2 loadings. In addition, there deposits on the surface and especially on the reboiler will affect the performance at large. However, these issues are beyond the scope of the research presented in this chapter.

8.7 Conclusions

- The comparative potential of the different power plants integrated to a MEA-based CO_2 capture system and CO_2 compression system for natural gas firing with and without EGR, subcritical coal and biomass firing, supercritical coal and biomass firing and supercritical co-firing of coal and biomass firing, were analysed. Furthermore, for solid fuel fired power plant constant heat input cases and constant fuel flow rate cases were investigated. For consistency, the gross power output was maintained at 800 MW_e for each of the cases modelled and simulated.

- The biomass firing results in about 40 % and 46 % increase in fuel flow rate in comparison to the coal firing for the super- and sub- critical system, respectively for the constant heat input case.
- The biomass firing results in about 30 % and 35 % derating of the power output in comparison to coal firing, for the super- and sub- critical systems, respectively, for the constant fuel flow rate case.
- The biomass firing results in about 4 % decrease in the exhaust gas flow rate in comparison to the coal firing for the constant heat input case and about 31 % decrease in the exhaust gas flow rate in comparison to the coal firing for the constant fuel flow rate case.
- The CO_2 concentration in the exhaust gas increases by 8 % and 6 % for the super- and sub- critical, respectively, for the biomass firing in comparison to the coal firing for both the constant heat input and fuel flow rates.
- A similar trend is observed in the case of the co-firing of the coal and biomass fired power plant, which results in decreased specific reboiler duty due to the increased CO_2 content and reduced flue gas flow rate, when the biomass portion in the fuel is increased.
- The FGD unit may not be required since the sulphur content in the biomass is less and the limitation of removing the SO_2 to the required level can be simply achieved by the SO_2 polisher present in the CO_2 capture plant.
- Similarly, it is observed that for the biomass firing, the ash handling requirements will be less.
- Solid fuel fired power plants with a constant fuel flow rate results in substantial power output de-rating in the case of a switch from coal to biomass due to the lower heating value of the biomass fuel.
- NGCC and NGCC with EGR integrated with CO_2 capture and CO_2 compression system shows higher net efficiency and the least efficiency penalty reduction in comparison to the coal and biomass fired power plants integrated with CO_2 capture and CO_2 compression system.
- Coal and biomass fired power plants when integrated with CO_2 capture and CO_2 compression system, results in higher specific CO_2 capture and least specific losses per unit of the CO_2 captured in comparison to the NGCC with and without EGR integrated with CO_2 capture and CO_2 compression system.

- A standalone biomass power plant integrated with CO_2 capture and CO_2 compression system will result in negative emissions if biomass is sustainably-grown.

Chapter 9
Conclusions and Future Recommendations

This chapter summarizes the conclusions of the research work presented in this thesis and recommendations are presented for possible future research work.

In this thesis, a process system analysis of the pilot-scale and commercial-scale natural gas fired system with CO_2 capture is investigated. The modelling, simulation and optimization of the process under investigation has been performed through the Aspen software. Further, the modifications of the existing system by the application of the exhaust gas recirculation has been analysed and optimised for both pilot-scale and commercial-scale applications.

The pilot-scale system explored was a micro gas turbine of 100 kW_e integrated to an amine-based pilot-scale CO_2 capture plant capable of capturing 1 ton per day of CO_2 based on MEA. The process models of both the MGT and pilot-scale CO_2 capture plants are validated against an extensive set of experimental data. Further, a sensitivity analysis of each of the systems is performed to judge the behaviour of the system at variable operating conditions and to develop the optimum operating range for the system. The optimized EGR is applied to the MGT to assess the performance of the system for varying EGR percentages and its impact on the behaviour of the pilot-scale CO_2 capture plant. In addition, the pure CO_2 is injected to simulate the EGR system at different part load conditions and validated against extensive experimental data. Furthermore, the additional modifications, such as steam injection, simultaneous steam and CO_2 injection, and humidification of the compressed air, were analysed to check their impact on the MGT performance.

At a commercial-scale level, the NGCC power plant at gross power output 650 MW_e is modelled and simulated based on the 2013 Report of the US Department of Energy [211]. The gas turbine considered is the F-Frame gas turbine and MEA-based CO_2 capture plant is integrated with the steam turbine section at three levels,

including the flue gas to the absorber column; the steam tapping from IP-LP steam turbine cross-over for the reboiler; and the condensate return from the reboiler to the deaerator of the steam turbine section. The techno-economic process design and/or scale up of the commercial-scale MEA-based CO_2 capture plant has been obtained for coupling to the commercial-scale NGCC power plant operated with 0, 15, 35 and 50 % EGR percentage.

Finally, a comparative potential is assessed for natural gas, coal and biomass fired power plants integrated to MEA-based CO_2 capture plant and CO_2 compression system.

A summary of the overall conclusions and recommendations for the research work presented in this thesis is presented in Sections 9.1 and 9.2, respectively, and the detailed conclusions and recommendations for the research work presented from Chapters 3 to 8 is presented along with some possible future recommendations for each chapter from Section 9.4 and onward.

9.1 Overall Conclusions

The process system analysis leads to the firm understanding of the power generation system with CO_2 capture, both at pilot- and commercial- scale. The process modelling resulted in developing possible modifications to the present natural gas fired gas turbine which results in the reduction of the specific reboiler duty of the PCC technology and lower energy penalty on integration with PCC plant and CO_2 compression systems.

The process model developed for the MGT is extensively validated against experimental data for the base case, varying CO_2 injection rates, varying steam injection rates, and varying simultaneous CO_2 and steam injection rates at different part load conditions, with mean percent absolute deviations for selected parameters within the acceptable range. The validated models were extended to study the behaviour of EGR, auto generated steam and humidification of the compressed air on the performance of the MGT. Furthermore, it is observed that the gas-CCS with EGR results in the least penalty on integration with the CO_2 capture and CO_2 compression system in comparison to the gas-CCS without EGR, coal and biomass fired power plants. However, coal and biomass fired power plants integrated with

CO_2 capture and CO_2 compression system results in maximum specific CO_2 capture and biomass in addition this result in negative emissions if biomass is sustainably-grown.

A summary of the overall conclusions for the research work presented in this thesis is presented below:

- The MGT model is developed in Aspen for the MGT available at the UKCCS research center PACT facility located in Sheffield, UK. Two base case models are developed for the power output of 100 kW_e as the results obtained are compared with the manufacturer's available data. The detailed model with less discrepancies is chosen for further analysis as it reduces the input boundary conditions for the model specification. Further, the model is tuned and validated against the extensive set of part load experimental data and the model predicted results are in good agreement with the reported PACT MGT data. The maximum percent absolute deviation observed between the experientially reported and model predicted results is 3.54 %.
- Further, the sensitivity analysis of the MGT model is performed for ambient conditions, including ambient temperature, ambient pressure and ambient humidity; also for recuperator effectiveness and fuel type. The sensitivity analysis shows the deviation of the model from the base case model results for the variation of the boundary conditions and results in the model robustness.
- The effect of the CO_2 enrichment on the performance of the MGT is analysed along with its impact on the performance of the pilot-scale CO_2 capture plant. This results in the synthetic EGR to the MGT at maximum EGR percentage of 288 % with the CO_2 concentration increasing to 5.04 mol% from 1.48 mol% at 50 kW_e. The higher EGR percentage is due to the fact that the MGT combustion is lean with higher excess air as compared to the commercial-scale gas turbines.
- Further, the validated MGT model is adopted for EGR application and these results in an increase in the CO_2 concentration to 3.5 mol% at EGR percentage of 55 % in comparison to 1.6 mol% without EGR. The thermodynamic analysis and potential comparison of some of the thermodynamic properties of the fluid at different locations of the MGT with

EGR assists in better understanding of the process details of the system under comparison.

- The detailed process analysis of the MGT-EGR for estimation of the best location and condition of the EGR results in an accurate demonstration of the optimized micro gas turbine configuration with EGR mode
- Steam injection and humid air turbine results in an electrical efficiency increase of 7.3 % and 6.3 %, respectively, and CO_2 enhancement by 1.2 and 1.1 times the CO_2 concentration in the MGT base case, respectively, which will be useful when integrated with a CO_2 capture system. However, the CO_2 enhancement is much less as compared to the CO_2 increase predicted due to the CO_2 injection and/or through the MGT-EGR model presented in Chapter 4.
- Due to the higher total efficiency, the EGR cycle is superior to the other two cycles, especially for the integration with a CO_2 capture system as a result of CO_2 enrichment. However, at a distributive level of power generation, where the sole purpose is to have the highest electrical power output, the STIG and HAT cycles will be the preferred choices due to the higher electrical efficiency. Therefore, in spite of the technical challenges, the innovative cycles show that the potential to improve the performance in terms of either efficiency or CO_2 capture readiness due to CO_2 enrichment. There is a trade-off between CO_2 enhancement and an increase in electrical efficiency and the choice of the MGT cycle adopted should depend on the implemented criteria.
- The pilot-scale amine-based CO_2 capture plant model is developed using a rate based calculation approach. The developed model is validated against two sets of the experimental data. The Laboratory of Engineering Thermodynamic, Kaiserslautern, Germany pilot-plant experimental data is extensive consisting of total 47 experiments covering a number of operating parameters. The UKCCS PACT, UK pilot-plant experimental data is based on a CO_2 enhanced flue gas to evaluate the process performance.
- Higher is the CO_2 concentration, the lower will be the specific reboiler duty. It is observed that the L/G ratio, lean solvent loading and solvent strength have strong impact on the specific reboiler duty. While the flue gas

temperature, liquid solvent temperature and stripper pressure effect on the specific reboiler duty is not significant.

- The carbon capture from the existing or new natural gas-fired power plants help to reduce the greenhouse gases by minor variation to the present cycle in the form of EGR, which results in fewer penalties in terms of the energy consumption and the cost incurred in comparison to a natural gas-fired power plant without EGR. The wide adoption of carbon capture, especially for fossil-fuelled power plants, will result in a better energy mix for the future low carbon economy.
- Instead of employing a process design analysis alone, a combined process economic analysis is an essential requirement for reaching the optimum design variables for a commercial-scale amine-based CO_2 capture plant. The optimum design results for the commercial-scale amine-based CO_2 capture plant are reported for a commercial-scale NGCC without EGR for a gross power output of 650 MW_e. This resulted in the optimum design and operational parameters for the commercial-scale amine-based CO_2 capture plant which can be integrated with NGCC without EGR and NGCC with EGR at 20, 35 and 50 % EGR percentages.
- The application of the EGR to the NGCC power plant integrated to CO_2 capture and CO_2 compression systems results in 5 and 9 % less efficiency penalty and specific losses per unit of the CO_2 captured.
- In the case of pulverised solid fuel fired power plants, the switching of fuel from coal to biomass either results in the de-rating of the power plant if the fuel flow rate is not changed or results in higher fuel feeding requirements to reach the required power output requirements.
- However, due to the lower flue gas flow rate, and higher CO_2 concentration in the case of the biomass fired power plants with CO_2 capture and CO_2 compression systems, results in higher specific CO_2 captured in comparison to the other cases reported. Further, the biomass firing may also result in fewer emission control technologies requirements in comparison to coal firing.
- In conclusion, the coal and biomass fired power plants with CCS will be a more reliable option to control and tackle the worsening effect of CO_2 emissions. However, in the present interest of gas-CCS, the NGCC with

EGR will be an attractive option to consider. In a nut shell, the next chapter presents the conclusions drawn by the research work carried out in this thesis and also suggests recommendations for future research work.

9.2 Overall Recommendations

A list of possible future recommendations for the research work presented from Chapter 3 to 8 are:

- The sensitivity analysis should be extended to further analyse the effect of the relative humidity at the ambient temperatures other than 15 ^{o}C. As at higher ambient temperatures, the saturation limit of the air will vary and it will carry more water in it and it is expected it will result in a severe drop in the electrical efficiency of the MGT.
- The combined sensitivity analysis effect of the ambient conditions, including ambient temperature, ambient pressure and relative humidity for MGT should be accessed to develop the optimized operating regime by simultaneously varying these parameters. It should also be extended to different alterations of MGT, including MGT-EGR, MGT, STIG and MGT-HAT.
- The robustness of the developed model should be enhanced by including the combustion kinetics in the combustor unit of the MGT model and its various alterations. Further, the combustor of the MGT can be linked with CFD for combustion kinetics to have advanced co- CFD-process model of the MGT.
- The dynamic behaviour of the MGT and its various alterations should be assessed for different part-load conditions to account the start-up and shut-down scenarios. Further, an alternative control strategy should be investigated for the MGT other than the default control strategy to better analyse the impact on the pilot-scale CO_2 capture plant at different part load conditions.
- Selective EGR by the application of the membrane should be analysed. Further, the selective EGR in series and in parallel and their impact on the pilot-scale CO_2 capture plant should also be investigated. The minimum oxygen concentration at combustor inlet and maximum achievable CO_2 concentration in the flue gas for selective EGR should be estimated.

- The other novel cycles including chemical recuperation, fuel cell and renewable integration as mentioned in Section 2.1.3 should also be investigated and their performance should be analysed with the base case cycle.
- A rigorous rate-based process model should be developed for other potential solvents and/or a blend of MEA with other solvents to analyse the performance of the other solvents and compared them with the baseline MEA solvent model performance.
- The impact of the different types of the column packing using rigorous process model should also be analysed to optimize the type of the packing for the particular solvent.
- The dynamic model of the pilot-scale CO_2 capture plant should be developed to analyse the start-up and shut down scenarios of the pilot-scale CO_2 capture plant which will be helpful for the commercial-scale application. Further, an optimized control strategy can be investigated using the dynamic model developed.
- The techno-economic analysis strategy adopted in this thesis should also be adopted for the design and/or scale-up of the commercial-scale CO_2 capture plants integrated with coal and biomass fired power plants and/or operated with different solvents and/or blends of different solvents; various types of column packings; and different configurations of the CO_2 capture system.
- A techno-economic of the NGCC power plant should also be considered to analyse the effect of the EGR on the cost of the gas turbine section of the power plant. Further, the impact of the steam tapping from the steam section of the power plant on the cost of the whole system when it is integrated with the commercial-scale CO_2 capture plant.
- Furthermore, the CO_2 compression system and its cost analysis should also be considered to have a bigger picture in terms of the power plant performance integrated to CO_2 capture and CO_2 compression system.
- The constant fuel flow rate co-firing of the coal and biomass should also be performed to better investigate the comparative potential of the each system.
- The economic or cost parameters should also be included for comparing the merits and demerits of each system to better comprehend the optimum system for commercial-scale application.

- The comparative potential of the aforementioned power plants integrated with a CO_2 capture and CO_2 compression system should also be investigated at the part load conditions of the power plant to assess the impact of the integration of the power plant with national grid for variable demand.
- The CFD can be linked with different sections of the power plants, including the combustor/burners, HRSG, super-heater, re-heater, economiser, and CO_2 capture plant columns to develop a robust model of the whole system.
- The pre-combustion CO_2 capture system and oxy-combustion CO_2 capture system along with PCC system at some rational basis should also be investigated to compare the potential of the each CO_2 capture technology.

Appendix A
Data for Chapters 3, 4 and 5

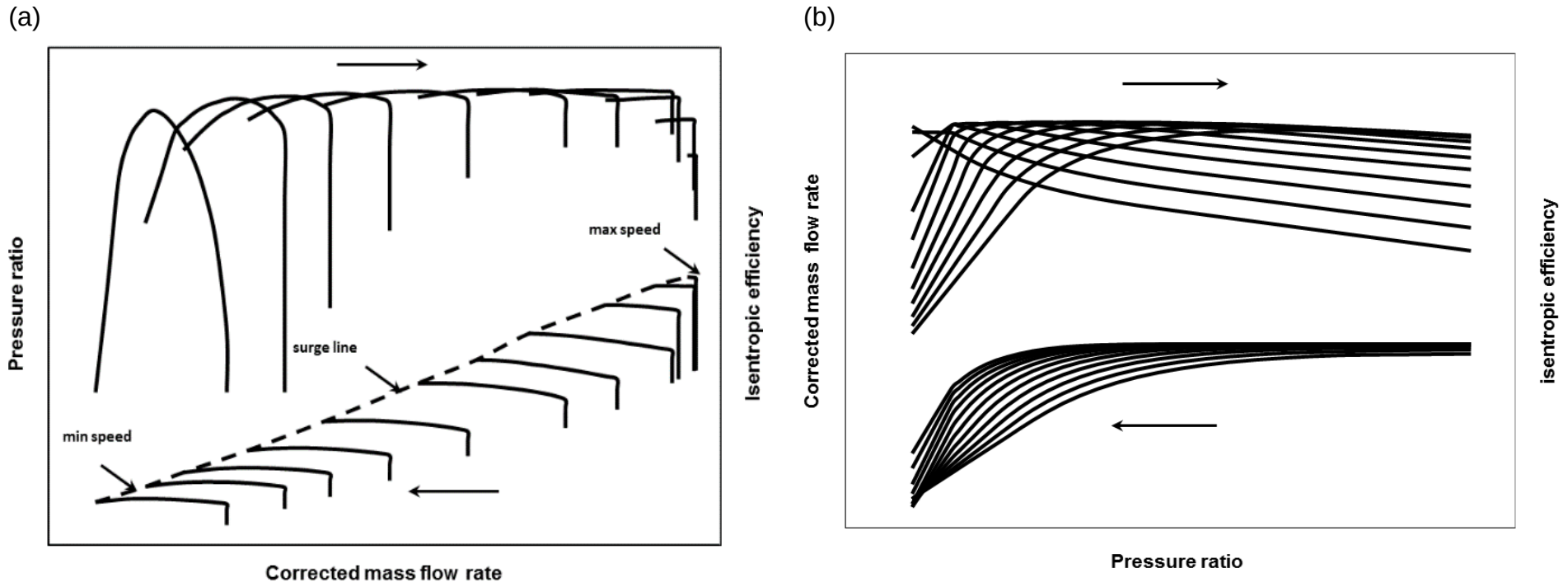

Figure A. 1 Performance maps for micro gas turbine series 2 (a) Performance maps for compressor, and (b) performance maps for expander [110].

A1.1Effect of Change in Fluid Properties on Characteristic Maps [186]

The classical dimensionless parameter groups are used to predict the behaviour of the compressor and turbine with a change in working fluid properties, according to the equations below, which have been derived for the compressor.

$$\dot{m}_{in,cr\ map} = \frac{\dot{m}_{in} \cdot \sqrt{\frac{T_{in}}{T_{in_{ref}}}}}{\frac{P}{P_{ref}} \cdot \sqrt{\frac{\gamma}{\gamma_{air}} \cdot \frac{R_{air}}{R}}} \quad \text{(A.1)}$$

$$N_{map} = \frac{N}{\sqrt{\gamma \cdot T_{in} \cdot R}} \cdot \sqrt{\gamma_{air} \cdot T_{in_{ref}} \cdot R_{air}} \quad \text{(A.2)}$$

$$PR_{map} = \frac{1}{PR_{ref}} \left[\frac{\left((PR)^{\frac{\gamma-1}{\gamma}} - 1 \right)}{\frac{\gamma - 1}{\gamma_{air} - 1}} + 1 \right]^{\gamma_{air}/(\gamma_{air}-1)} \quad \text{(A.3)}$$

Table A. 1 Measured and simulated results for parameters such as compressor discharge temperature, compressor discharge pressure, turbine inlet temperature and flue gas temperature as a function of power output for MGT for base line performance of the MGT.

Power output [kW_e]		Compressor discharge temperature [^oC]		Compressor discharge pressure [bar]		Turbine inlet temperature [^oC]		Flue gas temperature [^oC]	
Exp.	Sim.	Exp.	Sim.	Exp.	Sim.	Exp.	Sim.	Exp.	Sim.
50.01 ± 0.33	50.00	160.04 ± 0.25	155.7	3.22 ± 0.01	3.12	882.05 ± 0.30	837.1	143.67 ± 0.54	143.5
55.02 ± 0.36	55.03	164.54 ± 0.32	162.1	3.35 ± 0.01	3.35	888.68 ± 0.36	850.3	142.67 ± 0.44	142.0
60.01 ± 0.42	60.03	171.32 ± 0.18	170.9	3.49 ± 0.01	3.50	896.18 ± 0.29	864.2	144.11 ± 2.23	143.9
64.96 ± 0.46	64.95	178.30 ± 0.66	179.4	3.63 ± 0.01	3.70	903.77 ± 0.49	876.8	146.02 ± 0.76	146.8
70.00 ± 0.48	70.00	184.86 ± 0.29	186.2	3.78 ± 0.01	3.90	912.12 ± 0.37	889.2	152.34 ± 1.42	151.7
75.01 ± 0.44	75.00	193.12 ± 0.38	194.7	3.93 ±0.01	4.01	922.17 ± 0.61	898.1	154.10 ± 1.37	154.1
79.87 ± 1.57	79.88	201.84 ± 0.45	200.8	4.12 ± 0.02	4.27	934.07 ± 4.56	899.9	156.03 ± 1.43	156.8

Table A. 2 Measured and simulated results for parameters such as molar flue gas composition for O_2, H_2O and CO_2; and rotational speed as a function of power output for MGT for base line performance of the MGT.

Power output [kW_e]		O_2 composition in flue gas [mol%]		H_2O composition in flue gas [mol%]		CO_2 composition in flue gas [mol%]		Rotational speed [rpm]	
Exp.	Sim.	Exp.	Sim.	Exp.	Sim.	Exp.	Sim.	Exp.	Sim.
50.01 ± 0.33	50.00	18.5	17.66	3.23 ± 0.01	3.71	1.51 ± 0.01	1.48	59241.7 ± 41.5	59242
55.02 ± 0.36	55.03	18.4	17.58	3.33 ± 0.04	3.77	1.53 ±0.01	1.51	60400.9 ± 45.1	60401
60.01 ± 0.42	60.03	18.4	17.53	3.26 ± 0.06	3.81	1.54 ± 0.01	1.53	61747.9 ± 33.2	61748
64.96 ± 0.46	64.95	18.3	17.4	3.34 ± 0.04	3.93	1.59 ± 0.01	1.59	63066.4 ± 60.6	63066
70.00 ± 0.48	70.00	18.3	17.39	3.45 ± 0.03	3.94	1.64 ± 0.02	1.6	64311.5 ± 42.1	64312
75.01 ± 0.44	75.00	18.2	17.38	3.49 ± 0.05	3.94	1.67 ± 0.01	1.61	65808.7 ± 47.7	65809
79.87 ± 1.57	79.88	18.2	17.28	3.48 ± 0.04	4.03	1.69 ± 0.02	1.65	67531.8 ± 141.6	67532

Table A. 3 Measured and simulated results for parameters such as compressor discharge temperature, compressor discharge pressure, turbine inlet temperature and flue gas temperature as a function of power output for MGT for CO_2 injection of the MGT part load of 80 kW_e.

CO_2 injected [kg/h]	EGR percentage [%]	Power output [kW_e]		Compressor discharge temperature [^oC]		Compressor discharge pressure [bar]		Turbine inlet temperature [^oC]		Flue gas temperature [^oC]	
		Exp.	Sim.	Exp.	Sim.	Exp.	Sim.	Exp.	Sim.	Exp.	Sim.
0	0	79.87 ± 1.57	79.88	201.84 ± 0.45	200.8	4.12 ± 0.02	4.27	934.07 ± 4.56	899.9	156.03 ± 1.43	156.8
6	8.6	79.12 ± 1.41	79.14	192.91 ± 0.26	189.8	4.04 ± 0.01	4.11	920.29 ± 3.66	887.5	149.58 ± 0.69	149.8
18	25.3	79.19 ± 1.37	79.21	193.27 ± 0.28	190.2	4.05 ± 0.01	4.12	920.74 ± 3.54	888.1	150.58 ± 1.57	150.3
30	42.6	79.05 ± 2.09	79.05	193.28 ± 0.45	190.0	4.05 ± 0.02	4.12	920.79 ± 6.25	887.1	148.71 ± 0.51	148.5
50	70.7	79.17 ± 2.19	79.19	193.78 ± 0.40	190.1	4.05 ± 0.02	4.12	921.97 ± 6.49	886.9	151.53 ± 0.69	151.5
75	105.3	79.21 ± 2.14	79.21	193.94 ± 0.42	190.0	4.06 ± 0.02	4.12	921.55 ± 6.24	885.7	150.16 ± 1.61	150.1
100	104.3	79.32 ± 1.95	79.33	193.93 ± 0.59	189.4	4.07 ± 0.02	4.12	920.93 ± 6.03	883.9	151.41 ± 0.42	151.4
125	175.1	79.32 ± 1.80	79.30	195.63 ± 0.38	190.7	4.08 ± 0.02	4.12	923.97 ± 5.54	885.0	151.06 ± 1.53	151.2

Table A. 4 Measured and simulated results for parameters such as molar flue gas composition for O_2, H_2O and CO_2; and rotational speed as a function of power output for MGT for CO_2 injection of the MGT part load of 80 kW_e.

CO_2 injected [kg/h]	EGR percentage [%]	Power output [kW_e]		O_2 composition in flue gas [mol%]		H_2O composition in flue gas [mol%]		CO_2 composition in flue gas [mol%]		Rotational speed [rpm]	
		Exp.	Sim.	Exp.	Sim.	Exp.	Sim.	Exp.	Sim.	Exp.	Sim.
0	0	79.87 ± 1.57	79.88	18.17	17.28	3.48 ± 0.04	4.03	1.69 ± 0.02	1.65	67531.8 ± 141.6	67532.0
6	8.6	79.12 ± 1.41	79.14	18.40	18.13	3.31 ± 0.09	3.92	1.71 ± 0.01	1.74	66891.3 ± 74.32	66891.3
18	25.3	79.19 ± 1.37	79.21	18.33	18.07	3.26 ± 0.17	3.91	1.99 ± 0.02	2.05	66907.5 ± 75.33	66907.5
30	42.6	79.05 ± 2.09	79.05	18.27	18.01	3.10 ± 0.11	3.90	2.29 ± 0.02	2.35	66871.2 ± 139.23	66871.2
50	70.7	79.17 ± 2.19	79.19	18.20	17.93	3.39 ± 0.03	3.88	2.74 ± 0.02	2.85	66883.1 ± 143.13	66883.1
75	105.3	79.21 ± 2.14	79.21	18.10	17.79	3.14 ± 0.14	3.87	3.31 ± 0.04	3.48	66875.9 ± 143.66	66875.9
100	104.3	79.32 ± 1.95	79.33	17.90	17.71	3.37 ± 0.03	3.84	3.88 ± 0.02	4.09	66849.2 ± 142.06	66849.2
125	175.1	79.32 ± 1.80	79.30	17.75	17.57	3.19 ± 0.14	3.83	4.45 ± 0.01	4.71	66959.2 ± 127.81	66959.2

Table A. 5 Measured and simulated results for parameters such as compressor discharge temperature, compressor discharge pressure, turbine inlet temperature and flue gas temperature as a function of power output for MGT for CO_2 injection of the MGT part load of 70 kW_e.

CO_2 injected [kg/h]	EGR percentage [%]	Power output [kW_e]		Compressor discharge temperature [^oC]		Compressor discharge pressure [bar]		Turbine inlet temperature [^oC]		Flue gas temperature [^oC]	
		Exp.	Sim.	Exp.	Sim.	Exp.	Sim.	Exp.	Sim.	Exp.	Sim.
0	0	70.00 ± 0.48	70.00	184.86 ± 0.29	186.2	3.78 ± 0.01	3.90	912.12 ± 0.37	889.2	152.34 ± 1.42	151.7
5	8.0	69.96 ± 0.50	69.96	179.05 ± 0.69	180.1	3.74 ± 0.01	3.83	904.82 ± 1.06	883.9	147.72 ± 1.28	147.7
15	23.8	70.01 ± 0.46	69.99	180.26 ± 0.09	183.6	3.74 ± 0.01	3.70	906.79 ± 0.38	887.5	148.45 ± 2.25	148.4
28	45.1	70.00 ± 0.45	70.00	180.64 ± 0.05	186.3	3.74 ± 0.01	3.74	907.44 ± 0.29	898.4	148.68 ± 0.68	148.8
50	79.54	70.00 ± 0.52	70.01	179.70 ± 0.04	179.9	3.74 ± 0.01	3.70	904.56 ± 0.58	882.0	147.49 ± 0.48	147.7
75	119.3	70.01 ± 0.53	70.01	180.18 ± 0.57	180.3	3.75 ± 0.01	3.73	905.05 ± 0.42	882.2	146.88 ± 0.27	146.6
100	159.0	70.01 ± 0.42	70.02	179.76 ± 0.33	182.2	3.76 ± 0.01	3.75	903.78 ± 0.60	891.0	149.30 ± 1.96	148.9
125	198.9	70.02 ± 0.48	70.03	179.95 ± 0.16	185.3	3.76 ± 0.01	3.72	903.86 ± 0.40	884.6	150.85 ± 0.32	150.9

Table A. 6 Measured and simulated results for parameters such as molar flue gas composition for O_2, H_2O and CO_2; and rotational speed as a function of power output for MGT for CO_2 injection of the MGT part load of 70 kW_e.

CO_2 injected [kg/h]	EGR percentage [%]	Power output [kW_e]		O_2 composition in flue gas [mol%]		H_2O composition in flue gas [mol%]		CO_2 composition in flue gas [mol%]		Rotational speed [rpm]	
		Exp.	Sim.	Exp.	Sim.	Exp.	Sim.	Exp.	Sim.	Exp.	Sim.
0	0	70.00 ± 0.48	70.00	18.30	17.39	3.45 ± 0.03	3.94	1.64 ± 0.02	1.60	64311.5 ± 42.1	64312.0
5	8.0	69.96 ± 0.50	69.96	18.20	17.85	3.37 ± 0.03	3.74	1.61 ± 0.01	1.64	63880.0 ± 63.36	63880.0
15	23.8	70.01 ± 0.46	69.99	18.10	17.68	3.20 ± 0.10	3.64	1.85 ± 0.01	1.88	63956.5 ± 24.20	63956.5
28	45.1	70.00 ± 0.45	70.00	18.10	17.7	3.32 ± 0.06	3.63	2.18 ± 0.01	2.26	63963.3 ± 23.71	63963.3
50	79.54	70.00 ± 0.52	70.01	18.00	17.67	3.24 ± 0.11	3.48	2.75 ± 0.01	2.85	63867.8 ± 42.65	63867.8
75	119.3	70.01 ± 0.53	70.01	17.90	17.44	3.20 ± 0.06	3.46	3.37 ± 0.01	3.48	63857.0 ± 32.69	63857.0
100	159.0	70.01 ± 0.42	70.02	17.80	17.26	3.24 ± 0.02	3.48	3.98 ± 0.01	4.29	63748.4 ± 29.43	63748.5
125	198.9	70.02 ± 0.48	70.03	17.60	17.11	3.19 ± 0.00	3.47	4.60 ± 0.01	5.04	63707.3 ± 36.37	63707.3

Table A. 7 Measured and simulated results for parameters such as compressor discharge temperature, compressor discharge pressure, turbine inlet temperature and flue gas temperature as a function of power output for MGT for CO_2 injection of the MGT part load of 60 kW_e.

CO_2 injected [kg/h]	EGR percentage [%]	Power output [kW_e]		Compressor discharge temperature [^oC]		Compressor discharge pressure [bar]		Turbine inlet temperature [^oC]		Flue gas temperature [^oC]	
		Exp.	Sim.	Exp.	Sim.	Exp.	Sim.	Exp.	Sim.	Exp.	Sim.
0	0	60.01 ± 0.42	60.03	171.32 ± 0.18	170.9	3.49 ± 0.01	3.50	896.18 ± 0.29	864.2	144.11 ± 2.23	143.9
5	10.1	60.00 ± 0.31	60.00	168.0 ± 0.09	166.6	3.46 ± 0.01	3.49	890.93 ± 0.33	857.4	138.46 ± 0.60	138.6
15	27.9	60.00 ± 0.38	60.00	167.30 ± 0.11	166.5	3.46 ± 0.01	3.47	889.29 ± 0.35	857.4	138.16 ± 0.67	139
25	45.7	60.01 ± 0.33	60.00	166.93 ± 0.22	165.3	3.46 ± 0.01	3.50	887.38 ± 0.51	854.1	140.06 ± 1.63	140.1
50	88.9	60.01 ± 0.42	60.00	165.92 ± 0.24	164.0	3.47 ±0.01	3.49	886.52 ± 0.63	852.9	137.71 ± 0.71	137.6
75	133.1	60.01 ± 0.40	60.01	166.93 ± 0.51	166.3	3.47 ±0.01	3.44	888.43 ± 1.20	855.5	138.48 ± 0.60	138.5
100	176.9	60.02 ± 0.40	60.02	168.11 ±0.08	165.0	3.48 ± 0.01	3.47	890.57 ± 0.30	864.1	138.93 ± 0.62	138.7
125	220.8	59.99 ± 0.37	60.00	166.99 ± 0.23	168.4	3.48 ± 0.01	3.48	888.18 ± 0.60	856.8	138.63 ± 0.66	138.7

Table A. 8 Measured and simulated results for parameters such as molar flue gas composition for O_2, H_2O and CO_2; and rotational speed as a function of power output for MGT for CO_2 injection of the MGT part load of 60 kW_e.

CO_2 injected [kg/h]	EGR percentage [%]	Power output [kW_e]		O_2 composition in flue gas [mol%]		H_2O composition in flue gas [mol%]		CO_2 composition in flue gas [mol%]		Rotational speed [rpm]	
		Exp.	Sim.	Exp.	Sim.	Exp.	Sim.	Exp.	Sim.	Exp.	Sim.
0	0	60.01 ± 0.42	60.03	18.40	17.53	3.26 ± 0.06	3.81	1.54 ± 0.01	1.53	61747.9 ± 33.2	61748.0
5	10.1	60.00 ± 0.31	60.00	18.40	17.89	2.78 ± 0.09	3.72	1.58 ± 0.01	1.63	61675.5 ± 22.71	61675.5
15	27.9	60.00 ± 0.38	60.00	18.30	17.67	2.79 ± 0.08	3.60	1.84 ± 0.01	1.86	61594.6 ± 25.87	61594.7
25	45.7	60.01 ± 0.33	60.00	18.40	17.91	3.04 ± 0.17	3.59	2.13 ± 0.01	2.15	61655.1 ± 29.16	61655.1
50	88.9	60.01 ± 0.42	60.00	18.10	17.55	2.80 ± 0.08	3.52	2.80 ± 0.01	2.84	61382.5 ± 34.12	61382.5
75	133.1	60.01 ± 0.40	60.01	17.97	17.69	2.81 ± 0.08	3.43	3.46 ± 0.01	3.56	61383.7 ± 44.03	61383.7
100	176.9	60.02 ± 0.40	60.02	17.80	17.48	2.81 ± 0.08	3.34	4.13 ± 0.02	4.25	61398.5 ± 24.31	61398.5
125	220.8	59.99 ± 0.37	60.00	17.70	17.46	2.86 ± 0.08	3.16	4.78 ± 0.01	4.90	61246.6 ± 36.63	61246.6

Table A. 9 Measured and simulated results for parameters such as compressor discharge temperature, compressor discharge pressure, turbine inlet temperature and flue gas temperature as a function of power output for MGT for CO_2 injection of the MGT part load of 50 kW_e.

CO_2 injected [kg/h]	EGR percentage [%]	Power output [kW_e]		Compressor discharge temperature [^oC]		Compressor discharge pressure [bar]		Turbine inlet temperature [^oC]		Flue gas temperature [^oC]	
		Exp.	Sim.	Exp.	Sim.	Exp.	Sim.	Exp.	Sim.	Exp.	Sim.
0	0	50.01 ± 0.33	50.00	160.04 ± 0.25	155.7	3.22 ± 0.01	3.12	882.05 ± 0.30	837.1	143.67 ± 0.54	143.5
5	13.1	49.99 ± 0.33	49.98	163.14 ± 0.10	158.5	3.20 ± 0.01	3.12	884.60 ± 0.24	848.1	141.92 ± 1.85	141.5
14	30.6	50.03 ± 0.33	50.04	162.73 ± 0.16	157.9	3.20 ± 0.01	3.11	884.23 ± 0.26	847.6	143.30 ± 0.51	143.3
23	48.9	50.02 ± 0.30	50.02	162.28 ± 0.18	157.2	3.20 ± 0.01	3.11	883.82 ± 0.27	846.7	141.30 ± 1.96	141.2
50	104.6	50.09 ± 0.30	50.05	160.84 0.43	155.1	3.20 ± 0.01	3.12	882.40 ± 0.39	844.3	141.97 ±0.48	141.9
75	152.6	50.03 ± 0.46	50.01	152.95 ± 0.33	148.2	3.20 ± 0.01	3.14	871.88 ± 1.24	843.8	140.25 ± 0.27	140.4
100	203.7	50.05 ± 0.41	50.04	155.28 ± 0.11	149.2	3.20 ± 0.01	3.11	875.76 ± 1.37	847.6	139.65 ± 0.25	138.5
125	253.9	50.06 ± 0.40	50.06	154.22 ± 0.11	148.1	3.20 ± 0.01	3.12	873.48 ± 0.98	845.2	134.42 ± 0.83	134.5

Table A. 10 Measured and simulated results for parameters such as molar flue gas composition for O_2, H_2O and CO_2; and rotational speed as a function of power output for MGT for CO_2 injection of the MGT part load of 50 kW_e.

CO_2 injected [kg/h]	EGR percentage [%]	Power output [kW_e]		O_2 composition in flue gas [mol%]		H_2O composition in flue gas [mol%]		CO_2 composition in flue gas [mol%]		Rotational speed [rpm]	
		Exp.	Sim.	Exp.	Sim.	Exp.	Sim.	Exp.	Sim.	Exp.	Sim.
0	0	50.01 ± 0.33	50.00	18.50	17.66	3.23 ± 0.01	3.71	1.51 ± 0.01	1.48	59241.7 ± 41.5	59242.0
5	13.1	49.99 ± 0.33	49.98	18.40	17.84	2.98 ± 0.15	3.51	1.48 ± 0.01	1.52	59682.5 ± 26.11	59682.5
14	30.6	50.03 ± 0.33	50.04	18.30	17.91	3.19 ± 0.03	3.40	1.73 ± 0.01	1.73	59614.8 ± 30.10	59614.8
23	48.9	50.02 ± 0.30	50.02	18.30	17.85	2.91 ± 0.14	3.39	1.99 ± 0.01	2.00	59538.5 ± 29.03	59538.5
50	104.6	50.09 ± 0.30	50.05	18.10	17.77	3.12 ±0.07	3.35	2.78 ± 0.01	2.79	59301.4 ± 58.59	59301.4
75	152.6	50.03 ± 0.46	50.01	17.93	17.62	3.03 ± 0.01	3.31	3.52 ± 0.02	3.50	58371.9 ± 52.39	58371.9
100	203.7	50.05 ± 0.41	50.04	17.90	17.47	2.98 ± 0.01	3.30	4.27 ± 0.02	4.23	58647.8 ± 55.47	58647.8
125	253.9	50.06 ± 0.40	50.06	17.67	17.32	2.72 ± 0.10	3.29	4.98 ± 0.02	4.94	58570.9 ± 42.99	58570.9

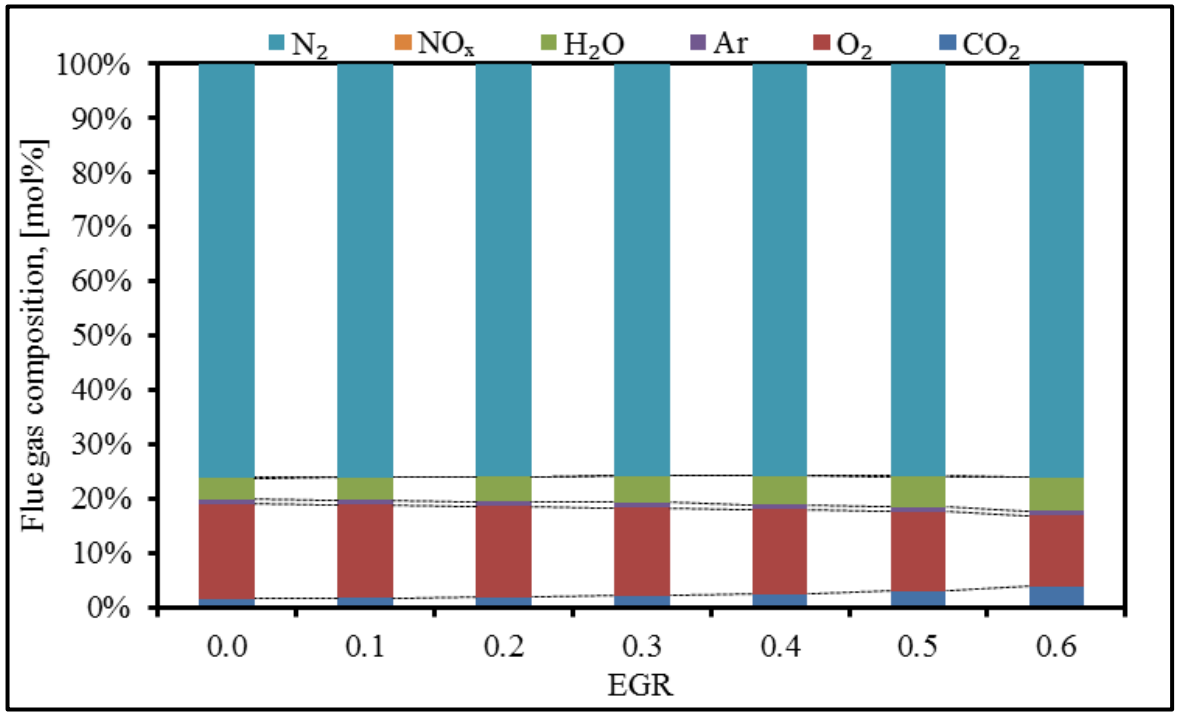

Figure A. 2 Effect of the EGR on the flue gas composition profile of the MGT-EGR.

Table A. 11 Measured and simulated results for parameters such as compressor discharge temperature, compressor discharge pressure, turbine inlet temperature and flue gas temperature as a function of power output for MGT for steam injection of the MGT part loads of 50, 55, 60 and 65 kW_e.

Steam injected [kg/h]	Power output [kW_e]		Compressor discharge temperature [^oC]		Compressor discharge pressure [bar]		Turbine inlet temperature [^oC]		Flue gas temperature [^oC]	
	Exp.	Sim.	Exp.	Sim.	Exp.	Sim.	Exp.	Sim.	Exp.	Sim.
0	50.01 ± 0.33	50.00	160.04 ± 0.25	155.7	3.22 ± 0.01	3.12	882.05 ± 0.30	837.1	143.67 ± 0.54	143.5
20	50.07 ± 0.38	50.07	121.77 ± 5.24	131.9	3.13 ± 0.01	2.94	868.01 ± 0.34	820.5	230.91 ± 0.19	247.6
40	50.39 ± 0.53	50.38	134.66 ± 4.00	134.8	3.10 ± 0.01	2.93	874.71 ± 0.82	821.7	233.00 ± 0.95	251.0
0	55.02 ± 0.36	55.03	164.54 ± 0.32	162.1	3.35 ± 0.01	3.35	888.68 ± 0.36	850.3	142.67 ± 0.44	142.0
20	55.04 ± 0.32	55.04	135.47 ± 4.63	135.0	3.26 ± 0.01	3.10	877.71 ± 0.35	834.9	237.12 ± 0.48	262.6
40	55.05 ± 0.46	55.06	144.07 ± 2.91	149.8	3.19 ± 0.01	3.01	879.19 ± 0.53	832.3	234.15 ± 0.55	255.9
0	60.01 ± 0.42	60.03	171.32 ± 0.18	170.9	3.49 ± 0.01	3.50	896.18 ± 0.29	864.2	144.11 ± 2.23	143.9
20	59.94 ± 0.35	59.96	141.63 ± 3.84	140.9	3.40 ± 0.01	3.29	883.41 ± 0.36	847.0	239.99 ± 0.67	270.2
40	59.91 ± 0.38	59.89	151.90 ± 1.91	158.5	3.32 ± 0.01	3.23	886.07 ± 0.43	846.2	239.10 ± 1.10	264.2
0	64.96 ± 0.46	64.95	178.30 ± 0.66	179.4	3.63 ± 0.01	3.70	903.77 ± 0.49	876.8	146.02 ± 0.76	146.8
20	64.95 ± 0.38	64.96	136.81 ± 11.63	138.0	3.33 ± 0.16	3.52	891.97 ± 0.36	862.5	238.36 ± 8.63	268.9
40	64.98 ± 0.39	64.98	158.10 ± 1.45	156.5	3.46 ± 0.01	3.43	893.02 ± 0.32	859.2	244.80 ± 1.05	263.4

Table A. 12 Measured and simulated results for parameters such as molar flue gas composition for O_2, H_2O and CO_2; and rotational speed as a function of power output for MGT for CO_2 injection of the MGT for steam injection of the MGT part loads of 50, 55, 60 and 65 kW_e.

Steam injected [kg/h]	Power output [kW_e]		O_2 composition in flue gas [mol%]		H_2O composition in flue gas [mol%]		CO_2 composition in flue gas [mol%]		Rotational speed [rpm]	
	Exp.	Sim.	Exp.	Sim.	Exp.	Sim.	Exp.	Sim.	Exp.	Sim.
0	50.01 ± 0.33	50.00	18.50	17.66	3.23 ± 0.01	3.71	1.51 ± 0.01	1.48	59241.70 ± 41.53	59241.7
20	50.07 ± 0.38	50.07	18.35	17.55	5.86 ± 0.10	4.98	1.40 ± 0.01	1.39	57927.62 ± 43.96	57927.6
40	50.39 ± 0.53	50.38	17.51	17.31	7.57 ± 0.30	6.33	1.35 ± 0.01	1.36	58005.59 ± 139.20	58005.6
0	55.02 ± 0.36	55.03	18.40	17.58	3.33 ± 0.04	3.77	1.53 ± 0.01	1.51	60400.92 ± 45.06	60400.9
20	55.04 ± 0.32	55.04	18.22	17.38	5.86 ± 0.10	5.11	1.44 ± 0.01	1.46	59340.14 ± 34.25	59340.1
40	55.05 ± 0.46	55.06	17.17	17.206	8.39 ± 0.27	6.40	1.38 ± 0.01	1.41	58902.87 ± 69.96	58902.9
0	60.01 ± 0.42	60.03	18.40	17.53	3.26 ± 0.06	3.81	1.54 ± 0.01	1.53	61747.90 ± 33.2	61747.9
20	59.94 ± 0.35	59.96	18.15	17.35	5.79 ±0.08	5.13	1.45 ± 0.01	1.47	60550.88 ± 38.10	60550.9
40	59.91 ± 0.38	59.89	17.25	17.08	8.13 ± 0.15	6.53	1.42 ± 0.00	1.46	60186.77 ± 56.63	60186.8
0	64.96 ± 0.46	64.95	18.30	17.395	3.34 ± 0.04	3.93	1.59 ± 0.01	1.59	63066.35 ± 60.61	63066.4
20	64.95 ± 0.38	64.96	17.91	17.17	5.78 ± 0.07	5.30	1.49 ± 0.01	1.56	61879.10 ± 36.00	61879.1
40	64.98 ± 0.39	64.98	17.04	16.92	8.07 ± 0.10	6.66	1.45 ± 0.01	1.53	61431.98 ± 34.21	61432.0

Table A. 13 Measured and simulated results for parameters such as compressor discharge temperature, compressor discharge pressure, turbine inlet temperature and flue gas temperature as a function of power output for MGT for simultaneous steam and CO_2 injection of the MGT part loads of 50 and 55 kW_e.

Steam injected [kg/h]	CO_2 injected [kg/h]	Power output [kW_e]		Compressor discharge temperature [^oC]		Compressor discharge pressure [bar]		Turbine inlet temperature [^oC]		Flue gas temperature [^oC]	
		Exp.	Sim.	Exp.	Sim.	Exp.	Sim.	Exp.	Sim.	Exp.	Sim.
0	0	50.01 ± 0.33	50.00	160.04 ± 0.25	155.7	3.22 ± 0.01	3.12	882.05 ± 0.30	837.1	143.67 ± 0.54	143.5
20	50	49.99 ± 0.37	49.96	130.62 ± 4.66	140.9	3.13 ± 0.01	2.94	866.27 ± 0.54	817.3	231.47 ± 0.16	244.5
20	75	50.11 ± 0.40	50.10	131.35 ± 5.26	140.7	3.13 ± 0.01	2.94	866.17 ± 0.62	816.7	232.76 ± 0.87	243.6
20	100	49.99 ± 0.36	49.98	130.14 ± 4.43	140.5	3.13 ± 0.01	2.92	866.69 ± 0.30	816.1	231.57 ± 0.15	241.9
20	125	50.11 ± 0.36	50.11	129.28 ± 4.75	141.1	3.14 ± 0.01	2.91	865.43 ± 0.40	816.8	232.05 ± 0.61	240.6
40	50	50.02 ± 0.34	50.01	139.62 ± 1.39	147.8	3.08 ± 0.01	2.95	871.76 ± 0.35	824.0	232.21 ± 0.16	248.3
40	75	50.00 ± 0.36	50.00	139.02 ± 1.62	146.6	3.09 ± 0.01	2.93	870.22 ± 0.37	822.5	231.68 ± 0.20	244.2
40	100	50.05 ± 0.40	50.02	138.21 ± 1.54	146.1	3.10 ± 0.01	2.95	868.90 ± 0.36	820.8	231.61 ± 0.18	240.6
40	125	50.05 ± 0.35	50.07	139.05 ± 1.58	148.3	3.10 ± 0.01	2.99	871.16 ± 0.38	822.3	232.95 ± 0.22	250.9
0	0	55.02 ± 0.36	55.03	164.54 ± 0.32	162.1	3.35 ± 0.01	3.35	888.68 ± 0.36	850.3	142.67 ± 0.44	142.0
20	50	54.98 ± 0.33	54.97	137.83 ± 4.99	148.7	3.27 ± 0.01	3.10	872.32 ± 0.44	828.7	234.96 ± 0.34	251.3
20	75	54.99 ± 0.36	54.96	139.15 ± 4.93	150.0	3.27 ± 0.01	3.12	874.76 ± 0.31	830.7	236.84 ± 0.18	254.1
20	100	54.97 ± 0.35	54.98	137.98 ±4.03	149.7	3.27 ± 0.01	3.12	874.57 ± 0.52	830.2	235.44 ± 0.88	251.4
20	125	55.00 ± 0.34	55.01	136.19 ± 5.18	148.3	3.27 ± 0.01	3.11	872.10 ± 0.44	827.1	236.54 ± 0.61	244.1
40	50	54.93 ± 0.35	54.93	145.74 ± 1.27	149.7	3.22 ± 0.01	3.03	878.62 ± 0.36	831.3	235.43 ± 0.51	251.8
40	75	55.01 ± 0.35	55.02	146.06 ± 1.22	149.0	3.22 ± 0.01	3.02	877.75 ± 0.40	830.0	236.04 ± 0.15	251.5
40	100	55.00 ± 0.40	54.99	146.19 ± 1.04	148.5	3.22 ± 0.01	3.01	877.50 ± 0.33	828.9	236.18 ± 0.11	252.6
40	125	55.01 ± 0.37	54.99	146.02 ± 0.97	147.6	3.22 ± 0.01	3.00	876.30 ± 0.34	827.2	235.95 ± 0.10	252.6

Table A. 14 Measured and simulated results for parameters such as compressor discharge temperature, compressor discharge pressure, turbine inlet temperature and flue gas temperature as a function of power output for MGT for simultaneous steam and CO_2 injection of the MGT part loads of 60 and 65 kW_e.

Steam injected [kg/hr]	CO_2 injected [kg/hr]	Power output [kW_e]		Compressor discharge temperature [^oC]		Compressor discharge pressure [bar]		Turbine inlet temperature [^oC]		Flue gas temperature [^oC]	
		Exp.	Sim.	Exp.	Sim.	Exp.	Sim.	Exp.	Sim.	Exp.	Sim.
0	0	60.01 ± 0.42	60.03	171.32 ± 0.18	170.9	3.49 ± 0.01	3.50	896.18 ± 0.29	864.2	144.11 ± 2.23	143.9
20	100	59.95 ± 0.36	59.94	145.86 ± 3.29	158.1	3.41 ± 0.01	3.33	881.34 ± 0.50	843.6	240.91 ± 0.95	259.5
20	125	60.11 ± 0.41	60.11	143.96 ± 5.46	157.7	3.42 ± 0.01	3.34	880.17 ± 0.42	841.9	243.16 ± 0.94	249.3
40	100	59.97 ± 0.33	59.96	150.74 ± 0.90	155.6	3.35 ± 0.01	3.25	880.71 ± 0.48	840.0	240.09 ± 0.14	259.0
40	125	59.95 ± 0.35	59.97	151.16 ± 0.87	155.5	3.36 ± 0.01	3.22	881.74 ± 0.61	839.4	239.80 ± 0.63	258.8
0	0	64.96 ± 0.46	64.95	178.30 ± 0.66	179.4	3.63 ± 0.01	3.70	903.77 ± 0.49	876.8	146.02 ± 0.76	146.8
20	125	65.03 ± 0.36	65.05	150.80 ± 5.27	166.3	3.56 ± 0.01	3.57	887.79 ± 0.36	856.0	248.0 ± 0.21	251.1
40	125	64.98 ± 0.34	64.98	156.32 ± 0.91	163.0	3.49 ± 0.01	3.47	886.31 ± 0.29	852.3	244.88 ± 0.49	257.7

Table A. 15 Measured and simulated results for parameters such as molar flue gas composition for O_2, H_2O and CO_2; and rotational speed as a function of power output for MGT for CO_2 injection of the MGT for simultaneous steam and CO_2 injection of the MGT part loads of 50 and 55 kW_e.

Steam injected [kg/h]	CO_2 injected [kg/h]	Power output [kW_e]		O_2 composition in flue gas [mol%]		H_2O composition in flue gas [mol%]		CO_2 composition in flue gas [mol%]		Rotational speed [rpm]	
		Exp.	Sim.	Exp.	Sim.	Exp.	Sim.	Exp.	Sim.	Exp.	Sim.
0	0	50.01 ± 0.33	50.00	18.50	17.66	3.23 ± 0.01	3.71	1.51 ± 0.01	1.48	59241.70 ± 41.53	59241.7
20	50	49.99 ± 0.37	49.96	17.17	17.26	5.74 ± 0.07	4.93	2.77 ± 0.02	2.86	57849.87 ± 40.05	57849.9
20	75	50.11 ± 0.40	50.10	17.10	17.12	5.76 ± 0.09	4.92	3.44 ± 0.02	3.50	57817.16 ± 48.99	57817.2
20	100	49.99 ± 0.36	49.98	17.20	16.97	5.83 ± 0.08	4.90	4.11 ± 0.01	4.33	57736.68 ± 30.11	57736.7
20	125	50.11 ± 0.36	50.11	17.21	16.76	5.89 ± 0.09	4.95	4.78 ± 0.02	5.10	57666.18 ± 39.20	58666.2
40	50	50.02 ± 0.34	50.01	17.49	16.98	7.85 ± 0.07	6.35	2.78 ± 0.02	2.85	57491.94 ± 28.29	58491.9
40	75	50.00 ± 0.36	50.00	17.16	16.84	7.81 ± 0.08	6.32	3.45 ± 0.02	3.50	57375.25 ± 32.04	58375.3
40	100	50.05 ± 0.40	50.02	17.49	16.67	7.77 ± 0.08	6.34	4.14 ± 0.02	4.33	57300.39 ± 32.91	58300.4
40	125	50.05 ± 0.35	50.07	16.68	16.52	7.55 ± 0.08	6.32	4.86 ± 0.01	5.00	57575.37 ± 33.20	58575.4
0	0	55.02 ± 0.36	55.03	18.40	17.58	3.33 ± 0.04	3.77	1.53 ± 0.01	1.51	60400.92 ± 45.06	60400.9
20	50	54.98 ± 0.33	54.97	17.15	17.11	5.66 ± 0.07	5.06	2.74 ± 0.01	2.90	59156.03 ± 32.58	59156.0
20	75	54.99 ± 0.36	54.96	17.10	16.93	5.68 ± 0.07	5.08	3.39 ± 0.01	3.60	59180.88 ± 35.22	59180.9
20	100	54.97 ± 0.35	54.98	17.26	16.77	5.76 ± 0.06	5.08	4.05 ± 0.01	4.40	59086.56 ± 41.84	59086.6
20	125	55.00 ± 0.34	55.01	17.33	16.67	5.84 ± 0.09	5.04	4.68 ± 0.01	5.10	58992.98 ± 31.57	58993.0
40	50	54.93 ± 0.35	54.93	17.41	16.87	7.71 ± 0.06	6.43	2.77 ± 0.01	2.88	58791.93 ± 34.45	58791.9
40	75	55.01 ± 0.35	55.02	17.47	16.73	7.76 ± 0.07	6.41	3.42 ± 0.01	3.60	58701.99 ±30.74	58702.0
40	100	55.00 ± 0.40	54.99	17.25	16.59	7.81 ± 0.05	6.39	4.08 ± 0.01	4.30	58609.93 ± 40.57	58609.9
40	125	55.01 ± 0.37	54.99	17.02	16.44	7.83 ± 0.04	6.37	4.76 ± 0.01	5.04	58513.88 ± 27.95	58513.9

Table A. 16 Measured and simulated results for parameters such as molar flue gas composition for O_2, H_2O and CO_2; and rotational speed as a function of power output for MGT for CO_2 injection of the MGT for simultaneous steam and CO_2 injection of the MGT part loads of 60 and 65 kW_e.

Steam injected [kg/h]	CO_2 injected [kg/h]	Power output [kW_e]		O_2 composition in flue gas [mol%]		H_2O composition in flue gas [mol%]		CO_2 composition in flue gas [mol%]		Rotational speed [rpm]	
		Exp.	Sim.	Exp.	Sim.	Exp.	Sim.	Exp.	Sim.	Exp.	Sim.
0	0	60.01 ± 0.42	60.03	18.40	17.53	3.26 ± 0.06	3.81	1.54 ± 0.01	1.53	61747.90 ± 33.2	61747.9
20	100	59.95 ± 0.36	59.94	17.62	16.71	5.67 ± 0.06	5.13	4.00 ± 0.01	4.40	60366.83 ± 51.91	60366.8
20	125	60.11 ± 0.41	60.11	17.37	16.59	5.77 ± 0.09	5.10	4.62 ± 0.01	5.13	60366.78 ± 41.20	60366.8
40	100	59.97 ± 0.33	59.96	17.35	16.44	7.69 ± 0.05	6.53	4.05 ± 0.01	4.41	59782.97 ± 28.97	59783.0
40	125	59.95 ± 0.35	59.97	17.01	16.33	7.68 ± 0.04	6.47	4.70 ± 0.01	5.09	59733.49 ± 35.56	59733.5
0	0	64.96 ± 0.46	64.95	18.30	17.395	3.34 ± 0.04	3.93	1.59 ± 0.01	1.59	63066.35 ± 60.61	63066.4
20	125	65.03 ± 0.36	65.05	17.34	16.43	5.71 ± 0.09	5.24	4.54 ± 0.02	5.21	61657.53 ± 32.88	61657.5
40	125	64.98 ± 0.34	64.98	17.01	16.11	7.57 ± 0.05	6.69	4.61 ± 0.01	5.30	60946.86 ± 27.85	60946.9

Appendix B
Data for Chapter 6

Table B. 1 Pilot-scale Amine-based CO_2 capture plant model validation against 1st set of experimental data reported by Notz et al. [139].

	CO_2 in flue gas, (mol %)		L/G ratio		Lean CO_2 loading (mol CO_2/mol MEA)		Rich CO_2 loading (mol CO_2/mol MEA)		Specific reboiler duty (GJ/tCO_2)		CO_2 captured (%)	
	Exp.	Sim.	Exp.	Sim.	Exp.	Sim.	Exp.	Sim.	Exp.	Sim.	Exp.	Sim.
1	5.5	5.4	2.78	2.8	0.265	0.279	0.386	0.391	5.01	5.23	75.9	76.4
2	10.9	10.9	2.76	2.8	0.308	0.321	0.464	0.481	3.98	3.96	51.3	51.5
3	3.6	3.5	2.77	2.8	0.230	0.234	0.308	0.307	7.18	8.00	84.9	84.9
4	5.7	5.6	2.79	2.8	0.268	0.269	0.397	0.388	5.05	5.13	76.5	76.9
5	8.5	8.5	2.79	2.8	0.306	0.313	0.446	0.456	4.19	4.17	60.7	60.9
6	13.4	13.2	2.77	2.8	0.317	0.341	0.464	0.499	3.85	3.83	43.7	43.9
7	11.1	10.9	2.77	2.8	0.356	0.365	0.478	0.495	3.91	3.94	40.3	40.4
8	10.9	10.8	2.76	2.8	0.228	0.223	0.444	0.443	4.22	4.17	76.5	77.4
9	11.0	10.9	2.77	2.8	0.147	0.146	0.393	0.386	5.49	5.64	88.3	88.8
10	5.6	5.6	2.78	2.8	0.299	0.299	0.402	0.409	5.65	8.39	69.4	69.6
11	5.7	5.7	2.79	2.8	0.280	0.280	0.396	0.398	5.12	7.03	72.1	72.3
12	5.6	5.6	2.78	2.8	0.256	0.272	0.372	0.376	4.91	5.45	75.3	75.8
13	5.2	5.2	2.78	2.8	0.287	0.293	0.400	0.401	4.52	5.13	77.2	77.4
14	5.4	5.3	2.78	2.8	0.253	0.247	0.369	0.365	5.48	5.49	76.2	76.8
15	5.6	5.4	2.78	2.8	0.241	0.241	0.359	0.363	5.84	5.79	75.6	75.9

16	5.7	5.5	1.01	1.0	0.096	0.097	0.414	0.388	7.38	7.67	74.9	75.4
17	5.7	5.4	1.51	1.5	0.166	0.166	0.371	0.369	5.47	5.69	75.7	75.5
18	5.8	5.5	2.01	2.0	0.215	0.202	0.387	0.374	5.35	5.33	75.4	75.6
19	5.7	5.4	3.52	3.5	0.247	0.237	0.354	0.337	6.27	6.26	75.8	76.5
20	5.5	5.5	2.81	2.8	0.261	0.261	0.395	0.380	5.10	5.31	77.4	77.5
21	5.4	5.4	2.82	2.8	0.270	0.270	0.400	0.385	5.18	5.13	77.5	78.3
22	5.8	5.8	2.77	2.8	0.263	0.270	0.389	0.387	5.10	5.26	75.1	75.4
23	6.0	5.9	2.80	2.8	0.274	0.276	0.393	0.394	5.11	5.48	73.3	72.8
24	5.5	5.4	2.79	2.8	0.251	0.251	0.392	0.386	5.11	5.28	74.6	75.1
25	5.5	5.4	2.79	2.8	0.166	0.130	0.435	0.395	5.46	5.50	68.6	68.5
26	10.9	10.8	2.75	2.7	0.288	0.291	0.474	0.488	4.13	4.11	49.3	49.5
27	11.0	10.9	2.76	2.8	0.169	0.176	0.501	0.517	4.77	4.75	42.3	42.4
28	11.0	10.8	1.98	2.0	0.266	0.282	0.470	0.492	3.68	3.63	53.4	54.2
29	10.9	10.7	2.63	2.6	0.306	0.320	0.465	0.479	3.92	3.88	53.7	54.3
30	10.7	10.5	3.33	3.3	0.316	0.316	0.459	0.468	4.38	4.03	55.9	56.3
31	107.0	106.5	3.63	3.6	0.338	0.313	0.454	0.469	4.30	4.27	55.6	56.1
32	10.5	10.3	3.92	3.9	0.335	0.326	0.449	0.465	4.57	4.52	55.4	56.1
33	10.6	10.4	4.54	4.5	0.360	0.339	0.441	0.467	4.35	4.31	54.6	55.3
34	5.4	5.3	1.07	1.1	0.146	0.151	0.417	0.419	4.85	4.97	75.9	76.3
35	5.5	5.4	1.43	1.4	0.208	0.212	0.411	0.412	4.27	4.49	76.6	76.6
36	5.4	5.3	2.11	2.1	0.252	0.255	0.393	0.399	4.68	4.87	76.0	74.9
37	5.4	5.3	2.81	2.8	0.296	0.288	0.398	0.402	5.11	5.10	74.5	75.0
38	5.5	5.4	3.50	3.5	0.308	0.303	0.385	0.395	5.40	5.40	74.7	74.7
39	5.4	5.4	3.84	3.8	0.319	0.318	0.400	0.397	5.23	3.72	74.8	75.7
40	5.3	5.3	1.77	1.8	0.111	0.112	0.297	0.282	10.24	10.81	91.2	91.1
41	5.3	5.2	2.12	2.1	0.130	0.127	0.297	0.282	9.76	9.86	90.8	91.1
42	5.5	5.4	2.85	2.8	0.190	0.197	0.310	0.319	7.16	7.15	88.4	88.7

43	5.3	5.2	2.82	2.8	0.200	0.208	0.318	0.313	6.87	6.86	85.8	85.8
44	5.3	5.3	3.52	3.5	0.209	0.213	0.314	0.305	7.18	7.56	85.9	86.0
45	5.5	5.4	3.84	3.8	0.219	0.221	0.324	0.308	7.09	7.48	86.0	86.0
46	5.4	5.4	2.86	2.9	0.318	0.314	0.417	0.419	4.68	4.62	67.51	68.12
47	5.5	5.4	2.86	2.9	0.255	0.251	0.366	0.370	5.50	5.51	81.56	80.06

Appendix C
Data for Chapter 7

Table C. 1 Comparison of the design results for amine-based CO_2 capture plant as reported for NGCC with and without EGR.

	Canepa et al. **[103]**		Biliyok et al. **[101]**		Biliyok and Yeung **[106]**		Sipocz and Tobiesen **[108]**		Luo et al. **[209]**	
Power plant type	without EGR	with EGR	without EGR	With EGR	without EGR	With EGR	without EGR	With EGR	without EGR	With EGR
Power plant size (MW_e) Gross	250	250	440	440	440	440	410.6	413.5	453	453
Gas turbine output (MW_e)	-	-	-	-	287.7	287.6	-	-	295.03	294.64
Flue gas flow rate (kg/s)	-	-	693.6	416.1	693.6	416.1	639.6	370.28	660.54	408.75
Liquid flow rate (kg/s)	720.46	675.6	721.7	675.2	721.6	675.3	-	-	1128.19	1036.81
Exhaust gas recirculation, EGR (%)	0	40	0	40	0	40	0	40	0	38
Liquid to gas ratio (mol basis)	2.29	3.32	1.314	-	1.31	2.09	0.68[a]	-	1.79	2.71
CO_2 in flue gas (mol %)	4.1	7	3.996	6.61	3.996	6.61	4.4	7.8	4.4	7.32
CO_2 capture rate (%)	90	90	90	90	90	90	90	90	90	90
MEA concentration (kg/kg)	0.3	0.3	0.3	0.3	0.3	0.3	0.3	-	0.325	0.325
Lean loading (mol/mol)	0.3	0.3	0.2343	0.3	0.234	-	0.132	0.128	0.32	0.32
Rich loading (mol/mol)	0.456	0.466	0.4952	-	0.4945	-	0.473	0.486	0.461	0.472
Number of absorber	2	2	4	3	4	3	1	-	-	-
Absorber Packing	IMTP	IMTP no.	Mellapak	Mellapak	Mellapak	Mellapak	Mellapak	Mellapak	IMTP no.	IMTP no.

	no.40	40	250X	250X	250X	250X	250	250	40	40
Absorber diameter (m)	9.5	8	10	-	10	-	9.13	6.87	19.81[c]	16.6[c]
Absorber packed height (m)	30	30	15	-	15	-	26.9	23.6	25	
Number of stripper	1	1	1	-	1	-	1	-	-	-
Stripper packing	Flexipack 1Y	Flexipack 1Y	Mellapak 250X	Mellapak 250X	Mellapak 250X	Mellapak 250X	Mellapak 250	Mellapak 250	Flexipack 1Y	Flexipack 1Y
Stripper diameter (m)	8.2	8	9	-	9	-	5.5	3.8	10.2[c]	9.8[c]
Stripper packed height (m)	30	30	15	-	15	-	23.5	21.2	15	-
Specific reboiler duty ($MJ/kgCO_2$)	4.97	4.68	3.992	3.726	4.0003	3.724	3.97	3.64	4.54	4.31
Stripper pressure (bar)	1.62	1.62	1.5	-	1.5	-	1.92[b]	1.92[b]	2.1	-

[a]L/G ratio reported was in mass basis.

[b]Regenerator temperature of 122 ^oC was reported.

[c]Diameter was estimated through the reported cross sectional area.

Table C. 2 Detailed results summary for the amine-based CO_2 capture plant for four different scenarios of the NGCC.

	NGCC without EGR	NGCC with 20 % EGR	NGCC with 35 % EGR	NGCC with 50 % EGR
Gross power plant size [MW_e]	650.7	622.5	621.3	622.5
Gas turbine power output [MW_e]	418.1	419.9	418.7	419.9
Steam turbine power output [MW_e]	232.6	202.6	202.6	202.6
Exhaust gas recirculation rate [%]	0	20	35	50
Natural gas flow rate [kg/hr]	84161	84260	84815	85450
CO_2 in flue gas [mol%]	3.91	5.13	6.2	8.19
Flue gas flow rate [kg/s]	1029.7	783.9	652.8	499.2
Recirculated gas flow rate [kg/s]	-	196.0	351.7	499.2
Optimum liquid flowrate [kg/s]	988.5	956.3	953.1	948.4
Optimum liquid to gas ratio [kg/kg]	0.96	1.22	1.46	1.9
Lean CO_2 loading [mol/mol] [16]	0.2	0.2	0.2	0.2
Optimum rich CO_2 loading [mol/mol]	0.480	0.485	0.487	0.489
Absorber				
Number of absorber	2	2	2	2
Absorber packing	Mellapak 250Y	Mellapak 250Y	Mellapak 250Y	Mellapak 250Y
Absorber diameter [m]	15.00	13.61	12.75	11.39
Optimum absorber height [m]	16.47	15.75	15.43	15.31
Stripper				
Number of stripper	1	1	1	1

Stripper packing	Mellapak 250Y	Mellapak 250Y	Mellapak 250Y	Mellapak 250Y
Stripper diameter [m]	9.20	9.06	9.02	9.00
Optimum stripper height [m]	29.73	29.46	28.67	27.88
Duty				
Specific reboiler duty [MJ/kg CO_2]	3.83	3.82	3.77	3.71
Specific condenser duty [MJ/kg CO_2]	1.65	1.51	1.50	1.48
Cross heat exchanger duty [MW]	135.6	149.8	157.3	224.3
Lean amine cooler duty [MW]	60.5	87.1	92.1	105.3
Lean amine pump duty [kW]	25.1	25.1	25.6	37.6
Rich amine pump duty [kW]	72.3	72.4	72.4	72.5
Capital and Operating Costs				
CAPEX [M £]	116.3	116.1	115.6	115.3
OPEX [M £/yr]	60.3	38.5	31.4	31.2
TOTEX [M £/yr]	74.0	52.1	45.0	44.8

Appendix D
Data for Chapter 8

Table D. 1 Detailed key performance results for NGCC with and without EGR integrated to CO_2 capture and CO_2 compression units.

Cases	NGCC	NGCC with EGR
Natural gas [kg/s | bar | ^oC]	29.2 | 28.4 | 38	29.5 | 28.4 | 39
Air [kg/s | bar | ^oC]	1177 | 1.01 | 15	771 | 1.01 | 16
EGR percentage [%]	0	35
EGR [kg/s | bar | ^oC]	-	398.8 | 1.03 |15
Flue gas, HRSG exit [kg/s | bar | ^oC]	1206.3 |1.01|159	779.6 | 1.01 |278
Flue gas composition, HRSG exit		
CO_2 [mol%]	4.16	5.53
H_2O [mol%]	8.90	9.22
N_2 [mol%]	74.23	75.76
O_2 [mol%]	11.83	7.59
Ar [mol%]	0.88	0.90
Steam Turbine	**NGCC**	**NGCC with EGR**
Main steam [kg/s | bar | ^oC]	134.8 |166.5 |565	134.8 |166.5 |566
Reheat to furnace/boiler [kg/s | bar | ^oC]	98.5 | 26.9 | 309	98.5 | 26.9 | 309
Reheat from furnace/boiler [kg/s | bar | ^oC]	98.5 | 24.8 | 566	98.5 | 24.8 | 566
Steam to stripper reboiler [kg/s | bar | ^oC]	110.3 | 5.2 | 338	108.1 | 5.2 | 338
Condensate return from stripper [kg/s | bar | ^oC]	110 | 3 | 130	108.1 | 3 | 130
Condensate, condenser outlet [kg/s | bar | ^oC]	22.2 | 28.4 | 48	24.4 | 28.4 | 49
Feed water [kg/s | bar | ^oC]	134.8 | 8.3 | 38	138.1 | 8.3 | 38
CO_2 in flue gas [kg/hr]	280253	282697
CO_2 Capture Plant	**NGCC**	**NGCC with EGR**
Flue gas, absorber inlet [kg/s | bar | ^oC]	1206.3 | 1.01 | 40	779.6 | 1.01 | 40
Flue gas, absorber outlet [kg/s | bar | ^oC	1081 | 1.01 | 29	671.7 | 1.01 | 32
Lean MEA solution, absorber inlet [kg/s | bar | ^oC]	1193.8 | 3 | 40	1166.6 | 3 | 40
Lean MEA solution, stripper outlet [kg/s | bar | ^oC]	1194 |1.62 | 117	1166 |1.62 | 117
Rich MEA solution, absorber outlet [kg/s | bar | ^oC]	1319 |1.01 | 38.7	1275| 1.01 | 39.1
Rich MEA solution, stripper inlet [kg/s | bar | ^oC]	1319 | 3 | 107	1275| 3 | 107
Flue gas composition, absorber outlet		
CO_2 [mol%]	0.45	0.75

H_2O [mol%]	1.95	2.08
N_2 [mol%]	83.34	87.40
O_2 [mol%]	13.28	7.50
Ar [mol%]	0.97	1.00
MEA concentration, CO_2 free basis [kg/kg]	0.3	0.3
Lean CO_2 loading [mol/mol]	0.2	0.2
Rich CO_2 loading [mol/mol]	0.4764	0.4783
Lean MEA solution cooler inlet temperature [^oC]	43.8	44.4
CO_2 captured [kg/s]	69.95	70.5
Reboiler heat duty [MW_{th}]	275.1	271.0
Specific reboiler duty [MJ/kg CO_2]	3.933	3.841
Stripper condenser duty [MW_{th}]	113.5	108.2
Lean MEA solution cooler duty [MW_{th}]	16.1	18.4
Lean/Rich heat exchanger duty [MW_{th}]	320.0	310.2
Lean MEA solution pump duty [kW_e]	193.3	188.9
Rich MEA solution pump duty [kW_e]	277.3	267.4
Absorber pressure drop [kPa]	4.20	1.87
Absorber fractional approach to flooding	0.69	0.52
Stripper pressure drop [kPa]	0.32	0.289
Stripper fractional approach to flooding	0.30	0.32
Stripper condenser pressure [bar]	1.62	1.62
Booster fan duty [MW_e]	20.7	18.4
CO_2 Compression System	NGCC	NGCC with EGR
Total compression duty [MW_e]	20.76	20.94
Total intercooling duty [MW_{th}]	35.50	35.81

Table D. 2 Detailed energy performance results for NGCC with and without EGR integrated to CO_2 capture and CO_2 compression units.

Cases	NGCC	NGCC with EGR
Fuel heat input, HHV [MW_{th}]	1528	1543
Gas turbine power, without steam extraction [MW_e]	551	550
Steam turbine power, without steam extraction [MW_e]	249	250
Total power, without steam extraction [MW_e]	800	800
Gas turbine power, with steam extraction [MW_e]	551	550
Steam turbine power, with steam extraction [MW_e]	163	160
Total power, with steam extraction [MW_e]	714	710
Power plant auxiliary loads [MW_e]	2.9	3.3
Other auxiliary loads* [MW_e]	11.5	14.3
CO_2 capture plant auxiliary loads [MW_e]	29.2	29.1
CO_2 Compression loads [MW_e]	20.8	20.9
Power output without CO_2 capture and compression [MW_e]	785	782
Power output with CO_2 capture only [MW_e]	670	672
Power output with CO_2 capture and compression [MW_e]	650	651
Efficiency without CO_2 capture and compression [%], HHV	51.40	50.60
Efficiency with CO_2 capture only [%], HHV	43.89	43.50
Efficiency with CO_2 capture and compression [%], HHV	42.53	42.15
Efficiency penalty with CO_2 capture only [%]	7.5	7.1
Efficiency penalty with CO_2 capture and compression [%]	8.9	8.5
Specific CO_2 emissions from power plant [g/kWh]	431	435
Specific CO_2 compression work [MJ/kg]	0.2968	0.2970
Specific losses per unit of CO_2 captured [%/kgs^{-1}]	0.11	0.10

* Based on auxiliary load reported by 2013 Report of US Department of Energy [211].

Table D. 3 Detailed key performance results for boiler, SCR, ESP, FGD and steam turbine sections of pulverised coal and biomass fired subcritical and supercritical power plants integrated with CO_2 capture and CO_2 compression system with constant heat input and constant fuel flow rate cases.

	Supercritical			Subcritical		
Case	Constant heat input	Constant heat input	Constant fuel flow	Constant heat input	Constant heat input	Constant fuel flow
Fuel type	Coal	Biomass	Biomass	Coal	Biomass	Biomass
Furnace/Boiler/SCR						
Coal [kg/s |bar |^{o}C]	71.3 |1.01 |15	99.6 |1.01 |15	71.3 |1.01 |15	74.1 |1.01 |15	108.7 |1.01 |15	74.1 |1.01 |15
Primary air [kg/s |bar |^{o}C]	168 |1.01 |15	162 |1.01 |15	116 |1.01 |15	178 |1.01 |15	177 |1.01 |15	120 |1.01 |15
Secondary Air [kg/s |bar |^{o}C]	548 |1.01 |15	528 |1.01 |15	377 | 1.01 |15	583 |1.01 |15	578 |1.01 |15	392 |1.01 |15
Air Infiltration [kg/s |bar |^{o}C]	12.4 |1.01 |15	11.4 |1.01 |15	9.6 |1.01 |15	13.5 |1.01 |15	13.0 |1.01 |15	9.99 |1.01 |15
NH_3 injected [kg/s |bar |^{o}C]	1.70 |7.24 |15	1.10 |7.24 |15	0.8 |7.24 |15	1.93 |7.24 |15	1.34 |7.24 |15	0.88 | 7.24 |15
Flue gas, ESP inlet [kg/s |bar |^{o}C]	795 |1.01 |169	802 |1.01 |169	574 |1.01 |169	844 |1.01 |169	886 |1.01|169	597 | 1.01 | 69
Slag [kg/s]	1.4	0.1	0.1	1.4	0.2	0.1
Primary air fans duty [MW_e]	1.8	1.7	1.2	1.9	1.9	1.2
Forced draft fans duty [MW_e]	2.5	2.4	1.7	2.7	2.7	1.9
Induced draft fans duty [MW_e]	6.0	6.3	4.5	6.5	7.0	4.7
Subcritical Steam Turbine						
Main steam [kg/s |bar |^{o}C]	630 |242.3 |593	630 |242.3 |593	452 |242.3 |593	641 |166.5 |566	641 |166.5 |566	419 |166.5 |566
Reheat to furnace/boiler [kg/s |bar |^{o}C]	514 |49 |348	514 |49 |348	367 |49 |348	606 |42.8 |361	606 |42.8 |361	394 |42.8 |361
Reheat from furnace/boiler [kg/s |bar |^{o}C]	514 |45.2 |593	514 |45.2 |593	367 |45.2 |593	606 |39 |566	606 |39 |566	394 |39 |566
Steam to stripper reboiler [kg/s |bar |^{o}C]	223 |5.07 |296	230 |5.07 |296	163 |5.07 |296	243 |5.07 |294	241 |5.07 |294	172 |5.07 |293
Condensate return from stripper [kg/s |bar |^{o}C]	223 |3 |130	230 |3 |130	163 |3 |130	243 |3 |130	241 |3 |130	172 |3 |130
Condensate, condenser outlet [kg/s |bar |^{o}C]	246 |0.07 |38	239 |0.07 |38	174 |0.07 |38	310 |0.07 |38	296 |0.07 |38	195 |0.07 |38

Boiler feed water, economiser inlet [kg/s |bar |^{o}C]	630 |288.5 |283	630 |288.5 |283	452 |288.5 |283	641 |240 |214	641 |240 |214	419 |240 |214
EPS/FGD						
Fly ash [kg/s]	5.53 |1.01 |169	0.55 |1.01 |169	0.39 |1.01 |170	4.77 |1.01 |170	0.60 |1.01 |170	0.41 |1.01 |169
Lime slurry [kg/s]	19.50|1.03 |15	0.21 |1.03 |15	0.15 |1.03 |15	14.20 |1.03 |15	0.22 |1.03 |15	0.15 |1.03 |15
Oxidation Air [kg/s]	3.69 |1.01 |15	0.04 |1.01 |15	0.03 |1.01 |15	3.80 |1.01 |15	0.04 |1.01 |15	0.03 |1.01 |15
Makeup water [kg/s]	54.38|1.01 |15	0.60 |1.01 |15	0.43 |1.01 |15	56.50 |1.01 |15	0.61 |1.01 |15	0.41 |1.01 |15
Flue gas, FGD outlet [kg/s |bar |^{o}C]	833 |1.01 |58	803 |1.01 |58	574 |1.01 |58	884 |1.01 |58	876 |1.01 |58	597 |1.01 |58
Gypsum, moisture-free (kg/s]	9.6	0.1	0.1	10.0	0.1	0.1
CO_2 emitted [kg/hr]	608623	627193	449004	632890	684428	466934

Table D. 4 Detailed key performance results for CO_2 capture and CO_2 compression sections of pulverised coal and biomass fired subcritical and supercritical power plants integrated with CO_2 capture and CO_2 compression system with constant heat input and constant fuel flow rate cases.

	Supercritical			Subcritical		
Case	Constant heat input	Constant heat input	Constant fuel flow	Constant heat input	Constant heat input	Constant fuel flow
Fuel type	Coal	Biomass	Biomass	Coal	Biomass	Biomass
CO_2 Capture Plant						
Flue gas, absorber inlet [kg/s |bar |^oC]	833 |1.2 |40	803 |1.20 |40	574 |1.20 |40	884 |1.20 |40	876 |1.20 |40	597 |1.20 |40
Flue gas, absorber outlet [kg/s |bar |^oC]	607 |1.01 |41	582 |1.01 |43	417 |1.01 |43	641 |1.01 |41	638 |1.01 |42	433 |1.01 |43
Lean MEA solution, absorber inlet [kg/s |bar |^oC]	2403 |3.00 |40	2470 |3.00 |40	1743 |3.00 |40	2605 |3.00 |40	2694 |3.00 |40	1816 | 3.00 |40
Lean MEA solution, stripper outlet [kg/s |bar |^oC]	2403 |1.62 |117	2470 |1.62 |117	1743 |1.62 |117	2605 |1.62 |117	2694 |1.62 |117	1816 |1.62 |117
Rich MEA solution, absorber outlet [kg/s |bar |^oC]	2628 |1.01 |44	2691 |1.01 |45	1900 |1.01 |45	2848 |1.01 |45	2932 |1.01 |45	1980 |1.01 |45
Rich MEA solution, stripper inlet [kg/s |bar |^oC]	2628 |3.00 |107	2691 |3.00 |107	1900 |3.00 |107	2848 |3.00 |107	2932 |3.00 |107	1980 |3.00 |107
MEA concentration, CO_2 free basis [kg/kg]	0.3	0.3	0.3	0.3	0.3	0.3
Lean CO_2 loading [mol/mol]	0.2	0.2	0.2	0.2	0.2	0.2
Rich CO_2 loading [mol/mol]	0.479	0.480	0.480	0.479	0.480	0.480
Lean MEA solution cooler inlet temperature [^oC]	48.4	49.2	48.5	48.7	49.4	48.6
CO_2 captured [kg/s]	152.0	157.1	112.1	164.9	170.9	116.7
Reboiler heat duty [MW_{th}]	560.1	577.1	407.4	607.5	629.3	424.4
Specific reboiler duty [MJ/kg CO_2]	3.686	3.673	3.634	3.685	3.683	3.638
Stripper condenser duty [MW_{th}]	226.6	231.0	164.2	245.6	272.5	171.0
Lean MEA solution cooler duty [MW_{th}]	72.3	81.8	53.1	80.9	90.7	55.8

Lean/Rich heat exchanger duty [MW_{th}]	604.4	613.9	437.6	652.7	668.0	455.4
Lean MEA solution pump duty [kW_e]	388.0	400.0	282.2	421.8	436.3	294.0
Rich MEA solution pump duty [kW_e]	550.8	563.7	397.7	597.1	614.3	414.4
Absorber pressure drop [kPa]	2.93	2.38	1.19	2.93	3.02	1.28
Absorber fractional approach to flooding	0.72	0.67	0.47	0.73	0.74	0.49
Stripper pressure drop [kPa]	1.48	1.12	5.81	1.25	1.35	6.25
Stripper fractional approach to flooding	0.71	0.66	0.47	0.70	0.73	0.49
Stripper condenser pressure [bar]	1.62	1.62	1.62	1.62	1.62	1.62
Booster fan duty (MW_e]	19.1	19.5	13.3	20.6	20.3	13.8
CO_2 Compression System						
Total compression duty [MW_e]	44.90	46.46	33.18	48.75	50.52	34.53
Total intercooling duty [MW_{th}]	76.90	79.64	56.83	83.58	86.61	59.14

Table D. 5 Detailed energy performance results for pulverised coal and biomass fired subcritical and supercritical power plants integrated with CO_2 capture and CO_2 compression system with constant heat input and constant fuel flow rate cases.

	Supercritical			Subcritical		
Case	Constant heat input	Constant heat input	Constant fuel flow	Constant heat input	Constant heat input	Constant fuel flow
Fuel type	Coal	Biomass	Biomass	Coal	Biomass	Biomass
Fuel heat input, HHV [MW_{th}]	1933	1933	1384	2010	2010	1371
Steam turbine power, without steam extraction [MW_e]	800	800	574	800	800	548
Steam turbine power, with steam extraction [MW_e]	664	656	473	664	658	410
Power plant auxiliary loads [MW_e]	12	11	8	12	12	8
Other auxiliary loads [MW_e]*	30	30	30	30	30	30
CO_2 capture plant auxiliary loads [MW_e]	20.04	19.55	13.98	21.68	21.30	14.50
CO_2 Compression loads [MW_e]	44.90	46.46	33.18	48.75	50.52	34.53
Power output without CO_2 capture and compression [MW_e]	758	758	536	757	757	510
Power output with CO_2 capture only [MW_e]	602	596	421	601	595	396
Power output with CO_2 capture and compression [MW_e]	557	549	388	556	544	361
Efficiency without CO_2 capture and compression [%], HHV	39.22	39.30	38.70	37.67	37.67	37.20
Efficiency with CO_2 capture only [%], HHV	31.16	30.82	30.40	29.91	29.59	28.87
Efficiency with CO_2 capture and compression [%], HHV	28.84	28.41	28.01	27.67	27.08	26.35
Efficiency penalty with CO_2 capture only [%]	8.1	8.5	8.3	7.8	8.1	8.3
Efficiency penalty with CO_2 capture and compression [%]	10.4	10.9	10.7	10.0	10.6	10.9
Specific CO_2 emissions from power plant [g/kWh]	1092	1142	1158	1138	1258	1293
Specific CO_2 compression work [MJ/kg]	0.2954	0.2957	0.2960	0.2956	0.2956	0.2959
Specific losses per unit of CO_2 captured [$\%/kgs^{-1}$]	0.0530	0.0540	0.0740	0.0471	0.0473	0.0714

* Based on auxiliary load reported by 2010 Report of US Department of Energy [263].

Table D. 6 Detailed flue gas composition at different locations for pulverised coal and biomass fired subcritical and supercritical power plants integrated with CO_2 capture and CO_2 compression system with constant heat input and constant fuel flow rate cases.

Location	SCR inlet						FGD inlet					
	Supercritical			Subcritical			Supercritical			Subcritical		
	Coal (CHI)	Biomass (CHI)	Biomass (CFF)	Coal (CHI)	Biomass (CHI)	Biomass (CFF)	Coal (CHI)	Biomass (CHI)	Biomass (CFF)	Coal (CHI)	Biomass (CHI)	Biomass (CFF)
T/[^oC]	297	297	297	245	245	245	176	176	176	176	176	176
P/[bara]	0.99	0.99	0.99	0.99	0.99	0.99	1.06	1.06	1.06	1.06	1.06	1.06
F/[kg/s]	754	763	546	800	846	567	795	802	574	823	890	59
Composition												
CO_2 [mol%]	14.97	15.13	15.14	14.67	14.89	15.14	14.14	14.36	14.38	13.84	14.13	14.38
H_2O [mol%]	8.94	14.38	14.38	8.78	14.16	14.38	9.05	14.05	14.06	8.93	13.87	14.08
N_2 [mol%]	72.90	67.90	67.89	72.97	68.04	67.89	73.16	68.38	68.38	73.23	68.52	68.38
O_2 [mol%]	1.69	1.53	1.52	2.06	1.83	1.51	2.56	2.38	2.37	2.91	2.66	2.36
Ar [mol%]	0.87	0.81	0.81	0.88	0.81	0.81	0.87	0.81	0.81	0.88	0.81	0.81
SO_2 [mol%]	0.22	0.00	0.00	0.22	0.00	0.00	0.21	0.00	0.00	0.20	0.00	0.00
NO [mol%]	0.39	0.25	0.25	0.42	0.27	0.27	0.00	0.00	0.00	0.00	0.00	0.00
NO_2 [ppmv]	0.00	0.01	0.01	0.01	0.01	0.01	0.00	0.00	0.00	0.00	0.00	0.00

Location	CO_2 absorber inlet						CO_2 absorber outlet					
	Supercritical			Subcritical			Supercritical			Subcritical		
	Coal (CHI)	Biomass (CHI)	Biomass (CFF)	Coal (CHI)	Biomass (CHI)	Biomass (CFF)	Coal (CHI)	Biomass (CHI)	Biomass (CFF)	Coal (CHI)	Biomass (CHI)	Biomass (CFF)
T/[^oC]	40	40	40	40	40	40	41	43	43	41	42	43
P/[bara]	1.20	1.20	1.20	1.20	1.20	1.20	1.01	1.01	1.01	1.01	1.01	1.01
F/[kg/s]	833	803	574	884	876	597	607	582	417	641	638	433
Composition												
CO_2 [mol%]	13.28	14.35	14.35	13.58	14.37	14.36	1.81	1.89	1.94	1.85	1.94	1.94
H_2O [mol%]	15.48	14.17	14.18	15.47	13.71	14.20	2.01	2.08	2.08	1.95	1.95	2.08
N_2 [mol%]	68.05	68.28	68.28	68.04	68.66	68.28	91.93	91.80	91.77	92.32	91.80	91.80
O_2 [mol%]	2.37	2.38	2.37	2.10	2.45	2.35	3.20	3.20	3.18	2.85	3.28	3.16
Ar [mol%]	0.81	0.81	0.81	0.81	0.82	0.81	1.01	1.01	1.01	1.02	1.02	1.01
SO_2 [mol%]	0.00	0.00	0.00	0.00	0.00	0.00	0.00	0.00	0.00	0.00	0.00	0.00
NO [mol%]	0.00	0.00	0.00	0.00	0.00	0.00	0.00	0.00	0.00	0.00	0.00	0.00
NO_2 [ppmv]	0.00	0.00	0.00	0.00	0.00	0.00	0.00	0.00	0.00	0.00	0.00	0.00

Table D. 7 Detailed key performance results for boiler, SCR, ESP, FGD and steam turbine sections of pulverised supercritical co-fired coal and biomass power plants integrated with CO_2 capture and CO_2 compression system.

Fuel type	Coal	C80/B20	C60/B40	C40/B60	C20/B80	Biomass
Furnace/Boiler/SCR						
Coal [kg/s |bar |^{o}C]	71.3 |1.01 |15	75.6 |1.01 |15	80.4 |1.01 |15	85.9 |1.01 |15	92.26 | 1.01 | 15	99.6 |1.01 |15
Primary air [kg/s |bar |^{o}C]	168 |1.01 |15	168 |1.01 |15	167 |1.01 |15	167 |1.01 |15	164.7 | 1.01 | 15	162 |1.01 |15
Secondary Air [kg/s |bar |^{o}C]	548 |1.01 |15	547 |1.01 |15	545 |1.01 |15	543 |1.01 |15	536.2 | 1.01 | 15	528 |1.01 |15
Air Infiltration [kg/s |bar |^{o}C]	12.4 |1.01 |15	11.19|1.01 |15	11.23 |1.01 |15	11.25 |1.01 |15	11.3 | 1.01 | 15	11.4 |1.01 |15
NH_3 injected [kg/s |bar |^{o}C]	1.70 |7.24 |15	1.60 |7.24 |15	1.50 |7.24 |15	1.4 |7.24 |15	1.27 | 7.24 | 15	1.10 |7.24 |15
Flue gas, ESP inlet [kg/s |bar |^{o}C]	795 |1.01 |169	797 |1.01 |169	800 |1.01 |169	804 |1.01 |169	803.4| 1.01 | 169	802 |1.01 |169
Slag [kg/s]	1.4	1.19	0.99	0.74	0.46	0.1
Primary air fans duty [MW_e]	1.8	1.8	1.8	1.8	1.7	1.7
Forced draft fans duty [MW_e]	2.5	2.5	2.5	2.5	2.5	2.4
Induced draft fans duty [MW_e]	6	6.0	6.2	6.3	6.3	6.3
Subcritical Steam Turbine						
Main steam [kg/s |bar |^{o}C]	630 |242.3 |593	630 |242.3 | 593	630 |242.3 |593	630 |242.3 |593	630 |242.3 |593	630 |242.3 |593
Reheat to furnace/boiler [kg/s |bar |^{o}C]	514 |49 |348	514 |49 |348	514 |49 |348	514 |49 |348	514 |49 |348	514 |49 |348
Reheat from furnace/boiler [kg/s |bar |^{o}C]	514 |45.2 |593	514 |45.2 |593	514 |45.2 |593	514 |45.2 |593	514 |45.2 |593	514 |45.2 |593
Steam to stripper reboiler [kg/s |bar |^{o}C]	233 |5.07 |296	225 |5.07 |296	226 |5.07 |296	228 |5.07 |296	223 |5.07 |296	230 |5.07 |296
Condensate return from stripper [kg/s |bar |^{o}C]	233 |3 |130	225 |3 |130	226 |3 |130	228 |3 |130	223 |3 |130	230 |3 |130
Condensate, condenser outlet [kg/s |bar |^{o}C]	246 |0.07 |38	225 |0.07 |38	243 |0.07 |38	242 |0.07 |38	240 |0.07 |38	239 |0.07 |38
Boiler feed water, economiser inlet [kg/s |bar	630 |288.5 |283	630|288.5 |283	630 |288.5 |283	630 |288.5 |283	630 |288.5 |283	630 |288.5 |283

	[°C]											
EPS/FGD												
Fly ash [kg/s]	5.53	1.01	169	4.77	1.01	169	3.93	1.01	169	2.96	1.01	169	1.8	1.01	169	0.55	1.01	169
Lime slurry [kg/s]	19.50	1.03	15	16.60	1.03	15	13.3	1.03	15	9.5	1.03	15	3.6	1.03	15	0.21	1.03	15
Oxidation Air [kg/s]	3.69	1.01	15	3.20	1.01	15	2.5	1.01	15	1.8	1.01	15	0.98	1.01	15	0.04	1.01	15
Makeup water [kg/s]	54.38	1.01	15	46.30	1.01	15	37	1.01	15	26.6	1.01	15	14.4	1.01	15	0.60	1.01	15
Flue gas, FGD outlet [kg/s |bar |[°C]	833	1.01	58	830	1.01	58	829	1.01	58	827	1.01	58	819	1.01	58	803	1.01	58
Gypsum, moisture-free (kg/s]	9.6			8.2			6.5			4.7			2.55			0.1		
CO_2 emitted [kg/hr]	608623			612995.0			617838			623450			625808			627193		

Table D. 8 Detailed key performance results for CO_2 capture and CO_2 compression sections of pulverised supercritical co-fired coal and biomass power plants integrated with CO_2 capture and CO_2 compression system.

Fuel type	Coal	C80/B20	C60/B40	C40/B60	C20/B80	Biomass
CO_2 Capture Plant						
Flue gas, absorber inlet [kg/s |bar |^oC]	833 |1.2 |40	830 |1.20 |40	829 |1.20 |40	827 |1.20 |40	819 |1.20 |40	597 |1.20 |40
Flue gas, absorber outlet [kg/s |bar |^oC]	607 |1.01 |41	604 |1.01 |42	603 |1.01 |41	582 |1.01 |43	591 |1.01 |42	433 |1.01 |43
Lean MEA solution, absorber inlet [kg/s |bar |^oC]	2403 |3.00 |40	2414 | 3.00 |40	2423 |3.00 |40	2453 | 3.00 |40	2464 | 3.00 |40	1816 | 3.00 |40
Lean MEA solution, stripper outlet [kg/s |bar |^oC]	2403 |1.62 |117	2414 |1.62 |117	2423 |1.62 |117	2453 |1.62 |117	2464 |1.62 |117	1816 |1.62 |117
Rich MEA solution, absorber outlet [kg/s |bar |^oC]	2628 |1.01 |44	2640 |1.01 | 44	2628 |1.01 |44	2681 |1.01 |45	2692 |1.01 |45	1980 |1.01 |45
Rich MEA solution, stripper inlet [kg/s |bar |^oC]	2628 |3.00 |107	2640 |3.00 |107	2628 |3.00 |107	2681 |3.00 |107	2692 |3.00 |107	1980 |3.00 |107
MEA concentration, CO_2 free basis [kg/kg]	0.3	0.3	0.3	0.3	0.3	0.3
Lean CO_2 loading [mol/mol]	0.2	0.2	0.2	0.2	0.2	0.2
Rich CO_2 loading [mol/mol]	0.479	0.479	0.479	0.480	0.480	0.480
Lean MEA solution cooler inlet temperature [^oC]	48.4	48.4	48.3	48.6	48.8	48.6
CO_2 captured [kg/s]	152.0	153.0	154.4	155.7	156.5	116.7
Reboiler heat duty [MW_{th}]	560.1	562.9	560.2	572.1	574.9	424.4
Specific reboiler duty [MJ/kg CO_2]	3.686	3.679	3.677	3.675	3.674	3.638
Stripper condenser duty [MW_{th}]	226.6	269.9	269.8	231.4	232.2	171.0
Lean MEA solution cooler duty [MW_{th}]	72.3	72.5	71.8	75.9	78.0	55.8
Lean/Rich heat exchanger duty [MW_{th}]	604.4	607.3	604.9	614.8	615.9	455.4
Lean MEA solution pump duty [kW_e]	388.0	390.9	389.1	397.2	399.0	294.0

Rich MEA solution pump duty [kW_e]	550.8	553.3	550.8	561.9	564.2	414.4
Absorber pressure drop [kPa]	2.93	2.46	2.88	2.46	2.43	1.28
Absorber fractional approach to flooding	0.72	0.68	0.72	0.68	0.68	0.49
Stripper pressure drop [kPa]	1.48	1.07	1.78	1.10	1.11	6.25
Stripper fractional approach to flooding	0.71	0.65	0.78	0.66	0.66	0.49
Stripper condenser pressure [bar]	1.62	1.62	1.62	1.62	1.62	1.62
Booster fan duty (MW_e]	19.1	19.4	19.0	19.3	19.1	13.8
CO_2 Compression System						
Total compression duty [MW_e]	44.90	45.26	45.03	46.04	46.29	34.53
Total intercooling duty [MW_{th}]	76.90	77.57	77.18	78.92	79.35	59.14

Table D. 9 Detailed energy performance results for pulverised supercritical co-fired coal and biomass power plants integrated with CO_2 capture and CO_2 compression system.

Fuel type	Coal	C80/B20	C60/B40	C40/B60	C20/B80	Biomass
Fuel heat input, HHV [MW_{th}]	1933	1932.9	1932.9	1932.9	1932.9	1371
Steam turbine power, without steam extraction [MW_e]	800	800	800	800	800	548
Steam turbine power, with steam extraction [MW_e]	664	661.5	659.4	658.2	657.1	410
Power plant auxiliary loads [MW_e]	12	11.56	11.47	11.38	11.2	8
Other auxiliary loads [MW_e]*	30	30	30	30	30	30
CO_2 capture plant auxiliary loads [MW_e]	20.04	20.37	19.92	20.27	20.07	14.50
CO_2 Compression loads [MW_e]	44.90	45.26	45.03	46.04	46.29	34.53
Power output without CO_2 capture and compression [MW_e]	758	758	758	758	758	510
Power output with CO_2 capture only [MW_e]	602	599.6	598	596.55	595.8	396
Power output with CO_2 capture and compression [MW_e]	557	554.32	552.98	550.51	549.53	361
Efficiency without CO_2 capture and compression [%], HHV	39.22	39.30	39.30	39.30	39.30	37.20
Efficiency with CO_2 capture only [%], HHV	31.16	31.02	30.94	30.86	30.83	28.87
Efficiency with CO_2 capture and compression [%], HHV	28.84	28.68	28.61	28.48	28.43	26.35
Efficiency penalty with CO_2 capture only [%]	8.1	8.3	8.4	8.4	8.5	8.3
Efficiency penalty with CO_2 capture and compression [%]	10.4	10.6	10.7	10.8	10.9	10.9
Specific CO_2 emissions from power plant [g/kWh]	1092	1105.9	1117.3	1132.5	1138.8	1293
Specific CO_2 compression work [MJ/kg]	0.2954	0.2958	0.2916	0.2957	0.2958	0.2959
Specific losses per unit of CO_2 captured [$\%/kgs^{-1}$]	0.0530	0.0541	0.0541	0.0542	0.0541	0.0714

* Based on auxiliary load reported by 2010 Report of US Department of Energy [263].

Table D. 10 Detailed flue gas composition at different locations for pulverised supercritical co-fired coal and biomass power plants integrated with CO_2 capture and CO_2 compression system.

Location	SCR inlet						FGD inlet					
	Coal	C80/B20	C60/B40	C40/B60	C20/B80	Biomass	Coal	C80/B20	C60/B40	C40/B60	C20/B80	Biomass
T/[^oC]	297	297	297	297	297	297	176	176	176	176	176	176
P/[bara]	0.99	0.99	0.99	0.99	0.99	0.99	1.06	1.06	1.06	1.06	1.06	1.06
F/[kg/s]	754	756	760	763	764	763	795	797	800	804	803	802
Composition												
CO_2 [mol%]	14.97	15.02	15.05	15.09	15.12	15.13	14.14	14.19	14.24	14.29	14.33	14.36
H_2O [mol%]	8.94	9.76	10.66	11.68	12.92	14.38	9.05	9.80	10.62	11.55	12.70	14.05
N_2 [mol%]	72.90	72.14	71.31	70.37	69.23	67.90	73.16	72.44	71.64	70.75	69.66	68.38
O_2 [mol%]	1.69	1.65	1.62	1.59	1.56	1.53	2.56	2.52	2.50	2.45	2.42	2.38
Ar [mol%]	0.87	0.86	0.85	0.84	0.83	0.81	0.87	0.86	0.85	0.84	0.83	0.81
SO_2 [mol%]	0.22	0.19	0.15	0.11	0.06	0.00	0.21	0.18	0.14	0.10	0.05	0.00
NO [mol%]	0.39	0.37	0.35	0.32	0.29	0.25	0.00	0.00	0.00	0.00	0.00	0.00
NO_2 [ppmv]	0.00	0.01	0.01	0.01	0.01	0.01	0.00	0.00	0.00	0.00	0.00	0.00

Location	CO_2 absorber inlet						CO_2 absorber outlet					
	Coal	C80/B20	C60/B40	C40/B60	C20/B80	Biomass	Coal	C80/B20	C60/B40	C40/B60	C20/B80	Biomass
T/[^oC]	40	40	40	40	40	40	41	42	41	42	42	43
P/[bara]	1.20	1.20	1.20	1.20	1.20	1.20	1.01	1.01	1.01	1.01	1.01	1.01
F/[kg/s]	833	830	829	827	819	803	607	604	603	598	591	582
Composition												
CO_2 [mol%]	13.28	13.42	13.56	13.73	13.93	14.35	1.81	1.83	2.06	1.88	1.88	1.89
H_2O [mol%]	15.48	15.48	15.48	15.50	15.40	14.17	2.01	2.08	1.94	2.08	2.08	2.08
N_2 [mol%]	68.05	67.94	67.80	67.64	67.53	68.28	91.93	91.87	91.78	91.84	91.83	91.80
O_2 [mol%]	2.37	2.35	2.35	2.34	2.34	2.38	3.20	3.18	3.18	3.18	3.18	3.20
Ar [mol%]	0.81	0.81	0.80	0.80	0.80	0.81	1.01	1.02	1.01	1.01	1.01	1.01
SO_2 [mol%]	0.00	0.00	0.00	0.00	0.00	0.00	0.00	0.00	0.00	0.00	0.00	0.00
NO [mol%]	0.00	0.00	0.00	0.00	0.00	0.00	0.00	0.00	0.00	0.00	0.00	0.00
NO_2 [ppmv]	0.00	0.00	0.00	0.00	0.00	0.00	0.00	0.00	0.00	0.00	0.00	0.00

List of References

1. IEA, *World Energy Outlook 2012*. 2012: OECD Publishing.
2. IEA, *World Energy Outlook 2015*. 2015: OECD/IEA Publishing.
3. WHO, *Tackling the Global Clean Air Challenge.* World Health Organization, 2011. Geneva.
4. Chen, L., S.Z. Yong, and A.F. Ghoniem, *Oxy-fuel combustion of pulverized coal: Characterization, fundamentals, stabilization and CFD modeling.* Progress in Energy and Combustion Science, 2012. 38(2): p. 156-214.
5. Protocol, K., *United Nations framework convention on climate change.* Kyoto Protocol, Kyoto, 1997.
6. IPCC, *Climate Change 2007-Mitigation of Climate Change*. 2007.
7. IEA Statistics, *CO_2 emissions from fuel combustion-highlights*. 2011, IEA.
8. Pachauri, R.K., M.R. Allen, V. Barros, J. Broome, W. Cramer, R. Christ, J. Church, L. Clarke, Q. Dahe, and P. Dasgupta, *Climate change 2014: synthesis Report. Contribution of working groups I, II and III to the fifth assessment report of the intergovernmental panel on climate change*. 2014: IPCC.
9. IEA, *Energy Policies of IEA Countries The United Kingdom 2012 Review.* OECD/IEA, 2012. Paris, France.
10. Climate Change, *The Scientific Basis. Intergovernmental Panel on Climate Change*, in *by JT Houghton, Y. Ding, DJ Griggs, et al*. 2001.
11. D'Aprile, A., *Advances and Slowdowns in Carbon Capture and Storage Technology Development.* 2016.
12. Boden, T.A., G. Marland, and R.J. Andres, *Global, Regional, and National Fossil-Fuel CO_2 Emissions.* , in *Carbon Dioxide Information Analysis Center, Oak Ridge National Laboratory*. 2010, U.S. Department of Energy: Oak Ridge, Tenn., U.S.A.
13. IPCC, *Mitigation of Climate Change. Contribution of Working Group III to the Fifth Assessment Report of the Intergovernmental Panel on Climate Change.* Cambridge University Press, Cambridge, UK and New York, NY, 2014.
14. Scripps Institution of Oceanography. *A Daily Record of Atmospheric Carbon Dioxide from Scripps Institution of Oceanography at UC San Diego*. [cited 2013 June 11]; Available from: http://keelingcurve.ucsd.edu/.
15. Meinshausen, M., N. Meinshausen, W. Hare, S.C. Raper, K. Frieler, R. Knutti, D.J. Frame, and M.R. Allen, *Greenhouse-gas emission targets for limiting global warming to 2 ^oC.* Nature, 2009. 458(7242): p. 1158-1162.
16. IEA, *Carbon Capture and Storage: The solution for deep emissions reductions*. 2015: OECD/IEA Publishing.
17. DECC, *CCS Roadmap Innovation and R&D.* DECC, 2012.
18. Burnard, K. and S. Bhattacharya, *Power Generation from Coal: Ongoing Developments and Outlook*. 2011, OECD Publishing.

19. IEA, *Fossil Fuel-Fired Power Generation Case Studies of Recently Constructed Coal-and Gas fired Power Plants*. 2007: OECD Publishing.
20. Finkenrath, M., J. Smith, and D. Volk, *CCS Retrofit: Analysis of the Globally Installed Coal-Fired Power Plant Fleet*. 2012, OECD Publishing.
21. Rohstoffe, B.B.f.G.u., *German Federal Institute for Geosciences and Natural Resources), "Energierohstoffe 2011, Reserven, Ressourcen, Verfügbarkeit", Tabellen (Energy Resources 2011, Reserves, Resources, Availability, Tables)*. BGR, Hannover, Germany.
22. IEA, *Gas Medium-Term Market Report 2015 - Market Analysis and Forecasts to 2020*. 2015: OECD/IEA Publishing.
23. Van der Hoeven, M., *World Energy Outlook 2013.* International Energy Agency: Tokyo, Japan, 2013.
24. Kurt, H., Z. Recebli, and E. Gedik, *Performance analysis of open cycle gas turbines.* International Journal of Energy Research, 2009. 33(3): p. 285-294.
25. Liss, W.E., *Natural gas power systems for the distributed generation market.* Proc. Power-Gen Int, 1999.
26. Demirbaş, A., *Sustainable cofiring of biomass with coal.* Energy Conversion and Management, 2003. 44(9): p. 1465-1479.
27. McKendry, P., *Energy production from biomass (part 1): overview of biomass.* Bioresource technology, 2002. 83(1): p. 37-46.
28. IEA, *Technology Roadmap - Bioenergy for Heat and Power*. 2012: OECD/IEA Publishing.
29. Frequently Asked Questions. *Answers to ten frequently asked questions about bioenergy, carbon sinks and their role in global climate change*. [cited 2016 January 21]; Available from: http://www.task38.org/.
30. Baxter, L., *Biomass-coal co-combustion: opportunity for affordable renewable energy.* Fuel, 2005. 84(10): p. 1295-1302.
31. Pires, J., F. Martins, M. Alvim-Ferraz, and M. Simões, *Recent developments on carbon capture and storage: An overview.* Chemical Engineering Research and Design, 2011. 89(9): p. 1446-1460.
32. Buhre, B.J.P., L.K. Elliott, C.D. Sheng, R.P. Gupta, and T.F. Wall, *Oxy-fuel combustion technology for coal-fired power generation.* Progress in Energy and Combustion Science, 2005. 31(4): p. 283-307.
33. Wall, T.F., *Combustion processes for carbon capture.* Proceedings of the Combustion Institute, 2007. 31(1): p. 31-47.
34. Figueroa, J.D., T. Fout, S. Plasynski, H. McIlvried, and R.D. Srivastava, *Advances in CO_2 capture technology—The US Department of Energy's Carbon Sequestration Program.* International Journal of Greenhouse Gas Control, 2008. 2(1): p. 9-20.
35. Bennaceur, K., D. Gielen, T. Kerr, and C. Tam, *CO_2 capture and storage: a key carbon abatement option*. 2008: OECD.
36. Metz, B., O. Davidson, H. De Coninck, M. Loos, and L. Meyer, *Carbon dioxide capture and storage.* 2005.
37. VGB PowerTech. *Electricity Generation - Facts and Figures*. [cited 2013 November 14]; Available from: http://www.vgb.org/en/data_powergeneration.html.

38. IEA, *Technology Roadmap Carbon Capture and Storage* 2013 edition ed. 2013: OECD/IEA Publishing.
39. IEA, *Tracking Clean Energy Progress 2016 - Energy Technology Perspectives 2016 Excerpt IEA Input to the Clean Energy Ministerial*. 2016: OECD/IEA Publisihing.
40. Gibbins, J., *Retrofitting CO2 capture to existing power plants.* IEA Greenhouse Gas Programme, Cheltenham, UK (Report No. 2011/2), 2011.
41. Gibbins, J., H. Chalmers, M. Lucquiaud, J. Li, N. McGlashan, X. Liang, and J. Davison, *Techno-economic assessment of CO 2 capture retrofit to existing power plants.* Energy Procedia, 2011. 4: p. 1835-1842.
42. IEAGHG, *Ready for CCS retrofit: The potential for equipping China's existing coal fleet with carbon capture and storage.* International Energy Agency, 2016. Paris.
43. Metz, B., O. Davidson, H. de Coninck, M. Loos, and L. Meyer, *IPCC special report on carbon dioxide capture and storage*. 2005, Intergovernmental Panel on Climate Change, Geneva (Switzerland). Working Group III.
44. Chmielniak, T., S. Lepszy, and K. Wójcik, *Analysis of gas turbine combined heat and power system for carbon capture installation of coal-fired power plant.* Energy, 2012. 45(1): p. 125-133.
45. Wang, M., A. Lawal, P. Stephenson, J. Sidders, and C. Ramshaw, *Post-combustion CO2 capture with chemical absorption: A state-of-the-art review.* Chemical Engineering Research and Design, 2011. 89(9): p. 1609-1624.
46. Toftegaard, M.B., J. Brix, P.A. Jensen, P. Glarborg, and A.D. Jensen, *Oxy-fuel combustion of solid fuels.* Progress in Energy and Combustion Science, 2010. 36(5): p. 581-625.
47. DECC, *Provisional estimates of UK Greenhouse Gas emissions for 2015, including quarterly emissions for 4th quarter 2015*. 2016: London.
48. Pilavachi, P., *Mini-and micro-gas turbines for combined heat and power.* Applied Thermal Engineering, 2002. 22(18): p. 2003-2014.
49. Pilavachi, P., *Power generation with gas turbine systems and combined heat and power.* Applied Thermal Engineering, 2000. 20(15): p. 1421-1429.
50. Eckardt, D. and P. Rufli, *Advanced gas turbine technology: ABB/BCC historical firsts.* Journal of engineering for gas turbines and power, 2002. 124(3): p. 542-549.
51. Giampaolo, T., *The gas turbine handbook: Principles and practices*. 2003: CRC Press.
52. Boyce, M.P., *Gas turbine engineering handbook*. 2012: Access Online via Elsevier.
53. Saravanamuttoo, H., G.F. Rogers, and H. Cohen, *Gas turbine theory*. 2001: Pearson Education.
54. Yeh, S. and E.S. Rubin, *A centurial history of technological change and learning curves for pulverized coal-fired utility boilers.* Energy, 2007. 32(10): p. 1996-2005.

55. Lee, J.J., D.W. Kang, and T.S. Kim, *Development of a gas turbine performance analysis program and its application.* Energy, 2011. 36(8): p. 5274-5285.
56. Kim, T. and S. Hwang, *Part load performance analysis of recuperated gas turbines considering engine configuration and operation strategy.* Energy, 2006. 31(2): p. 260-277.
57. Badran, O.O., *Gas-turbine performance improvements.* Applied Energy, 1999. 64(1): p. 263-273.
58. Massardo, A. and M. Scialo, *Thermoeconomic analysis of gas turbine based cycles.* Journal of engineering for gas turbines and power, 2000. 122(4): p. 664-671.
59. Jeong, D.H., S.H. Yoon, J.J. Lee, and T.S. Kim, *Evaluation of component characteristics of a reheat cycle gas turbine using measured performance data.* Journal of Mechanical Science and Technology, 2008. 22(2): p. 350-360.
60. Zhanga, J., L. Ma, Z. Li, and W. Ni, *Modeling an Air-Cooled Gas Turbine of the Integrated Gasification Combined Cycle in Aspen plus.* Young, 2012. 4: p. 5.
61. Zhang, N. and N. Lior, *A novel near-zero CO_2 emission thermal cycle with LNG cryogenic exergy utilization.* Energy, 2006. 31(10): p. 1666-1679.
62. Chiaramonti, D., A.M. Rizzo, A. Spadi, M. Prussi, G. Riccio, and F. Martelli, *Exhaust emissions from liquid fuel micro gas turbine fed with diesel oil, biodiesel and vegetable oil.* Applied Energy, 2013. 101: p. 349-356.
63. Tyagi, A. and Y.K. Chauhan, *A Prospective on Modeling and Performance Analysis of Micro-turbine Generation System.*
64. Jonsson, M. and J. Yan, *Humidified gas turbines - a review of proposed and implemented cycles.* Energy, 2005. 30(7): p. 1013-1078.
65. Lee, J.J., J.E. Yoon, T.S. Kim, and J.L. Sohn, *Performance test and component characteristics evaluation of a micro gas turbine.* Journal of mechanical science and technology, 2007. 21(1): p. 141-152.
66. Guda, S., C. Wang, and M. Nehrir, *Modeling of microturbine power generation systems.* Electric Power Components and Systems, 2006. 34(9): p. 1027-1041.
67. Zaltash, A., A. Petrov, D. Rizy, S. Labinov, E. Vineyard, and R. Linkous, *Laboratory R&D on integrated energy systems (IES).* Applied thermal engineering, 2006. 26(1): p. 28-35.
68. do Nascimento, M.A.R., L. de Oliveira Rodrigues, E.C. dos Santos, E.E.B. Gomes, F.L.G. Dias, E.I.G. Velásques, and R.A.M. Carrillo, *Micro Gas Turbine Engine: A Review.* 2013.
69. Henke, M., T. Monz, and M. Aigner, *Inverted Brayton Cycle With Exhaust Gas Recirculation—A Numerical Investigation.* Journal of Engineering for Gas Turbines and Power, 2013. 135(9): p. 091203.
70. Poullikkas, A., *An overview of current and future sustainable gas turbine technologies.* Renewable and Sustainable Energy Reviews, 2005. 9(5): p. 409-443.
71. Heppenstall, T., *Advanced gas turbine cycles for power generation: a critical review.* Applied Thermal Engineering, 1998. 18(9): p. 837-846.

72. Galanti, L. and A.F. Massardo, *Micro gas turbine thermodynamic and economic analysis up to 500kW$_e$ size.* Applied Energy, 2011. 88(12): p. 4795-4802.
73. McDonald, C.F., *Low-cost compact primary surface recuperator concept for microturbines.* Applied Thermal Engineering, 2000. 20(5): p. 471-497.
74. Traverso, A., F. Calzolari, and A. Massardo, *Transient analysis of and control system for advanced cycles based on micro gas turbine technology.* Journal of engineering for gas turbines and power, 2005. 127(2): p. 340-347.
75. Peirs, J., D. Reynaerts, and F. Verplaetsen, *A microturbine for electric power generation.* Sensors and Actuators A: Physical, 2004. 113(1): p. 86-93.
76. Colombo, L.P., F. Armanasco, and O. Perego, *Experimentation on a cogenerative system based on a microturbine.* Applied thermal engineering, 2007. 27(4): p. 705-711.
77. Lee, J.J., M.S. Jeon, and T.S. Kim, *The influence of water and steam injection on the performance of a recuperated cycle microturbine for combined heat and power application.* Applied energy, 2010. 87(4): p. 1307-1316.
78. De Sa, A. and S. Al Zubaidy, *Gas turbine performance at varying ambient temperature.* Applied Thermal Engineering, 2011. 31(14): p. 2735-2739.
79. Farzaneh-Gord, M. and M. Deymi-Dashtebayaz, *A new approach for enhancing performance of a gas turbine (case study: Khangiran refinery).* Applied Energy, 2009. 86(12): p. 2750-2759.
80. Earnest, E.R., *Turbine engine with exhaust gas recirculation*. 1981, Google Patents.
81. Ferrari, M.L., M. Pascenti, L. Magistri, and A.F. Massardo, *Micro gas turbine recuperator: steady-state and transient experimental investigation.* Journal of engineering for gas turbines and power, 2010. 132(2).
82. Ferrari, M.L., A. Sorce, M. Pascenti, and A.F. Massardo, *Recuperator dynamic performance: Experimental investigation with a microgas turbine test rig.* Applied Energy, 2011. 88(12): p. 5090-5096.
83. Kesseli, J., T. Wolf, J. Nash, and S. Freedman. *Micro, industrial, and advanced gas turbines employing recuperators*. 2003. ASME.
84. Nishida, K., T. Takagi, and S. Kinoshita, *Regenerative steam-injection gas-turbine systems.* Applied Energy, 2005. 81(3): p. 231-246.
85. Delattin, F., S. Bram, S. Knoops, and J. De Ruyck, *Effects of steam injection on microturbine efficiency and performance.* Energy, 2008. 33(2): p. 241-247.
86. Rao, A.D. and W.H. Day, *Mitigation of greenhouse gases from gas turbine power plants.* Energy conversion and management, 1996. 37(6): p. 909-914.
87. Parente, J., A. Traverso, and A. Massardo. *Micro Humid Air Cycle: Part A - Thermodynamic and Technical Aspects*. 2003. ASME.
88. Parente, J., A. Traverso, and A. Massardo. *Micro Humid Air Cycle: Part B - Thermoeconomic Analysis*. 2003. ASME.

89. Bolland, O. and P. Mathieu, *Comparison of two CO_2 removal options in combined cycle power plants.* Energy Conversion and Management, 1998. 39(16): p. 1653-1663.
90. Ditaranto, M., J. Hals, and T. Bjørge, *Investigation on the in-flame NO reburning in turbine exhaust gas.* Proceedings of the Combustion Institute, 2009. 32(2): p. 2659-2666.
91. ElKady, A.M., T.P. Ursin, A. Lynghjem, A. Evulet, and A. Brand, *Application of exhaust gas recirculation in a DLN F-class combustion system for postcombustion carbon capture.* Journal of Engineering for Gas Turbines and Power, 2009. 131(3): p. 034505.
92. Evulet, A.T., A.M. ELKady, A.R. Branda, and D. Chinn, *On the Performance and Operability of GE's Dry Low NO_x Combustors utilizing Exhaust Gas Recirculation for PostCombustion Carbon Capture.* Energy Procedia, 2009. 1(1): p. 3809-3816.
93. Cameretti, M.C., R. Piazzesi, F. Reale, and R. Tuccillo, *Combustion simulation of an exhaust gas recirculation operated micro-gas turbine.* Journal of engineering for gas turbines and power, 2009. 131(5).
94. Cameretti, M.C., F. Reale, and R. Tuccillo, *Cycle optimization and combustion analysis in a low-NO_x micro-gas turbine.* Journal of engineering for gas turbines and power, 2007. 129(4): p. 994-1003.
95. Cameretti, M.C., F. Reale, and R. Tuccillo. *NO_x suppression from a Micro-gas turbine approaching the mild-combustion regime*. 2007. ASME.
96. Cameretti, M.C., R. Tuccillo, and R. Piazzesi, *Study of an EGR Equipped Micro Gas Turbine supplied with bio-fuels.* Applied Thermal Engineering, 2013.
97. Cavaliere, A. and M. de Joannon, *Mild combustion.* Progress in Energy and Combustion science, 2004. 30(4): p. 329-366.
98. Levy, Y., V. Sherbaum, and V. Erenburg. *Fundamentals of Low-NO_x Gas Turbine Adiabatic Combustor*. 2005. ASME.
99. SipÃķcz, N. and M. Assadi, *Combined cycles with CO_2 capture: two alternatives for system integration.* Journal of Engineering for Gas Turbines and Power, 2010. 132(6): p. 061701.
100. Jonshagen, K., N. Sipöcz, and M. Genrup. *Optimal Combined cycle for CO_2 capture with EGR*. in *ASME Turbo Expo 2010: Power for Land, Sea, and Air*. 2010. American Society of Mechanical Engineers.
101. Biliyok, C., R. Canepa, M. Wang, and H. Yeung, *Techno-Economic Analysis of a Natural Gas Combined Cycle Power Plant with CO_2 Capture*, in *Computer Aided Chemical Engineering*, K. Andrzej and T. Ilkka, Editors. 2013, Elsevier. p. 187-192.
102. Botero, C., M. Finkenrath, M. Bartlett, R. Chu, G. Choi, and D. Chinn, *Redesign, Optimization, and Economic Evaluation of a Natural Gas Combined Cycle with the Best Integrated Technology CO_2 Capture.* Energy Procedia, 2009. 1(1): p. 3835-3842.
103. Canepa, R., M. Wang, C. Biliyok, and A. Satta, *Thermodynamic analysis of combined cycle gas turbine power plant with post-combustion CO_2 capture and exhaust gas recirculation.* Proceedings of the Institution of Mechanical Engineers, Part E: Journal of Process Mechanical Engineering, 2013. 227(2): p. 89-105.
104. Li, H., M. Ditaranto, and D. Berstad, *Technologies for increasing CO_2 concentration in exhaust gas from natural gas-fired power production*

with post-combustion, amine-based CO_2 capture. Energy, 2011. 36(2): p. 1124-1133.
105. Li, H., G. Haugen, M. Ditaranto, D. Berstad, and K. Jordal, *Impacts of exhaust gas recirculation (EGR) on the natural gas combined cycle integrated with chemical absorption CO_2 capture technology.* Energy Procedia, 2011. 4: p. 1411-1418.
106. Biliyok, C. and H. Yeung, *Evaluation of natural gas combined cycle power plant for post-combustion CO_2 capture integration.* International Journal of Greenhouse Gas Control, 2013. 19(0): p. 396-405.
107. Canepa, R. and M. Wang, *Techno-economic analysis of a CO_2 capture plant integrated with a commercial scale combined cycle gas turbine (CCGT) power plant.* Applied Thermal Engineering, 2015. 74(0): p. 10-19.
108. Sipöcz, N. and F.A. Tobiesen, *Natural gas combined cycle power plants with CO_2 capture – Opportunities to reduce cost.* International Journal of Greenhouse Gas Control, 2012. 7(0): p. 98-106.
109. Majoumerd, M.M., H.N. Somehsaraei, M. Assadi, and P. Breuhaus, *Micro gas turbine configurations with carbon capture-Performance assessment using a validated thermodynamic model.* Applied Thermal Engineering, 2014.
110. Nikpey, H., M.M. Majoumerd, M. Assadi, and P. Breuhaus, *Thermodynamic analysis of innovative micro gas turbine cycles*, in *ASME Turbo Expo 2014: Germany*. 2014, American Society of Mechanical Engineers.
111. Akram, M., B. Khandelwal, S. Blakey, and C.W. Wilson. *Preliminary Calculations on Post Combustion Carbon Capture From Gas Turbines With Flue Gas Recycle*. in *ASME Turbo Expo 2013: Turbine Technical Conference and Exposition*. 2013. American Society of Mechanical Engineers.
112. Smith, J., *Van ness, Abbott, MM, Introduction to Chemical Engineering Thermodynamic.* McGraw-Hill, Boston, 2001. 329: p. 354.
113. Sonntag, R.E., C. Borgnakke, G.J. Van Wylen, and S. Van Wyk, *Fundamentals of thermodynamics*. 1998: Wiley New York.
114. Simões-Moreira, J.R., *Fundamentals of Thermodynamics Applied to Thermal Power Plants*, in *Thermal Power Plant Performance Analysis*. 2012, Springer. p. 7-39.
115. Moran, M.J., H.N. Shapiro, D.D. Boettner, and M. Bailey, *Fundamentals of engineering thermodynamics*. 2010: Wiley. com.
116. Rao, A.B. and E.S. Rubin, *A technical, economic, and environmental assessment of amine-based CO_2 capture technology for power plant greenhouse gas control.* Environmental science & technology, 2002. 36(20): p. 4467-4475.
117. Davison, J., *Performance and costs of power plants with capture and storage of CO_2.* Energy, 2007. 32(7): p. 1163-1176.
118. Kohl, A.L. and R. Nielsen, *Gas purification*. 1997: Gulf Professional Publishing.
119. Besong, M.T., M.M. Maroto-Valer, and A.J. Finn, *Study of design parameters affecting the performance of CO_2 purification units in oxy-fuel combustion.* International Journal of Greenhouse Gas Control, 2013. 12(0): p. 441-449.

120. Horn, F.L. and M. Steinberg, *Control of carbon dioxide emissions from a power plant (and use in enhanced oil recovery).* Fuel, 1982. 61(5): p. 415-422.
121. IEA, *Microalgae removal of CO_2 from flue gas*. 2015: London.
122. Molburg, J.C., R. Doctor, N.F. Brockmeier, and S. Plasynski. *CO_2 capture from PC boilers with O_2-firing*. in *18th Annual International Pittsburgh Coal Conference, Newcastle, New South Wales, Australia*. 2001.
123. Sayre, R., *Microalgae: the potential for carbon capture.* Bioscience, 2010. 60(9): p. 722-727.
124. Van Den Hende, S., H. Vervaeren, and N. Boon, *Flue gas compounds and microalgae:(Bio-) chemical interactions leading to biotechnological opportunities.* Biotechnology advances, 2012. 30(6): p. 1405-1424.
125. Bottoms, R., *Organic bases for gas purification.* Industrial & Engineering Chemistry, 1931. 23(5): p. 501-504.
126. Bottoms, R.R., *Process for separating acidic gases*, in *U.S. Patent No. 1,783,901*, U.S. Patent No. 1, 901, Editor. 1930, Google Patents.
127. Morrison, R.T. and R.N. Boyd, *Organic chemistry.* Englewood Cliffs (NJ): Prentice-Hall, 1992. 552: p. 1120.
128. Campbell, J.M., *Gas conditioning and processing. vol. 1.* 1979.
129. Akram, M., U. Ali, T. Best, S. Blakey, K. Finney, and M. Pourkashanian, *Performance evaluation of PACT Pilot-plant for CO_2 capture from gas turbines with Exhaust Gas Recycle.* International Journal of Greenhouse Gas Control, 2016. 47: p. 137-150.
130. Brigman, N., M.I. Shah, O. Falk-Pedersen, T. Cents, V. Smith, T. De Cazenove, A.K. Morken, O.A. Hvidsten, M. Chhaganlal, and J.K. Feste, *Results of amine plant operations from 30 wt% and 40 wt% aqueous MEA testing at the CO_2 Technology Centre Mongstad.* Energy Procedia, 2014. 63: p. 6012-6022.
131. Carey, J., K. Damen, F. Fitzgerald, and R. Gardiner, *CCPilot100+ Operating Experience and Test Results.* Energy Procedia, 2013. 37: p. 6170-6178.
132. Cottrell, A., J. McGregor, J. Jansen, Y. Artanto, N. Dave, S. Morgan, P. Pearson, M. Attalla, L. Wardhaugh, and H. Yu, *Post-combustion capture R&D and pilot plant operation in Australia.* Energy Procedia, 2009. 1(1): p. 1003-1010.
133. Hamborg, E.S., V. Smith, T. Cents, N. Brigman, O. Falk-Pedersen, T. De Cazenove, M. Chhaganlal, J.K. Feste, Ø. Ullestad, and H. Ulvatn, *Results from MEA testing at the CO_2 Technology Centre Mongstad. Part II: Verification of baseline results.* Energy Procedia, 2014. 63: p. 5994-6011.
134. Idem, R., M. Wilson, P. Tontiwachwuthikul, A. Chakma, A. Veawab, A. Aroonwilas, and D. Gelowitz, *Pilot plant studies of the CO_2 capture performance of aqueous MEA and mixed MEA/MDEA solvents at the University of Regina CO_2 capture technology development plant and the Boundary Dam CO_2 capture demonstration plant.* Industrial & engineering chemistry research, 2006. 45(8): p. 2414-2420.
135. Knudsen, J.N., J.N. Jensen, P.-J. Vilhelmsen, and O. Biede, *Experience with CO_2 capture from coal flue gas in pilot-scale: testing of different amine solvents.* Energy Procedia, 2009. 1(1): p. 783-790.

136. Meuleman, E., Y. Artanto, J. Jansen, M. Osborn, P. Pearson, A. Cottrell, and P. Feron. *CO_2 capture performance of MEA and blended amine solvents in CSIRO's pilot plant with flue gas from a brown coalfired power station*. in *6th International Technical Conference on Clean Coal & Fuel Systems*. 2010.
137. Morken, A.K., B. Nenseter, S. Pedersen, M. Chhaganlal, J.K. Feste, R.B. Tyborgnes, Ø. Ullestad, H. Ulvatn, L. Zhu, and T. Mikoviny, *Emission results of amine plant operations from MEA testing at the CO_2 Technology Centre Mongstad.* Energy Procedia, 2014. 63: p. 6023-6038.
138. Muhammad, A. and Y. GadelHak, *Simulation based improvement techniques for acid gases sweetening by chemical absorption: A review.* International Journal of Greenhouse Gas Control, 2015. 37: p. 481-491.
139. Notz, R., H.P. Mangalapally, and H. Hasse, *Post combustion CO_2 capture by reactive absorption: Pilot plant description and results of systematic studies with MEA.* International Journal of Greenhouse Gas Control, 2012. 6: p. 84-112.
140. Thimsen, D., A. Maxson, V. Smith, T. Cents, O. Falk-Pedersen, O. Gorset, and E.S. Hamborg, *Results from MEA testing at the CO_2 Technology Centre Mongstad. Part I: Post-Combustion CO_2 capture testing methodology.* Energy Procedia, 2014. 63: p. 5938-5958.
141. Davidson, R.M., *Post-combustion carbon capture from coal fired plants: solvent scrubbing*. 2007: IEA Clean Coal Centre London.
142. Sexton, A.J. and G.T. Rochelle, *Reaction products from the oxidative degradation of monoethanolamine.* Industrial & Engineering Chemistry Research, 2010. 50(2): p. 667-673.
143. Fredriksen, S. and K.-J. Jens, *Oxidative degradation of aqueous amine solutions of MEA, AMP, MDEA, PZ: A review.* Energy Procedia, 2013. 37: p. 1770-1777.
144. Gouedard, C., D. Picq, F. Launay, and P.L. Carrette, *Amine degradation in CO_2 capture. I. A review.* International Journal of Greenhouse Gas Control, 2012. 10: p. 244-270.
145. Lepaumier, H., D. Picq, and P.-L. Carrette, *New amines for CO_2 capture. I. Mechanisms of amine degradation in the presence of CO_2.* Industrial & Engineering Chemistry Research, 2009. 48(20): p. 9061-9067.
146. DuPart, M., T. Bacon, and D. Edwards, *Understanding corrosion in alkanolamine gas treating plants: Part 1.* Hydrocarbon Processing;(United States), 1993. 72(4).
147. DuPart, M., T. Bacon, and D. Edwards, *Understanding corrosion in alkanolamine gas treating plants: Part 2.* Hydrocarbon Processing;(United States), 1993. 72(5).
148. Kittel, J., R. Idem, D. Gelowitz, P. Tontiwachwuthikul, G. Parrain, and A. Bonneau, *Corrosion in MEA units for CO_2 capture: pilot plant studies.* Energy Procedia, 2009. 1(1): p. 791-797.
149. Zhang, Y. and C.-C. Chen, *Thermodynamic modeling for CO_2 absorption in aqueous MDEA solution with electrolyte NRTL model.* Industrial & Engineering Chemistry Research, 2010. 50(1): p. 163-175.

150. Closmann, F., T. Nguyen, and G.T. Rochelle, *MDEA/Piperazine as a solvent for CO_2 capture.* Energy Procedia, 2009. 1(1): p. 1351-1357.
151. Tan, Z., *Air pollution and greenhouse gases: from basic concepts to engineering applications for air emission control*. 2014: Springer.
152. Baron, H., *Oil and gas engineering guide*. 2010: Editions Technip.
153. Lecomte, F., P. Broutin, and É. Lebas, *CO_2 Capture: Technologies to Reduce Greenhouse Gas Emissions*. 2010: Editions Technip.
154. Vaidya, P.D. and E.Y. Kenig, *CO_2- Alkanolamine Reaction Kinetics: A Review of Recent Studies.* Chemical Engineering & Technology, 2007. 30(11): p. 1467-1474.
155. Stéphenne, K., *Start-Up of World's First Commercial Post-Combustion Coal Fired CCS Project: Contribution of Shell Cansolv to SaskPower Boundary Dam ICCS Project.* 2013.
156. Uilenreef, J. and M. Kombrink, *Flow Assurance and control philosophy: Rotterdam Opslag en Afvang Demonstratie (ROAD) project. Special report for the global carbon capture and storage institute*. 2013, Global CCS Institution Ltd.: Melbourne.
157. ErikØi, L., *Comparison of Aspen HYSYS and Aspen Plus simulation of CO_2 Absorption into MEA from Atmospheric Gas.* Energy Procedia, 2012. 23: p. 360-369.
158. Zhang, Y. and C.-C. Chen, *Modeling CO_2 Absorption and Desorption by Aqueous Monoethanolamine Solution with Aspen Rate-based Model.* Energy Procedia, 2013. 37: p. 1584-1596.
159. Agbonghae, E.O., K.J. Hughes, D.B. Ingham, L. Ma, and M. Pourkashanian, *Optimal Process Design of Commercial-Scale Amine-Based CO_2 Capture Plants.* Industrial & Engineering Chemistry Research, 2014. 53(38): p. 14815-14829.
160. Berstad, D., A. Arasto, K. Jordal, and G. Haugen, *Parametric study and benchmarking of NGCC, coal and biomass power cycles integrated with MEA-based post-combustion CO_2 capture.* Energy Procedia, 2011. 4: p. 1737-1744.
161. Oko, E., M. Wang, and A.K. Olaleye, *Simplification of detailed rate-based model of post-combustion CO_2 capture for full chain CCS integration studies.* Fuel, 2015. 142: p. 87-93.
162. Hetland, J., H.M. Kvamsdal, G. Haugen, F. Major, V. Kårstad, and G. Tjellander, *Integrating a full carbon capture scheme onto a 450MW_e NGCC electric power generation hub for offshore operations: Presenting the Sevan GTW concept.* Applied Energy, 2009. 86(11): p. 2298-2307.
163. Lindqvist, K., K. Jordal, G. Haugen, K.A. Hoff, and R. Anantharaman, *Integration aspects of reactive absorption for post-combustion CO_2 capture from NGCC (natural gas combined cycle) power plants.* Energy, 2014. 78: p. 758-767.
164. Peeters, A., A. Faaij, and W. Turkenburg, *Techno-economic analysis of natural gas combined cycles with post-combustion CO_2 absorption, including a detailed evaluation of the development potential.* International Journal of Greenhouse gas control, 2007. 1(4): p. 396-417.
165. Ali, U., C.F. Palma, K.J. Hughes, D.B. Ingham, L. Ma, and M. Pourkashanian. *Thermodynamic analysis and process system comparison of the exhaust gas recirculated, steam injected and*

humidified micro gas turbine. in *Turbine Technical Conference and Exposition*. 2015. Montreal, Canada: GT2015-42454,Proceedings of ASME Turbo Expo 2015.

166. Jonshagen, K., N. SipÃķcz, and M. Genrup, *A novel approach of retrofitting a combined cycle with post combustion CO_2 capture.* Journal of Engineering for Gas Turbines and Power, 2011. 133(1): p. 011703.
167. Bouillon, P.-A., S. Hennes, and C. Mahieux, *ECO_2: Post-combustion or Oxyfuel–A comparison between coal power plants with integrated CO_2 capture.* Energy Procedia, 2009. 1(1): p. 4015-4022.
168. Seltzer, A.H., Z. Fan, and T. Fout. *An optimized supercritical oxygen-fired pulverized coal power plant for CO2 capture*. in *31st International Coal Utilization and Fuel Systems Conference*. 2006.
169. Kim, S., H. Ahn, S. Choi, and T. Kim, *Impurity effects on the oxy-coal combustion power generation system.* International Journal of Greenhouse Gas Control, 2012. 11: p. 262-270.
170. Li, H., J. Yan, and M. Anheden, *Impurity impacts on the purification process in oxy-fuel combustion based CO< sub> 2</sub> capture and storage system.* Applied Energy, 2009. 86(2): p. 202-213.
171. Gautier, F., F. Châtel-Pélage, R.K. Varagani, P. Pranda, D. McDonald, D. Devault, H. Farzan, R.L. Schoff, J. Ciferno, and A.C. Bose, *Oxy-Combustion Process for CO2 Capture from Coal-Fired Power Plants: Engineering Case Studies and Engineering Feasibility Analysis.* Fifth Annual Conference on Carbon Sequestration, Alexandria, VA, 2006.
172. Seltzer, A., Z. Fan, and H. Hack. *Zero Emission Oxyfuel Power Generation for CO_2 Capture*. in *Power-Gen International 2010 Conference Orlando, Fl, USA December*. 2010.
173. AspenTech, *Aspen Engineering Suite V8.0.* Aspen Technology, 2012(Burlington).
174. Lipták, B.G., *Instrument Engineers' Handbook, Volume Two: Process Control and Optimization*. Vol. 2. 2010: CRC press.
175. Process System Enterprise Limited. *Advanced Process Modelling - Differences from Other Process Modelling Technologies*. [cited 2013 July 13]; Available from: http://www.psenterprise.com/concepts/apm_differences.html.
176. AspenTech. *About AspenTech*. [cited 2013 July 13]; Available from: http://www.aspentech.com/Company/About-AspenTech/.
177. AspenTech. *Process Industry Leadership*. [cited 2013 July 13]; Available from: http://www.aspentech.com/Company/Process-Industry-Leadership/.
178. Carlson, E.C., *Don't gamble with physical properties for simulations.* Chemical Engineering Progress, 1996. 92(10): p. 35-46.
179. Cumpsty, N.A., *Jet Propulsion: A simple guide to the aerodynamic and thermodynamic design and performance of jet engines*. Vol. 2. 2003: Cambridge University Press.
180. Hunecke, K., *Jet Engines: Fundamentals of Theory, Design, and Operation*. 1997: Zenith Press.
181. Nikpey Somehsaraei, H., M. Mansouri Majoumerd, P. Breuhaus, and M. Assadi, *Performance analysis of a biogas-fueled micro gas turbine*

using a validated thermodynamic model. Applied Thermal Engineering, 2014. 66(1): p. 181-190.
182. De Paepe, W., F. Delattin, S. Bram, and J. De Ruyck, *Steam injection experiments in a microturbine - A thermodynamic performance analysis.* Applied Energy, 2012. 97: p. 569-576.
183. Schultz, J.M., *The polytropic analysis of centrifugal compressors.* Journal of Engineering for Power, 1962. 84(1): p. 69-82.
184. Huntington, R., *Evaluation of polytropic calculation methods for turbomachinery performance.* Journal of Engineering for gas Turbines and Power, 1985. 107(4): p. 872-876.
185. ISO, *Turbocompressors – Performance test code Standard ISO 5389:2005.* 2005.
186. Walsh, P.P. and P. Fletcher, *Gas turbine performance*. 2004: John Wiley & Sons.
187. ISO, *Gas turbines - Procurement - Part 2: Standard reference conditions and ratings*, in *ISO 3977-2:*. 1997, International Organization for Standardization: Geneva, Switzerland.
188. Kautz, M. and U. Hansen, *The externally-fired gas-turbine (EFGT-Cycle) for decentralized use of biomass.* Applied Energy, 2007. 84(7): p. 795-805.
189. Turbec, A.B., *Technical description - T100 microturbine system*. 2000, Turbec Company. Italy. Turbec AB.
190. Ali, U., C. Font-Palma, H. Nikpey, M. Mansouri, M. Akram, K.N. Finney, T. Best, N.B. Mohd Said, M. Assadi, and M. Pourkashanian, *Benchmarking of a micro gas turbine model integrated with post-combustion CO_2 capture.* Energy 2016 [Submitted].
191. Hosseinalipour, S., E. Abdolahi, and M. Razaghi, *Static and Dynamic Mathematical Modeling of a Micro Gas Turbine.* Journal of Mechanics: p. 1-9.
192. MacKay, D.J. and T.J. Stone, *Potential greenhouse gas emissions associated with shale gas extraction and use.* London, UK: Department of Energy and Climate Change, 2013.
193. Persson, M., *Evaluation of upgrading techniques for biogas.* Report SGC, 2003. 142.
194. Akram, M., S. Blakey, and M. Pourkashanian, *Influence of gas turbine exhaust CO_2 concentration on the performance of Post combustion carbon capture plant*, in *GT2015*. 2015, Proceedings of ASME Turbo Expo 2015: Turbine Technical Conference and Exposition: Montreal, Canada.
195. Mangalapally, H.P. and H. Hasse, *Pilot plant experiments for post combustion carbon dioxide capture by reactive absorption with novel solvents.* Energy Procedia, 2011. 4: p. 1-8.
196. NETL, *Carbon Capture Approaches for Natural Gas Combined Cycle Systems", National Energy Technology Laboratory.* U.S Department of Energy, 2010: p. DOE/NETL-2011/1470.
197. Belokon, A.A., K.M. Khritov, L.A. Klyachko, S.A. Tschepin, V.M. Zakharov, and G. Opdyke. *Prediction of Combustion Efficiency and NO_x Levels for Diffusion Flame Combustors in HAT Cycles*. in *ASME Turbo Expo 2002: Power for Land, Sea, and Air*. 2002. American Society of Mechanical Engineers.

198. Hermann, F., J. Klingmann, and R. Gabrielsson. *Computational and experimental investigation of emissions in a highly humidified premixed flame*. in *ASME Turbo Expo 2003, collocated with the 2003 International Joint Power Generation Conference*. 2003. American Society of Mechanical Engineers.
199. De Paepe, W., F. Delattin, S. Bram, and J. De Ruyck, *Water injection in a micro gas turbine - Assessment of the performance using a black box method.* Applied Energy, 2013. 112: p. 1291-1302.
200. De Paepe, W., F. Contino, F. Delattin, S. Bram, and J. De Ruyck, *New concept of spray saturation tower for micro Humid Air Turbine applications.* Applied Energy, 2014.
201. De Paepe, W., M.M. Carrero, S. Bram, and F. Contino. *T100 Micro Gas Turbine Converted to Full Humid Air Operation: Test Rig Evaluation*. in *ASME Turbo Expo 2014: Turbine Technical Conference and Exposition*. 2014. American Society of Mechanical Engineers.
202. Zhang, Y., H. Que, and C.-C. Chen, *Thermodynamic modeling for CO_2 absorption in aqueous MEA solution with electrolyte NRTL model.* Fluid Phase Equilibria, 2011. 311: p. 67-75.
203. Bravo, J.L., J. Rocha, and J. Fair, *Mass transfer in gauze packings.* Hydrocarbon Processing, 1985. 64(1): p. 91-95.
204. Kister, H.Z., *Distillation design*. Vol. 223. 1992: McGraw-Hill New York.
205. Strigle, R.F., *Packed tower design and applications: random and structured packings*. 2nd ed. 1994, Houston, TX: Gulf Publishing Co.
206. Chapel, D.G., C.L. Mariz, and J. Ernest. *Recovery of CO2 from flue gases: commercial trends*. in *Canadian Society of Chemical Engineers Annual Meeting*. 1999.
207. Mangalapally, H.P., R. Notz, S. Hoch, N. Asprion, G. Sieder, H. Garcia, and H. Hasse, *Pilot plant experimental studies of post combustion CO_2 capture by reactive absorption with MEA and new solvents.* Energy Procedia, 2009. 1(1): p. 963-970.
208. Dugas, R.E., *Pilot plant study of carbon dioxide capture by aqueous monoethanolamine.* MSE Thesis, University of Texas at Austin, 2006.
209. Luo, X., M. Wang, and J. Chen, *Heat integration of natural gas combined cycle power plant integrated with post-combustion CO_2 capture and compression.* Fuel, 2015. 151: p. 110-117.
210. Kvamsdal, H.M., J. Hetland, G. Haugen, H.F. Svendsen, F. Major, V. Kårstad, and G. Tjellander, *Maintaining a neutral water balance in a 450MW_e NGCC-CCS power system with post-combustion carbon dioxide capture aimed at offshore operation.* International Journal of Greenhouse Gas Control, 2010. 4(4): p. 613-622.
211. U.S.DOE., *Current and Future Technologies for Natural Gas Combined Cycle (NGCC) Power Plants*, [DOE/NETL-341/061013], Editor. 2013 [DOE/NETL-341/061013], U.S. Department of Energy: Washington, DC.
212. Green, D.W., *Perry's chemical engineers' handbook*. 8 ed. Vol. 796. 2008: McGraw-hill New York.
213. Rubin, E.S., C. Short, G. Booras, J. Davison, C. Ekstrom, M. Matuszewski, and S. McCoy, *A proposed methodology for CO_2*

capture and storage cost estimates. International Journal of Greenhouse Gas Control, 2013. 17: p. 488-503.
214. Rubin, E.S. and H. Zhai, *The cost of carbon capture and storage for natural gas combined cycle power plants.* Environmental science & technology, 2012. 46(6): p. 3076-3084.
215. Ali, U., C.F. Palma, K.J. Hughes, D.B. Ingham, L. Ma, and M. Pourkashanian, *Impact of the operating conditions and position of exhaust gas recirculation on the performance of a micro gas turbine*, in *Computer Aided Chemical Engineering*, J.K.H. Krist V. Gernaey and G. Rafiqul, Editors. 2015, Elsevier. p. 2417-2422.
216. Bhave, A., R.H.S. Taylor, P. Fennell, W.R. Livingstond, N. Shah, N.M. Dowell, J. Dennis, M. Kraft, M. Pourkashanian, M. Insa, J. Jones, N. Burdett, A. Bauen, C. Beal, A. Samllbone, and J. Akroyd, *Screening and techno-economic assessment of biomass-based power generation with CCS technologies to meet 2050 CO_2 targets.* University of Cambridge, 2014: p. 14.
217. McIlveen-Wright, D.R., Y. Huang, S. Rezvani, D. Redpath, M. Anderson, A. Dave, and N.J. Hewitt, *A technical and economic analysis of three large scale biomass combustion plants in the UK.* Applied energy, 2013. 112: p. 396-404.
218. Thornley, P., *Increasing biomass based power generation in the UK.* Energy Policy, 2006. 34(15): p. 2087-2099.
219. Thornley, P., J. Rogers, and Y. Huang, *Quantification of employment from biomass power plants.* Renewable Energy, 2008. 33(8): p. 1922-1927.
220. McKendry, P., *Energy production from biomass (part 2): conversion technologies.* Bioresource technology, 2002. 83(1): p. 47-54.
221. Demirbas, M.F., M. Balat, and H. Balat, *Potential contribution of biomass to the sustainable energy development.* Energy Conversion and Management, 2009. 50(7): p. 1746-1760.
222. Eisentraut, A. and A. Brown, *Technology roadmap–bioenergy for heat and power.* International Energy Agency, IEA Renewable Energy Division, 2012.
223. Faaij, A.P., *Bio-energy in Europe: changing technology choices.* Energy policy, 2006. 34(3): p. 322-342.
224. Van den Broek, R., S. Teeuwisse, K. Healion, T. Kent, A. Van Wijk, A. Faaij, and W. Turkenburg, *Potentials for electricity production from wood in Ireland.* Energy, 2001. 26(11): p. 991-1013.
225. Kraxner, F., K. Aoki, S. Leduc, G. Kindermann, S. Fuss, J. Yang, Y. Yamagata, K.-I. Tak, and M. Obersteiner, *BECCS in South Korea—analyzing the negative emissions potential of bioenergy as a mitigation tool.* Renewable Energy, 2014. 61: p. 102-108.
226. Sebastián, F., J. Royo, and M. Gómez, *Cofiring versus biomass-fired power plants: GHG (Greenhouse Gases) emissions savings comparison by means of LCA (Life Cycle Assessment) methodology.* Energy, 2011. 36(4): p. 2029-2037.
227. Hein, K. and J. Bemtgen, *EU clean coal technology - co-combustion of coal and biomass.* Fuel processing technology, 1998. 54(1): p. 159-169.

228. Sami, M., K. Annamalai, and M. Wooldridge, *Co-firing of coal and biomass fuel blends.* Progress in energy and combustion science, 2001. 27(2): p. 171-214.
229. Tillman, D.A., *Cofiring benefits for coal and biomass.* Biomass and bioenergy, 2000. 19(6): p. 363-364.
230. Basu, P., J. Butler, and M.A. Leon, *Biomass co-firing options on the emission reduction and electricity generation costs in coal-fired power plants.* Renewable Energy, 2011. 36(1): p. 282-288.
231. IEA. *Biomass combustion and co-firing: global scenario*. Task 32 of the IEA bioenergy agreement [cited 2016 Januray 19]; Available from: http://www.ieabcc.nl/.
232. McIlveen-Wright, D., Y. Huang, S. Rezvani, J.D. Mondol, D. Redpath, M. Anderson, N. Hewitt, and B. Williams, *A techno-economic assessment of the reduction of carbon dioxide emissions through the use of biomass co-combustion.* Fuel, 2011. 90(1): p. 11-18.
233. Williams, A., M. Pourkashanian, and J. Jones, *Combustion of pulverised coal and biomass.* Progress in Energy and Combustion Science, 2001. 27(6): p. 587-610.
234. Mann, M. and P. Spath, *A life cycle assessment of biomass cofiring in a coal-fired power plant.* Clean Products and Processes, 2001. 3(2): p. 81-91.
235. Spliethoff, H. and K. Hein, *Effect of co-combustion of biomass on emissions in pulverized fuel furnaces.* Fuel processing technology, 1998. 54(1): p. 189-205.
236. Wang, C., Y. Wu, Q. Liu, H. Yang, and F. Wang, *Analysis of the behaviour of pollutant gas emissions during wheat straw/coal cofiring by TG-FTIR.* Fuel Processing Technology, 2011. 92(5): p. 1037-1041.
237. McIlveen-Wright, D., Y. Huang, S. Rezvani, and Y. Wang, *A technical and environmental analysis of co-combustion of coal and biomass in fluidised bed technologies.* Fuel, 2007. 86(14): p. 2032-2042.
238. Mehmood, S., B.V. Reddy, and M.A. Rosen, *Energy analysis of a biomass co-firing based pulverized coal power generation system.* Sustainability, 2012. 4(4): p. 462-490.
239. Kumar, A., J.B. Cameron, and P.C. Flynn, *Biomass power cost and optimum plant size in western Canada.* Biomass and Bioenergy, 2003. 24(6): p. 445-464.
240. De, S. and M. Assadi, *Impact of cofiring biomass with coal in power plants - A techno-economic assessment.* Biomass and Bioenergy, 2009. 33(2): p. 283-293.
241. Al-Qayim, K., W. Nimmo, and M. Pourkashanian, *Comparative techno-economic assessment of biomass and coal with CCS technologies in a pulverized combustion power plant in the United Kingdom.* International Journal of Greenhouse Gas Control, 2015. 43: p. 82-92.
242. IEA, G., *Biomass CCS Study: Techno-Economic Evaluation of Biomass Fired or Co-Fired Power Plant with Post-Combustion CO_2 Capture.* IEAGHG: Cheltenham, UK, 2009.
243. Domenichini, R., F. Gasparini, P. Cotone, and S. Santos, *Techno-economic evaluation of biomass fired or co-fired power plants with post combustion CO_2 capture.* Energy Procedia, 2011. 4: p. 1851-1860.

244. Abu-Zahra, M.R., J.P. Niederer, P.H. Feron, and G.F. Versteeg, *CO_2 capture from power plants: Part II. A parametric study of the economical performance based on mono-ethanolamine.* International journal of greenhouse gas control, 2007. 1(2): p. 135-142.
245. Abu-Zahra, M.R., L.H. Schneiders, J.P. Niederer, P.H. Feron, and G.F. Versteeg, *CO_2 capture from power plants: Part I. A parametric study of the technical performance based on monoethanolamine.* International Journal of Greenhouse gas control, 2007. 1(1): p. 37-46.
246. Aroonwilas, A. and A. Veawab, *Integration of CO_2 capture unit using single-and blended-amines into supercritical coal-fired power plants: implications for emission and energy management.* International Journal of Greenhouse Gas Control, 2007. 1(2): p. 143-150.
247. Lawal, A., M. Wang, P. Stephenson, and O. Obi, *Demonstrating full-scale post-combustion CO_2 capture for coal-fired power plants through dynamic modelling and simulation.* Fuel, 2012. 101: p. 115-128.
248. Mac Dowell, N. and N. Shah, *Dynamic modelling and analysis of a coal-fired power plant integrated with a novel split-flow configuration post-combustion CO_2 capture process.* International Journal of Greenhouse Gas Control, 2014. 27: p. 103-119.
249. Cifre, P.G., K. Brechtel, S. Hoch, H. García, N. Asprion, H. Hasse, and G. Scheffknecht, *Integration of a chemical process model in a power plant modelling tool for the simulation of an amine based CO_2 scrubber.* Fuel, 2009. 88(12): p. 2481-2488.
250. Duan, L., M. Zhao, and Y. Yang, *Integration and optimization study on the coal-fired power plant with CO_2 capture using MEA.* Energy, 2012. 45(1): p. 107-116.
251. Gibbins, J. and R. Crane, *Scope for reductions in the cost of CO_2 capture using flue gas scrubbing with amine solvents.* Proceedings of the Institution of Mechanical Engineers, Part A: Journal of Power and Energy, 2004. 218(4): p. 231-239.
252. Hanak, D.P., C. Biliyok, H. Yeung, and R. Białecki, *Heat integration and exergy analysis for a supercritical high-ash coal-fired power plant integrated with a post-combustion carbon capture process.* Fuel, 2014. 134: p. 126-139.
253. Khalilpour, R. and A. Abbas, *HEN optimization for efficient retrofitting of coal-fired power plants with post-combustion carbon capture.* International journal of greenhouse gas control, 2011. 5(2): p. 189-199.
254. Lucquiaud, M. and J. Gibbins, *On the integration of CO_2 capture with coal-fired power plants: a methodology to assess and optimise solvent-based post-combustion capture systems.* Chemical Engineering Research and Design, 2011. 89(9): p. 1553-1571.
255. Lucquiaud, M. and J. Gibbins, *Effective retrofitting of post-combustion CO_2 capture to coal-fired power plants and insensitivity of CO_2 abatement costs to base plant efficiency.* International Journal of Greenhouse Gas Control, 2011. 5(3): p. 427-438.
256. Pfaff, I., J. Oexmann, and A. Kather, *Optimised integration of post-combustion CO_2 capture process in greenfield power plants.* Energy, 2010. 35(10): p. 4030-4041.

257. Rao, A.B. and E.S. Rubin, *Identifying cost-effective CO_2 control levels for amine-based CO_2 capture systems.* Industrial & engineering chemistry research, 2006. 45(8): p. 2421-2429.
258. Romeo, L.M., I. Bolea, and J.M. Escosa, *Integration of power plant and amine scrubbing to reduce CO_2 capture costs.* Applied Thermal Engineering, 2008. 28(8): p. 1039-1046.
259. Sanpasertparnich, T., R. Idem, I. Bolea, and P. Tontiwachwuthikul, *Integration of post-combustion capture and storage into a pulverized coal-fired power plant.* International Journal of Greenhouse Gas Control, 2010. 4(3): p. 499-510.
260. Strube, R. and G. Manfrida, *CO_2 capture in coal-fired power plants - Impact on plant performance.* International Journal of Greenhouse Gas Control, 2011. 5(4): p. 710-726.
261. Hasan, M.F., R.C. Baliban, J.A. Elia, and C.A. Floudas, *Modeling, simulation, and optimization of postcombustion CO_2 capture for variable feed concentration and flow rate. 1. Chemical absorption and membrane processes.* Industrial & Engineering Chemistry Research, 2012. 51(48): p. 15642-15664.
262. Agbonghae, E.O., *Modelling and Optimization of Coal-Fired Power Plant Generation Systems with CO_2 Capture* in *School of Chemical and Process Engineering*. 2015, PhD Thesis, University of Leeds: Leeds, UK. p. 301.
263. Black, J., *Cost and performance baseline for fossil energy plants volume 1: bituminous coal and natural gas to electricity.* National Energy Technology Laboratory: Washington, DC, USA, 2010.
264. Veatch, B., *Power Plant Engineering*. 1996, Springer Science, New York.
265. Chou, V., D. Keairns, M. Turner, M. Woods, and A. Zoelle, *Quality guidelines for energy system studies: process modeling design parameters (National Energy Technology Laboratory) NETL*. 2012, DOE-341/051314 pp 13–21.
266. Chou, V., D. Keairns, M. Turner, M. Woods, and A. Zoelle, *Quality guidelines for energy system studies: process modeling design parameters (National Energy Technology Laboratory) NETL*. 2014, DOE-341/051314 pp 13–21.
268. Schallert, B., Neuhaus, S., & Satterley, C. J. (2013). Do we underestimate the impact of particles in coal-derived flue gas on amine-based CO 2 capture processes?. Energy Procedia, 37, 817-825.